UNIVERSITY OF SOUTHAMPTON

FACULTY OF NATURAL AND ENVIRONMENTAL SCIENCES

School of Ocean and Earth Science

Functional and life-history traits in deep-sea fishes

by

Ming-Tsung Chung

Thesis for the degree of Doctor of Philosophy

September_2015

UNIVERSITY OF SOUTHAMPTON

ABSTRACT

FACULTY OF NATURAL AND ENVIRONMENTAL SCIENCES

SCHOOL OF OCEAN AND EARTH SCIENCE

Doctor of Philosophy

FUNCTIONAL AND LIFE-HISTORY TRAITS IN DEEP-SEA FISHES

Ming-Tsung Chung

The deep sea is one of the largest ecosystems on the earth and fishes play an important role of transporting energy and structuring communities in the deep-sea ecosystem. However, the evaluation of functional and life-history traits (behaviours) in deep-sea fishes is challenging and problematic to directly study at sea. Therefore, this research investigates sensory capabilities from functional tissues in deep-sea fishes to identify functional groups and reconstruct vertical migration patterns and ontogenetic metabolic histories of representative species.

Visual fields and resolving power, indicated by the ganglion cells density and topography on the retina provide the information of diet preferences, habitats and space usage. Otolith morphology, i.e. the outline, the weight and sensory epithelium areas, displays acoustic and vestibular demands in feeding behaviours. These sensory abilities differ between pelagic- and benthic-foraging species or active and passive feeders, and show that depth exerts a stronger pressure on sensory adaptation in pelagic-foraging species. Pelagic foragers with visual-based hunting respond sensitively to the decrease of light intensity with increasing depth through enhanced visual acuity but are also released from the selective pressure of rapid swimming.

Ontogenetic growth, vertical migration and metabolism in four representative deep-water fishes (*Alepocephalus bairdii*, *Antimora rostrata*, *Coryphaenoides rupestris* and *Spectrunculus grandis*) are reconstructed by the otolith microstructure and stable oxygen and carbon isotopes, respectively. *C. rupestris, S. grandis* and other passive/benthic foraging fishes, have evolved interspecific consistency in life history traits, with common large-scale ontogenetic vertical migration, transformations of feeding behaviours between life stages and a dramatic decrease of mass-specific metabolism in the early life. In contrast, *A.bairdii*, *A. rostrata* and active/pelagic foraging species, develop diverse and inconsistent patterns. This study is first to combine morphological and geochemical data to identify functional and life-history traits, and the diverse datasets greatly aids classification where direct observation is difficult.

Table of Contents

List of tables

List of figures

DECLARATION OF AUTHORSHIP

I, Ming-Tsung Chung

declare that this thesis entitled

“Functional and life-history traits in deep-sea fishes”

and the work presented in it are my own and has been generated by me as the result of my own original research.

I confirm that:

1. This work was done wholly or mainly while in candidature for a research degree at this University;
2. Where any part of this thesis has previously been submitted for a degree or any other qualification at this University or any other institution, this has been clearly stated;
3. Where I have consulted the published work of others, this is always clearly attributed;
4. Where I have quoted from the work of others, the source is always given. With the exception of such quotations, this thesis is entirely my own work;
5. I have acknowledged all main sources of help;
6. Where the thesis is based on work done by myself jointly with others, I have made clear exactly what was done by others and what I have contributed myself;
7. None of this work has been published before submission.

Signed: ……

Date: ……

Acknowledgements

This study would not have been possible without the help of a number of people and organisations. First and foremost, I would like to thank my supervisor, Dr. Clive Trueman, for his supervision and patience in the past five years including my MRes degree. I really appreciate that he inspires me to make my PhD project possible and provides numerous opportunities for cooperations with other prestigious institutions. I would also thank to Dr. Francis Neat (Marine Scotland Science) giving helpful advices in deep-sea fishes, supports of samples and feedbacks for papers.

In the National Oceanography Centre, Southampton, I am deeply grateful to everyone whom giving help. Dr. Sven Thatje for chairing my panel; John Ford, Bob Jones and Matt O'Shaughnessy for technique help; Diana Shores, Rui Vieira, Sarah Magozzi, Katie Davies, Kirsteen MacKenzie, Rhiannon Meier, Joe Scutt Phillips and all people in our best SUMIE research group; Ben Hume, Alastair Brown, Nina Rosset and Richard Davy as wonderful office mates. I specially thank to Chiara Marieni, Chris Daniel, Amonsak Sawusdee, Khaira Ismail and Jiraporn Charoenvattanaporn for friendship supports in many aspects. Many thanks also to my friends for making my life in Southampton very pleasant.

At Marine Scotland Science, many thanks to all scientists and crews in the 2012-2013 Deep Water Survey from whom I learnt lot of deep-sea knowledge.

I would like to say a big thank to Dr. Chia-Hui Wang (National Taiwan Ocean University) and Professor Chen-Feng You (National Cheng Kung University) for encouraging me studying abroad and lots of supports throughout these years.

Finally, all my love to my whole family. Thanks for your mental and financial supports that make me without any worry while studying in UK and always cheering me up in the most difficult time.

This study is supported by Taiwan Government Fellowship for Studying Abroad.

Chapter 1: Thesis introduction

1.1 Deep-sea environment

1.1.1 Zonation

The open ocean is strongly zoned by vertical gradients rather than by horizontal gradients because topography, temperature, light penetration and food availability vary with depths. According to the topography, the continental shelf, slope, abyssal plain and hadal zone are generally defined as having depths of 0-200m, 200-3000m, 3000-6000m and over 6000m respectively (Angel 1997, Gage & Tyler 1991, Merrett & Haedrich 1997) (Fig. 1.1).

In the pelagic realm, boundaries are set at the depths 200m, 1000m, 3000m and 6000m. Above 200m, the euphotic area is defined as the epipelagic zone, and the primary production in this area supports the life beneath. In terms of a definition, the deep sea is viewed as the environment below the epipelagic zone. In the dimmer environment between 200m and 1000m, known as the mesopelagic zone, light penetration decreases, and below 1000m, daylight ceases to be detectable. Besides light penetrations, below 1000m, other oceanographic conditions, such as temperature, tend to be more stable below a permanent thermocline. A boundary around 3000m separates the bathypelagic (1000-3000 m) and the abyssopelagic (3000-6000 m) zones, due to the possibility of topographic transition (continental rise) from slope to abyssal plain. The abyssal plain extends to the mid-ocean ridge at the passive continental margin, and the sea floor plummets to the hadalelagic zone (under 6000m) at the active continental margin.

The demersal community extends from the costal shelf to the abyssal plain and comprises the benthic fauna, living and feeding on the seafloor, and benthopelagic fauna, swimming or drifting in the water column close to the bottom. According to topography, demersal assemblages can be classified as bathaldemersal (200-3000m, the depth range of continental slope) and abyssal (3000-6000m, the depth range of abyssal plain) demersal species.

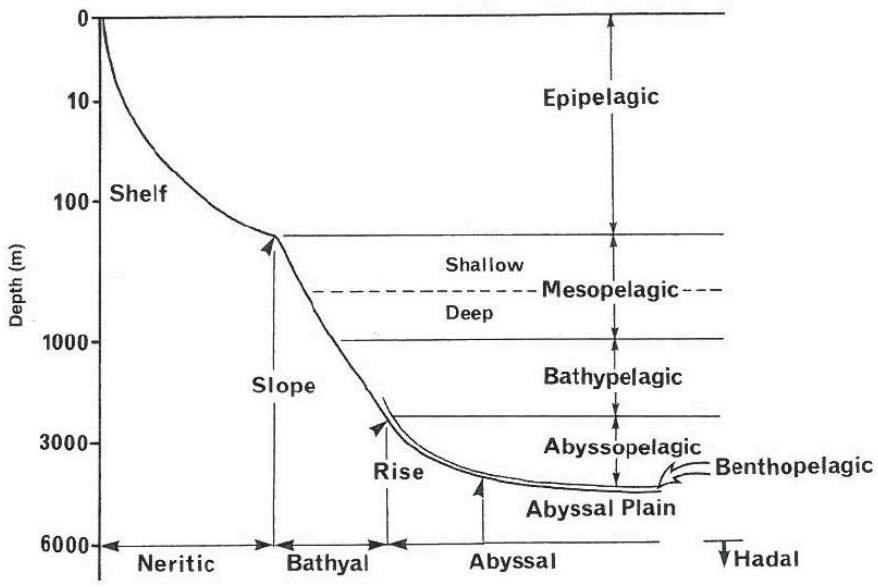

Figure 1.1. Zonation in the deep sea (Angel 1997).

1.1.2 Light

There are numerous factors controlling the zonation of deep-sea organisms and showing a depth related gradient, and as described above, light is one of the most important factors. Sunlight is important for photosynthesis and animals' vision in the ocean, but light intensity exponentially decreases with depth in clear water (Clarke & Denton 1962) (Fig. 1.2):

$$\frac{I}{I_0} = e^{-kL}$$

where I and I_0 are the light intensity of two depths and L is the distance between these two depths. The vertical extinction coefficient, k, varies between water masses and locations, with values such as 0.46-0.15 for coastal waters but with a tiny value of 0.046 for clear oceanic regions. In the open ocean, the intensity dramatically decreases in the shallower layer above 100m because of absorption by phytoplankton and organic matters. However, below this depth, the trend keeps constant at an order of magnitude of 1.5x decrease for every 100m (Warrant & Johnsen 2013). The mesopelagic zone is divided into shallow and deep zones according to the appearance of organisms, which are dependent on the change of light intensity (Angel 1997). Fishes with mirrored sides and dark backs (for example, myctophids) and crustaceans with half-red and half-transparent bodies are observed above 600-700m. The animals are hiding in the environment and away from predators, relying on the fact that the black backs blur the vision of overhead predators and their red body is functionally black given that the red

wavelength of light is absorbed in the deep sea. At the depth of 700-1000m, the sunlight is very weak and nearly all the fish and crustaceans have uniformly black and red bodies. Basically, no sunlight can be detected at a greater depth than 1000m.

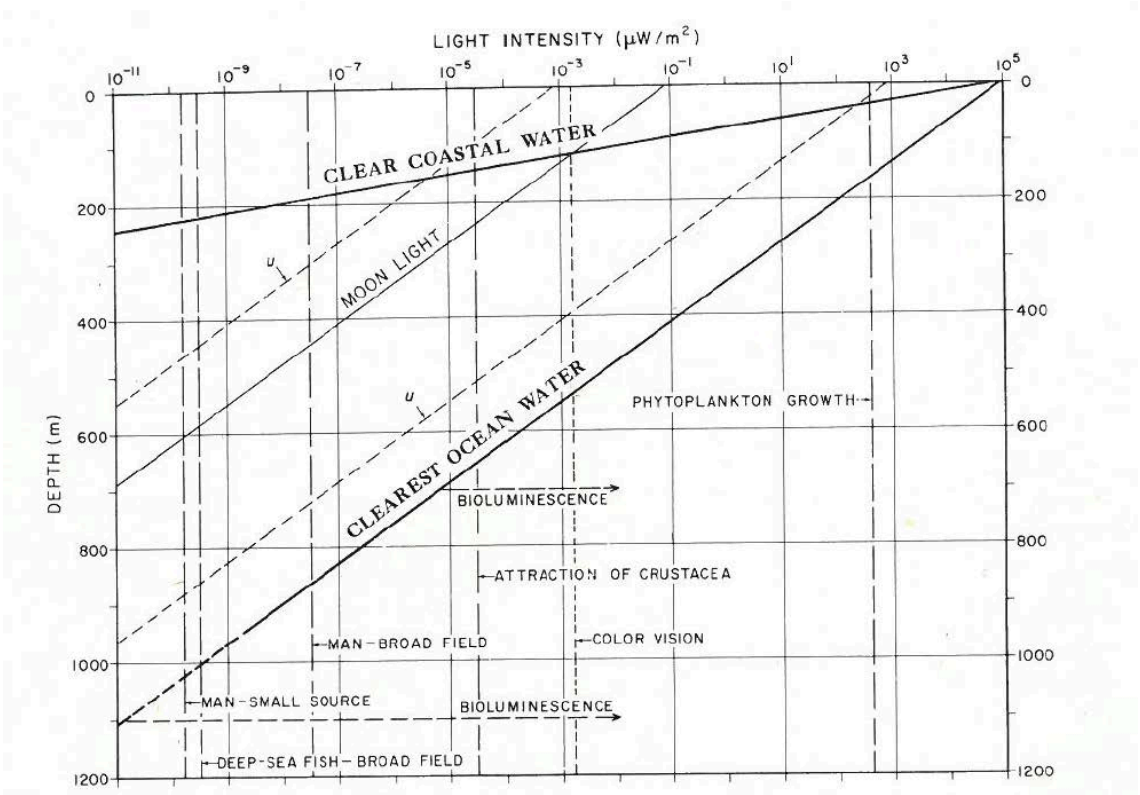

Figure 1.2. Light intensity with depth gradients in log scale. (Clarke & Denton 1962).

The importance of bioluminescence increases with depth, revealling that pointed light replaces light in a broader space (sunghlight) in the deep sea. This changes visual behaviours and life strategies of organisms. Bioluminescence has been found in a broad range of taxa from bacteria to fish, distributed from shallow water to the deep (Haddock *et al*. 2010). However, the bioluminescent events also decrease with depth because of in a decrease of biomass (Craig *et al*. 2009; Craig *et al*. 2011; Gillibrand *et al*. 2007a).

1.1.3 Temperature

Surface water receives solar radiation and the heat can be transmitted hundreds of metres down by the mixing of layers through the power of waves, wind-drive currents and convection. The ocean mixed layer maintains a high temperature, but temperature dramatically decreases in the layer beneath, which is called the thermocline. The depth

of the thermocline and the level of temperature changes depend on the latitude as shown in Figure 1.3a. However, below the thermocline, the temperature decreases with depth less rapidly and is more constant in cold and dense water masses, with the exception of areas around hydrothermal vents which can reach temperatures of up to 200-360°C (Gage & Tyler 1991). In the Northeast Atlantic (the research area for this thesis), the temperature sharply decreases around 1000m, on the upper continental slope (Fig. 1.3b) and animals inhabiting in this depth range experience a dramatic decrease in temperature.

1.1.4 Oxygen

Generally, the maximum oxygen concentration is recorded in the surface layer of the ocean. Photosynthesis is the main input of oxygen and the photosynthesis rate follows the pattern of light intensity in that it decreases with depth gradients (Ryther 1956). However, the imbalance of oxygen generation (photosynthesis) and consumption (organisms' utilization) causes a dramatic decline of oxygen concentration from shallower waters till the oxygen minimum zone around 400-1000m (Fig. 1.3a) (Childress & Seibel 1998). Gas transfer across the air-sea interface is the second input of oxygen. The process is temperature dependent in that cold waters, especially in the polar regions, have a higher capacity to absorb dissolved oxygen derived from the atmosphere. Furthermore, owing to a higher density, the cold and O_2-rich water in the polar regions sink and flow equatorward to form the deep-water layer above the ocean basins. This water mass supplies oxygen to the deep sea, explaining the increase of oxygen concentration below the minimum oxygen zone (Fig. 1.3a).

Animals living in oxygen minimum zones have prominent strategies of adaptation (Childress & Seibel 1998; Seibel 2011). A larger gill size, a shorter diffusion distance between water and blood and a higher affinity of O_2 enhance the oxygen extraction from the hypoxic environment. In addition, the anaerobic metabolism is promoted and energy consumption is suppressed.

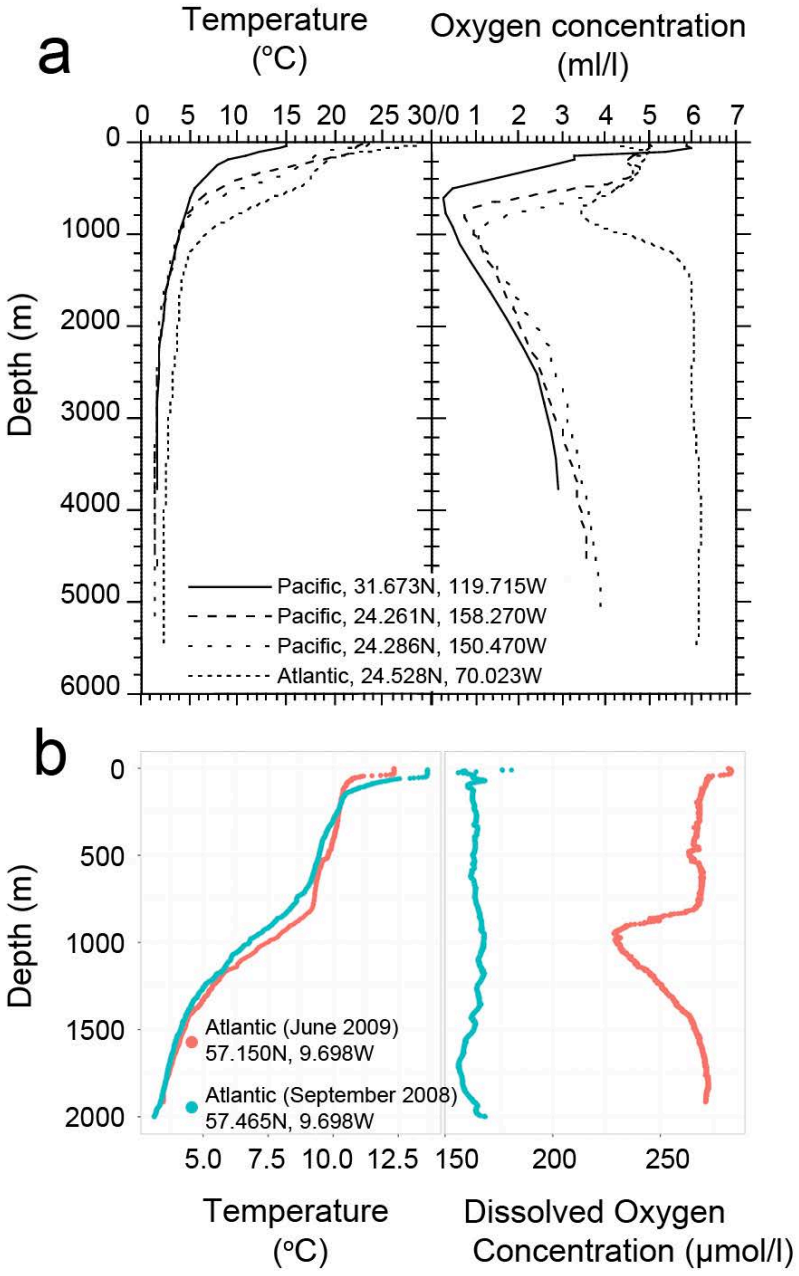

Figure 1.3. Temperature and dissolved oxygen concentration with depth gradients. (a) Childress and Seibel (1998). (b) The Northeast Atlantic (the sampling location in this thesis).

1.1.5 Hydrostatic pressure

The hydrostatic pressure in the ocean is related to depth and seawater density. Although the pressure varies from site to site, the relationship with depth can be simplified as an increase of 1 atm per 10 metres depth (Pinet 2009). According to the

information from Sea-Bird Scientific (http://sea-birdscientific.com), the empirical formula between depth and pressure is shown below with an assumption of 0°C (temperature) and 35 PSU (salinity) for water mass:

$$Depth = \left[\left(\left((-1.82\times10^{-15} * Pressure + 2.279\times10^{-10}) * Pressure - 2.2512\times10^{-5}\right) * Pressure + 9.72659\right) * Pressure\right] / Gravity$$

$$Gravity = 9.780318 * [1.0 + (5.2788\times10^{-3} + 2.36\times10^{-5} * X) * X] + 1.092\times10^{-6} * Pressure$$

$$X = [\sin(latitude/57.29578)]^2$$

where the units of depth, gravity and pressure are metres, meter per square second (m/s^2) and decibars, respectively. This equation will be further utilised in Chapter 4.

Neritic animals are restricted from penetrating into deep water owing to high hydrostatic pressure, but deep-sea species develop stable cellular structures (i.e. enzymes, proteins and membrane-based systems) in adaptation to the high-pressure environment (Somero 1992). However, the limit of fish occurrence is reported to be no more than 8400m because of the biochemical constraint in osmoregulation (Yancey *et al*. 2014).

1.1.6 Food availability

Organic matter transferred from the surface into the deep ocean maintains life in the deep-sea ecosystem. Two mechanisms in deep-sea ecology, the passive and biological transportation, have been pointed out (Gage 2003) (Fig. 1.4).

Small organic particles and large animal or plant remains passively sink to the deep. The small particles are important organic materials from the euphotic zone entering the deep ocean, and particles include faecal pellets, moults, salps and phytodetritus. The amount of organic matter strongly depends on the primary production in the surface ocean and considerably declines in the mixing layer (Lampitt *et al*. 1993). About 5-15% of organic matter generated from primary production is exported from the surface layer loop and exported to the deep sea (Fowler & Knauer 1986; Frigstad *et al.* 2015; Giering *et al.*, 2014; Henson *et al.* 2011; Laws *et al.* 2000). As they are consumed by zooplankton and nekton, the size of particles determines their residence time in the

water column, and particle aggregations, known as marine snow, have higher residence time and sinking rates as they are transported to a deeper environment. Moreover, larger food fallings, such as animal carcasses, have a higher opportunity of reaching the deep as a food source for necrophages, such as amphipods, ophiuroids and fish (Gage 2003 and citation therein). Although large food-falls are rare events, they represent a significant energy flow into the deep ocean (Stockton & DeLaca 1982).

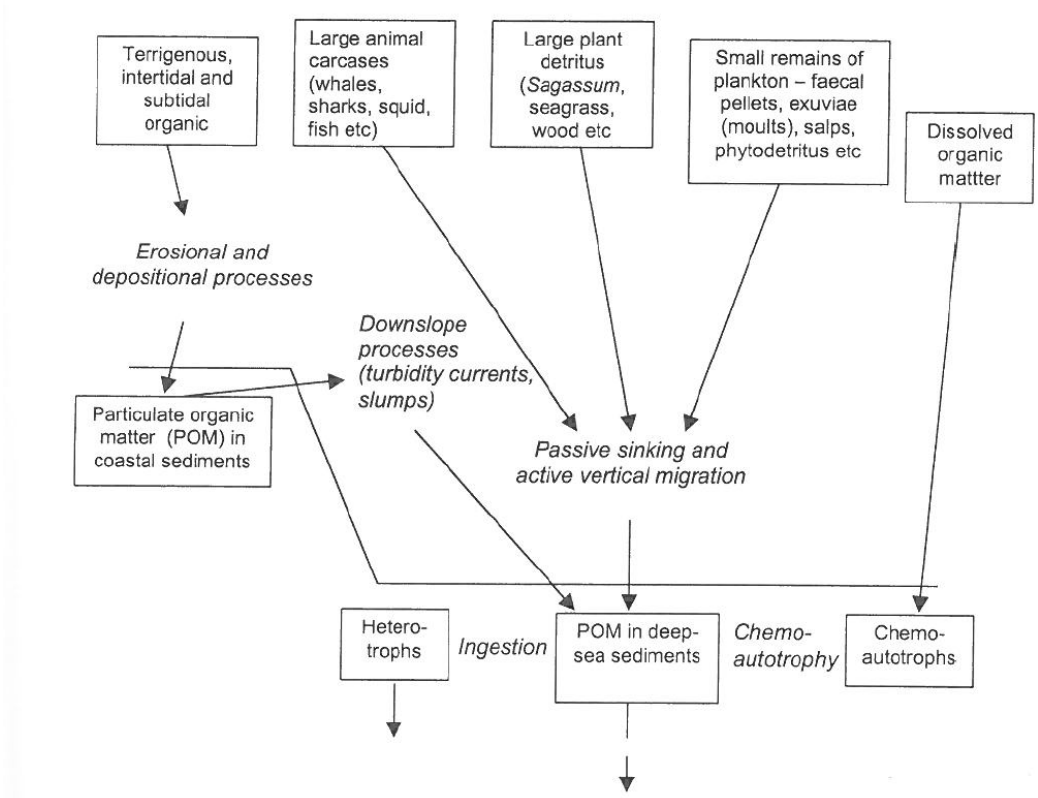

Figure 1.4. Sources of organic matters transported to the deep sea (Gage 2003).

The second mechanism for transport of food into the deep sea is through transport by migratory species, which link the epipelagic layer to the deep benthos through daily vertical migrations. The daily migration pattern is observed that some pelagic deep-sea organisms (such as copepods and lanternfish) forage in the shallower water layer for higher food availability, but descend to deep waters to evade high predation pressure at the surface. In deeper waters these migrating organisms are, however, preyed on by resident deep water species (Mauchline & Gordon 1991). No matter whether the migration is diel or ontogenetic, it facilitates energy transportation to the deep-sea ecosystem (Mauchline & Gordon 1991; Trueman *et al*., 2014).

Another possible food source is dissolved organic matter in sediments, which contain a higher concentration of dissolved organic matter than the water layer above has. Although the importance of this food source is uncertain, several studies have proved that dissolved organic carbon is utilised by deep-sea invertebrates (Gage 2003 and citation therein) and supports life in the deep.

1.2 Deep-sea demersal fishes

According to Headrich (1997), the deep sea species account for 10-15% of global fish fauna, according to data recorded in 1970. With more new species found in past decades, Mora *et al*. (2008) indicated that the proportion of deep sea species may exceed 27%. In deep-sea fish assemblages, demersal species are identified as having a higher diversity than the pelagic species (Mora *et al*. 2008). Environmental heterogeneities give an explanation of the high diversity of deep-sea fishes and the difference between pelagic and demersal assemblages (Levin *et al*. 2001). Brown and Thatje (2014) further explain that the physiological stress response to dramatic environmental changes (especially of temperature decreases and pressure increases) drives speciation, resulting in a higher diversity of deep-sea animals on the continental slope. For example, in the North Atlantic, deep-sea demersal fishes reach peak diversity at 1500-2000m, within the range of continental slope (Priede *et al*. 2010; Rex & Etter 2010) (Fig. 1.5). Moreover, depth-dependent energy flows and types of food are also possibly driving forces of increasing diversity in this depth range (Trueman *et al.* 2014)

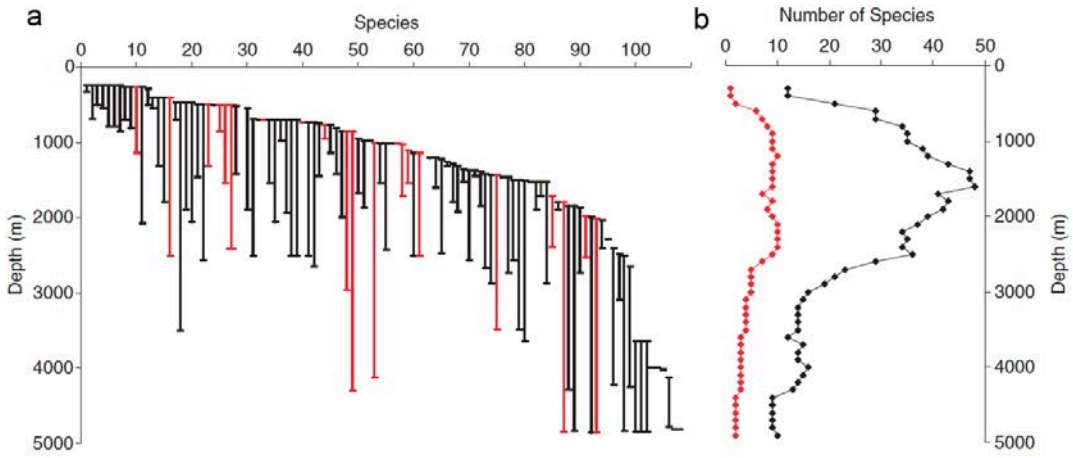

Figure 1.5. Species diversity with depth gradients (Priede *et al*. 2010). (a) The depth range of distributions in individual species. (b) Accumulated species

numbers with depth. Black and red bars/dots represent the non-scavenging and scavenging species.

1.2.1 Population Ecology on the continental slope of the Rockall Trough

Although some deep-sea species or taxa are widely distributed across different geographical locations, such as the orange roughy (*Hoplostethus atlanticus*), the deep-sea demersal assemblages are not viewed as globally homogeneous and show regional dissimilarity of species compositions and abundance (Clark *et al*. 2010). In the Northeast Atlantic, Neat *et al*. (2008) reported that 185 species (composed of teleosts, sharks and Chimaerids) have been recognised from within the ecosystem of the continental slope and the seamounts (Fig. 1.6). Teleosts as in family Gadidae (codfishes), Macrouridae (grenadiers), Meluccidae (hakes), Moridae (Morid codfishes), Scorpaenidae (redfish), Synaphobranchidae (cutthroat eels), Alepocephalidae (smoothheads), Argentinidae (Argentines), Trichuridae (scabbard fish) and Zoarcidae (eelpouts) are abundant in this ecosystem. However, the taxa composition shows a strong depth zonation (Fig. 1.7) and varies between locations, for example, more abundant blue whiting (*Micromesistius poutassou*) and Baird's smoothhead (*Alepocephalus bairdii*) on the Rosemary Bank, but a large number of black scabbard fish (*Aphanopus carbo*) found on the Anton Dohrn Seamount (Neat *et al*. 2008).

The population structure is closely related to life history traits and the behaviours of deep-sea fishes. For example, the similar diet preferences lead to shallower distributions of Baird's smoothhead than Agassiz's smoothhead (*Alepocephalus agassizi*) in order to avoid competitions (Mauchline & Gordon 1983). The population of blue whiting is more stable on the continental slope rather than on the Rockall Bank, because larval drifts and returning mature individuals mainly follow the route between spawning (Porcupine Bank) and feeding ground (Norwegian Sea) along the continental shelf edge (Was *et al*. 2008; Payne *et al*. 2012). Such differences cause regional variety in the compositions of deep-sea fish; however, there is a poor understanding of population ecology owing to the limited knowledge of life history traits in the majority of deep-sea species.

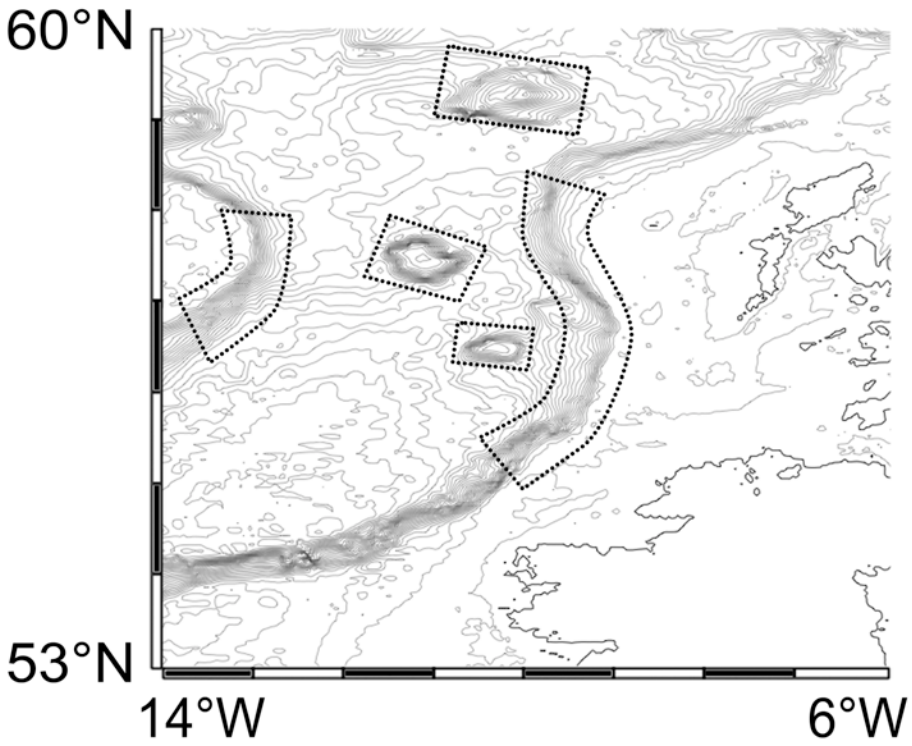

Figure 1.6. Deep-water surveys in the Rockall Trough area, conducted by Marine-Scotland Science. The dot-line areas are sampling locations.

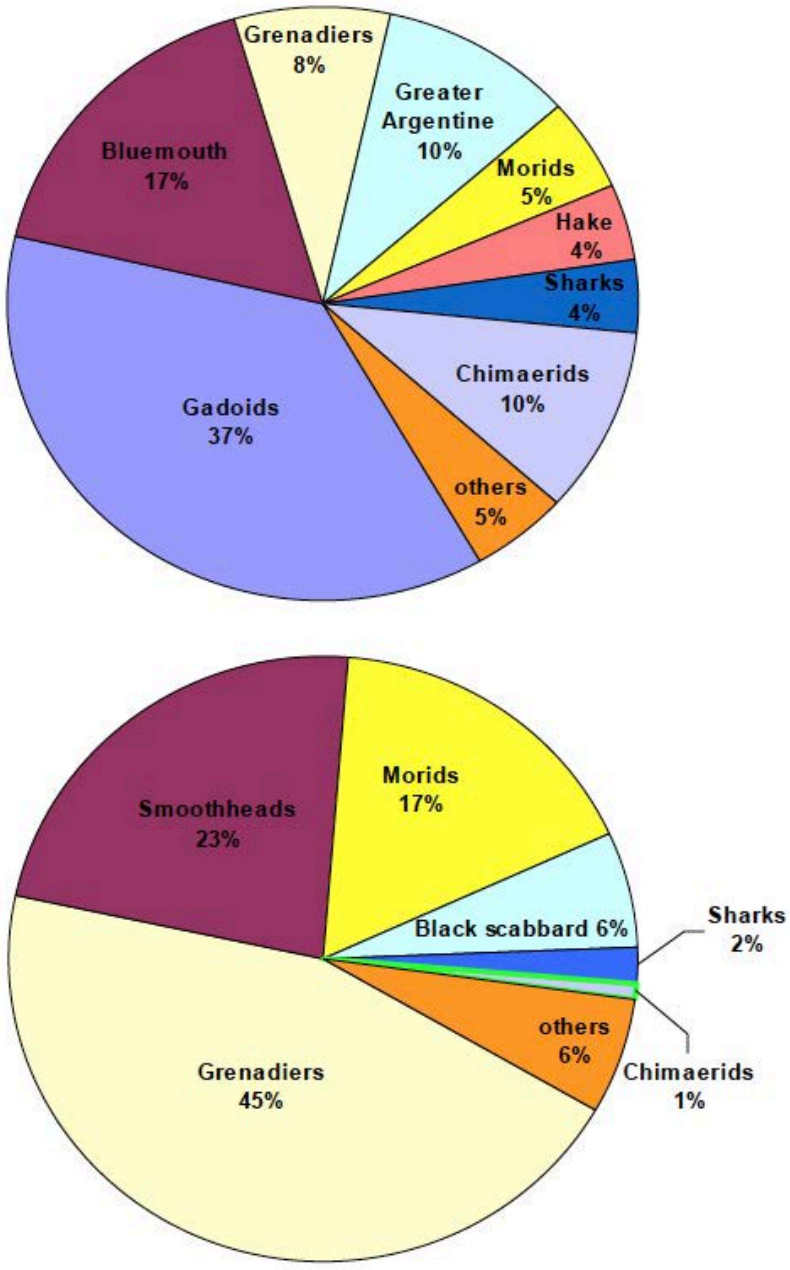

Figure 1.7. Species compositions in the Northeast Atlantic (Neat *et al*. 2008). Upper pie chart is the composition at 500m and lower at 1000m. The percentage represents the abundance of individuals in each taxonomic group.

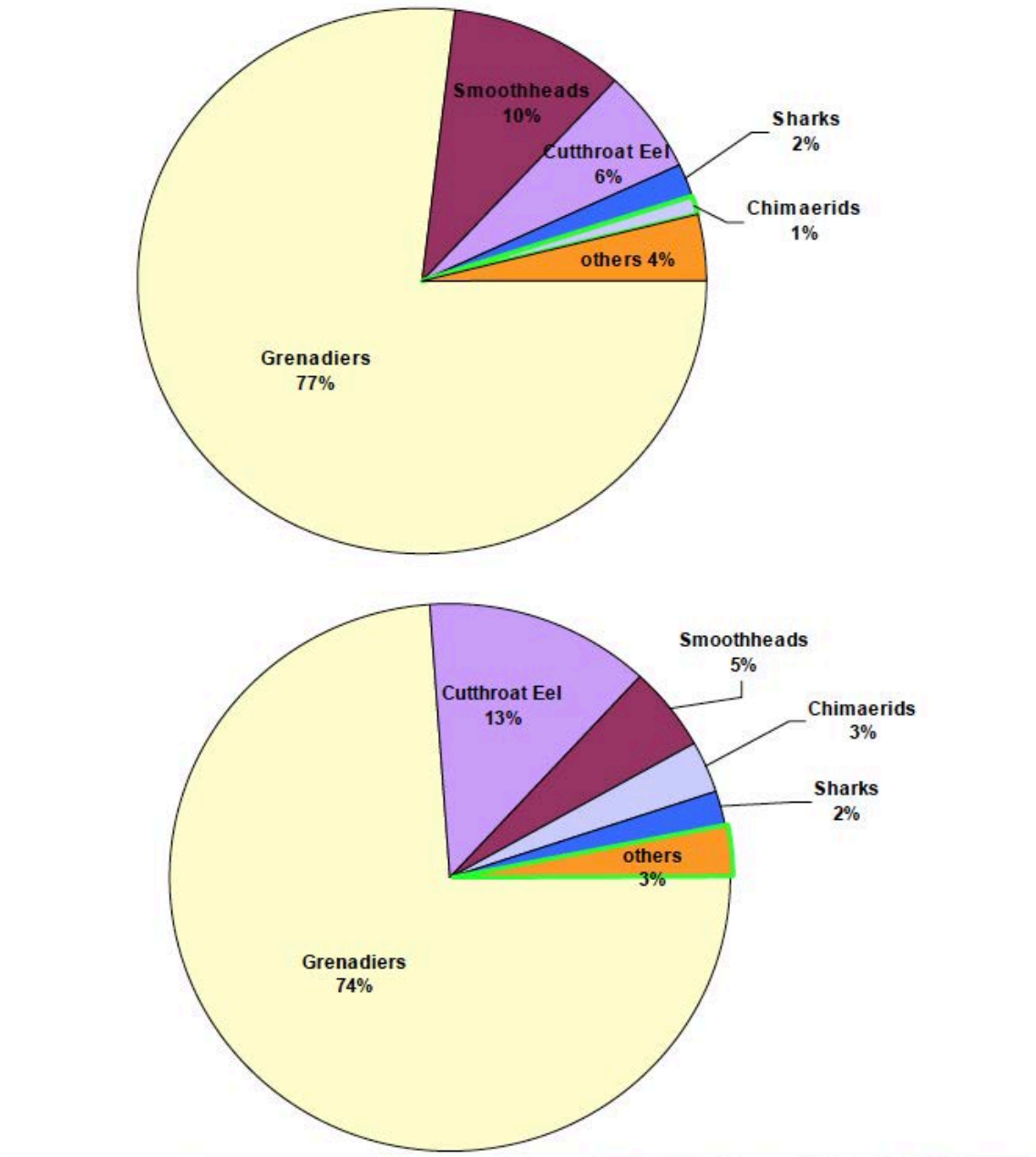

Figure 1.7 (continued). Upper pie chart is the composition at 1500m and lower at 1800m. The percentage represents the abundance of individuals in each taxonomic group.

1.2.2 Phylogeny

The trait evolution is a key to understanding why some species or taxa successfully live in the deep environment and what distinct functional behaviours they develop. Andriashev (1953) pointed out two categories in the phylogeny of deep-sea fish as the ancient and the secondary groupings. The ancient taxa revealed by the molecular phylogeny are Notacanthiforms, Angulliformes, Osmeriformes, Stomiiformes, Aulopiformes and Myctophiformes (Near *et al*. 2012) (Fig. 1.8). The ancient species evolved early into deep water species and they inhabit a wide range of depths and have various specialized morphological functions (Priede & Froese 2013). On the other hand, the secondary deep-sea grouping comprises the recent teleost taxa, which belong to Acanthopterygii as Zeiformes, Scorpaneiformes and Perciformes. Most of these species show less variability in morphology (Priede & Froese 2013). Moreover, Priede and Froese (2013) further define Paracenthopterygii (Gadiformes, Ophidiiformes and Lophiiformes) as the intermediate group between ancient and secondary groupings. This broad view of deep-sea fish phylogeny explains that ancient species have evolved in Earth's history for a longer period than recent taxa, and ancient species develop physiological adaptations to extreme environmental conditions such as lower temperature, higher hydrostatic pressure and lower food availability. Although several uncertainties of fish evolution have not yet been resolved, the overall phylogenetic relationship (Fig. 1.8) gives a basic criterion for comparing fish life history and functional behaviours in phylogeny.

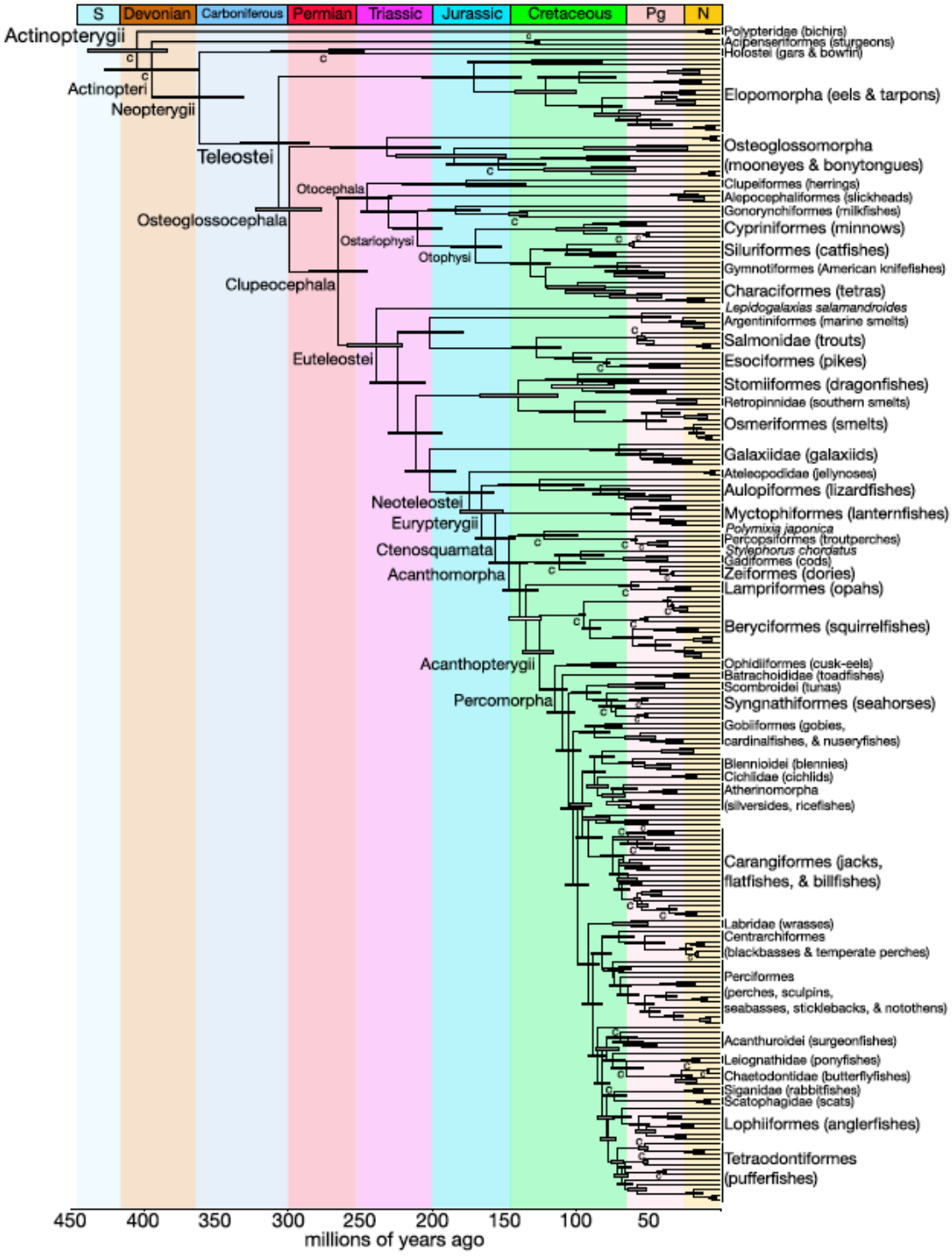

Figure 1.8. Time-calibrated phylogeny in ray-finned fishes, including 232 fish species. This is established based on genetic information and fossil records (Near *et al*. 2012).

1.3 Surveys of deep-sea fish ecology, life history and behaviours in literatures

1.3.1 Sampling for specimens

Deep-sea fish sampling can be conducted with baited longlines, baited traps and trawls (Haedrich & Merrett 1988; Hareide 1995; Jørgensen 1995) that give direct evidences of fish ecology in the aspects of species assemblages (Gordon & Bergstad 1992; Merrett & Marshall 1980; Neat *et al*. 2008; Priede *et al*. 1994; Priede *et al*. 2010), vertical distribution (Merrett & Marshall 1980; Priede *et al*. 2010), habitat usage (Husebø *et al*. 2002), size structures (Mauchline & Gordon, 1983, 1984a, 1984b, 1984c), biodiversity (Campbell *et al*. 2011; Danovaro et al. 2010) and dietary preferences (more descriptions in section 1.1.3). With the technological progress, such as a development of suction samplers mounted on a remotely operated vehicle (ROV) (Drazen and Robison 2004; Ross & Quattrini 2009), deep-water sampling reaches a deeper environment, offering a wider survey in fish ecological issues.

In addition, most of studies rely on the collection of fish specimens to further explain behavioural ecology, for example, fish body form indicating swimming capability (Neat & Campbell 2013), specified organs or tissue evolved in the deep-sea fishes (Deng *et al*. 2011; Wagner *et al*. 1998), biochemistry revealing physiological adaptation (Drazen & Seibel 2007; Graham *et al*. 1985) and genotypic variation between fish stocks (Longmore *et al*. 2014). Sampling for specimens provides direct and indirect evidences of fish populations and behaviours, which are important and essential to comprehend the deep-water fish ecology.

1.3.2 In situ observations

The remotely operated vehicle (ROV) equipped with video has been widely used in the investigation of deep-sea organisms and also applied to the surveys of fish occurrence, abundance, population size, habitat specificity and regional assemblages (Baker *et al.* 2012*;* Stein *et al.* 2005; Trenkel *et al.* 2004a*;* Trenkel *et al*. 2004b). However, this approach causes disturbances during a survey (Lorance & Trenkel 2006; Uiblein *et al*. 2003) and a short-term monitoring may bias identifications of fish's in situ behaviours.

The autonomous instrument carrier system, the Lander (a free-fall system), is also applied to deep-sea research. Usually, the Lander is configured with baits to record the feeding behaviours of scavengers, such as macrourids, morids, cusl eels, cutthroat eels and so on (Yeh & Drazen 2011; Henriques *et al*. 2002; Bailey *et al*. 2007). The advantage of the Lander is that the additional instruments can be mounted on this carrier system, which is designed for a specific experimental purpose. For example, a survey of swimming mode and a measurement of in situ oxygen consumption are conducted by the redesigned Lander with cages (Bailey *et al.* 2003; Bailey *et al*. 2002). Another advantage of Lander is that there are fewer disturbances during the investigation and the observation can last for up to several months (Bailey *et al*. 2007). However, this is constrained if the species are not scavengers. Therefore, with the existing limitations of in situ observations, the indirect evidences from other approaches are necessary for supporting the findings about deep-sea fish ecology.

1.3.3 Stomach content analysis

Stomach content analysis is a conventional method to analyse the feeding behaviours and the trophic structure of fish. Mauchline and Gordon (1980, 1983, 1984a, 1984b, 1984c, 1986) have widely surveyed deep-sea species in the Northeast Atlantic and explain the habitat usage and feeding strategies of different taxa. Stomach content analysis provides important information about the prey and predator relationship in the ecosystem and give clues as to energy transfer through deep-sea fishes (Bergstad *et al.* 2003). Nevertheless, stomach analysis has some limitations. For example, seasonal changes of prey species compositions and availabilities bias identifications of fish diets (González *et al*. 2000). Secondly, insufficient sample sizes result from empty stomachs or everted stomachs owing to a sharp decrease of pressure causing the expansion of gas filled bladders during the sampling (Bulman & Koslow 1992). Thirdly, items in the stomach are hard to identify, especially the gelatinous prey species. In order to overcome these difficulties, long-term and massive sample collections are necessary, but these lead to great expense.

1.3.4 Stable carbon and nitrogen isotope analysis

Since 1980s, the stable isotopes, especially those of nitrogen and carbon, have been widely utilised in discussions of trophic ecology in terrestrial and aquatic systems (Minagawa & Wada 1984; Peterson & Fry 1987; van der Merwe 1982). Stable isotopes provide a tool for quantifying trophic levels, giving support to stomach content analysis. The basic theory is based on the isotope fractionation in the physiological process, that

the lighter isotope is preferentially extracted by respiration, extraction and metabolism, leaving newly formed tissues relatively enriched in the heavier isotope (Fig. 1.9). According to the above mechanism, isotope values increase (become more enriched in the heavier isotope) from primary production to top predators in the food web. The isotope fractionation in a single trophic transfer ranges from less than 2‰ to 5‰ for $\delta^{15}N$ and from 0‰ to 2.0‰ for $\delta^{13}C$, and the mean value among multiple trophic pathways is 3.4‰ and 0.4‰ per trophic level for $\delta^{15}N$ and $\delta^{13}C$, respectively (Post 2002; Peterson & Fry 1987) (Fig. 1.9). To determine absolutely the trophic position or compare trophic positions between different ecosystems, the issue of how to choose and measure an appropriate isotope baseline is critical for stable isotope analysis.

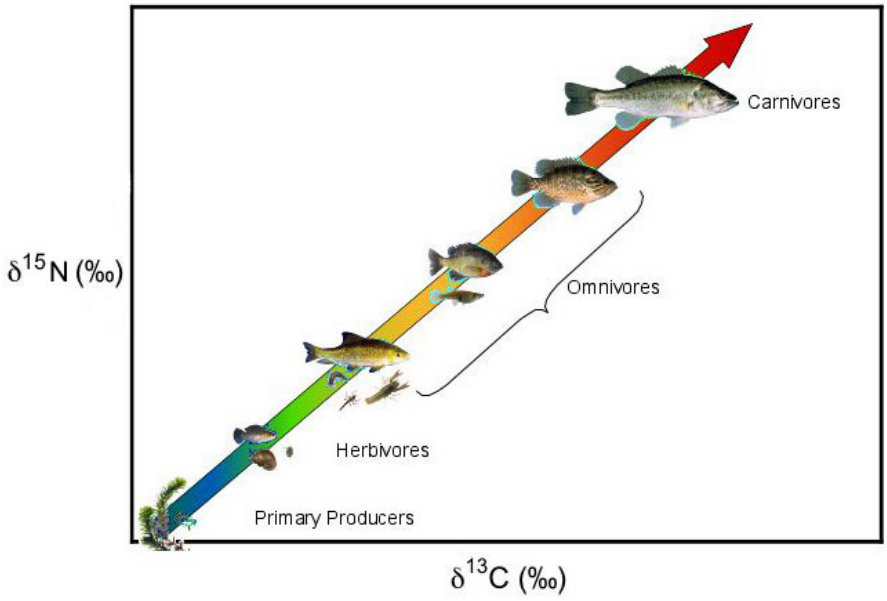

Figure 1.9 Increasing trend of $\delta^{15}N$ and $\delta^{13}C$ values (in muscle tissues) with an increase of trophic levels (Bemis 2003).

The applications of stable isotope on deep-sea fish ecology include the role of fish in deep-sea benthic communities and food web structures (Iken *et al*. 2001; Polunin *et al*. 2001), the trophic ecology of fish assemblages (Stowasser *et al*. 2009; Boyle *et al*. 2012; Trueman *et al.* 2014), the trophic position of specific species in the ecosystem (Drazen *et al*. 2008; Stowasser *et al*. 2009; Fanelli & Cartes 2010; Santos *et al*. 2013) and the trophic dynamics in relation to temporal changes or ontogeny (Fanelli & Cartes 2010; Santos *et al*. 2013; Stowasser *et al.* 2009). The studies of stable isotope analysis on deep-sea fish are still few in number and there are some unresolved issues, such as the turnover rate of tissue in long-lived animals, the influence of pelagic-benthic coupling in trophic dynamics. Nevertheless, stable isotopes analysis provides one kind of evidences to complete the knowledge in deep-sea fish.

1.3.5 Otolith applications

The otolith, an auditory and vestibular sense organ in teleosts, continuously grows in the capsule of the inner ear. The microstructure of otolith, a calcified tissue, shows a periodic pattern of alternations of opaque and translucent bands, which reveal endogenous rhythm synchronised with environmental variations (Morales-Nin 2000). These growth increments from the basis of fish ageing are in most temperate systems. High food supplies and temperature in daytime/summer cause the otolith to form wider increments than in nighttime/winter because the higher absorption of organic matters in the interim accelerates calcification rates (Wright *et al*. 2002). Organic matter in the otolith comprise less than 5% (Campana 1999), but it plays an important role as scaffolds for carbonate deposition. Without the protein aggregates, otolith calcification is slowed down (Hüssy 2008; Pannella 1971; Petko *et al*. 2008; Murayama *et al*. 2002; Murayama *et al*. 2005). In spite of daily or seasonal increments, growth rings provide a tool with which to determine the age of fish.

The deep sea is regarded as a relatively homogenous environment with constant temperature, aseasonality and no photoperiod, but regular temporal variations are seen in some variables, such as food supply (Lampitt 1985; Rice *et al*. 1986). Downward-settling organic particles produced in shallower layers are transported to the seabed as the energy sources for organisms in deep waters (Gage & Tyler 1991). The seasonal pulses arouse activity in benthic communities and influence abundance and biomass of megafauna (Bett *et al*. 2001; Witbaard *et al*. 2000). Whatever the mechanism, the otoliths of deep-water fishes display clear, regular variations in opacity which correspond to somatic growth rates, and thus it possible to discuss the seasonal growth pattern in deep-sea fish otoliths. For example, Swan and Gordon (2001) examined marginal increments of macrourid otoliths and validated that the seasonal timing of zone formation is present in the deep sea. Moreover, radioactive dating confirms that the age of deep-sea fish, estimated from otolith increments, is reasonable for some long-lived species (Andrews *et al*. 2009; Cailliet *et al*. 2001; Kerr *et al*. 2004). Thus, the age determination from otolith growth rings has been widely conducted with numerous deep-sea fish species (Vieira *et al*. 2009; Vieira *et al*. 2013; Sequeira *et al*. 2009; Fossen & Bergstad 2006; Bergstad *et al*. 2012; Allain & Lorance 2000; Casas & Pineiro 2000; Kelly *et al*. 1997; Kelly *et al*. 1999; Morales-Nin & Sena-Carvalho 1996).

Besides ageing, there are other important applications for otolith analyses on fish ecology. Firstly, the stock and population structures of deep-sea fish are successfully discriminated by otolith morphology and/or chemical compositions, which record distinct signals and regional variations while fish live and grow in different locations (Longmore *et al*. 2010; Longmore *et al*. 2011; Swan *et al*. 2003; Swan, Gordon & Shimmield 2003; Swan *et al*. 2006; Cardinale *et al*. 2004; Carlsson *et al*. 2011). Secondly, the chronological record of stable isotopes in otolith can be utilised as a tracer for migration pathways ($\delta^{18}O$) and as an indicator of ontogenetic metabolism ($\delta^{13}C$) (Shephard *et al*. 2007; Lin *et al*. 2012; Schwarcz *et al*. 1998; Jamieson *et al*. 2004). Thirdly, the eco-morphological study of otolith (ecology constrains the development of otolith morphology or the function-related morphology responds to environmental effects) explains functional behaviours of fishes (Gauldie *et al*. 2002; Torres *et al*. 2000; Tuset *et al*. 2010). According to these findings, we can expect to acquire more ecological information from deep-sea fish otoliths.

1.4 Aim, objectives and hypotheses

The marine ecosystem is structured by functional components, defined as several species sharing similar functional traits and showing similar responses to the environment (Steneck 2001; Blondel 2003). However, there is limited knowledge about functional compositions in deep-sea fish ecology and about the fish life history traits corresponding to specific functional behaviours. Thus, this thesis aims to provide a better understating of ecosystem functions of deep-sea fish and, specifically, the objectives of the project are as follows, to:

- Identify functional groups of deep-sea fishes based on sensory perception adaptations
- Explain prominent functional feeding behaviours in relation to the deep-sea environment
- Investigate the life history traits between functional groups

The continental slope of the Rockall Trough (Fig. 1.6) is the main deep-sea ecosystem discussed in this thesis and teleosts are the target species. To achieve the goals, the main hypotheses to be tested are:

- The sensory morphology of the eye will vary between broad functional groups of fishes, and will vary according to depth. This hypothesis is based on an assumption of connections between light attenuation, evolutionary trade-offs between predators and prey, and variations in food availability.
- Functional groups of deep-sea fishes can also be distinguished by auditory and vestibular abilities. Otoliths are the auditory and vestibular sense organs and otolith morphology has been found to vary with fish hearing and swimming activity. Similar to the hypothesis above, variations in food availability and predator-prey interactions are expected to drive differential adaptative trajectories in auditory and vestibular performance.
- Fishes falling into different functional groups as identified from sensory morphology, will have different life history traits. These life history traits include age, growth rates, metabolic rates and migratory behaviours.

1.5 Thesis structure and overview

This project comprises several approaches to discuss functional behaviours and life history traits and each approach has different analysis methodologies. Each hypothesis is tested in separate chapter, and thus the thesis structure is designed such that chapters 2 to 4 illustrate one application with a specific methodology, and chapter 5 integrates all the information and gives a conclusion.

- Chapter 2: Visual directions of deep-sea fish as a functional trait of feeding performance.

  The visual field is reconstructed from the density of ganglion cells on the retina, a functional tissue in the eye. The uneven distribution of ganglion cells reveals the dominant visual direction and this information is combined with fish diet preferences and trophic levels to indicate the feeding behaviour between groups.

- Chapter 3: Otolith form predicts functional groupings of deep-sea fishes.

  Otolith morphology is measured with five shape-related indices and two function-related indices. A wide range of deep-sea fish species are grouped by the otolith morphological indices and a functional difference between groups is discussed with function-related indices, diet preferences, trophic levels and sensory responses to environmental changes.

- Chapter 4: Otolith microchemistry reveals life history traits (vertical migration and metabolism) of four abundant deep-sea fishes.

  The otoliths provide a lifelong record of isotopic compositions of aragonite, and $\delta^{18}O$ and $\delta^{13}C$ values across otolith reveal the ontogenetic trend in depth and metabolic rate. Water depth and metabolic life histories for four abundant species representing different functional groups are examined in this chapter.

- Chapter 5: Synthesis

  This chapter give a systematic analysis to explain functional demands and development of fishes living in the deep. The analysis integrates the results in this thesis and information extracted from the relevant literatures. These

multiple evidences will indicate the sensory adaptation and functional compositions in the deep sea and give preliminary clues of adaptive strategies of abundant species in the extreme environment.

Chapter 2: Visual directions of deep-sea fish as a functional trait of feeding performance

2.1 Introduction

2.1.1 Visual demands in the deep

Sunlight provides the basis for visual-based acuity in most of the aquatic environment, but its prominence declines with depth because of absorption and scattering by the water (Clarke & Denton 1962):

$$\frac{I}{I_0} = e^{-kL}$$

I and I_0 are the light intensity of two depths and the L is the distance between these two depths. The vertical extinction coefficient, k, varies between water masses and locations, such as 0.46-0.15 for costal waters but 0.046 for clear oceanic regions. In the ocean, daylight no longer penetrates below 1000m and marine animals inhabiting below this depth cannot detect it. The bioluminescent source progressively replaces the role of daylight in the mesopelagic zone starting from a depth of 200m to 1000m, and dominates the visual scene in deeper water (Warrant & Locket 2004). Bioluminescent organisms occupy a wide range of habitats from the shallower layer to the deep sea floor, and include various marine phyla, from bacteria to fish (Haddock *et al.* 2010). Not only pelagic species have been found with bioluminescence (Heger *et al.* 2008; Widder 2002; Gillibrand *et al.* 2007b; S. Haddock & Case 1999), but also benthic organisms are indicated with bioluminescent events (Gillibrand *et al.* 2007a; Craig *et al.* 2011; Johnsen *et al.* 2012). Owing to the common presence of bioluminescence, fish still rely on vision for many purposes in the dark ocean, such as orientation, searching for prey, detecting predators, finding mates and recognizing items (Warrant & Locket 2004; Haddock *et al.* 2010). Furthermore, several adaptive evidences support the importance of vision in the deep sea. For example, a well-developed and dominant visual perception area in the brain has been found from numerous deep-sea fishes (Wagner 2001a, 2001b). Deep-sea fish develop specialized eye structures for receiving dim light (Partridge *et al*. 2014; Wagner *et al*. 1998) and have diverse retinal designs for specific visual behaviours (Douglas *et al.* 1998; Wagner *et al.* 1998).

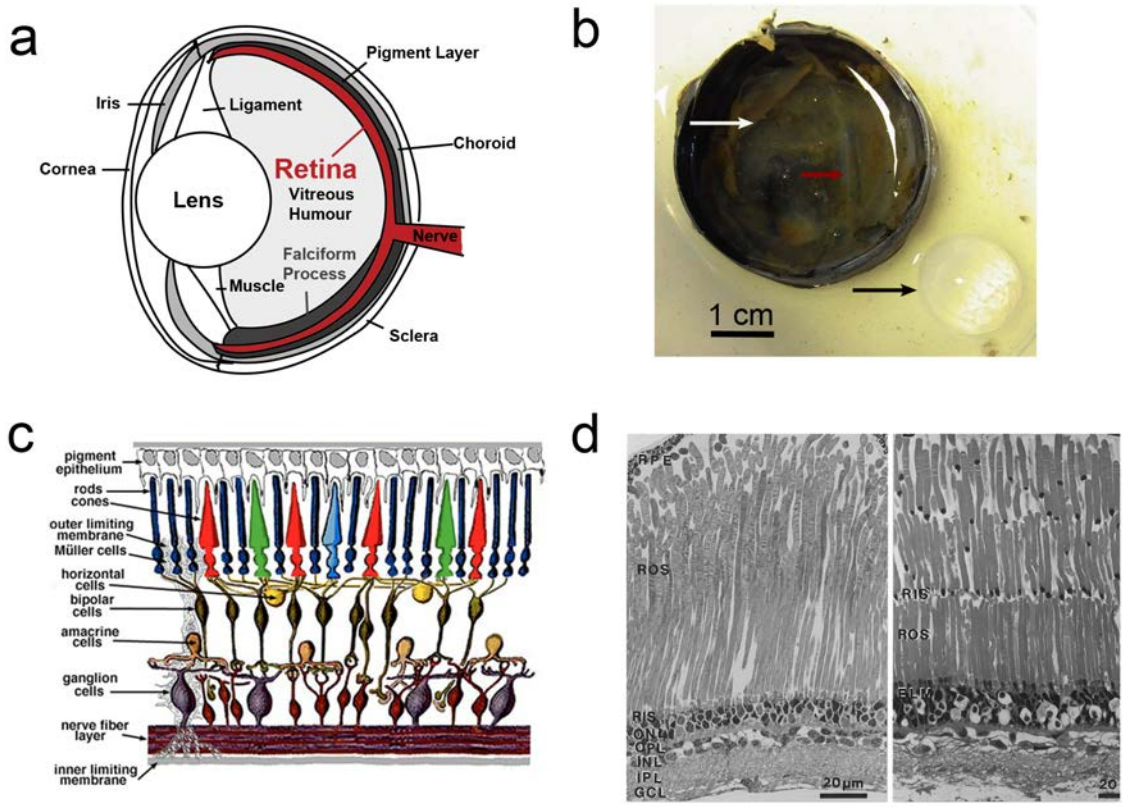

Figure 2.1. The structure of the eye and the retina in deep-sea fish. (a) The profile of fish eyeball. (b) An example of fish eyeball profiles from *Aphanopus carbo*. The black, white and red arrows indicate the lens, the retina and the falciform process, respectively. (c) The cutting section of retinae that optic information is received from photoreceptors and transmitted to ganglion cells (Webvision: webvision.med.utah.edu). (d) Two examples of specialised retinal cells in deep-sea fishes (Wagner *et al*. 1998). Elongated photoreceptors (left) or multiple banks of photoreceptor layers (right) are found in fish species, *Xenodermichthys copei* and *Notacanthus chemnitzii*, respectively.

Fish eye structures and the position of retina are shown in Figure 2.1. Light enters the eyeball, is refracted by the lens, goes through the vitreous humor and then reaches the retinal tissue (Fig. 2.1a). The retina is the only tissue dealing with light signals in the eye and it is composed of minor layers with different functional neurons. Photoreceptors as rods and cones in the first layer receive light stimuli, and transfer the signals to ganglion cells via bipolar cells (Fig. 2.1c). Ganglion cells (GCs) in the final layer of retina integrate visual information and relay signals to the central nerve system. This is a general pathway of signal transduction. However, in order to detect less

signals in the dim environment, deep-sea fish develop rod-pure retinae to enhance the sensitivity of light rather than colour information (Locket 1977). Moreover, some species have a long rod inter and outer segment (RIOS) (*Xenodermichthys copei*) or multiple banks of RIOSs (*Notacanthus chemnitzii*), and these adaptive changes reflect the selective pressure of light intensity (Wagner *et al.* 1998) (Fig. 2.1d).

The distribution pattern of GCs across the retina provides information of fish visual behaviours (Bozzano & Catalán 2002; Wagner *et al.* 1998; Collin & Partridge 1996; Fritsches *et al.* 2003; Collin & Shand 2003; Bozzano 2004). Two general patterns of the GCs' distribution in deep-sea fishes are given by Wagner *et al.* (1998) (Fig. 2.2). A large group of pelagic deep-sea fishes has a uniform distribution (the first pattern), which shows a peripheral increase of the GCs density. This pattern enables fish to sensitively detect objects entering or leaving the lateral field. Latternfish is a typical example with the uniform cell distribution. In contrast, the area centralis, as the second pattern, with one or multiple high-density centres in the retina is observed for various species, including pelagic and demersal fish. Uneven distribution of GCs shows the directional visual acuity, where GCs concentrate on the area (peak density area) of main visual direction. For example, scavenging behaviour is supported by increased cell density in the dorsal retinal field in *Synaphobranchus kaupii*, enabling searching downward for food falls (Fig. 2.2c). Furthermore, the visual direction is also related to the head or eye morphology, lifestyle and so on. Tubular eyes are usually associated with ventral GCs peaks on the retina providing a dorsal visual field (Fig. 2.2d).

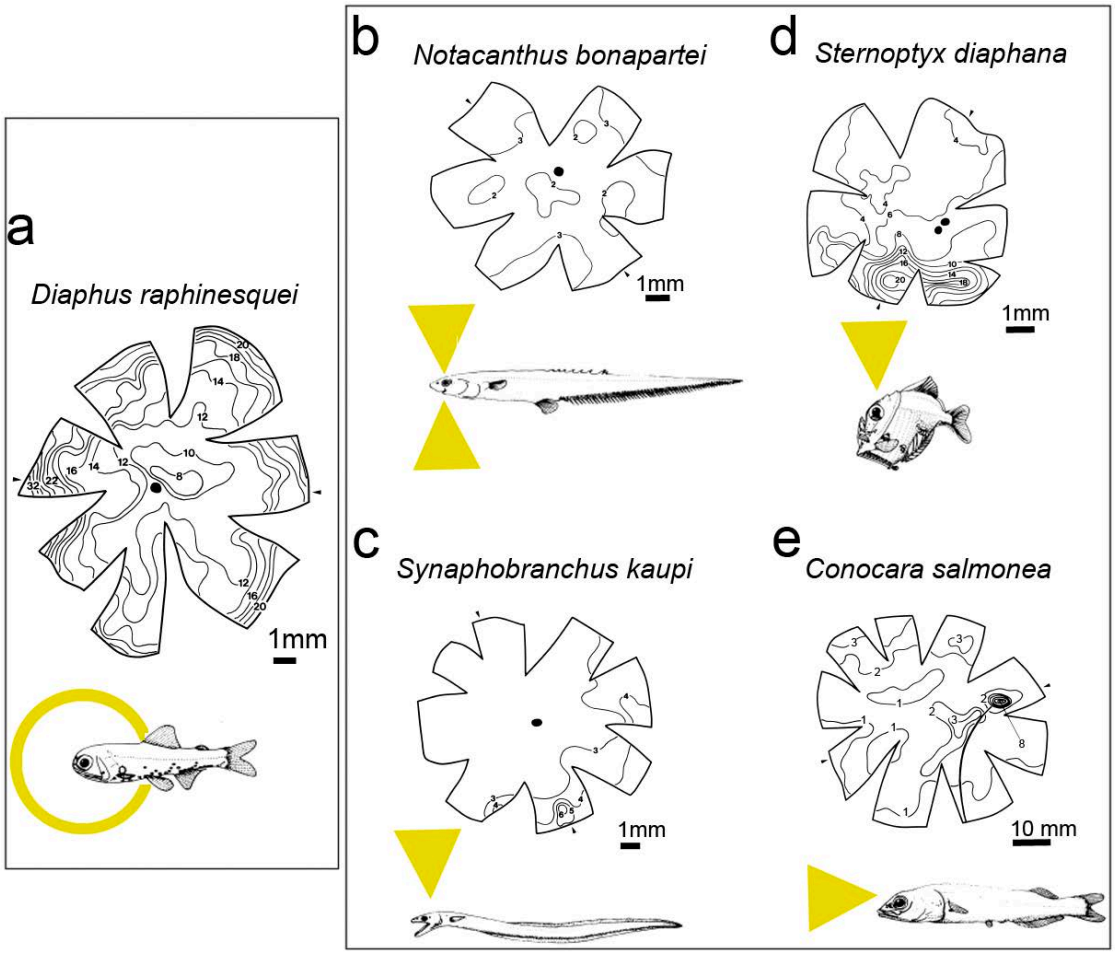

Figure 2.2. Types of retinal topography in deep-sea fishes. The figure is revised and summarized from Wagner *et al.* (1998) that show two types of retinal designs. The first one is an unspecialised retina, revealing a peripheral increase of GCs density (a). The second type is a specialised retina with single (c-e) or multiple peaks of GCs density (b). The position of GCs peak determines the visual direction of fish; for example, *Synaphobranchus kaupi* has GCs density peak at the ventral end on the retina, indicating the importance of dorsal view (see text). Two modified structures as tubular eyes (d, found in hatchet fishes) or foveae on the retinae (e, extremely high GCs density on the retinae for sharp visual acuity that is usually found in Alepocephalidae fishes) are all included in the second type.

2.1.2 Visual capability of deep-sea fish

As mentioned above, the adaptive changes of photoreceptors enhance visual sensitivity in the dark environment. According to de Busserolles *et al.* (2014, and

citations therein), two equations of visual sensitivities to sunlight and bioluminescence are given:

$$S\ (sensitivity\ to\ downward\ light) = \left(\frac{\pi}{4}\right)^2 A^2 \left(\frac{d}{f}\right)^2 \left(1 - e^{-kl}\right)$$

$$N\ (senstivity\ to\ bioluminensence) = \frac{EA^2}{16r^2} e^{-\alpha r}\left(1 - e^{-kl}\right)$$

A is the diameter of the pupil and E is the number of photons emitted from the bioluminescent sources. The photoreceptor related factors, *d*, *k* and *l*, represent the diameter, outer segment length and absorption coefficient, respectively. Other terms in the equations have meanings as follows: *f* is the focal length of the eye (2.55*radius of lens), *r* is the distance between the eye and the bioluminescent source and α is the attenuation coefficient of bioluminescence. While the length of rod outer segment (i.e. long or multiple banks of RIOS) increases, deep-sea fish have higher sensitivity for both sunlight and bioluminescence.

Not only sensitivity, but also spatial resolution of visual information is important in the deep sea. As point-like bioluminescence gradually replaces the space light with depths, fish need a better spatial resolving power. The spatial resolution of deep-sea fish sharply increases above 1000m and the variation across species reduces in the deeper water (Warrant 2000). Fish inhabiting in the mesopelagic zone may develop as different functional groups, such as sunlight-dependent species, bioluminescence-dependent species or mixed-lifestyle species.

2.1.3 Aim

GCs distribution patterns give clues to differentiate fish between feeding types and habitats, and this study tests the hypothesis of determining functional groups from directional visual acuity in deep-sea fish. In addition, the visual capacity between functional groups is examined according to the density of GCs. Second, pronounced depth-related environmental gradients (light intensity and sources) exist in the deep-sea environment, and therefore the depth-related trend of visual capacity among functional groups is further investigated.

2.2 Materials and Methods

Fish samples were collected from the Irish continental slope and the Rosemary Bank (Fig. 2.3), based on the 2012 deep-water survey undertaken by Marine Scotland-

Science. The collections using bottom trawl ranged from 500m to 2030m in depth. Fish were caught, wet body mass and length were recorded, and paired eyeballs were removed from the orbits, marked at the dorsal end with a pin and stored in a freezer. 22 species were examined as part of this study (Table 2.1). Ideally, fish samples should be mature individuals to avoid ontogenetic changes influencing the visual directions. However, little information about maturity is known owing to the limited research into the reproductive biology of many deep-sea fishes. Thus samples were chosen of individual in the top 50 percentile of sizes known from sampling. However, four species (*Coryphaenoides guentheri*, *C. rupestris*, *Molva dypterygia* and *Nezumia aequalis*) were under the criterion because eyes from the biggest individuals were used in pilot work to determine methodologies.

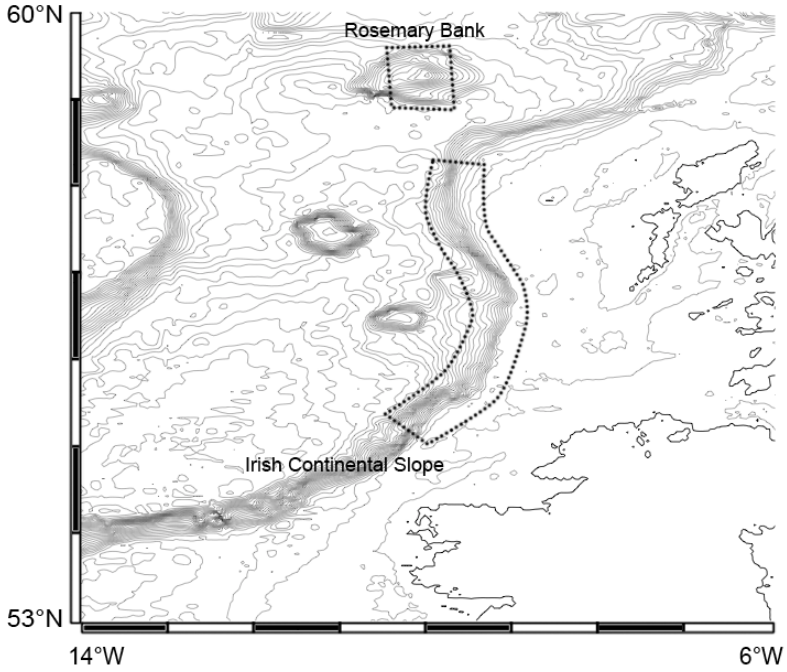

Figure 2.3. Sampling location in the Northeast Atlantic.

Table 2.1. Information of samples. TL: total length; PAFL: pre-anal fin length; SL: standard length.

Order	Family	Species	Length (cm)	Length quality	Weight (g)
Aulopiformes	Bathysauridae	*Bathysaurus ferox*	48	TL	485
Beryciformes	Trachichthyidae	*Hoplostethus atlanticus*	63	TL	NA
Gadiformes	Gadidae	*Micromesistius poutassou*	37	TL	340
	Lotidae	*Molva dypterygia*	94	TL	2754
	Macrouridae	*Coryphaenoides guentheri*	10	PAFL	118
		Coryphaenoides mediterranea	20	PAFL	1550
		Coryphaenoides rupestris	16	PAFL	900
		Nezumia aequalis	5	PAFL	39.7
		Trachyrincus murrayi	NA	PAFL	267
	Moridae	*Antimora rostrata*	60	TL	2146
		Halargyreus johnsonii	27	TL	113
		Lepidion eques	27	TL	148
		Mora moro	54	TL	1408
	Phycidae	*Phycis blennoides*	52	TL	1095
Notacanthiformes	Halosauridae	*Halosauropsis macrochir*	69	TL	318
Ophidiiformes	Ophidiidae	*Spectrunculus grandis*	48	TL	658
Osmeriformes	Alepocephalidae	*Alepocephalus agassizi*	64	SL	2090
		Alepocephalus bairdii	68	SL	3662
	Argentinidae	*Argentina silus*	43	TL	596
Perciformes	Epigonidae	*Epigonus telescopus*	46	TL	1296
	Trichiuridae	*Aphanopus carbo*	99	TL	1250
Scorpaeniformes	Sebastidae	*Helicolenus dactylopterus*	26	TL	312

2.2.1 Retinal whole mounting

The cornea was removed from the defrosted eyeball, and then the lens was removed leaving a cup-like hollow structure. In addition to the artificial location mark (pin) placed at the dorsal end of the eyeball, sometimes the biological landmarks on the retina, such as the falciform process (Fig. 2.1b), also helped identify the orientation. Following a well-established protocol of retinal whole mounting from Ullmann *et al.* (2012), the retina was chemically fixed before it was extracted from the eyecup. The eyecup was immersed in a fixation solution (4% paraformaldehyde in 0.1M phosphate buffer - the phosphate buffer at pH 7.4 was made from two stock solutions, 0.2M

monobasic sodium phosphate and dibasic sodium phosphate, in a ratio of 19:81) for two hours. The fixation time was extended for large-sized retinae up to four hours. The fixed eyecup was then washed three times with a 0.1M phosphate buffer for one minute. After the fixation, the adherent tissues (vitreous humour) and the sclera were gently peeled and cut away from the retina. The retinal pigment epithelium (RPE), a layer of tissue with dark colour, will impede the staining of ganglion cells, therefore a physical cleaning with a pen brush and a scalpel was conducted to remove the RPE. Owing to difficulties of cleaning the RPE completely, the extracted retina was immersed in a bleaching solution (a mixture of 90 ml of 0.1 M phosphate buffer, 10 ml of 30% hydrogen peroxide and 80 ml of 1.0 M potassium hydroxide) until the retina was clear, and rinsed in 0.1M phosphate buffers.

The clean retina was placed inner side-up on a gelatinised glass slide, which was prepared in advance by dipping clean glass slides into a gelatin solution and oven drying at 37°C overnight. Radial cuts were made on the periphery of the retina to release any stress from curling. In addition, the soaking up of redundant buffer liquid strengthened the adhesion of the retinae on the slide. The retina was recoded as the original size before drying.

The dried retina was stained with cresyl violet, following the protocol in Table 2.2 (Ullmann *et al.* 2012) and sealed by the mounting media and the cover slip.

Table 2.2. Staining protocol. [1]A mixture of 0.4g of cresyl violet, 10ml of glacial acetic acid, 10ml of 1.0M sodium acetate and 380ml of distilled water. [2]A mixture of 900ml of 95% ethanol and 1ml glacial acid.

Stage	Treatment	Time
1	Histoclear	10 min
2	Histoclear	10 min
3	100% ethanol	2 min
4	100% ethanol	2 min
5	90% ethanol	2 min
6	70% ethanol	2 min
7	20% ethanol	2 min
8	Distilled water	2 min
9	0.1% cresyl violet[1]	20 min
10	Distilled water	Quick rinse
11	100% ethanol	30 s
12	100% ethanol	30 s
13	100% ethanol	30 s
14	Differentiation solution[2]	1 min
15	100% ethanol	1 min
16	100% ethanol	1 min
17	Histoclear	2 min
18	Histoclear	2 min

2.2.2 Ganglion cell counting

Around 200 counting areas were evenly selected on each retina and photographed under a stereomicroscope using a Nikon SMZ800 equipped with a Qimaging MicroPublisher RTV 5.0 digital camera. The cells were counted from images with "*Cell Counter*" functions in ImageJ (developed by the U.S. National Institute of Health). The size of the counting area was controlled in a grid of 0.01mm^2 (Fig. 2.4), but the GCs density in the topography map was transformed to cells per 1mm^2 and calibrated with the shrinkage of retina after drying and staining:

$$\text{GCs density}\left(\frac{\text{cells}}{\text{mm}^2}\right) = \frac{\text{GCs(cells)}}{0.01(\text{mm}^2)} \times 100 \times \text{SR}$$

$$\text{Shrinkage rate (SR)} = \frac{\text{A}'(\text{mm}^2)}{\text{A}(\text{mm}^2)} \times 100\%$$

A and A' are the area of original and stained retina, respectively. The topography of GCs density was made according to around 200 counting grids with calibrated density values.

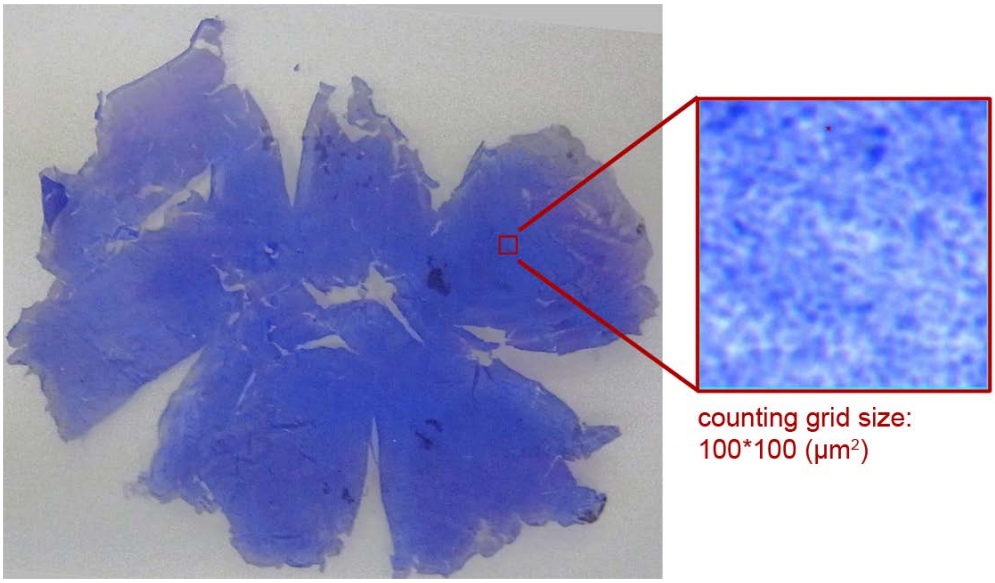

Figure 2.4. Stained retina, GCs image and counting grid size.

2.2.3 Fish's primary visual direction revealed by stereographic projection

It is hard to establish the specific visual angle from a flattened retina due to the presence of cuts and slits generated during the process of wholemounting. Thus, we (1) reconstructed the three-dimensional structure of the retina and (2) displayed the 3D information on a 2D plane according using stereographic projection.

The retina in the eyeball was assumed as a perfect sphere to facilitate the reconstruction of 3D structures. Two types of visual angles were defined during the reconstruction: (1) the lateral visual angle (*l-angle*); (2) the frontal plane angle (z-*angle*) (Fig. 2.5). Following the outline of retina, a circle was made (called the MaxCircle) to determine the centre and the diameter of the retina (Fig. 2.5a). For this project, this was conducted through a "*Fit Circle*" function in ImageJ. Using the same centre as the MaxCircle, minor circles were made (called the circle') across each GCs peak area/point of GCs density (Fig. 2.5a). The dorsal end of the retina was set as 0°/360°, and the lateral visual angle (*l-angle*) was calculated with the following equation (Fig. 2.5b):

$$l - angle = \left(X - Angle_{splits}\right) \times \frac{360}{360 - Angle_{SPLITS}}$$

X is the angle from the dorsal end to the peak area. $Angle_{splits}$ is the sum of angles of splits between the dorsal end and the peak area, and $Angle_{SPLITS}$ is the sum of angles of all splits on the circle' (an additional explanation can be found in Fig. 2.5). This process considered the proportion of splits existing in the retina and back-calculates the real angle (*l-angle*) of each peak area.

If the lateral visual angle is 90° or 150°, another angle is observed as varying on the frontal plane (of the fish body) (Fig. 2.5c). As the sagittal plane of the fish body is set as an x-y plane, this angle always changes along the z-axis, and therefore the angle is called *z-angle* in this study. The edge of the MaxCircle was defined as 0° for the *z-angle* and the centre as the maxima of 90°. The z-angle was calculated through the proportion of the radius of the MaxCircle and 'the circle' (Fig. 2.5c):

$$z - angle = 90 - 90 \times \frac{r}{R}$$

The r and R represent the radius of 'the circle' and the MaxCircle, respectively.

Among approximately 200 counting areas in each retina, the ones with a density value above the 95th percentile were chosen for examination of the main visual direction. The values of two defined angles, *l-angle* and *z-angle*, in each peak area were plotted on a 2D circular grid by using a stereographic projection program, Stereonet 9 (Allmendinger 2011). The stereographic projection projects a plane/line onto the sphere into a line/dot on the circular grid (Fig. 2.6).

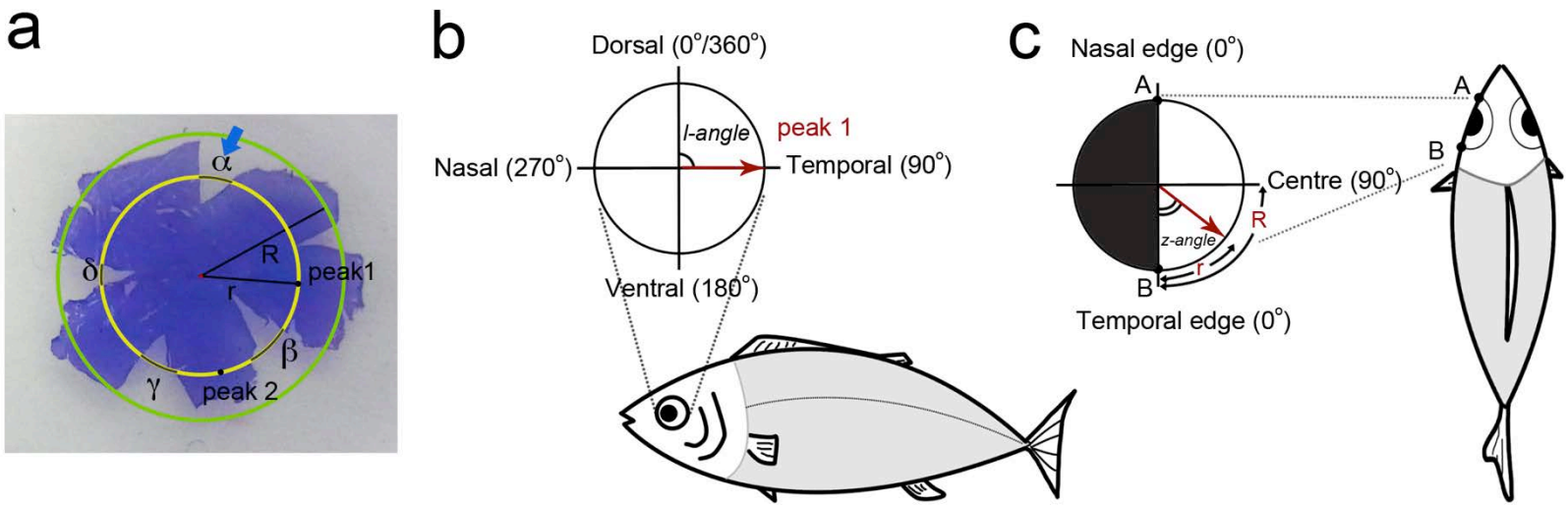

Figure 2.5. Calculation of three-dimensional information from the flattened retina. (a) The green and yellow circle are the MaxCircle and circle', and the radius of two circles are R and r, respectively. The blue arrow is the dorsal mark set as 0°/360°. As this example, the circle' is drawn across two peaks of GCs density. Following the content, X value is the angle measured from the dorsal mark to the peak (peak 1 or peak 2). $Angle_{SPLITS}$ is calculated as α+β+γ+δ, and $Angle_{splits}$ is α for peak 1 and α+β for peak 2. (b) The *l-angle* (of peak 1) is shown on the reconstructed 3D retina as a view of the sagittal plane of fish body. (c) The *z-angle* (of peak 1) is shown on the reconstructed 3D retina as a view of the frontal plane of fish body.

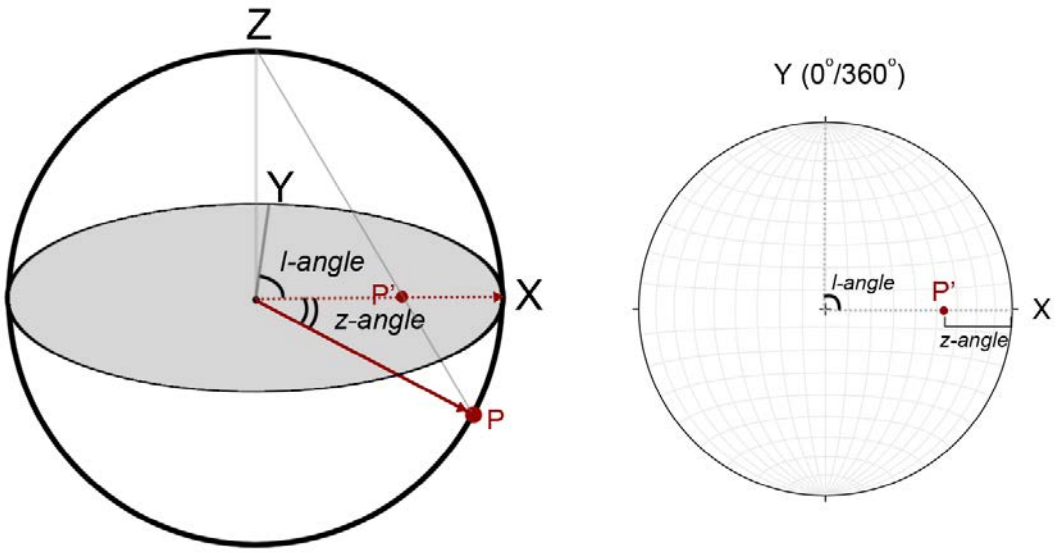

Figure 2.6. Schematic diagram of 3D information plotted on the 2D circular grid.

2.2.4 Spatial resolution

The spatial resolving power was calculated using equations below (Collin & Pettigrew 1989; Ullmann *et al*. 2012) (Fig. 2.7):

$$PND = 2.55 \times r$$

r is the radius of the lens, which was measured with fresh material by calipers instead of measuring the frozen lens section. It avoids shrinkage of the lens influencing on the measurement. PND is the distance from the centre of a lens to the retina and. Owing to the difficulty of precise measurement, the PND was deduced by the equation shown above, following the methodology in Ullmann *et al* (2012). The number of 2.55 is Matthiessen's ratio for the teleost.

$$\tan \alpha = \frac{1mm}{PND}$$

$$cells\ per\ degree = \frac{\sqrt{peak\ density\ of\ GCs}}{angle\ of\ PND\ (\alpha)}$$

$$cycles\ per\ degree = \frac{cells\ per\ degree}{2}$$

The two cells for disguising light and dark boundaries are combined to complete one cycle grating of the highest resolvable frequency, hence cells per degree are divided by

2. Following the discussion in Warrant (2000), the spatial resolving power was also represented in a unit of angular measurement (as a minute of arc or arcmin) (Fig. 2.7).

$$Spatial\ resolving\ power\ (arcmin) = \frac{\tan^{-1}\frac{1}{PND}\times 3437.7}{\sqrt{peak\ density\ of\ GCs}}\times 2$$

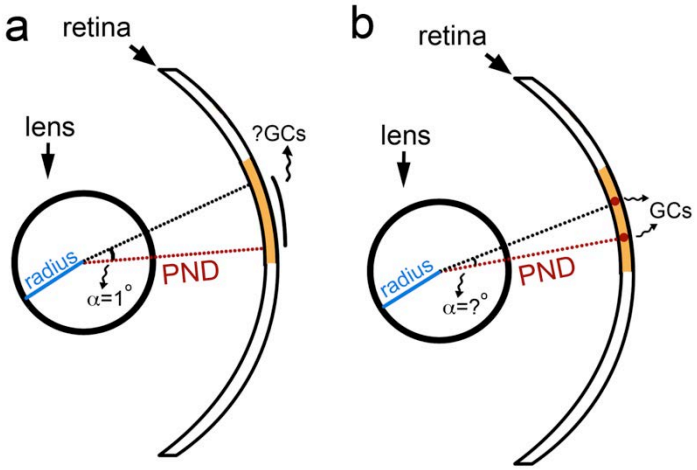

Figure 2.7. Calculations of spatial resolving power by two different units: (a) cells per degree (how many GCs are present across in one degree of retinal surface); (b) arcmin (what the average angular distance between two GCs in the peak area is). PND equals to 2.55*radius of lens. The yellow band is the area of GCs peak density.

2.2.5 Ecological trend

To investigate the ecological trend of visual capability among deep-sea fish, the information of ganglion cell density and the spatial resolution from 35 deep-sea fish species in Wagner *et al*. (1998), 1 species (*Merluccius merluccius*) in Bozzano & Catalán (2002) and 22 species in this study were assimilated (Appendix A). The depth of fish occurrence and categories of fish habitat were extracted from Neat & Campbell (2013) and FishBase (Froese & Pauly, 2013). The occurrence was generally reported as a whole depth range, but the mean value was utilized for each species.

2.2.6 Statistical analyses

The comparison of GCs peak density and spatial resolving power between functional groups (defined by visual fields) was conducted by one-way ANOVA in statistical programme R (R Development Core Team 2012). In addition, two-way

ANOVA tested influences of both habitat depths and functional groups on two visual performance indices (the GCs peak density and the spatial resolving power).

2.3 Results

The visual fields of 22 species, collected in this study, generally corresponded to their assumed feeding behaviours, according to stomach diet analyses in the literature, in that benthic feeders had dorsal/ventral visual fields and pelagic feeders had temporal/nasal visual fields (Table 2.3). The visual fields were defined by the distribution of the GCs, based on both topography (Fig. 2.12) and stereographic projection (Fig. 2.13). We considered the distributions of 95th percentile density peaks and then compared the whole general patterns to determine dorsal/ventral and temporal/nasal visual fields. To expand comparisons, 58 deep-sea fishes in the assimilated data (from literatures and this study) were further defined by habitat categories and visual fields as 6 functional groups, which were species with tubular eyes (TE), species with peripheral fields (P), pelagic species with temporal/nasal fields (PTN), pelagic species with dorsal/ventral fields (PDV), demersal species with temporal/nasal fields (DTN) and demersal species with dorsal/ventral fields (DDV). The retina position in the tubular eyes was different from lateral eyes, demanding a separate category for these species. Moreover, the species with tubular eyes and peripheral fields were all observed as living in the pelagic zone.

Functional groups differed in peak density of GCs and spatial resolving power (ANOVA, GCs peak density: $n=58$, $df=5$, $F=9.418$, $p<0.01$; spatial resolving power, cells per degree: $n=36$, $df=5$, $F=11.27$, $p<0.01$; arcmin: $n=34$, $df=5$, $F=8.621$, $p<0.01$). Group TE showed the highest GCs peak density, but Group DTN and PDV had better spatial resolution than other groups (Fig. 2.8). The differences were not only influenced by functional behaviours but also by depth effects (Table 2.4). The GCs peak density sharply decreased with depths till 1000-1500m and slightly increased below this depth range (Fig. 2.9). Compared to GCs density, a totally inverse trend was observed from the spatial resolving power (Fig. 2.9).

A transition between functional groups with depth was observed from pelagic fish: Above 1000m, pelagic fish species mainly have tubular eyes and peripheral field vision, but this visual style is replaced by temporal/nasal visual fields at depths >1000m (Fig. 2.10). This group transition explained the significant depth-related decrease of GCs and the increase of spatial power resolution in pelagic fish. However, the depth effect on group transition and visual capacity was less obvious on demersal fish groups.

In order to test the relationships between trophic levels and visual field functional groups, muscle $\delta^{15}N$ and $\delta^{13}C$ values of 26 deep-sea fish species (Appendix A, data described in Trueman et al. 2014) were analysed. $\delta^{15}N$ values showed no significant difference between the five functional groups (n=26, df=4, F=2.69, p=0.0592), but a slightly lower value was observed from the Group P and PTN (Fig. 2.11). In contrast, a significant difference of muscle $\delta^{13}C$ values between groups was observed (n=26, df=4, F=3.98, p=0.0148) and the Group P and PTN have the lowest muscle $\delta^{13}C$ values. Lower muscle $\delta^{15}N$ and $\delta^{13}C$ values are therefore associated fish species preying on more pelagic diets.

Table 2.3. Visual directions in relation to diet preferences in 22 deep-sea demersal fishes. [1] Mauchline & Gordon (1984b); [2] Mauchline & Gordon (1983); [3] Whitehead *et al*. (1984); [4] Whitehead *et al*. (1986); [5] Sulak *et al*. (1985); [6] Mauchline & Gordon (1984c); [7] Bergstad (1991); [8] Mauchline & Gordon (1987); [9] Mauchline & Gordon (1984a); [10] Carrassón *et al*. (1997); [11] Morte *et al* (2002).

Visual direction	Feeding behaviour	Primary dietary items
Peripheral field	Pelagic feeder	*Halargyreus johnsonii*: copepods and mysids[1]
Temporal and nasal visual fields	Benthopelagic feeder	*Argentina silus*: salps and ctenophores[2]
		Alepocephalus agassizi: ctenophores, crustaceans, echinoderms and polychaetes[3]
	Active forager	*Alepocephalus bairdii*: medusa, mysids, decapods, squid and fish[2]
		Aphanopus carbo: fish, cephalopods and crustaceans[4]
	Generalist feeder	*Bathysaurus ferox: fish*[5]
		Epigonus telescopus: copepods, mysids and decapods[6]
		Helicolenus dactylopterus: widely feed on pelagic and benthic organisms[4]
		Micromesistius poutassou: euphausiids[1]
		Molva dypterygia: fish and crustaceans[7]
Dorsal and ventral visual fields	Benthic feeder	*Antimora rostrata*: fish, cephalopods and crustaceans[7]
		Halosauropsis macrochir : amphipods, mysids and decapods[8]
	Passive feeder	*Hoplostethus atlanticus*: decapods, mysids, squids and fish[6]
		Coryphaenoides guentheri: copepods, amphipods and mysids[6]
		Coryphaenoides mediterranea: copepods, amphipods and mysids[9]
		Coryphaenoides rupestris: copepods[9]
		Lepidion eques: amphipods and decapods[1]
		Mora moro: decapods, cephalopods and fish[10]
		Phycis blennoides: decapods, mysids and fish[11]
		Spectrunculus grandis: echinoderms and amphipods[6]
		Nezumia aequalis: copepods, mysids, polychaetes, isopods and decapods[9]
		Trachyrincus murrayi: decapods, copepods, amphipods and polychaetes[9]

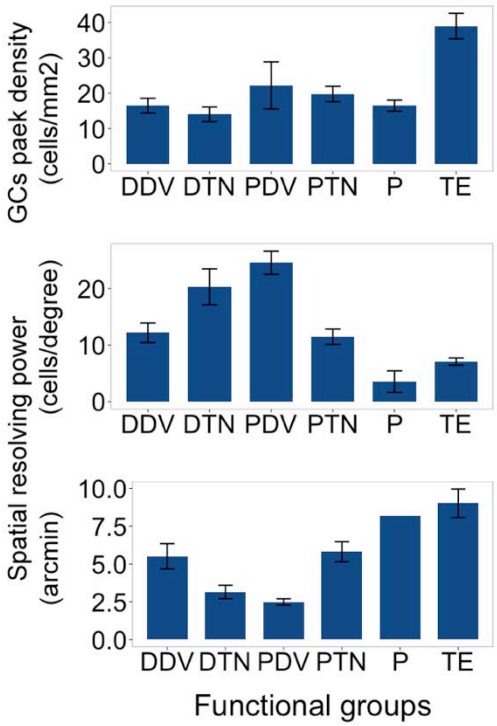

Figure 2.8. Visual capabilities between functional groups. The error bar represents the standard error.

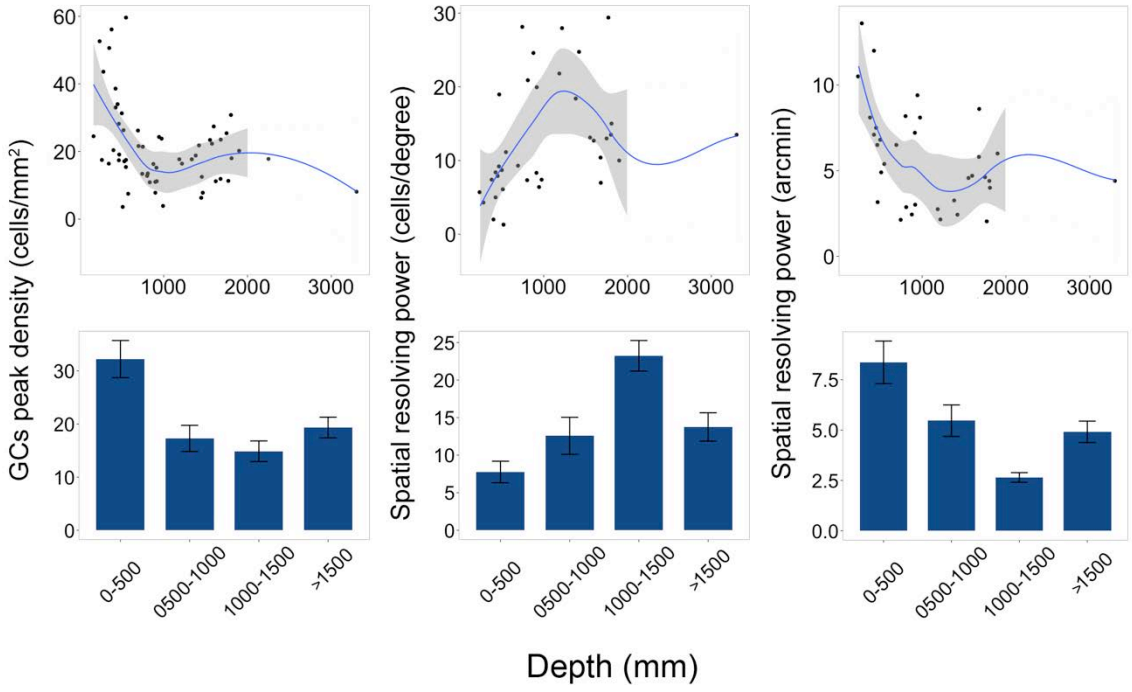

Figure 2.9. Visual capabilities with depth gradients. The smooth line in the dot plot is calculated by the local polynomial regression fitting method and grey area is 95% confidence interval. The error bar in the bar chart represents the standard error.

Table 2.4. Two-way ANOVA: depth effects and group influences on visual capabilities of deep-sea fishes.

Model:

GCs peak density~ depth*functional groups

	Df	Sum Sq	Mean Sq	F value	Pr(>F)
Depth	1	1146	1146	17.1	<0.01
Functional groups	5	3126	625	9.31	<0.01
Depth:Functional groups	5	1344	269	4.00	<0.01
Residuals	46	3090	67.2		

Model:

Spatial resolving power (cells per degree)~ depth*functional groups

	Df	Sum Sq	Mean Sq	F value	Pr(>F)
Depth	1	223	223	8.46	<0.01
Functional groups	5	1160	232	8.79	<0.01
Depth:Functional groups	5	40.7	8.14	0.308	0.903
Residuals	24	633	26.4		

Model:

Spatial resolving power (arcmin)~ depth*functional groups

	Df	Sum Sq	Mean Sq	F value	Pr(>F)
Depth	1	47.5	47.5	13.5	<0.01
Functional groups	5	130	26	7.39	<0.01
Depth:Functional groups	4	23.5	5.86	1.67	0.192
Residuals	23	80.9	3.52		

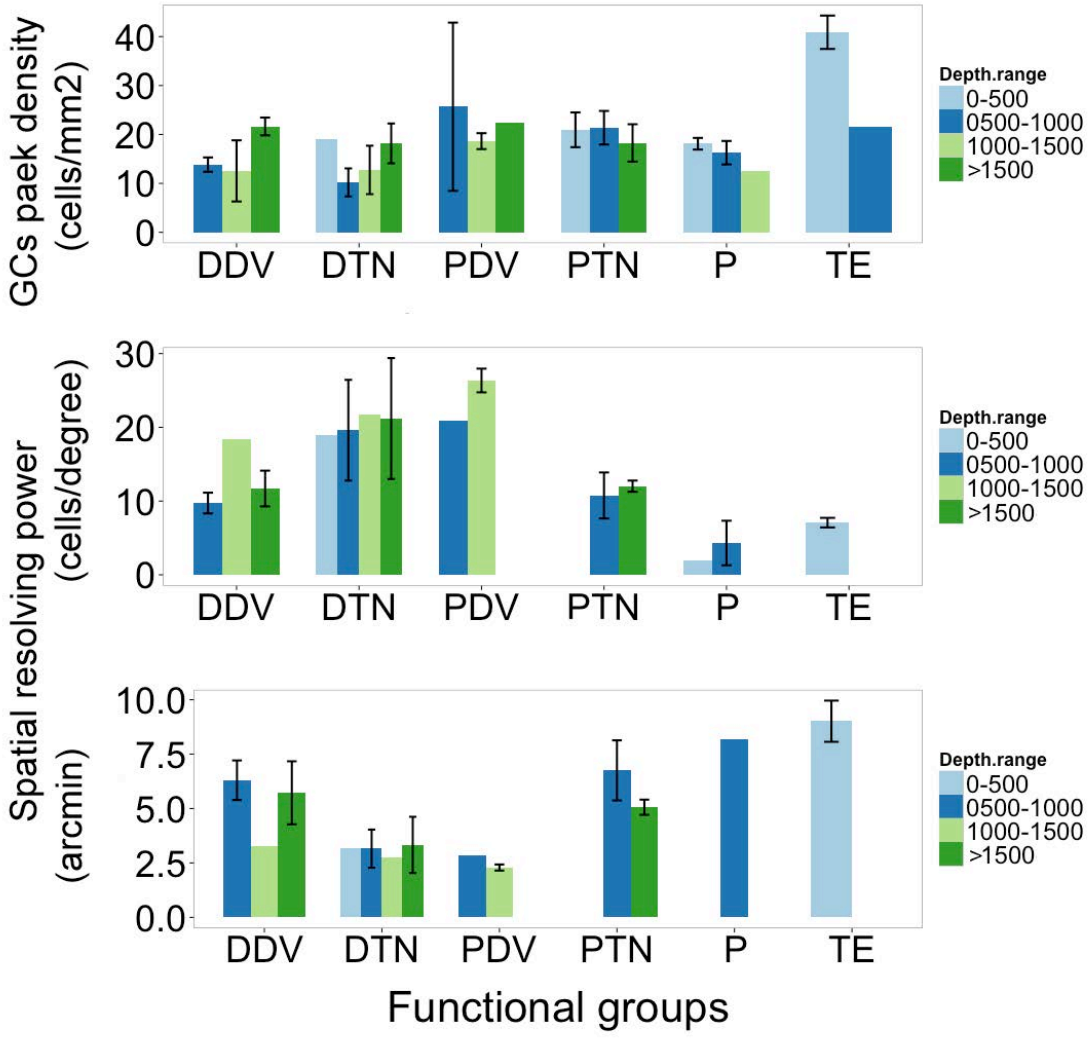

Figure 2.10. Visual capability between functional groups and depths. The error bar represents the standard error.

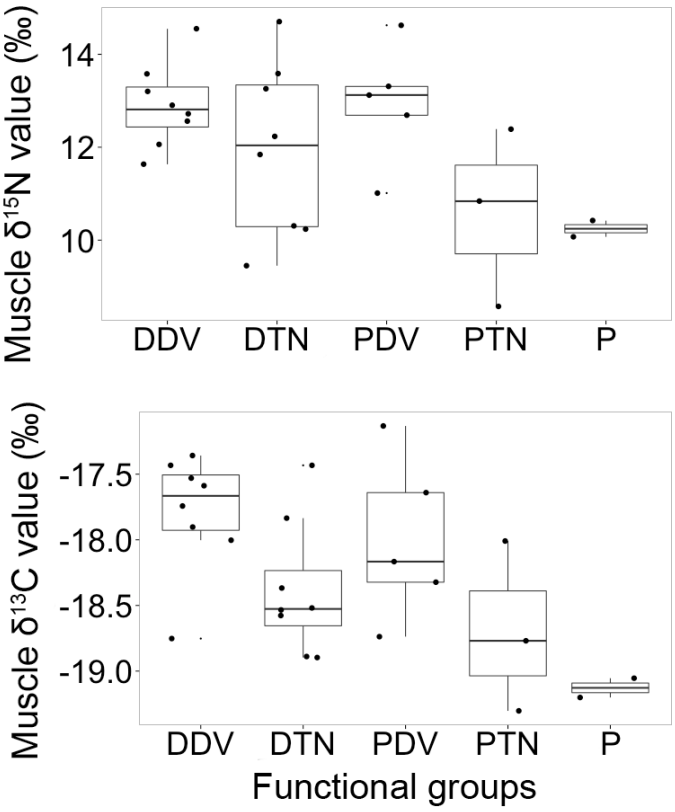

Figure 2.11. Stable isotope signals (in muscle) between functional groups. Each dot represents the species average.

2.4 Discussion

Even in the dim environment of the deep sea, fishes have a reliable visual ability and a well developed optical tectum in their brain sensory area to support them in receiving light signals (Wagner 2001a; Wagner 2001b). Visual perception is used for many purposes, such as offenses, defences and attracting mates. In the present study, the visual field of deep-sea demersal fish is described in the context of foraging ecology, and according to both functional trait and taxonomic classifications. The topography of the GCs density and the stereographic projections are shown in Fig. 2.12 and Fig. 2.13, respectively.

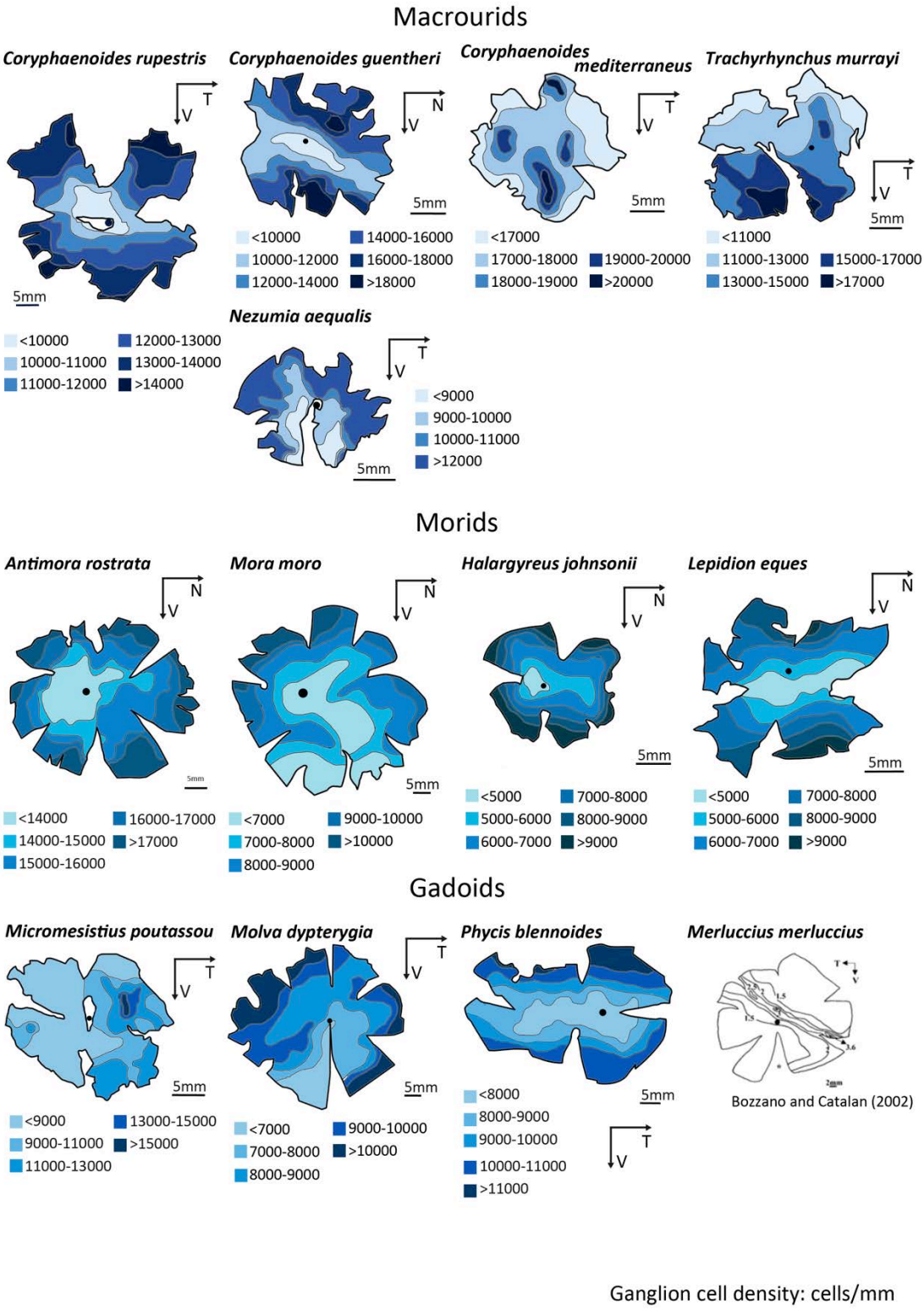

Figure 2.12. Topography of GCs density in 29 species (22 species in this study and 7 species from literatures). The abbreviations of directions represent nasal (N), temporal (T), dorsal (D) and ventral (V).

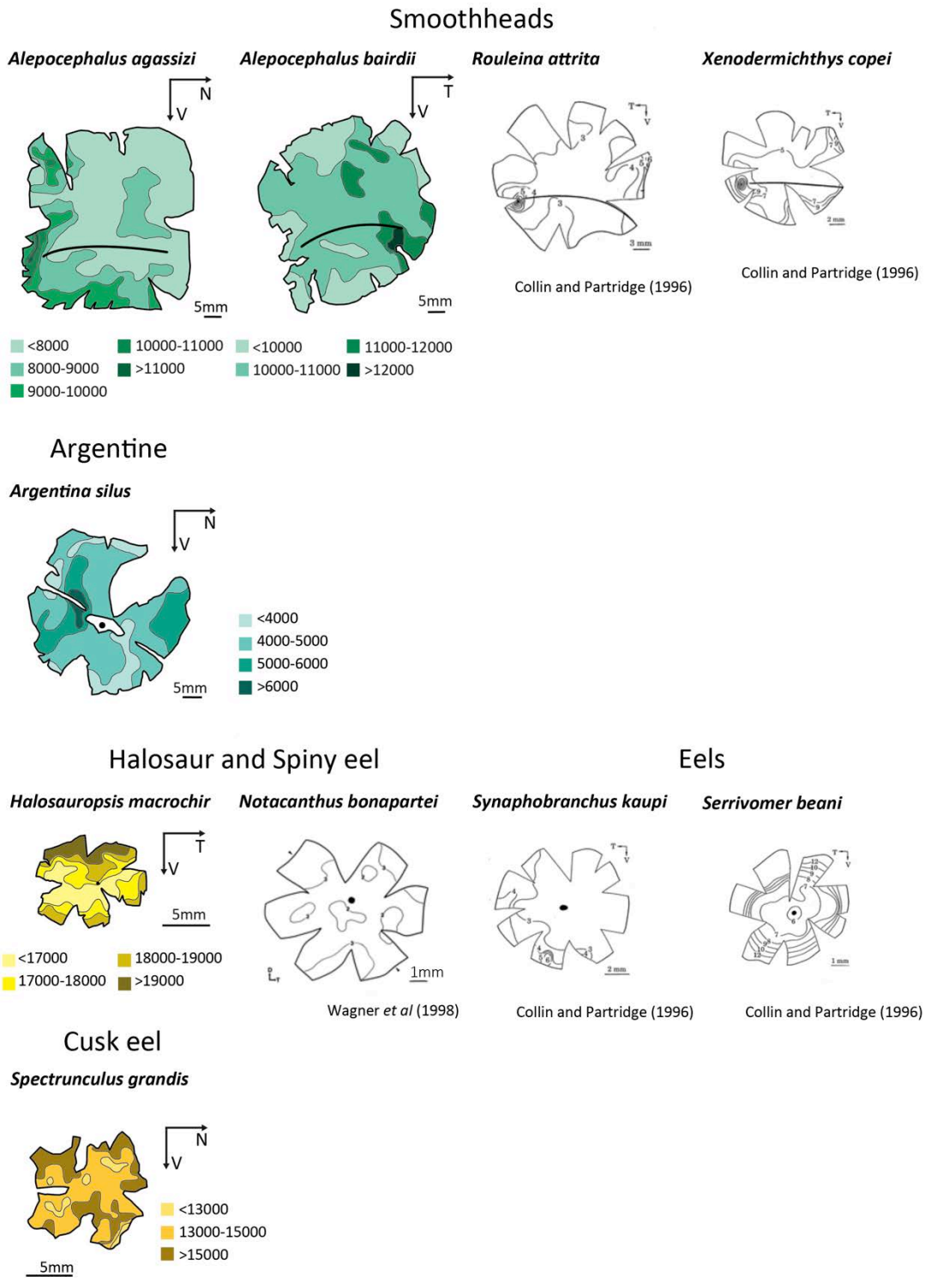

Figure 2.12 (continued).

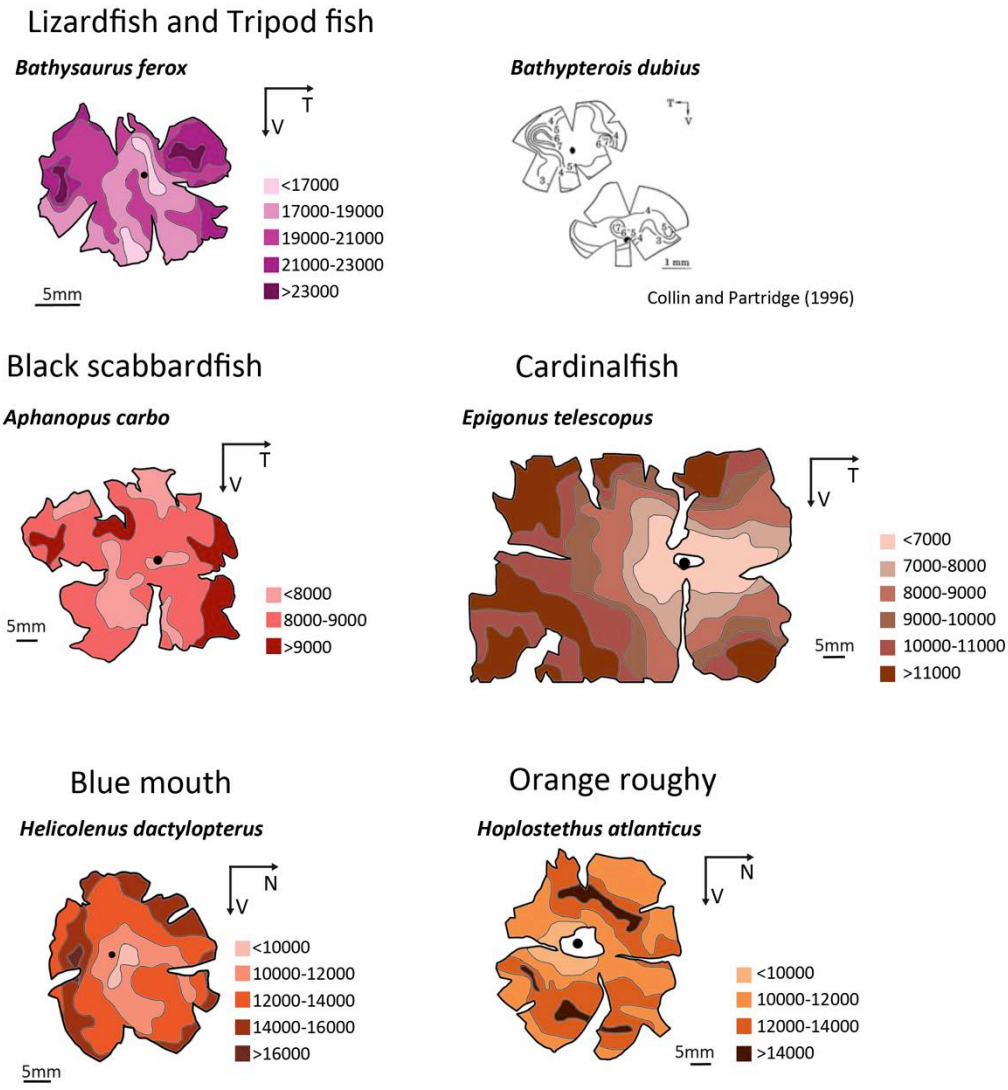

Figure 2.12 (continued).

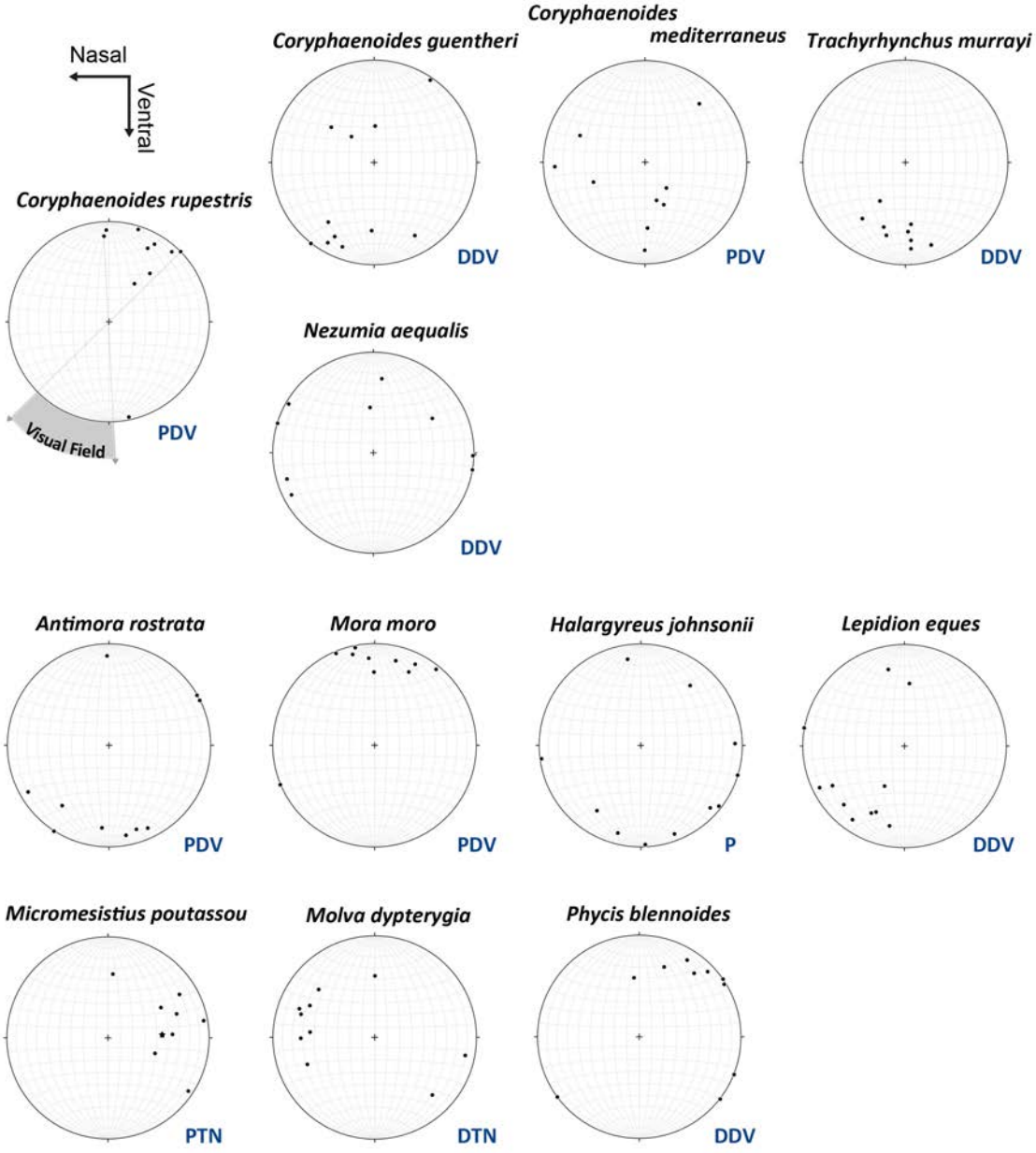

Figure 2.13. Stereographic projections of GCs density peaks (95th percentile). The smaller projection in *S. grandis* is based on the density values above 90th percentile. The assigned functional groups in each species are next to the stereographic projection.

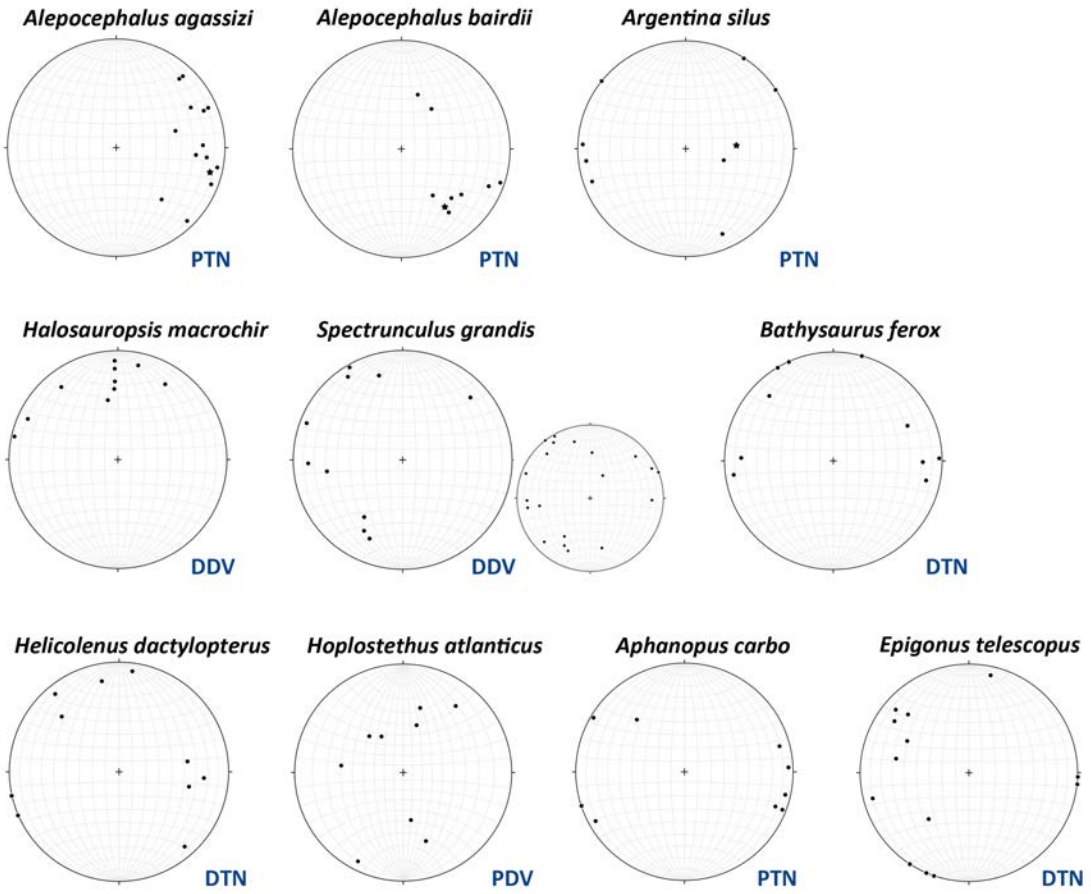

Figure 2.13 (continued).

2.4.1 Trait distribution between functional groups and along depth gradients

Functional groups are defined by adaptations of fish to the deep sea setting. For instance, tubular eyes and peripheral field are only found in the mesopelagic species. In the mesopelagic zone, fish develop tubular eyes for receiving downward sunlight or to broaden their visual angle in the 3-dimensional environment. In contrast, fish having the area centralis of GCs distributions on the retina are found across a wide depth range of occurrences and diverse habitat environments, implying that this type of visual functional trait is less constrained by environmental changes. Visual directions revealed by the location of the area centralis successfully predict the feeding behaviours of deep-sea fish (Table 2.3). Compared to visual fields, habitat categories provide a clue of positions in the water column.

According to evidences from not only habitat categories and visual directions but also prey items and muscle $\delta^{15}N$ and $\delta^{13}C$ values, the examined taxa can be divided into six functional groups: pelagic (species with tubular eyes TE, species with peripheral fields P, and pelagic species with temporal/nasal fields PTN), benthopelagic (pelagic species with dorsal/ventral fields PDV and demersal species with temporal/nasal fields DTN) and benthic foragers (demersal species with dorsal/ventral fields DDV) (Fig. 2.14). Although the Group PDV is originally categorized in a pelagic habitat from FishBase data, they have greater intake of benthic prey as indicated by muscle $\delta^{15}N$ and $\delta^{13}C$ values (Fig. 2.11), revealing the importance of benthic diets and the possibility of living in the water column close to the seafloor.

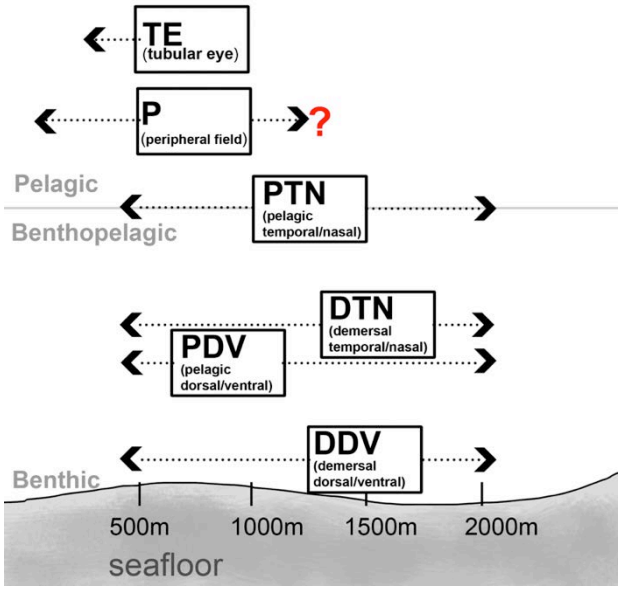

Figure 2.14. Space usage between functional groups.

GCs integrate all the optic information in the retina and therefore a decrease in cell density corresponds to weaker light density and less optic signal information in the deeper environment. Depth-dependent decreases in GC density are found in pelagic fish but are less clear in demersal species (benthopelagic and benthic feeders), showing the pelagic functional group to be more strongly influenced by the depth-dependent reduction in light intensity (Fig. 2.10; more discussions in Section 5.1.1 and Fig. 5.1). However the corresponding depth-dependent increasing trend of spatial resolving power across all functional groups implies that greater visual acuity for discriminating point light sources is more important when the bioluminescence substitutes for space light. As defined by Collin and Pettigrew (1989), spatial resolving power is positively correlated to two factors, peak density of ganglion cells and size of lens.

$$Spatial\ resolving\ power\ (cycles\ per\ degree) = \frac{\sqrt{peak\ density\ of\ GCs}}{\tan^{-1}\left[\frac{1}{2.55\times(lens\ size)}\right]} \div 2$$

Considering the depth-related decrease of GC density described above, the higher spatial resolving power of deep-sea pelagic fish apparently results from the increase of lens/eye size. The eye size of deep-sea fishes increases with depths till 1000m and below the depth, fish have smaller eyes (Montgomery & Pankhurst 1997) because developing large eyes is energetically expensive in the deeper environment (Warrant & Johnsen 2013).

Large eyes also enhance fish visual sensitivity. Following the defined equation in the Introduction (shown below) and assuming pupil diameter (A) varies in proportion with the lens diameter (f), the visual sensitivity to sunlight is not influenced by the size of lens. The larger lens, however, increases the sensitivity to bioluminescence.

$$S\ (sensitivity\ to\ downward\ light) = \left(\frac{\pi}{4}\right)^2 A^2 \left(\frac{d}{f}\right)^2 \left(1 - e^{-kl}\right)$$

$$N\ (senstivity\ to\ bioluminensence) = \frac{EA^2}{16r^2} e^{-\alpha r}\left(1 - e^{-kl}\right)$$

Undoubtedly, it is too simple to discuss the visual sensitivity of fish without consideration of other factors, but it theoretically explains the advantage of large lens/eyes for fish living in the deep, especially above 1000m.

2.4.2 Taxonomic description of visual fields

2.4.2.1 Gadiformes

Gadiformes constitute a considerable proportion of deep-sea fish species, in which macrourids dominate the benthopelagic fauna. Benthos are the primary food source for macrourids, such as copepods amphipods, polychaetes and others (Mauchline & Gordon 1984a; Whitehead *et al.* 1986), and therefore, a common feature of a downward visual field was found in most species. Particularly *Nazumia aequalis,* as it only has a ventral visual field, corresponding to dominant epibenthic items found in the stomach content analysis (Mauchline & Gordon 1984a). In contrast, detecting organisms or food falling from the top is facilitated through the dorsal visual field, which also explains the behaviour of scavenging observed from macrourids (Yeh & Drazen 2011; Drazen *et al.* 2001). However, *Trachyrhynchus murrayi* has no downward, but an upward visual field that is associated with their distinct head morphology from other genera. The genus Trachyrhynchus has a long and flat rostrum and a protrusible mouth underneath the rostrum that facilitates digging the soft seabed for feeding on epifauna and infauna (McLellan 1977). Functionally, the unique head morphology of the *T. murrayi* weakens the dependence of the ventral field and this species may not physically see downwards. Moreover, according to genetic evidences, the phylogenetic relationship of the genus Trachyrhynchus in the order Gadiformes is revised and this genus is classified into the suborder Gadoidei (gadoid and morid fishes) rather than the suborder Macrouroidei (macrourid fishes) (Roa-Varón & Ortí 2009). It may explain the

visual specificity (a upward visual field only) of *T. murrayi* compared to other macrourid fishes.

Morids are also abundant in the deep sea and distribute from 500m to 2900m. For the four common species in the Northeast Atlantic (Table 2.1), the GCs density increases from the centre to the periphery, but the peak cell density is located in different areas. The peak values concentrate on the ventral retina (as a dorsal visual field) for *Antimora rostrata*, the deepest morid fish, which corresponds to intakes of pelagic food and the behaviour of scavenging (Collins *et al.* 1999; Priede *et al.* 1994). In addition, this visual field may aid *A. rostrata* for the avoidance of pelagic predators. Nevertheless, a few peaks on the dorsal retina are found, implying that *A. rostrata* searches for benthic organisms, especially for benthic crustaceans, as seen in their diet (Mauchline & Gordon 1984b). *Lepidion eques* also links the pelagic and benthic food web, revealed by fatty acid signals in muscle *(Stowasser et al.* 2009), and has the same dorsal and ventral visual directions as *A. rostrata*. Based on muscle $\delta^{15}N$ values, both species have a similar dietary signals and ecological role (Trueman *et al.*, 2014). In order to avoid competition, two species have different habitat depth that *L. eques* has a shallower distribution (500m-900m than *A. rostrata* (1300-2500m) (Whitehead *et al.* 1986). Although *Mora moro* and *Halargyreus johnsonii* inhabit on upper and middle slope as similar depth ranges to *L. eques*, their diet preferences are different. Carrassón *et al.* (1997) indicated that epibenthic or suprabenthic organisms are the main food sources for *M moro* and the dominant downward vision support this observation. In contrast, *H. johnsonii* mainly forages on pelagic prey, such as copepods and chaetognaths (Mauchline & Gordon 1984b) that is also supported by the peripheral field, usually found in deep-sea pelagic fish. Not much information of morid ecology has been established in literatures, but according to our results, three shallower species (*H. johnsonii*, *L. eques* and *M. moro*) have obvious differences in regards to the trophic niche to reduce competitions. The deepest one, *A. rostrata*, behaves similarly to *L. eques*.

Gadoid fish inhabit at shallower layers than macrourids and morids, and diverse dietary items can be found in their stomachs. Usually, the nasal field (sometimes with the temporal field) supports gadoid fish actively pursuing pelagic or swimming organisms. For example, the *Micromesistius poutassou*, with nasal/temporal fields, forage on euphausiids, fish and cephalopods in the midwater (Mauchline & Gordon 1984b). *Molva dypterygia* is highly piscivorous and has better sensitivities in regards to the nasal and temporal vision to detect animals with a higher mobility in their visual fields (Bergstad 1991). Another piscivorous species, *Merluccius merluccius*, also

displays a better horizontal vision (Cartes *et al.* 2009; Bozzano & Catalán 2002) (Fig. 2.12). However, not all gadoid fish prey on pelagic or active organisms, and some such as *Phycis blennoides* and tend to feed more on benthic crustaceans (Morte *et al.* 2002), which is reflected in their downward visual field.

2.4.2.2 Osmeriformes

Alepocephalids are the most abundant deep-sea fishes in Osmeriformes. A specialised structure of the retina, called the fovea, is widely observed in smoothheads, offering a higher spatial resolution for bioluminescent points (Wagner *et al.* 1998). The fovea accompanied with the highest GCs density locates at the temporal retina, indicating the dominant forward vision of the alepocephalids (Collin & Partridge 1996) (see four species in Fig. 2.12). Alepocephalids are not themselves bioluminescent, and the forward visual field combined with the pronounced fovea indicates a strong diet preference for bioluminescent species, such as medusae and ctenophores (Mauchline & Gordon 1983; Whitehead *et al.* 1984; Haddock *et al.* 2010; S. Haddock & Case 1999).

The *Argentina silus*, an Argentinidae fish, shows a similar diet preference (ctenophores and salps) as alepocephalids (Mauchline & Gordon 1983), explaining the importance of the nasal visual field. *A. silus* does not show a prominent fovea, however, perhaps reflecting their relatively shallow occurrence and reliance on sunlight. In addition, backward vision is also important in *A. silus*, presumably to detect piscivorous predators, such as the *M. dypterygia.*

2.4.2.3 Notacanthiformes

Only one notacanthiform species, the *Notacanthus bonapartei*, has been studied in the past (Wagner *et al.* 1998). There are two main visual fields, the ventral and dorsal fields, utilised to capture sessile and mobile organisms, respectively. The present study analyses another species, the *Halosauropsis macrochir*, and finds that GCs densities increase along the dorsal and ventral directions. But the ventral vision is the primary field used for preying on the epibenthos, such as crustaceans and polychaetes (Gordon & Duncan 1987).

2.4.2.4 Ophidiiformes

The interval of the GCs density is small in regards to the *Spectrunculus grandis*, and the highest cell densities are found at the outer portion of retina, especially at the dorsal and ventral ends. This pattern is similar to the *N. bonapartei.* The two visual

fields for *S. grandis* are utilised for feeding on benthopelagic crustaceans (mobile prey) and polychaetes and echinoderms (immobile prey) (Mauchline & Gordon 1984c).

2.4.2.5 Aulopiformes

Two species of Aulopiformes fish, the *Bathysaurus ferox* (this study) and the *Bathypterois dubius* (Collin & Partridge 1996), have similar GCs density patterns, where two peaks are located at the temporal and nasal areas. Although the two species perch on the seafloor and have the same feeding strategy of 'sit-and-wait' (Gartner *et al.* 1997), their diet compositions are considerably different. *B. dubius* may use the rostral visual field to feed on small prey carried by the current, and perceive the approach of predators by the caudal visual field (Collin & Partridge 1996). However, the apex predator, *B. ferox*, may use both areas in detecting swimming fish in their visual field (Sulak *et al.* 1985).

2.4.2.6 Perciformes

Piscivorous fish, the *Aphanopus carbo* (Mauchline & Gordon 1984c), have a similar visual field as other active predators in that the fish sensitively detect swimming animals in their temporal and nasal field. In accordance with the stereographic projection of the GCs distribution, the same visual fields are found in the *Epigonus telescopus*. This species feeds on benthopelagic crustaceans (Mauchline & Gordon 1984c), which may explain the requirement for these visual directions. However, the density topography of *E. telescopus* provides different fields in temporo-dorsal, temporo-ventral, naso-dorsal and naso-ventral areas. The huge and elliptical eyeball may cause a bias in stereographic projection in this case, and therefore more samples are needed to further investigate the *E. telescopus*.

2.4.2.7 Scorpaeniformes

The 'sit-and-wait' feeding strategy (Gartner *et al.* 1997) and diverse diet compositions (Mauchline & Gordon 1985; Whitehead *et al.* 1986) predict the GCs distribution for the *Helicolenus dactylopterus*. The high GCs density at periphery enables *H. dactylopterus* to perceive either pelagic or benthic prey in their visual field. Unlike pelagic fish living in the water column, *H. dactylopterus* perches close to the sea floor. As a consequence this species has more benthos diet choices. Moreover, the temporal peak of the GCs density, observed from other active foragers or fish eaters, indicates that the *H. dactylopterus* has a good ability to capture fish, cephalopods and other swimming animals.

2.4.2.8 Beryciformes

According to body morphology, *H atlanticus* has a relatively large gape compared to most of the other deep-sea fishes (Fig. 2.15), implying that they relies less on the accuracy for locating if they apply gape suction to feed. This feeding behaviour is also reflecting on their visual field. In the present study, species with a dorso-ventral visual field generally have low value *z-angles* and strongly rely on benthos or food fallings as passive feeders. *Hoplostethus atlanticus* does have this kind of visual field, but in a bigger *z-angle* around 45°, therefore implying that the *H. atlanticus* shows less dependence on sedentary organisms, but may search for benthopelagic/swimming prey in the water column close to the seafloor. The high metabolic rate and varied diet composed of crustaceans, fish and cephalopods support this assumption (Mauchline & Gordon 1984c; Bulman & Koslow 1992). However, typical active fish, such as the piscivorous species (*A. carbo* and *M. dypterygia*) and pelagic foragers (osmeriform fish), hunt for swimming prey with the aid of naso-temporal visual fields, rather than dorso-ventral fields. In order to explain the behaviour of *H. atlanticus*, two observations are given. First, *H. atlanticus* forages for smaller fish (myctophids and deep-sea smelts) and swimming crustaceans (Mauchline & Gordon 1984c). Secondly, the factor that *H. atlanticus* forms large aggregations nature may be the trigger for the higher incidences of feeding activity (Bulman & Koslow 1992). In the aggregating period, *H. atlanticus* can save energy in regards to locating and chasing its quarries. These two observations imply that: (1) the wide visual field (observed from a wide range of *l-angle*) for searching prey is much more important than the accuracy of prey position for opportunistic feeding or feeding in a food-rich environment; (2) The *H. atlanticus* behaves between active/pelagic feeders (different *l-angle,* but similar *z-angle*) and passive/benthic feeders (similar *l-angle,* but different *z-angle*).

2.5 Summary

Visual acuity is still important for deep-sea demersal fishes and retinal cell distributions vary between functional groups as predicted from stomach content. While detailed diet information is absent, retinal cell analysis could reveal foraging habits. Visual fields are not constraint by depth (except fishes with tubular eyes) but sensitivity and spatial resolution display depth-related trends. This could provide us the information of visual adaptation within and between functional groups. For example, bioluminescence dominates light sources in depth deeper than 1000m, driving fishes

developing large eyes size for better spatial resolving power. This is obviously found in pelagic/benthopelagic assemblages other than benthic fishes. In the same taxonomic group, similar visual behaviours between species are common, but while the interspecific differences are observed, it may reveal fishes avoid niche overlapping and develop distinct visual hunting behaviours.

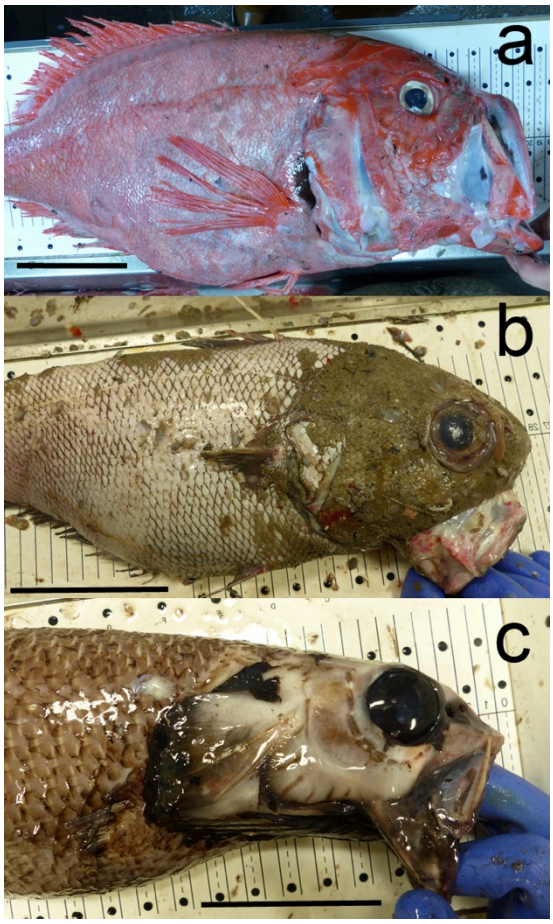

Figure 2.15. Head morphology and mouth opening of three abundant deep-sea species. *H. atlanticus* has a larger mouth opening than *C. rupestris* and *A. bairdii.* Scale bar equals to 10cm.

Chapter 3: Otolith form predicts functional groupings of deep-sea fishes

3.1 Introduction

3.1.1 The physiological function of otolith

Teleosts have coupled inner ear structures, composed of semicircular canals and three otolithic end organs (Popper 1977). The semicircular canal perceives angular accelerations and otolithic organs detect auditory and vestibular stimulations (Wright *et al*. 2003). There are three otolithic organs each with their own distinct otolith; the sagitta in the saccule, the lapillus in the utricle and the asteriscus in the legena. Sagittae are the largest of three-paired otoliths for most adult fish (except for *otophysan* fish with larger asteriscii) and are most widely used in biological studies (Campana 2004). Following the orientation of the fish body, the otolith has dorsoventral and anterior-axes surface (Campana 2004; Tuset *et al*. 2003). Generally, a notch at the anterior end, called excisura, separates rostrum and antirostrum and shows an inward extension to form a grooved structure on the proximal surface. The sulcus acusticus, the grooved structure, contacts with hair cells of sensory epithelium. A relative displacement between the otolith and the sensory epithelium, induced by acoustic vibration or swimming, results in the physical bending of hair cells as a trigger of signal transductions in the nerve system (Popper & Fay 1993; Popper & Lu 2000). The relative sulcus size is defined as a ratio of sulcus area to otolith area (SO ratio) and the value corresponds to the auditory threshold frequency and locomotion pattern (Gauldie 1998). Sulcus area develops with fish growth and allometric changes of sulcus acusticus in some species can lead to an ontogenetic increase of SO ratio (Aguirre 2003; Aguirre & Lombarte 1999; Arellano *et al*., 1995; Lombarte 1992). This change may be associated with environmental factors, such as depth and temperature (Lombarte 1992).

Continuous accretions of calcium carbonate on the otolith change the tolerant ranges of acoustic and vestibular stimulations throughout ontogeny growth (Lychakov & Rebane 2000) that can lead to an increase in sound sensitivities and a shift of the frequency (Wysocki & Ladich 2001). Greater increases of otolith size are observed in demersal fish than from pelagic species, implying that demersal fish have a noticeable change of acoustic capabilities (Lychakov & Rebane 2000). Secondly, the sensitivity

and resolving power of vestibular stimuli increase with an increase of otolith mass, but the tolerant range of acceleration becomes narrower. This reflects the different performance of locomotory movement between functional groups in that pelagic fish with smaller otoliths can swim at a variety of accelerations whereas demersal fish have a better ability to dodge obstacles near the bottom with a functional support by large otoliths (Lychakov & Rebane 2000). The size of otoliths is also correlated with the depth of fish habitats. Lombarte and Cruz (2007) found that demersal communities at the depth of 200-750 m showed a positive trend between otolith size and distribution depths, because fish in the deeper environment are supposed to strongly rely on the auditory rather than visual stimuli. This morpho-functional feature suggests that not only the ontogeny, but also exogenous factors determine otolith size (Aguirre & Lombarte 1999; Lombarte & Lleonart 1993).

3.1.2 Phylogenetic and environmental regulations of otolith morphology

Otolith shape shows phylogenetic relationships (Lombarte & Castellón 1991) and the functional demand of auditory and vestibular abilities are genetically regulated (Lombarte *et al*. 2010; Lychakov & Rebane 2000; Volpedo & Echeverria 2003; Volpedo *et al*. 2008). However, environmental effects, such as the depth, water temperature and food supply, also contribute to morphological variations (Hüssy 2008; Gagliano & McCormick 2004; Lombarte & Lleonart 1993; Mérigot *et al*. 2007). It has been suggested that the otolith is synergistically shaped by genetic and environmental effects (Cardinale *et al*. 2004) and that environmental effects constrain the overall shape of otolith while the genetic effects have a local influence (Vignon & Morat 2010). According to these regulations, otolith morphology has been successfully applied to fish taxonomy (Tuset *et al*. 2003; Tuset *et al*. 2006), and the regional difference of otolith shape within species has been utilized in stock identification and management (Cardinale *et al*. 2004; Jónsdóttir *et al*. 2006; Mérigot *et al*. 2007).

3.1.3 Aim

The aim of the present study was to characterise interspecific diversity of otolith morphology in relation to phylogenetic (endogenous) and environmental (exogenous) effects. Deep-sea demersal fishes have evolved various feeding behaviours, which provides a strong comparative basis for a functional analysis of otolith shape.

3.2 Materials and Methods

3.2.1 Sample collection

Fish samples were collected from the Rockall Trough area based on annual deep-water fisheries trawl surveys from 2006 to 2012 undertaken by Marine Scotland-Science. Samples were collected from a depth range of 500-2030m along the continental slope at Rockall Bank, Rosemary Bank and Anton Dohrn Seamount (Fig. 3.1). All fish were identified and body weight and length measured (Table 3.1). Paired sagittal otoliths were extracted, cleaned, dried and reserved in plastic trays. In an attempt to control for ontogenetic variability of otolith morphology, samples for each species were chosen from individuals larger or heavier than the record of their maturity length or maturity weight. For those species where size at maturity was unknown, samples were taken from the collection from individuals with relatively large body sizes. In total, 898 sagittal otoliths from 39 species in 10 orders of deep-sea fish were analysed.

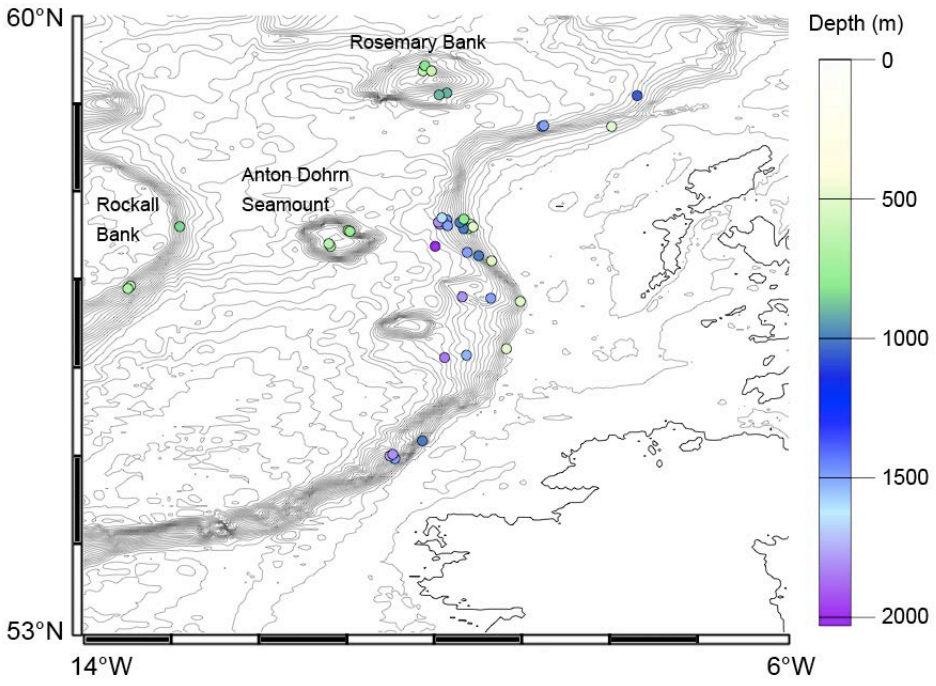

Figure 3.1. Sampling locations.

Table 3.1. Sample list. Macrourids were measured with pre-anal fin length, smoothheads with standard length, and others with total length.

Species	N	Depth (m)	Length (cm)	Weight (g)
Anguilliformes				
Serrivomer beani	3	1750	73-81	105-189
Synaphobranchus kaupi	10	1800	NA	82-256
Aulopiformes				
Bathypterois dubius	6	1530	17-20	43-73
Bathysaurus ferox	1	1800	48	485
Beryciformes				
Hoplostethus atlanticus	15	1500	48-64	2062-4591
Gadiformes				
Brosme brosme	4	540,760	52-59	1486-2714
Merluccius merluccius	10	500	NA	474-3678
Micromesistius poutassou	17	500	27-39	108-364
Molva dypterygia	37	680, 760, 910, 1000,1050	60-124	656-8400
Molva molva	3	500	NA	780-2060
Phycis blennoides	15	500	37-65	372-2038
Coelorhynchus coelorhynchus	17	540	10-13	119-296
Coelorhynchus labiatus	10	1800	11.5-12.5	74-111
Coryphaenoides guentheri	21	1500, 1850	7.5-11	60-400
Coryphaenoides mediterranea	10	1800	18.5-21	789-1748
Coryphaenoides rupestris	21	1500	8-26	106-2484
Nezumia aequalis	21	650	5-5.5	38-75
Trachyrincus murrayi	15	1500, 1850	8-16.5	38-259
Antimora rostrata	13	1800, 1850, 2030	52-60	1250-2146
Halargyreus johnsonii	14	760, 1000	19-28	40-119
Lepidion eques	20	760, 1000	30-40	115-442
Mora moro	18	610,650, 760, 810	48-64	1012-2754

Table 3.1 (continued).

Species	N	Depth (m)	Length (cm)	Weight (g)
Notacanthiformes				
Halosauropsis macrochir	10	1750, 1800	58-72	195-426
Polyacanthonotus rissoanus	7	1800	37-55	33-190
Ophidiiformes				
Cataetyx laticeps	25	1500, 1650, 1800	73-91	2812-5662
Spectrunculus grandis	11	1850	37-51	262-834
Osmeriformes				
Argentina silus	19	500	35-44	302-764
Alepocephalus agassizi	10	1650	52-68	1572-4645
Alepocephalus bairdii	26	1000, 1500	26-80	116-3930
Rouleina attrita	5	1750	NA	343-822
Xenodermichthys copei	10	1000	14-17	21-43
Stomiiformes				
Borostomias antarcticus	2	1800	NA	107-201
Perciformes				
Aphanopus carbo	23	850	82-109	598-1894
Centrolophus niger	2	500	48 (one is NA)	984-1260
Epigonus telescopus	4	900, 1000	41-54	998-2118
Lycodes atlanticus	3	1500	25-30	51-106
Nesiarchus nasutus	2	800	77-80	1078-1168
Scorpaeniformes				
Helicolenus dactylopterus	49	680	23-35	192-716
Sebastes mentella	14	600	41-50	968-1842

3.2.2 Morphological and functional indices of otolith

Each otolith was first weighed, and then photographed under a stereomicroscope using a Nikon SMZ800 equipped with Qimaging MicroPublisher RTV 5.0 digital camera. Using the image of the otolith proximal surface, five two-dimensional parameters, the feret length, feret width, perimeter, total area and sulcus area, were measured by imageJ (developed by National Institute of Health, the U.S.). Following Tuset *et al*. (2003), five otolith morphological indices, calculated from the first four parameters, were used to describe the outline of otolith (Fig. 3.2). The indices approximately illustrated otolith shape as square (formfactor), round (roundness), irregular (circularity), rectangular (rectangularity) and elongate (ellipticity), respectively.

Size parameters	Morphological indices	Functional indices
Feret length (L)	Formfactor = $(4\pi OA)/P^2$	SO ratio = SA/OA
Feret width (W)	Roundness = $(4OA)/\pi L^2$	OW
Perimeter (P)	Circularity = P^2/OA	OB ratio = OW/BW
Otolith area (OA)	Rectangularity = OA/LW	
Sulcus area (SA)	Ellipticity = (L-W)/(L+W)	
Otolith weight (OW, mg)		
Fish body weight (BW, g)		

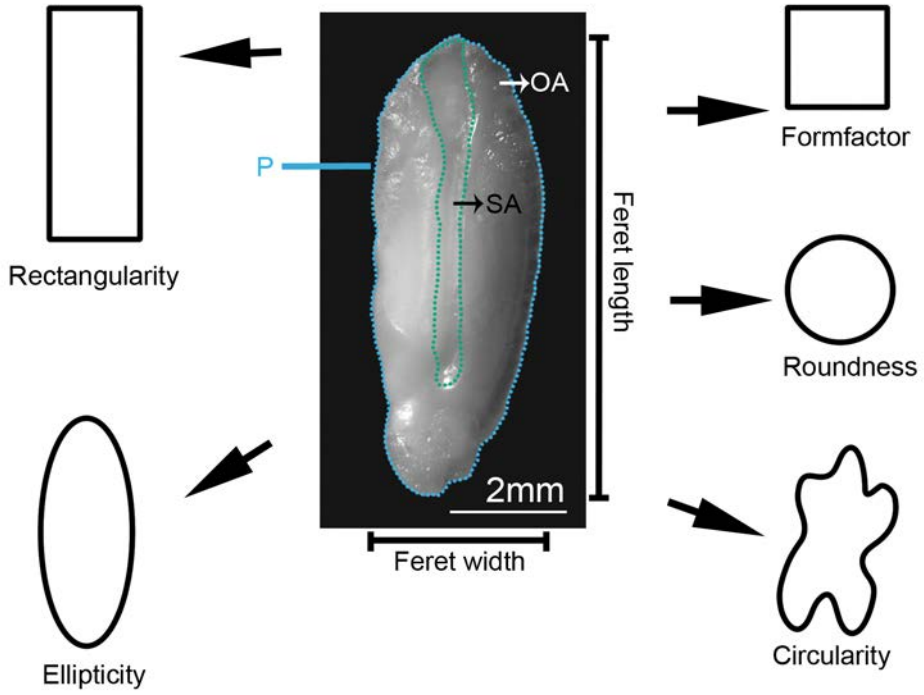

Figure 3.2. Measurement of morphological and functional indices from size parameters.

Based on the assumption that otolith shape relates to different functions of hearing and balance control, two types of functional indices were introduced (the definition in Fig. 3.2 and the value in Appendix B). The SO ratio (sulcus area/otolith area) and otolith size are regarded as indices of feeding behaviours of pelagic or benthic tendency because both determine auditory threshold frequencies and accelerations to meet demands of the fish in different feeding modes (Gauldie 1998; Lychakov & Rebane 2000). For otolith size, two mass related indices, otolith weight and OB ratio, were used and OB ratio was defined as the value of otolith weight scaled to fish body weight. Values of otolith weight and OB ratio were $\log_{10}$-transformed to decrease extreme numerical intervals, which may affect the statistical analysis in terms of non-normal distributions.

3.2.3 Statistical analyses

All statistical analyses were conducted using the software R (R Development Core Team, 2012) and graphics were produced by package “ggplot2 (Wickham 2009).

The relationship between functional indices and morphological indices was examined by Pearson correlation from two aspects. One was a comparison between individuals, and the other was compared with average values between species.

39 species were classified into functional groups by features of otolith outline, and the values of morphological indices were averaged at species level. First, principal component analysis (PCA) was performed to transform five morphological indices to new PCA components. This procedure reduced the redundant morphology information and standardized indices from various measurement scales. Then, 39 species with new five component values were grouped by agglomerative hierarchical clustering.

Following the clustering, the difference of SO ratio between groups was tested by the analysis of variance (one-way ANOVA) to evaluate the functional performance of fish in identified groups. The same statistical analysis was also applied on the comparison of otolith weight and OB ratio.

Considering the environmental influence (depth), functional indices were regressed on the depth of fish occurrence. The captured depth in this study and usual depth recorded in literatures were applied to assess the environmental effect on functional indices. Usual depth of each species was extracted from literatures and median of depth range was applied on the linear regression model to prevent bias from an abnormally shallow or deep habitat. If the depth showed a relationship with functional

indices, an analysis was conducted to discuss the influence of a covariate, depth, on functional indices between morphological groups.

3.2.4 Phylogenetic effects on otolith morphology and function: comparative analysis by independent contrasts

In conventional statistics, variances are usually assumed to be independent. However, closely related species show similarities in otolith morphology, indicating a strong phylogenetic dependence (Nolf 1993; Campana 2004). To deal with such non-independent data points in a diverse collection of fish species, comparative analysis of independent contrast (CAIC) was applied for comparing discrete or continuous traits in a phylogeny (Pagel 1992). As no fully resolved phylogenetic tree for deep-sea fishes was available, a new one we established based on DNA sequences from the online database, the National Center for Biotechnology Information (NCBI) (Geer *et al*. 2010). The DNA sequence used in this study was partial mitochondrial cytochrome *c* oxidase I gene (COI gene). Among 39 species in the sample collection, only 33 species of COI gene information were available from NCBI nucleotide database. The COI gene of 493 base pairs was analysed in a GTR+G+I model with the maximum likelihood method by the computer program MEGA version 5.2.2 (Tamura 2011). Bootstrap analysis was set to 100 replicates.

The comparative analyses were performed in R software and the original otolith dataset was combined with the information from the phylogenetic tree by package "*caper*" (Orme 2012). First, the phylogenetic signal, Pagel's lambda (λ), was measured with package "*phytool*" (Revell 2012) and tested the degree of phylogenetic dependence of each trait (five morphological and two functional indices). The phylogenetic signal was introduced by Pagel (1999) and varied between 0 and 1 where a value of 0 means phylogenetically independent and a value of 1 indicates the trait evolved in shared histories between species under Brownian motion process. The observed phylogenetic signal from empirical data was compared with λ=0 and λ=1 by the likelihood ratio test, which examined significant differences between observed and theoretical signals. Second, two analyses were conducted again with phylogenetic information: the relationship between functional indices and depths, and the differences of functional indices between groups. Phylogenetic generalized least square regression (PGLS) was performed to assess the relationship between functional indices and occurrence depth by package "*caper*". PGLS is designed as a linear regression model but incorporates phylogenetic information in terms of the length of branches from the phylogenetic tree (Freckleton *et al*. 2002). The model quantifies the variance of

observations and covariance between observations in the shared history and gives the strength of phylogenetic dependence of the regression. The signal λ was estimated by maximum likelihood methods and compared to λ=0 (no phylogenetic dependence) and λ=1 (strong phylogenetic dependence) by likelihood ratio test.

The difference of functional indices between groups was tested by phylogenetic ANOVA with the package "*geiger*" (Harmon *et al*. 2008). Phylogenetic ANOVA compares empirical F statistics with a null distribution of the F statistic, in which the null distribution is generated by simulations of trait evolution in the phylogenetic tree with a Brownian motion model (Garland *et al*. 1993). The traits explored are the functional indices, SO ratio, otolith weight and OB ratio, respectively.

3.3 Results

3.3.1 Morphological indices vs. Functional indices

The sulcus area was assumed to be the same as the sensory epithelium, but according to Deng *et al*. (2011), the area of sensory epithelium in *Antimora rostrata* was less than the grooved structure on the otolith. Thus the SO ratio of morid fish might be overestimated in this study (Fig. 3.3). The sulcus area of *A. rostrata* can be calibrated based on the observation from Deng *et al*. (2011) and the SO ratio was retained. However, given limited knowledge and little research of sulcus areas in other three morid species sampled, their SO ratio cannot be calibrated and these three morids were removed from any analysis related to the SO ratio.

All otolith samples showed that SO ratio was significantly correlated with morphological indices (Fig. 3.4). The correlation was positive for the circularity and ellipticity, but negative for the other three. The coefficient, except of rectangularity, was much higher when the correlation was on the comparison at a species level.

Otolith weight showed a positive correlation with rectangularity and ellipticity but negative with formfactor and roundness (Fig. 3.4). However, the roundness was the only one morphological index showing the negative correlation with OB ratio, and the most correlation coefficients were lower than with otolith weight (Fig. 3.4).

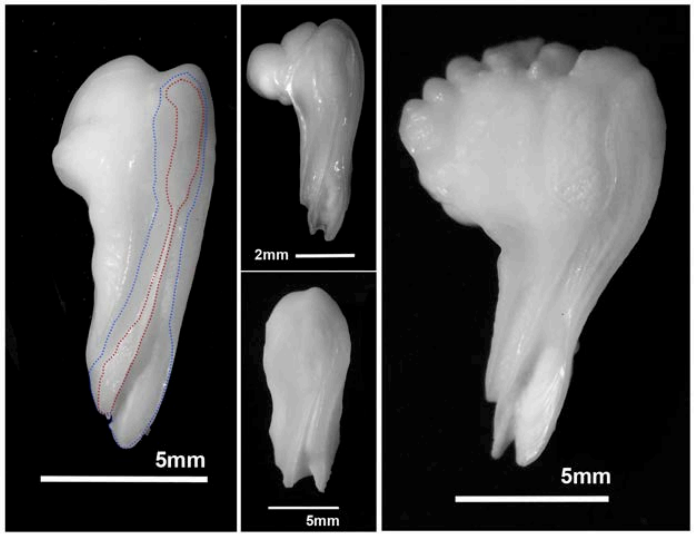

Figure 3.3. The proximal surface of morid otoliths (left: *Antimora rostrata*; middle-up: *Halargyreus johnsonii*; middle-down: *Lepidion eques*; right: *Mora moro*). The specific area of sensory epithelium in *A. rostrata* (red dot line) is smaller than the grooved structure on the otolith (blue dot line). Although the grooved structure is obvious in morid fish, it does not represent the sulcus area of otolith. *A. rostrata* is the only one of four morid species has been investigated in the specific area of sensory epithelium on otolith.

	Individual level			Species level		
	SO ratio	Otolith weight	OB ratio	SO ratio	Otolith Weight	OB ratio
Formfactor	-0.43***	-0.23***	0.065	-0.47***	-0.33*	0.020
Roundness	-0.57***	-0.50***	-0.26***	-0.62***	-0.58***	-0.33*
Rectangularity	-0.070*	0.11***	0.13***	-0.030	0.079	0.014
Circularity	0.39***	-0.051	0.25***	0.43**	-0.022	0.33*
Ellipticity	0.57***	0.48***	0.24***	0.62***	0.53***	0.30

*** p<0.001, **0.001<p<0.01, *0.01<p<0.05

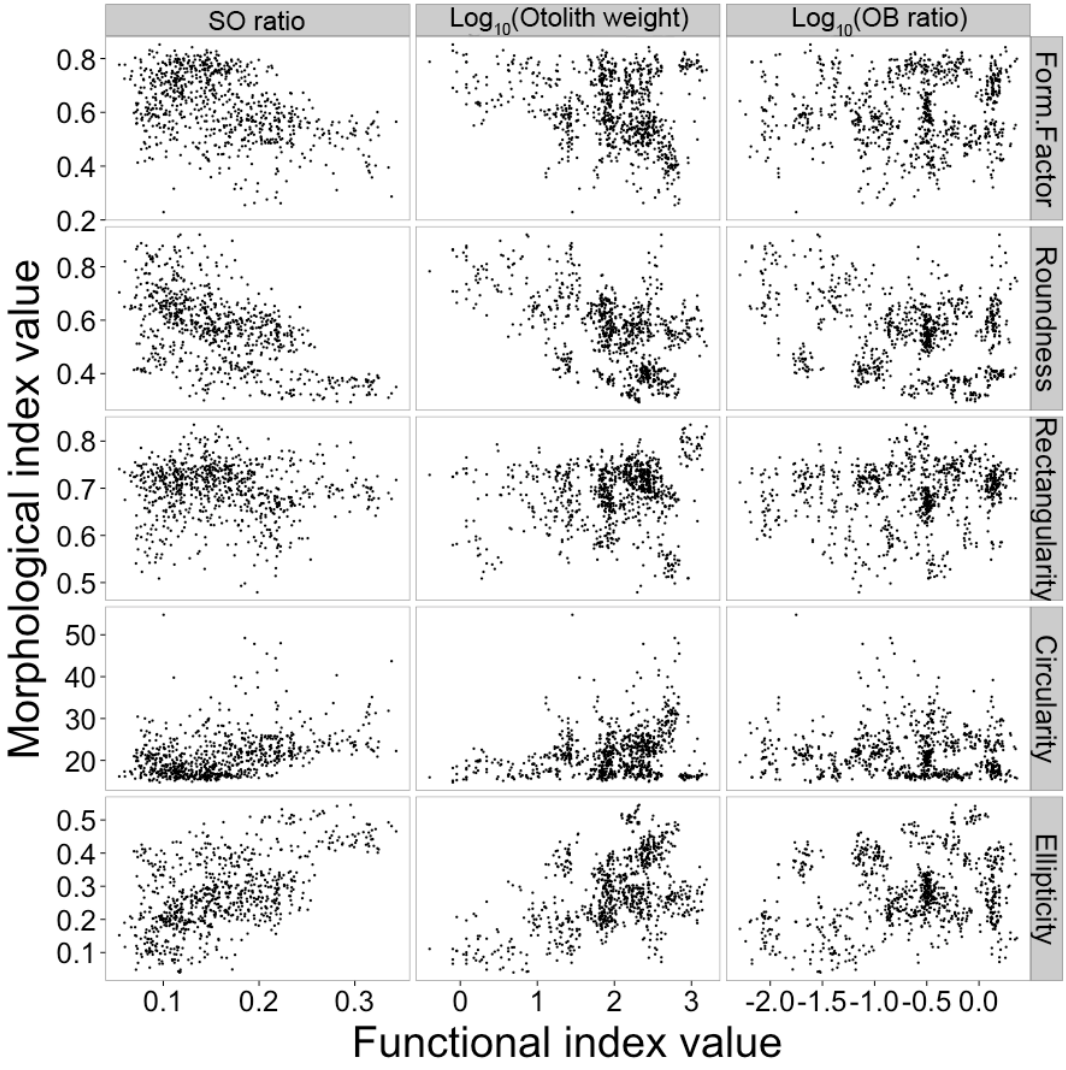

Figure 3.4. Correlations between morphological and functional indices. Pearson coefficients in each comparison at two levels (individual and species levels) are given in the upper table. The dot chart shows the trend of morphological and functional indices at the individual level.

3.3.2 Clustering

Four discriminative groups were identified by the clustering analysis with PCA scores (Fig. 3.5) and the group assignment of each species is shown on Table 3.1. Group A was composed of argentine, smooth-head, snaggletooth and deep-water cardinal fish with round and slightly irregular otoliths. Group B had discoid and rectangular otoliths, which were observed from macrourids, abyssal halosaurs, tripod fish, eels, cusk eels and spiny eels. Group C was characterized as obviously elliptical otolith from gadoids, morids, redfish, scabbardfish, lizardfish and blackfish. Group D consisted of only two species of *M. moro* and *Hoplostethus atlanticus*, with notably irregular otoliths.

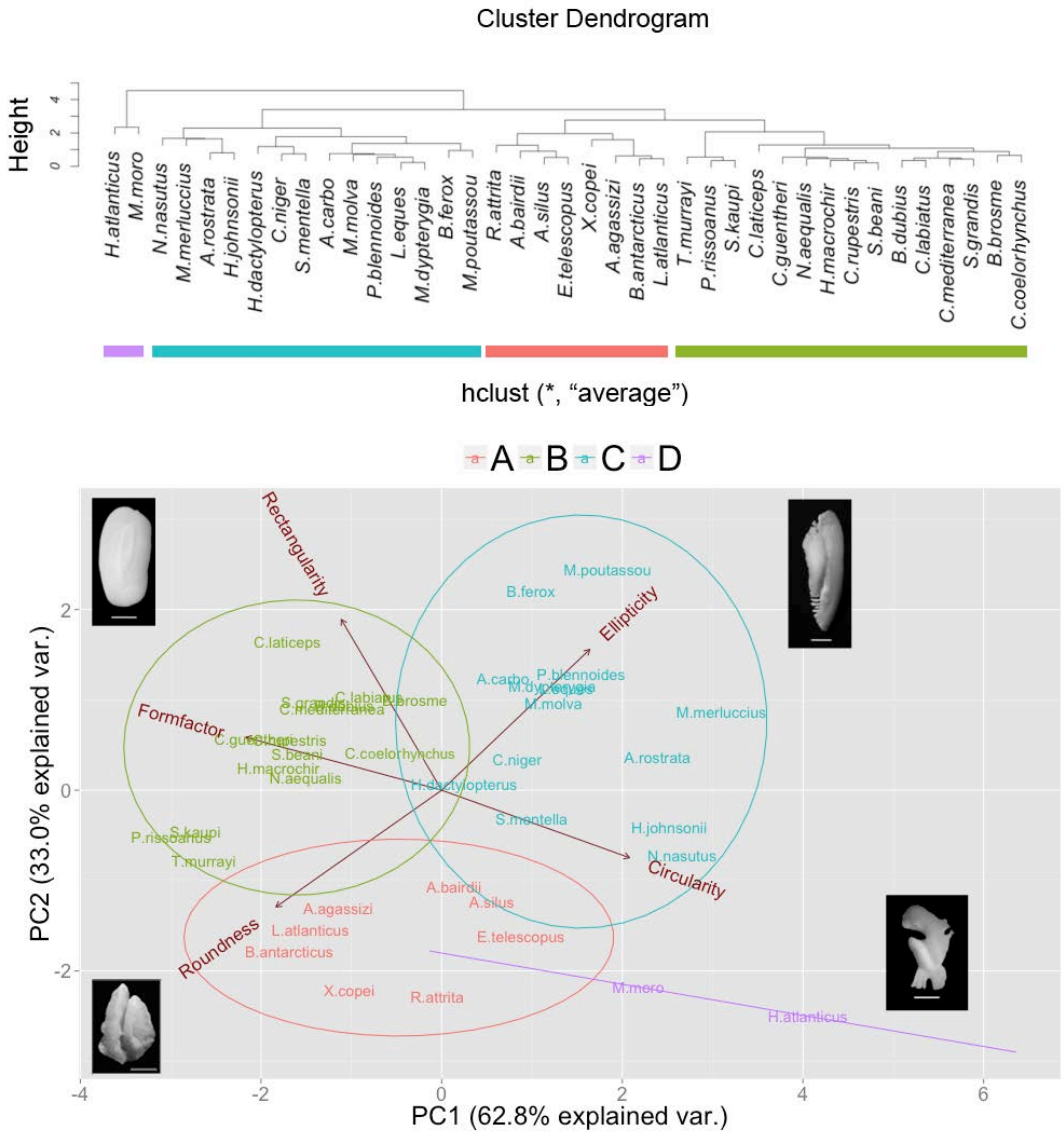

Figure 3.5. PCA and cluster analysis of 39 species with five otolith morphological indices. In PCA biplot, the circle represents 95% confidence interval. Four otolith photos represent typical shapes in each morphological group: bottom left – *Alepocephalus bairdii* in group A (scale: 2mm); upper left - *Cataetyx laticeps* in group B (scale: 5mm); upper right: *Merluccius merluccius* in group C (scale: 5mm); bottom right - *Hoplostethus atlanticus* in group D (scale: 5mm).

3.3.3 Functional indices vs. Groups

SO ratio and otolith weight differed significantly between groups (ANOVA, SO ratio: df=3, F=3.86, p=0.018; log10-transformed otolith weight; df=3, F=3.40, p=0.0285) (Fig.

3.6). However, OB ratio was not significantly different between groups (ANOVA, log10-transformed OB ratio: df=3, F=1.55, p=0.218).

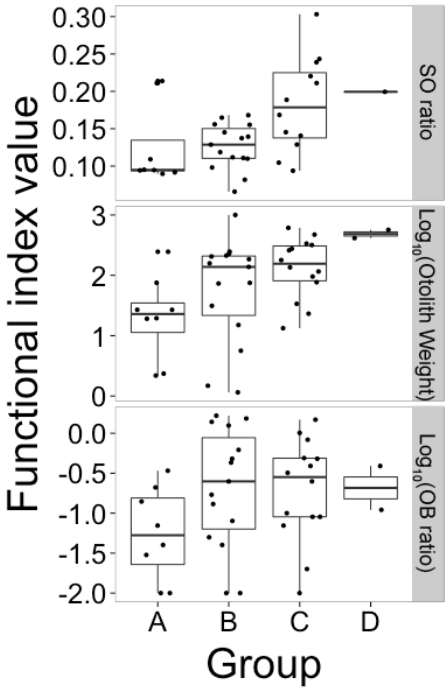

Figure 3.6. Values of functional indices between morphological groups.

3.3.4 Environmental effect (depth) on functional indices

SO ratio decreased with distribution depth of fish (linear regression, usual depth: n=36, R^2=0.362, t=-4.57, p<0.01; captured depth: n=36, R^2=0.342, t=-4.382, p<0.01) and the decreasing trends of SO ratio were significantly different between morphological groups (Fig. 3.7). The trends were significant in Group A and C rather than Group B when the usual and captured depth were applied to the model (usual depth: Group A: n=8, t=-2.77, p<0.01; Group B: n=15, t=-0.530, p=0.600; Group C: n=15, t=-2.49, p=0.0186; captured depth, Group A: n=8, t=-2.81, p<0.01; Group B: n=15, t=-0.275, p=0.785; Group C: n=15, t=-3.02, p<0.01). The regression model was not applicable in Group D because of only one species being included (*M. mora*, was removed from the analysis related to SO ratio).

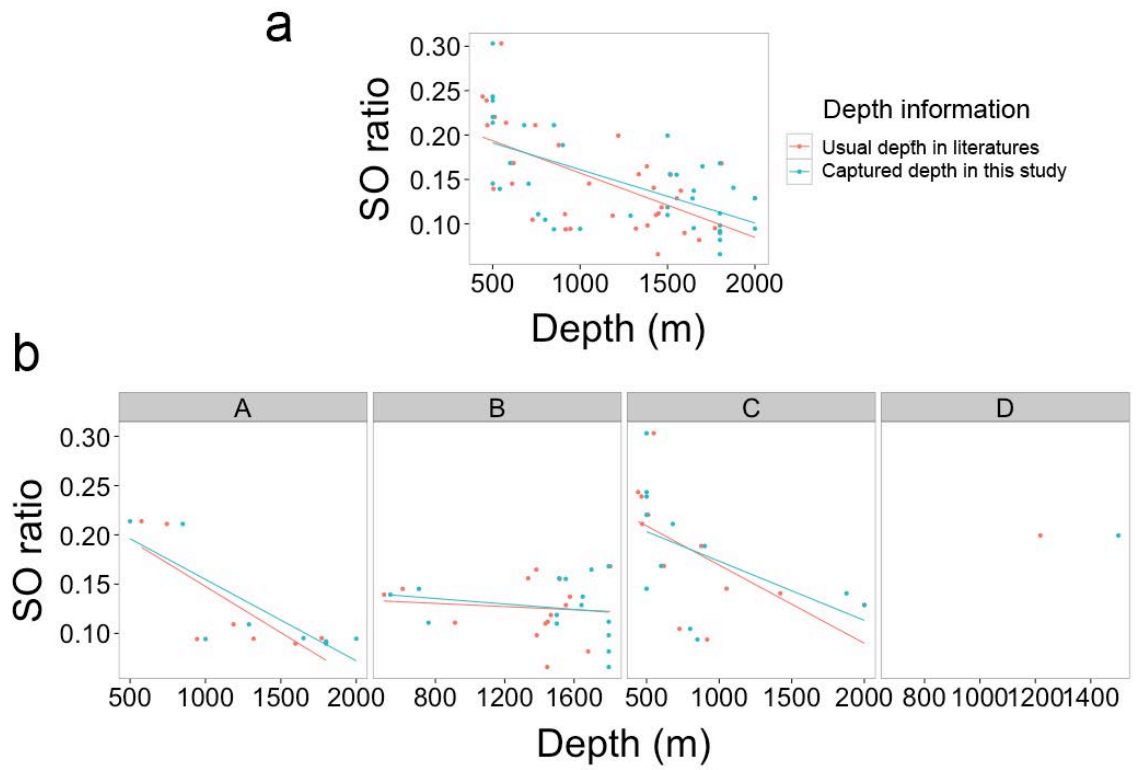

Figure 3.7. Regression of SO ratio on the depth of fish occurrences. (a) All species. (b) Three morphological groups.

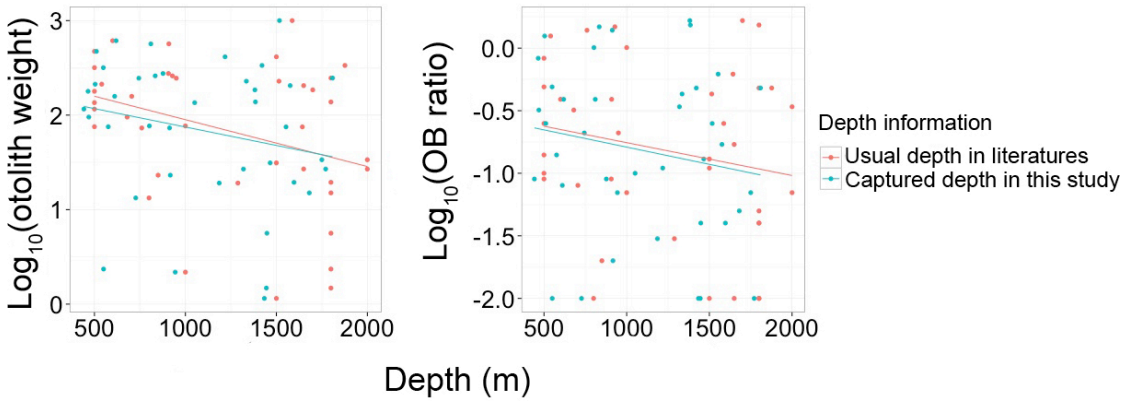

Figure 3.8. Regression of otolith mass-related indices on the depth of fish occurrences. The decreasing trends are not significant (statistical values shown in section 3.3.4).

The depth effect generally had no influence on mass-related indices. Although the otolith weight significantly decreased with captured depth, the explained variance was low, and the trend of usual depth on otolith weight was not significant (Linear regression, usual depth, log10-transformed otolith weight: n=39, R^2=0.0254, t=-1.41,

p=0.167; log10-transformed OB ratio: n=39, R^2=0.0118, t=-1.21, p=0.236. Captured depth: log10-transformed otolith weight: n=39, R^2=0.0961, t=-2.25, p=0.0308; log10-transformed OB ratio: n=39, R^2=0.0094, t=-1.17, p=0.251. Fig. 3.8).

3.3.5 Comparative analyses of independent contrast

Based on the phylogenetic tree built in the present study (Fig. 3.9), the phylogenetic signal, Pagel's λ, of each trait is shown in Table 1. Pagel's λ was 1 or close to 1 for five morphological indices that indicated an obvious phylogenetic relationship. In addition, functional indices also revealed the phylogenetic dependence (Table 3.2). According to phylogenetic ANOVA, all the functional indices have no significant difference between the four morphological groups (SO ratio: df=3, F=3.27, phylogenetic p=0.118; log10-transformed otolith weight: df=3, F=2.15, phylogenetic p=0.294; log10-transformed OB ratio: df=3, F=1.25, phylogenetic p=0.451). This implied that the functional behaviours associated with otolith morphology were all phylogenetically determined.

The apparent environment (depth) influence on otolith morphology should therefore be re-evaluated as a strong phylogenetic effect was found on functional indices. Considering the potential phylogenetic effect on both distribution depth and functional indices, PGLS was conducted, adjusting data to correct for the observed phylogenetic relationship between species in the linear regression model. Under PGLS regression, the relationship between depth and SO ratio was still significant (usual depth, PGLS: n=30, R^2=0.110, t=-2.14, p=0.041; captured depth, PGLS: n=30, R^2=0.211, t=-2.96, p<0.01). However, no significant relationship was observed between mass-related functional indices and depth, even when incorporating phylogenetic information (usual depth, log10-transformed otolith weight: n=30, R^2=-0.0136, t=0.783, p=0.440; log10-transformed OB ratio n=30, R^2=-0.0351, t=-0.133, p=0.895; captured depth, log10-transformed otolith weight: n=30, R^2=-0.0301, t=-0.392, p=0.698; log10-transformed OB ratio n=30, R^2=-0.0189, t=-0.687, p=0.498.).

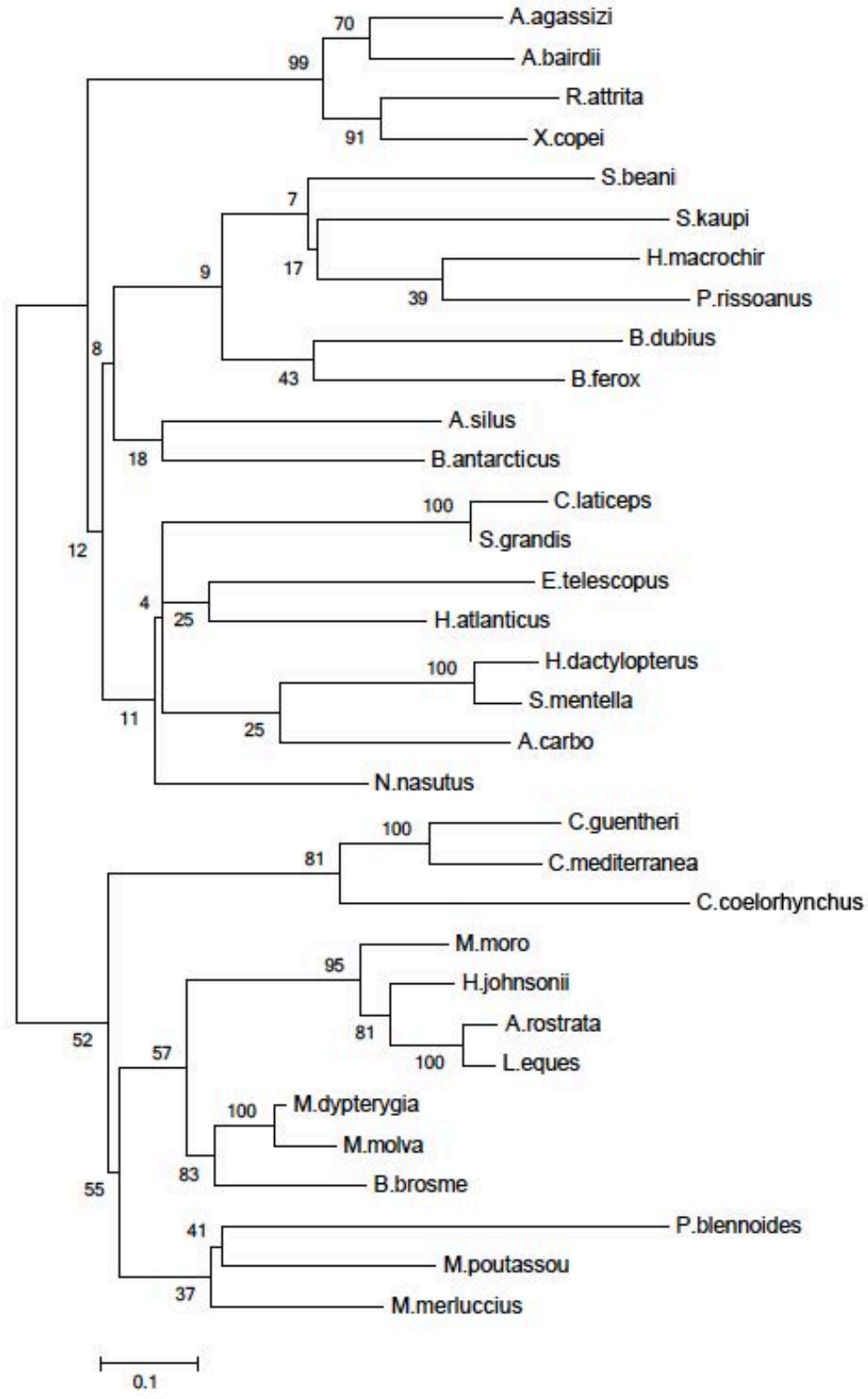

Figure 3.9. Phylogenetic tree of 33 deep-sea fishes established from partial COI genes. The numbers in each node are bootstrap replicate scores.

Table 3.2. Estimations of phylogenetic signals from each morphological and functional index and depth distribution. The superscript is the significance (p value) between empirical and theoretical λ value (left: λ=0; right: λ=1).

Variables	Pagel's λ
Formfactor	$1^{<0.01,\ 1}$
Roundness	$1^{<0.01,\ 1}$
Rectangularity	$0.969^{<0.01,\ 0.677}$
Circularity	$1^{<0.01,\ 1}$
Ellipticity	$1^{<0.01,\ 1}$
SO ratio	$0.939^{<0.01,\ 0.545}$
Log10-transformed otolith weight	$0.842^{<0.01,\ 0.141}$
Log10-transformed OB ratio	$0.995^{<0.01,\ 0.949}$
Usual depth	$0.862^{<0.01,\ 0.188}$
Captured depth	$0.962^{<0.01,\ 0.678}$

3.4 Discussion

3.4.1 Characteristics of functional indices

Sulcus area is correlated to otolith shape, and wider areas are observed from the irregular and elongate otoliths compared with the round and square otoliths. This reveals that the sulcus area develops along the otolith length rather than otolith width. However, the otolith shape is not purely characterized with one morphological index. For example, smoothheads with slightly irregular otoliths might be predicted to have higher SO ratios, but the roundness constrains the development of sulcus and has a negative effect on the SO ratio.

Both environment (depth) and phylogenetic effects influence the variation of the SO ratio in deep-sea fishes. The lower SO ratio observed in otoliths from fishes of the deeper ocean is under environmental constraint but specific fish taxa are more

successfully adapted to the extreme environment, such as grenadiers. Both driving forces also explain why the group C fishes, especially gadoids, have higher SO ratio but exist in the shallower layers.

Otolith weight considerably increases in more elliptical otoliths (and decreased in rounder otoliths), explaining higher otolith weight in group C than in group A. Considering fish body size (OB ratio), the otolith weight shows less discrimination between groups and a weak correlation with otolith morphology, because the large variations of OB ratio decrease the discriminative power.

Although the change of otolith size with depth has been found in the previous study (Lombarte & Crusz 2007), no significant relationship is found in our results; this may be caused by the fact that otolith weight is used instead of otolith area as a size indicator and the depth is not set as categories but as a continuous variable in this study.

Unsurprisingly, phylogeny, one of the factors influencing otolith size (Lombarte & Cruz 2007; Lombarte & Lleonart 1993), influences on the otolith weight and OB ratio. Group A with lower otolith size can be explained as being a composition of several fish orders with smaller otoliths, such as Osmeriformes and Stomiiformes. Therefore, phylogeny seems a primary effect on the difference of otolith size between groups. Compared to SO ratio, the phylogenetic effect is much stronger than the ecological influence on otolith size.

3.4.2 Food preferences between groups

The diet of many deep-sea fishes has been investigated by stomach content analysis. According to literatures, there appears to some strong similarities of food preferences within our groupings (Table 3.3). In group A, fishes can be described as benthopelagic feeders with a higher percentage of pelagic intakes. Particularly, macroplanktonic and benthopelagic organisms, such as jellyfish and crustaceans (copepods, mysids and decapods), are the dominant items in their diet compositions. There is one exception, *Lycodes atlanticus*, which feeds on benthos. In the classification, this species locates at the boundary between group A and B that may cause the bias of grouping, and their feeding behaviour closer to species in group B.

In group B, benthopelagic organisms are also important food sources, but bottom-living crustaceans and invertebrates, such as amphipods, polychaetes and echinoderms, account for a notable percentage in fish diet compositions. This kind of passive benthic feeding is observed from macrourids, spiny eels, cusk eels and one

gadoid, *Brosme brosme.* Although pelagic items are found in the diets of eels and tripodfish, *Bathypterois dubius*, these fish species are regarded as passive feeders according to their feeding strategy as scavenging and sit-and-wait (Gordon & Mauchline 1996; Sulak 1977).

The diet preferences of fishes in group C is similar to group B that the benthopelagic and benthic fauna are the dominant items, such as for morids (*Lepidion eques* and *Halagyreus johnsonii*) and redfish (*Sebastes mentella*). However, the importance of swimming prey, in terms of fish and cephalopods, increases. For example, *Phycis bennoides*, *Micromesistius poutassou*, *Centrolophus niger* and *Helicolenus dactylopterus* have diverse selectivity of food items from small planktonic crustaceans to active fish and squids. Furthermore, a wide variety of picscivory types is observed from gadoid (*Merluccius merluccius, Molva molva* and *Molva dypterygia*), morid (*A. rostrata*), scabbardfish (*Aphanopus carbo and Nesiarchus nasutus*) and deep-sea lizardfish (*Bathysaurus ferox*). Thus, compared to group B, groups C show a higher activity in feeding.

There are only two species, *M. moro* and *H. atlanticus*, in group D and they display high diversity in their diet composition, including crustaceans, invertebrate, cephalopods and fish.

Table 3.3. Diet preferences of fishes between otolith morphological groups. Trophic guild is based on the descriptions by Gartner *et al* (1997)

Group	Feeding characteristics	Trophic guild	Species	Primary dietary items
A	• Benthopelagic feeders with higher percentage of pelagic diets	• Macronekton foragers • Macroplanktonivores	*Argentina silus*	Salps and ctenophores[1]
			Alepocephalus agassizi	Ctenophores, crustaceans, echinoderms
			Alepocephalus bairdii	Medusa, mysids, decapods, squid and
			Rouleina attrite	NA
			Xenodermichthys copei	Copepods, ostracods and jellyfish[1]
			Borostomias antarcticus	Fish and cnidarians[3]
			Epigonus telescopus	Copepods, mysids and decapods[4]
			Lycodes atlanticus	Polychaetes and mollusks[5]
B	• Benthopelagic feeders with higher percentage of benthic diets • Benthic feeders • Passive feeders	• Macronekton foragers • Micronekton/epibenthos predators • Microphagous epifaunal browsers • Specialist necrophages	*Serrivomer beani*	Euphausiids and small fish[6]
			Synaphobranchus kaupi	Pelagic fish and decapods[7]
			Bathypterois dubius	Benthopelagic plankton[2]
			Brosme brosme	Mollusks and crustaceans[6]
			Coelorhynchus	Polychaetes and isopods[8]
			Coelorhynchus labiatus	Small fish, polychaetes and crustaceans[6]
			Coryphaenoides guentheri	Copepods, amphipods and mysids8
			Coryphaenoides	Copepods, amphipods and mysids[8]
			Coryphaenoides rupestris	Copepods[8]
			Nezumia aequalis	Copepods, mysids, polychaetes, isopods
			Trachyrincus murrayi	Decapods, copepods, amphipods and
			Halosauropsis macrochir	Amphipods, mysids and decapods[9]
			Polyacanthonotus rissoanus	Bottom invertebrates[6]
			Cataetyx laticeps	NA
			Spectrunculus grandis	Echinoderms and amphipods[4]

Table 3.3. (continued).

Group	Feeding characteristics	Trophic guild	Species	Primary dietary items
C	• Active foragers • Generalist feeders	• Piscivores • Macronekton foragers • Micronekton/epbenthos predators	*Bathysaurus ferox*	Fish[10]
			Merluccius merluccius	Euphausiids and small fish[11]
			Micromesistius poutassou	Euphausiids[12]
			Molva dypterygia	Fish and crustaceans[13]
			Molva molva	Fish and crustaceans[13]
			Phycis blennoides	Decapods, mysids and fish[14]
			Antimora rostrata	Fish, cephalopods and crustaceans[12]
			Halargyreus johnsonii	Copepods and mysids[12]
			Lepidion eques	Amphipods and decapods[12]
			Aphanopus carbo	Fish, cephalopods and crustaceans[6]
			Centrolophus niger	Plankton, pelagic crustaceans, fish and squids[6]
			Nesiarchus nasutus	Fish, squids and crustacean[6]
			Helicolenus dactylopterus	Widely feed on pelagic and benthic organisms[6]
			Sebastes mentella	Copepods and hyperiids[15]
D	• Active foragers	• Macronekton foragers	*Hoplostethus atlanticus*	Decapods, mysids, squids and fish[4]
			Mora moro	Decapods, cephalopods and fish[16]

[1]Mauchline and Gordon (1983); [2]Whitehead *et al*. (1984); [3]Gaskett *et al*. (2001); [4]Mauchline and Gordon (1984c); [5]Sedberry and Musick (1978); [6]Whitehead *et al*. (1986); [7]Gordon and Mauchline (1996); [8]Mauchline and Gordon (1984a); [9]Gordon and Duncan (1987); [10]Sulak *et al*. (1985); [11]Carte *et al*. (2009); [12]Mauchline and Gordon (1984b); [13]Bergstad (1991); [14]Morte *et al*. (2002); [15]Albikovskaya and Gerasimova (1993); [16]Carrassón *et al*. (1997).

3.4.3 Otolith morphology and functional behaviours between groups

Pelagic fishes have smaller otoliths than the demersal species and that could provide better acceleration abilities when fish chase pelagic prey (Lychakov & Rebane 2000). The relatively small otolith in pelagic fishes is also characterized by ornamented margins (Fig. 3.10), a prominent rostrum, the deep V-shaped excisure and higher SO ratio (Gauldie 1988; Lombarte & Cruz 2007; Volpedo & Echeverría 2003). Deep-water fishes in group A, especially smoothheads, have smaller otoliths than species in other groups, but their otolith has less ornamented margins and, most importantly, a lower SO ratio than typical epipelagic or mesopelagic fish. Volpedo *et al*. (2008) suggested that small otoliths with regular edges and low SO ratios are indicative of the "pelagization" of demersal fish. This means that demersal fish develop functions to live in the water column away from the bottom, behaving more like pelagic species. The predominant pelagic prey items in group A supports the assumption, but there is little phylogenetic or fossil evidence to support a benthic ancestry for smoothheads.

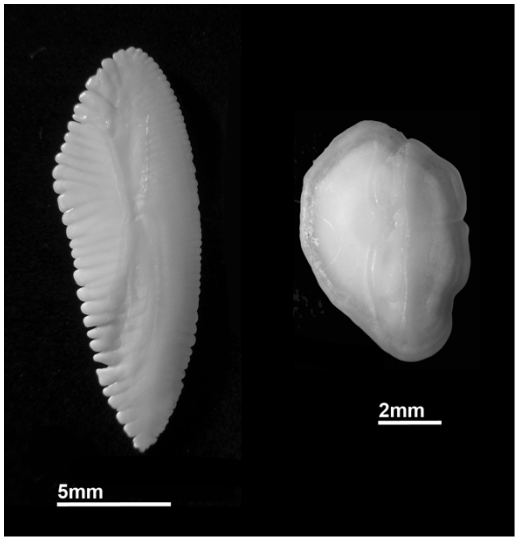

Figure 3.10. Two types of the otolith margin. *Merluccius merluccius* has ornamented margin, which means numerous lobes or domes observed around the edges of otolith (left). On the second hand, *Nezumia aequalis* has regular margin with smooth outline (right).

Typical demersal fish have large otoliths, which are recognized by two morphological types described by Volpedo and Echererría (2003). Fish living on soft

bottoms typically have polygonal or round otoliths with a less evident rostrum (as seen in group B fishes such as macrourids), whereas species associated with rocky substrate have elongate otoliths with ornamented margins and varieties of rostra. The latter is also found with higher SO ratios than the former (Aguirre & Lombarte 1999; Volpedo & Echeverría 2003). We postulate that fish associated with soft bottoms heavily rely on the benthos as benthic feeders, but, in a rocky seabed environment, fish must have better swimming ability to chase prey because less food is available from the bottom (Arellano *et al*. 1995). Elongate otoliths support the sulcus area development (proved in the present study) and that gives a better mobility ability. Although it is impossible to clearly classify the habitats of each deep-sea fish, our results verify the connections between otolith shapes, SO ratio and feeding behaviours based on the comparison between group B and C. First, the elongate otolith with the ornamented margin is a noticeable characteristic of group C and is coincident with higher SO ratio than the polygonal otolith of group B. Second, from the evidences of their diet preferences, group C fish feed on a higher percentage of swimming prey, indicating that they behave more actively. Third, the ornamented margins may result from higher food consumption (Hüssy & Mosegaard 2004), which is linked to the high metabolic rate in an active feeding mode. Note however, that our sample is constrained by sea bottom conditions conductive to trawl sampling (i.e. relatively flat, soft bottom ground). We hypothesise that group B fishes will be less abundant in rough grounds associated with (for instant) deep-water corals or canons.

Irregular otoliths are generally observed among pelagic fishes with small otoliths (Volpedo & Echeverría 2003), but *M. moro and H. atlanticus* (in group D) do have large otoliths. Thus, comparing with other morphological groups, group D has a higher SO ratio, larger otoliths and similar food preferences to group C, giving a preliminary conclusion that these two species may behave actively.

3.4.4 Depth effect on SO ratio

In order to further explain the decreasing trend of SO ratio with depth, the SO ratio was measured for wide range of marine fishes, including both shallow and deep-sea species using otolith images in Campana (2004). Although SO ratio was acquired from only one otolith photo in each species, up to 175 comparable species in 20 orders were analysed to minimize the bias from the low sample size and the ontogenetic change within species. The depth of fish occurrence and categories of fish habitat were extracted from Neat and Campbell (2013), FishBase (Froese & Pauly 2013) and Whitehead *et al*. (1984, 1986) (Appendix C). According to habitats listed in FishBase,

fish species were simply categorized as pelagic (relatively active) and demersal species (relatively passive foraging species, including benthopelagic and benthic fishes). SO ratio, from the dataset of 36 deep-sea species in the present study and 175 species in this section, was regressed on the mean value of occurrence depth and then by following the two categories of feeding behaviours.

A significant linear decrease of SO ratio with depth was already observed in the deep-sea species (Fig. 3.7). However, the SO ratio dramatically decreased at the shallowest layer above 500m when more species were taken into account, and the general trend of SO ratio exponentially decreased with depth gradients (Fig. 3.11). Therefore, considering the exponential relationship between SO ratio and distribution depth, the regression models mentioned in section 3.3.4 and 3.3.5 were conducted again and all showed significant decrease of SO ratio with depth, except for group B.

The integrated data including 211 species in total revealed significantly different depth-dependent trends of SO ratio between the two functional groups. The response was more pronounced in pelagic species (linear regression of log10-transformed depth on SO ratio, n=86, R^2=0.462, t=-8.61, p<0.01) than demersal fishes (linear regression, n=125, R^2=0.0905, t=-3.65, p<0.01) (Fig. 3.12). Below 500m, the SO ratio of pelagic foraging fishes dropped to a similar or lower level than the values of passive foraging species.

Two possibilities, associated with the auditory and vestibular function of otolith, are proposed to explain the observed relationship between SO ratio, depth and functional group. First, Aguirre and Lombarte (1999) pointed out that fish have higher SO ratios provide greater sensitivity to acoustic signals in a noisy environment. In fact, many factors, such as biological sources, wind, wave, storm and so on, make shallower layers of ocean noisier and the intensity of noise decreases with depth (Urick 1984). Ambient noise may impede fish from receiving acoustic signals to locate their prey, which clarifies shallower species having higher SO ratio for hearing sensitivities.

Second, a high SO ratio provides mobile fish with better vestibular capabilities whilst searching for and chasing their quarry (Arellano 2003; Gauldie 1988). With increasing depth, ambient temperature and light levels decrease, likely together with food availability and predator-prey interaction frequency, acting to reduce the selective pressure for active pursuit locomotion (Drazen & Haedrich 2012; Drazen & Seibel 2007). Thus, with an increase of depth, the functional demand of locomotion is getting lower, resulting in a decreasing trend of SO ratio.

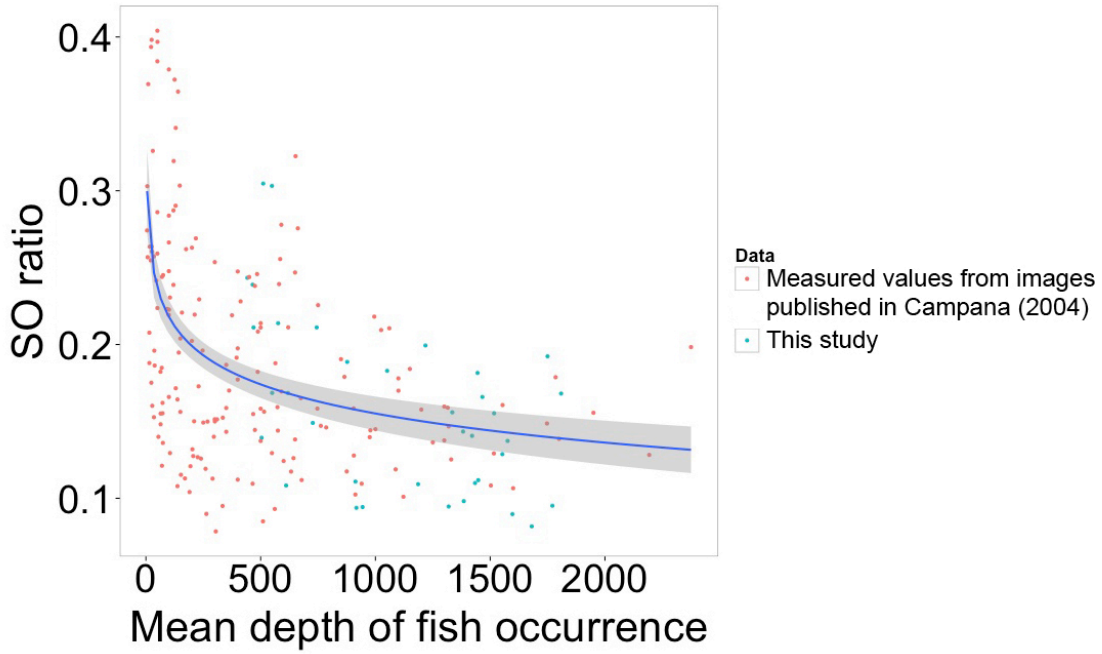

Figure 3.11. Relationship between fish habitat depth and SO ratio. An exponential decrease is observed from a wide range of fish species ($y=0.389x^{-0.130}$, $p<0.01$). The grey area is 95% confident interval.

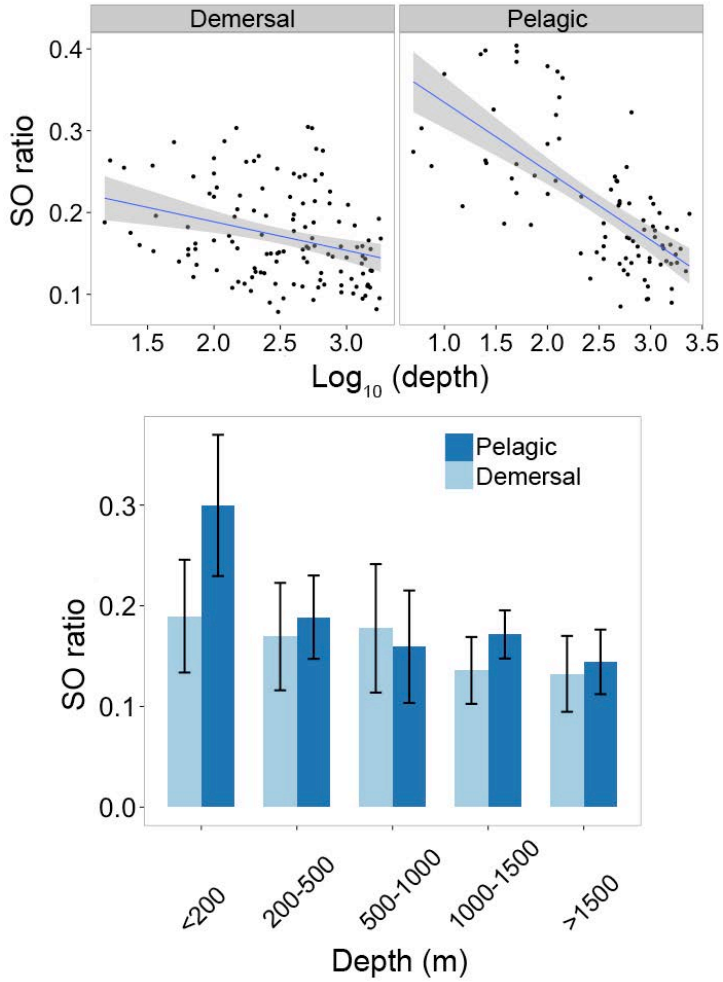

Figure 3.12. Trends of SO ratio between functional groups. (A) The SO ratio regressed on log_{10}-transformed depths with 95% confident interval (the dark grey area) (pelagic: $y=-8.42*10^{-2}x+0.419$; demersal: $y=-3.51*10^{-2}x+0.259$). (B) The change of SO ratio with depth categories. The error bars represent standard errors.

The SO ratio of fishes in group B, however, is not sensitive to depth, unlike groups A and C (Fig. 3.7). Group B fishes are predominantly benthic foragers, and their sense of smell and taste assist them in feeding more than hearing (Wagner 2001a; Wagner 2001b). Furthermore, foraging for cryptic, sessile or infaunal benthic prey reduce the need for active swimming ability even in shallow water. Although several species in group B are not benthic feeders, such as *S. kaupi* and *B. dubius*, they are still viewed as passive feeders. Compared to group B, fishes in groups A and C feed on more pelagic organisms and/or swimming prey (supported by the evidences of muscle $\delta^{15}N$ and $\delta^{13}C$ values discussed in the next section, Fig. 3.13). Thus, depth-dependent declines in SO ratio in group A and C reflect release of pelagic foragers from pressures of pursuing active prey in a noisy visual-based shallow water environment. Metabolic rates also decline faster with depth in pelagic compared to benthic fishes (Drazen & Seibel 2007) consistent with our explanations that active foragers respond to increases in depth more obviously than passive or benthic feeders.

Some species migrate to deeper habitats though growth, accompanied with an increase of SO ratio, for example the genus *Merluccius* (Lombarte 1992). This is a reverse trend between depths and SO ratio, compared to our results. A gradual function transformation in their life span may explain observed increases of SO ratio with depth. Particularly, juvenile European hake (*M. merluccius*) prey on benthic crustaceans and generally live between 100 and 200m, while adults are mostly piscivorous and move down to 750m (DuBui 1996; Bozzano *et al*. 1997). The change of feeding modes from benthic foraging to active foraging is also supported by changes of visual directions throughout their life (Bozzano & Catalán 2002). Therefore, in this case, the increase of SO ratio may be more associated with changes of life history traits from passive to active feeding rather than environmental driving forces.

3.4.5 Trophic structure

Stable nitrogen and carbon isotope signals in muscle tissues give clues of diet sources and trophic levels of organisms (Trueman *et al*. 2014). $\delta^{15}N$ and $\delta^{13}C$ values of four defined groups confirm that groups A and B are pelagic and benthic feeders, respectively (Appendix B, Trueman *et al*. 2014) (Fig. 3.13). $\delta^{13}C$ values indicate dietary preferences of group C in a wide range of organisms from pelagic to benthic prey items, but $\delta^{15}N$ values revel theses species having a relatively high trophic level more similar to fishes group B. These also imply fishes in group C connect the pelagic and

benthic food webs. Given their higher trophic level, group-C species may prey on larger pelagic animals compared to group A, and it further explains the different foraging activities (revealed by SO ratio) and trophic levels between these two groups. Although high $\delta^{15}N$ and $\delta^{13}C$ values are found in group D and similar to group B, group-D species are supposed to behave like group-C species as benthopelagic feeders according to the SO ratio, diet preferences and occurrence depth. Therefore, energy transportation is expected from the pelagic foragers (group A) to benthopelagic feeder (group C and D) and then to benthic feeders (group B) in the deep-sea fish ecosystem.

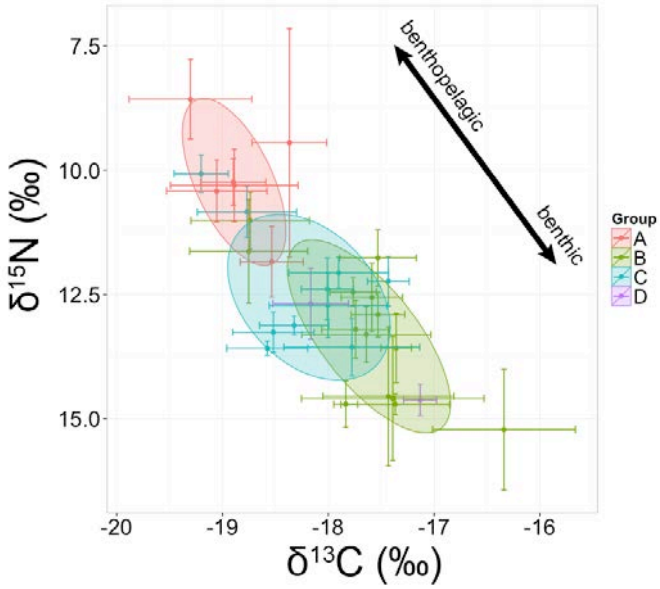

Figure 3.13. Stable isotope values in muscle tissues between otolith morphological groups. The reverse y-axis of $\delta^{15}N$ values demonstrates relative positions between benthopelagic and benthic fish in the water column above the sea floor.

3.4.6 Conclusions and future works

Otolith morphology has been discussed in the context of fish behaviours, and phylogenetic and environmental effects were mentioned to explain the diversity and variations of otolith shape. In addition, otolith functions regulated by otolith size and sulcus area have been pointed out in the previous research. By connecting several lines of evidences, this study assigns deep water species into ecologically meaningful functional groupings on the basis of otolith morphology, indicates the functional meanings of otolith shapes, and further clarifies the relationship between otolith functions and environmental or phylogenetic controls at a interspecies level. However, phylogenetic tests of functional traits in this study are based on own COI-derived

distance with limited genetic information, and it may bias the assessment of phylogenetic relationship between fish species. In order to resolving this issue, the future research works will be extended by integrating well-established phylogenetic information from literatures, such as revised taxonomy in the order Gadiformes (Roa-Varón & Ortí 2009) and a broad phylogenetic survey in teleosts (Near *et al*. 2012), and analysing a wider range of fish species.

Chapter 4: Otolith microchemistry reveals life history traits (vertical migration and metabolism) of four abundant deep-sea fishes

4.1 Introduction

4.1.1 Life history traits of fishes

Animals are traditionally classified as r or K selected according to their life history traits (MacArthur & Wilson 1967). Kawasaki (1980) expanded the classification for marine fishes as three types: (1) type IA corresponds to r selection, with traits such as short life spans, small sizes and early maturation; (2) type II corresponds to K selection with opposite traits to r selection, such as long life spans, large sizes and late maturation; (3) type IB which is an immediate type between IA and II with traits such as long-life spans and medium in size. Furthermore, Winemiller and Rose (1992) indicated three life-history modes from a model incorporating life history traits, phylogenetic information and ecological parameters: (1) opportunistic strategists maximizing population growth rate through a short life generation and high reproductive effort; (2) periodic strategists having long lifespan, late maturation, and large adult body size to maximize fecundities at specific age; (3) equilibrium strategists having higher juvenile survivorship though the provision of parental care and thus have relatively large eggs, lower productive effort and lower fecundity. No matter how life history traits are classified, the assemblage of life history traits expressed in a community reflects environmental selection pressure.

Deep-sea fishes are traditionally viewed as K-selected species or periodic strategists; however, it is likely that a spectrum of life history traits exists in any single slope assemblage. Fishes inhabiting the sea floor on the continental slopes experience some of the most extreme environmental gradients along depths (Gage & Tyler 1991). These environmental gradients, such as decreases of temperature, sunlight intensity and food availability make fish develop adaptive behaviours and life-history traits (Drazen & Haedrich 2012). For example, the increase of longevity found in deeper species reflects lower temperatures, potentially reduced food availability and consequently lower metabolic rates (Drazen & Haedrich 2012). Technical issues constrain the direct investigation of life history traits in deep-sea fishes, and thus this

study describes an approach using fish otolith chemistry as a tool to obtain more life history information.

4.1.2 Otolith microstructure and stable oxygen and carbon isotope

Elements comprising the otolith are derived from both ambient water (inorganic sources) and food (organic sources). The elements from both sources follow the same pathway going through blood plasma, and endolymph, and are finally deposited into the otoliths. Although the otolith is isolated from the external aqueous environment and surrounded by endolymph, the isotopic composition of oxygen in otolith aragonite is in equilibrium with (or close to) ambient waters, suggesting that the water is the primary source of oxygen (Thorrold *et al.* 1997; Kalish 1991a). Fractionation of oxygen isotopes between ambient water and otolith aragonite is temperature dependent, with greater exclusion of the heavy isotope at higher temperatures (Kalish 1991a; Kalish 1991b). According to Hoie *et al*. (2004), the relationship between temperature and $\delta^{18}O$ values in water and cod otoliths is expressed below:

$$\delta^{18}O_{oto} - \delta^{18}O_w = 3.9 - 0.2(T℃)$$

where $\delta^{18}O_{oto}$ and $\delta^{18}O_w$ represent the oxygen isotope values of the otolith and seawater, respectively. The isotopic composition of oxygen in ambient seawater ($\delta^{18}O_w$) is primarily regulated by salinity. Thus, if $\delta^{18}O_w$ is known or can be inferred, the isotopic composition of oxygen in the otolith is regarded as a tracer of fish movements across thermal gradients. As water temperature decreases systematically with depth on the continental slope, $\delta^{18}O_{oto}$ values serve as a tracer for ontogenetic vertical migrations of deep-sea fishes (Lin et al. 2012, Shiao et al. 2014).

The carbon in otolith aragonite is derived from dissolved inorganic carbon (DIC) in the ambient water, and metabolized organic carbon derived from food (Gauldie 1996; Schwarcz *et al*. 1998; Thorrold *et al*. 1997). The metabolically derived organic carbon has more negative isotope values than seawater DIC (typically depleted by more than 10 per mil). Mixing of the two carbon sources therefore drives the carbon isotope composition of otolith aragonite away from the environmental equilibrium. The relationship between $\delta^{13}C_{oto}$, $\delta^{13}C_{DIC}$ values and the proportion of diet-derived carbon in otolith aragonite can be described by a two-component mixing model (Schwarcz *et al*. 1998):

$$\delta^{13}C_{oto} = \mathrm{M}\,(\,\delta^{13}C_{diet}) + (1 - \mathrm{M})(\delta^{13}C_w) + 2$$

where M is the percentage of metabolic carbon in the otoliths, and $\delta^{13}C_{diet}$ and $\delta^{13}C_w$ are the incorporated isotope values from diet and ambient water, respectively.

The value of $\delta^{13}C_w$ varies by ~2‰ between ocean water bodies (Tagliabue & Bopp 2008). In contrast, the carbon isotope composition of potential prey tissues averages around -17‰ (Fig. 4.1). $\delta^{13}C_{oto}$ values are typically in the range 0:-6‰ (Kalish 1991b; Sherwood & Rose 2003), and estimates of M derived from the literature typically range from c. 10% in adult cod to around 30% in metabolically active fishes such as salmon and tuna (Schwarcz *et al*. 1998; Kalish 1991b).

Schwarcz *et al.* (1998) pointed out that a dietary shift and a decrease of metabolic CO_2 deposition result in an ontogenetic change in carbon isotope values (with examples of Atlantic cod, *Gadus morhua*). Sherwood and Rose (2003) further explained that feeding activity controlling metabolic rates plays a more significant role in the disequilibrium of otolith carbon isotope than the diet shift. As the majority of carbon in otoliths is derived from DIC, $\delta^{13}C_{oto}$ values are more sensitive to variation in metabolic rate and $\delta^{13}C_w$ than $\delta^{13}C_{diet}$. Moreover, in the North East Atlantic, $\delta^{13}C_w$ value is estimated at about 1‰ and the depth-dependent variation is less than 0.8‰ (Kroopnick 1985). Following these examples and observations, carbon isotope values recorded in otoliths can provide a tool with which to illustrate the ontogenetic changes of metabolism.

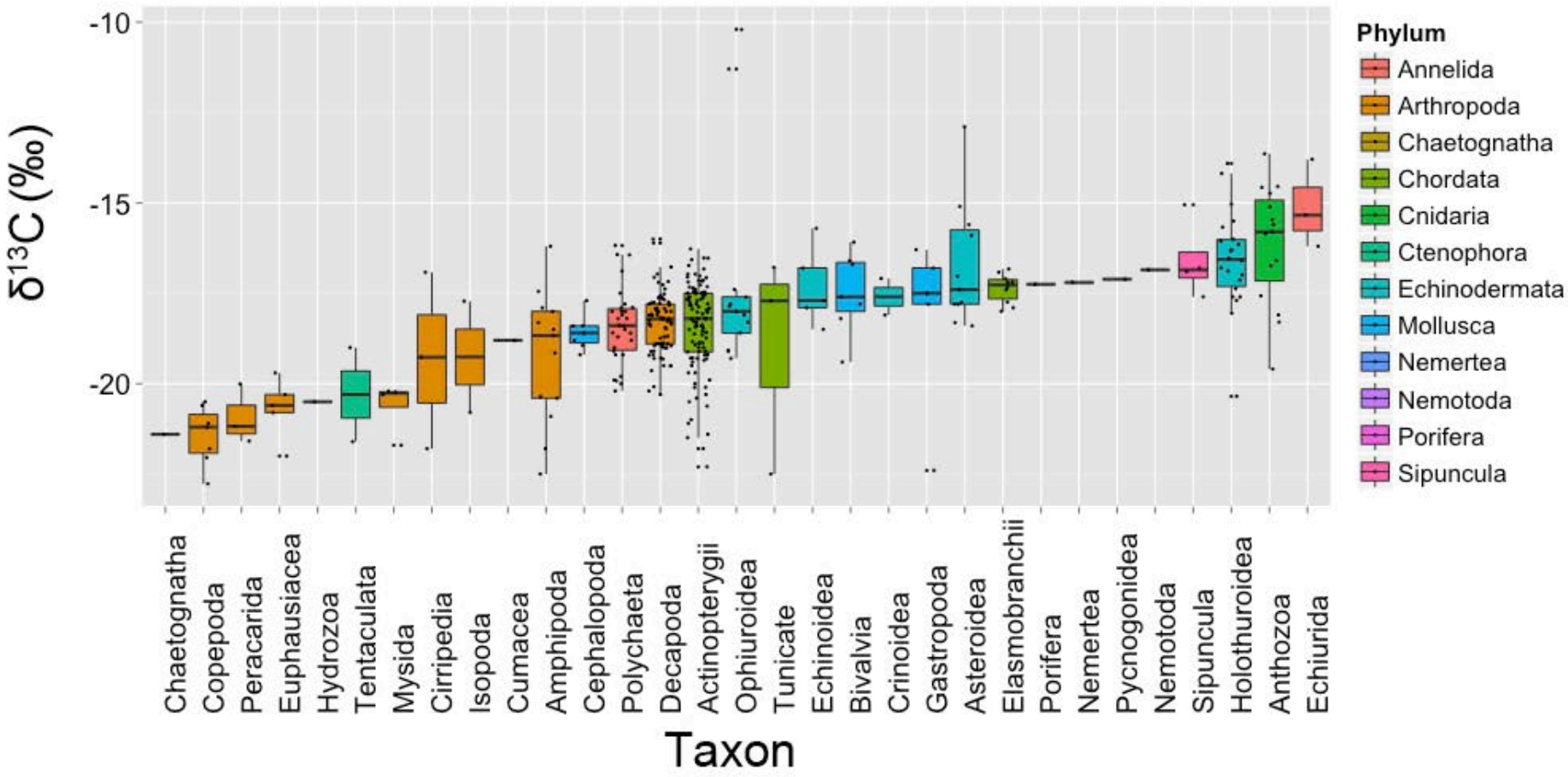

Figure 4.1. $\delta^{13}C$ values of potential dietary items for deep-sea fishes (Boyle *et al*., 2012; Iken *et al*., 2001; Polunin *et al*., 2001; Renaud *et al*., 2011; Sherwood & Rose 2005).

4.1.3 Aim

This study tries to establish life history traits based on otolith stable isotope composition in four model deep-water demersal species, *Alepocephalus bairdii*, *Coryphaenoides rupestris*, *Antimora rostrata* and *Spectrunculus grandis*. The chosen species are abundant in the Rockall area, inhabit similar depth strata of the Northeast Atlantic and show different diet preferences and trophic guilds (Mauchline & Gordon 1983; Mauchline & Gordon 1984a; Mauchline & Gordon 1984c; Mauchline & Gordon 1984b). Their life spans, growth rates and fecundity have been primarily investigated and indicate that these species have different functional or feeding behaviours (traits) to adapt in the deep-sea environment (Mauchline & Gordon 1983, 1984a, 1984b; Allain & Lorance 2000; Magnússon 2001; Fossen & Bergstad 2006; Lorance *et al*. 2008 and citations therein). However, not all life history traits in each species are well known, especially migration patterns and metabolic ecology. Therefore, this study tries to reconstruct ontogenetic migrations and ontogenetic variation in metabolic rates, and to determine whether fishes with differing diet behaviours has contrasting life history traits.

4.2 Materials and Methods

4.2.1 Sampling

Fish samples were collected from the Rockall Trough area based on annual deep-water fisheries' trawl surveys in 2012 undertaken by Marine Scotland-Science. Four target species were collected from a depth range of 1000-2000m along the continental slope of Rockall Trough (Fig. 2.3) and measured in terms of body weight and length (Table 4.1). Paired sagittal otoliths in each individual were extracted from the cranium, cleaned, dried and reserved in plastic trays.

Table 4.1. Sample information. SL: standard length; PANL: pre-anal fin length; TL: total length. *Used in stable isotope analyses.

Body length (SL, cm)	Body weight (g)	Average numbers of growth rings	Capture depth (m)	Body length (PANL, cm)	Body weight (g)	Average numbers of growth rings	Capture depth (m)	Body length (TL, cm)	Body weight (g)	Average numbers of growth rings	Capture depth (m)
Alepocephalus bairdii				*Coryphaenoides rupestris*				*Antimora rostrata*			
80	3930	26	1500	20	1374	39	1500	58*	1872	23	1800
79*	3546	24	1500	19	1408	36	1500	59	1500	21	1800
78	3442	22	1500	18	1196	33	1500	57	1660	26	1800
72	3346	21	1000	18	1026	35	1500	55*	1457	22	2000
68	3662	18	1000	17	952	33	1500	53*	1040	16	2000
68	3360	21	1000	17	936		1500	52	1250	24	2000
68	2154	20	1500	17	908	34	1500	52*	1169	18	2000
66*	2986	22	1000	16.5	910	32	1500	52	1134	17	2000
66*	2696	19	1000	16*	900	28	1500	52*	993	17	1800
65	2268	16	1000	16	862	33	1500	42	498	13	1800
64	2758	17	1000	15*	722	23	1500	34	271	11	1800
62	2400	16	1000	14	466	21	1500	27	124	8	1800
61	2376	18	1000	12.5	388	15	1500				
61*	2350	17	1000	12*	378	15	1500	*Spectrunculus grandis*			
52	896	13	1500	10.5	232	12	1500	51	834	37	1800
48	778	13	1500	8.5	120	10	1500	48*	658	34	1800
46	576	11	1500	8	104	10	1500	47*	542	31	1800
								46	606	27	1800
								44	454	25	1800
								43	490	25	1800
								43	436	27	1800
								43	382	24	1800
								42*	472	22	1800
								37	262	22	1800

4.2.2 Otolith thin section preparation and examination of growth rings

Fish age can be estimated by counting growth rings from whole otoliths (Kelly *et al*. 1999; Morales-Nin & Sena-Carvalho 1996; Sequeira *et al*. 2009; Filiz *et al*. 2006; Allain & Lorance 2000) or sectioned otoliths (Kelly *et al*. 1999; Sequeira *et al*. 2009; Allain & Lorance 2000; Casas & Pineiro 2000). However, the sectioned otolith provides a higher resolution of otolith microstructure and is suitable for studying the whole life of individual deep-sea fish, because the rings are less identifiable in whole otoliths in species with high longevity. Increment age assessment assumes that each increment represents a year of life. Annual increment formation has only been directly validated in a few deep-water fishes (e.g. rockfish, orange roughy). Here we assume annual increment formation but accept that this validation may be incorrect. Considering the micromilling in the following steps, the transverse plane of the otolith is determined as the sectioning plane. In the micromilling, the z dimension is not easy to control for the growth ring discrimination. Therefore, as the z-axis in the micromilling is set along the maximum growth axis of the otolith (in terms of transverse plane sectioning), it could minimise the bias of controlling growth ring numbers (Fig. 4.2).

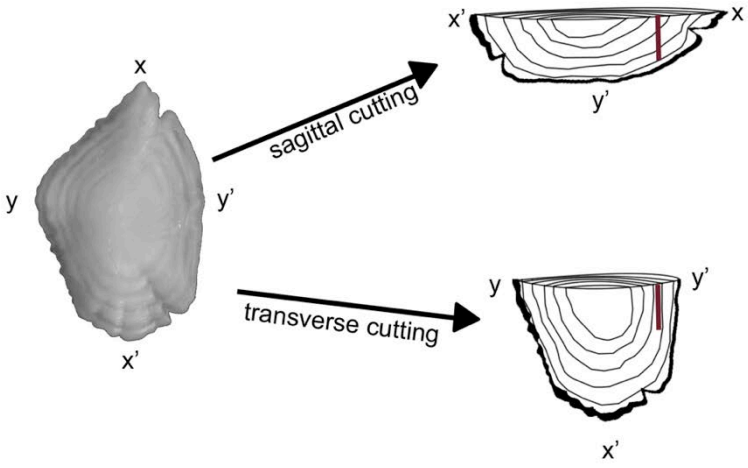

Figure 4.2. Cutting planes of otoliths. If the depth (z dimension) of drilling is set as the same value (red bands) in two different cutting planes, the growth ring is much easier to control in the same number (or fewer numbers) when the transverse plane is applied.

Otoliths were embedded in epoxy resin (the epoxy clod mounting of mixture of resin and hardener, Epofix Kit, Struers Ltd.) and then cut by a Buehler Isomet Low Speed Saw with 102 mm x 0.3 mm Diamond Wafering Blade. If the core was vague and hidden behind the cutting plane, this section was ground with grit paper until the nucleus showed on the surface of the sections. The final step of polishing was conducted with diamond suspension in a sequence from 15, 9, 6, 3, to 1μm grit size (Buehler Metadi Diamond Suspension). Each section was controlled, 0.9-1.0 mm thick, during the procedure and the thickness was thin enough to observe growth rings under the microscope with transmitted light, but still thick to provide a sufficient sample amount (in z dimension) in micromilling.

Otolith section profiles were examined under a stereomicroscope, Nikon SMZ800, and photographed with Qimage. Based on the periodic pattern of alternations of opaque and translucent bands, the growth rings in each otolith were counted in three repeats (monthly intervals). The counting was conducted with ImageJ. The average value of age in each individual was applied in a von Bertalanffy growth equation:

$$L_t = L_\infty\left[1 - e^{-k(t-t_0)}\right]$$

where L_t is the body length at age t, L_∞ the mean theoretical maximum total length, k the growth rate parameter (year^{-1}) and t_0 the theoretical age at zero length. Secondly, according to the fact that otolith length increases in proportion to fish length (Campana 2004), the width of each otolith increment was measured and accumulated widths (from the core to the ring at age t) were used as an index of the fish body length at age t. This procedure double-checked the growth rate value, k.

4.2.3 Microdrilling and stable isotope analyses

Five otoliths of larger individuals in each species were micromilled in high temporal resolution by a computer-controlled micromill (NewWave Research). Each drilling area was set as 2.2 x 10^7 μm^3 with a constant depth (z dimension) of 200 μm to provide a minimum of 30 μg of aragonite powder for stable isotope analysis. The theoretical size of the drilling area was calculated from an assumed otolith density of 2.3 g/ml^3 of otolith density (Hunt 1992) and 60% recovery of otolith powder collections. Samples were analysed with the isotope ratio mass spectrometer at Stable Isotope Laboratory, University of East Anglia, and the isotope value followed the δ notation related to the Pee Dee Belemnite (PDB) standard:

$$\delta = \left(\frac{R_{sample}}{R_{standard}} - 1\right) \times 1000\ ‰$$

where *R* is the $^{18}O/^{16}O$ or $^{13}C/^{12}C$ ratio in the sample or the standard.

4.2.3.1 Stable oxygen isotope

According to the equation described above ($\delta^{18}O_{oto} - \delta^{18}O_{water}$ = 3.9-0.2*T°C), the relationship between $\delta^{18}O_{oto}$ and ambient water temperature was established and based on a relative shallower species, Atlantic cod (*Gadus morhua*). Thus, in order to investigate deeper water species, we examined the relationship of $\delta^{18}O_{oto}$ and ambient water temperature in the Rockall area and established the temperature equation. The equation incorporated $\delta^{18}O_{oto}$ values at the outermost portion of otoliths and temperature at captured depth in 4 of our target species from 1000m to 2000m, and 17 species from 500m to 1500m published in Trueman et al. (2013). The seawater $\delta^{18}O_{water}$ value was calculated with known salinity according to the equation from (Craig & Gordon 1965) :

$$\delta^{18}O_{water(SMOW)} = (-21.6 + 0.61S)$$

where S is the salinity and the $\delta^{18}O_w$ value is relative to Standard Mean Ocean Water (SMOW). The seawater temperature and salinity with depth gradients were acquired from the International Council for the Exploration of the Sea (ICES) oceanographic CTD database (http://ices.dk/marine-data/Pages/default.aspx) (Fig. 4.3).

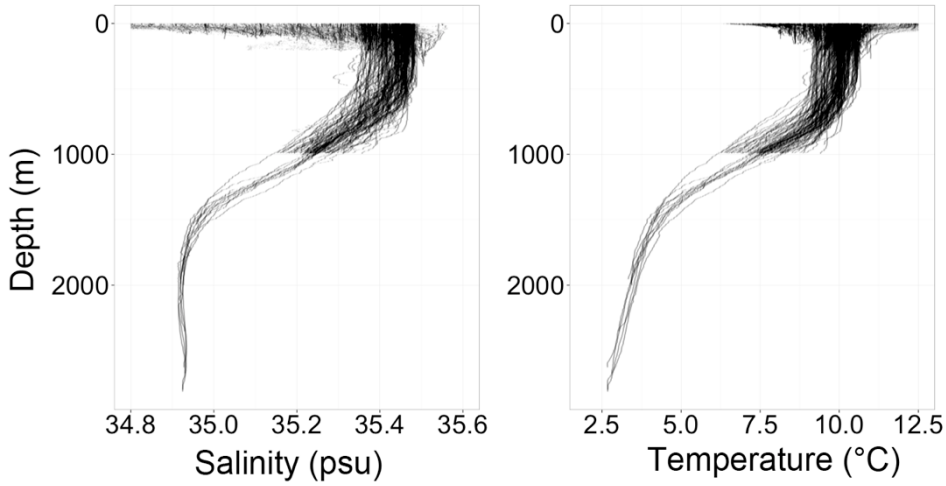

Figure 4.3. Temperature and salinity profiles in depth gradients in the survey of the area as 8-12°W and 53-60°N from 2010-2013. (Data source: ICES oceanographic CTD database).

4.2.3.2 Stable carbon isotopes

In order to use stable carbon isotopes to provide a reliable proxy for metabolic rates of fish, two aspects should be considered: (1) factors that influence the relationship between $\delta^{13}C_{oto}$ values and metabolic rates, such as $\delta^{13}C_w$ and $\delta^{13}C_{diet}$ values; (2) factors that directly influence metabolic rates, such as ambient temperature, growth rates, body size and foraging activity. To answer the first question, the mass balance equation from Schwarcz et al (1998) was used:

$$\delta^{13}C_{oto} = \mathrm{M}\,(\,\delta^{13}C_{diet}) + (1 - \mathrm{M})(\delta^{13}C_w) + 2$$

The relationship between $\delta^{13}C_{oto}$ values and M was predicted by the following assumptions: $\delta^{13}C_{diet}$ values were taken from $\delta^{13}C$ values measured in muscle tissues ($\delta^{13}C_{muscle}$) from deep demersal fishes from the Rockall Trough (Trueman unpublished data, Table 4.2). The expected $\delta^{13}C_{diet}$ was reasonably located in the range of potential $\delta^{13}C_{diet}$ values (-13~-22‰, Fig. 4.1) of deep-sea fishes. $\delta^{13}C_w$ values considerably varied above 100m, but below this depth, the value kept a constant value around 1‰ (as a range between 1.18 and 0.85‰) in the Northeast Atlantic (Kroopnick 1985) and thus the $\delta^{13}C_w$ value was simply assumed as 1‰. Furthermore, we applied the mass balance equation to $\delta^{13}C_{oto}$ data from four target species to examine the difference between estimated relative metabolic rates of the two life stages (juveniles and adults) and to evaluate the diet preference effect on ontogenetic changes of $\delta^{13}C_{oto}$ values. $\delta^{13}C_{oto}$ values of otolith core and the most outer portion represented the values in the juvenile and adult stage.

For the second question, three factors were taken into account. First, any ontogenetic downward migration causes a decrease of ambient temperature, which will reduce the metabolic rate. According to the metabolic theory of ecology (Brown et al. 2004), metabolic rates increase exponentially with temperature:

$$Metabolic\ rate \propto e^{-\frac{E}{kT}}$$

$$log(Metabolic\ rate) \propto -\frac{1}{T}$$

E is the activation energy, k is Boltzmann's constant and T is the absolute temperature (K). Therefore, $\delta^{18}O_{oto}$ values were used to estimate the expected temperature effect on metabolic rates and compared to $\delta^{13}C_{oto}$ values. Second, the growth rate has been observed as a proportional increase with metabolic rates in organisms (Weiser 1994)

causing the disequilibrium of otolith carbon isotope values (Thorrold *et al*. 1997). As otolith growth-ring widths reflect the somatic growth rates (Reichert *et al.* 2000), the increment widths were used to evaluate the influence of growth rates on metabolism. Third, higher body mass increases whole body metabolic rates (but decreases mass-specific metabolic rates), which may further influence $\delta^{13}C_{oto}$ values throughout the ontogeny. Previous studies pointed out that $\delta^{13}C_{oto}$ values become more positive (lower metabolic rate) with increasing fish size, demonstrating that $\delta^{13}C_{oto}$ values reflect mass-specific metabolic rates rather than the whole-animal metabolic rates (as expected given the isotopic effect is caused by the proportional amount of metabolically-derived carbon relative to the total blood carbon). To calculate size at age, the otolith accumulated increment width was taken as a measure of size at age, as the index of fish length at age *t* was determined above, and the reconstructed length was applied to length-weight relationship, extracted from Neat and Campbell (2013), to back-calculate the body mass (more explanations in Fig. 4.4).

Metabolic theory predicts the relationship between mass-specific metabolic rates and mass as:

$$Metabolic\ rate \propto Mass^{-\frac{1}{4}}$$

$$log(Metabolic\ rate) \propto log(Mass)$$

Thus, we can establish body mass from otolith accumulated increment widths and compare $\delta^{13}C_{oto}$ values to body mass index following the equation shown above .

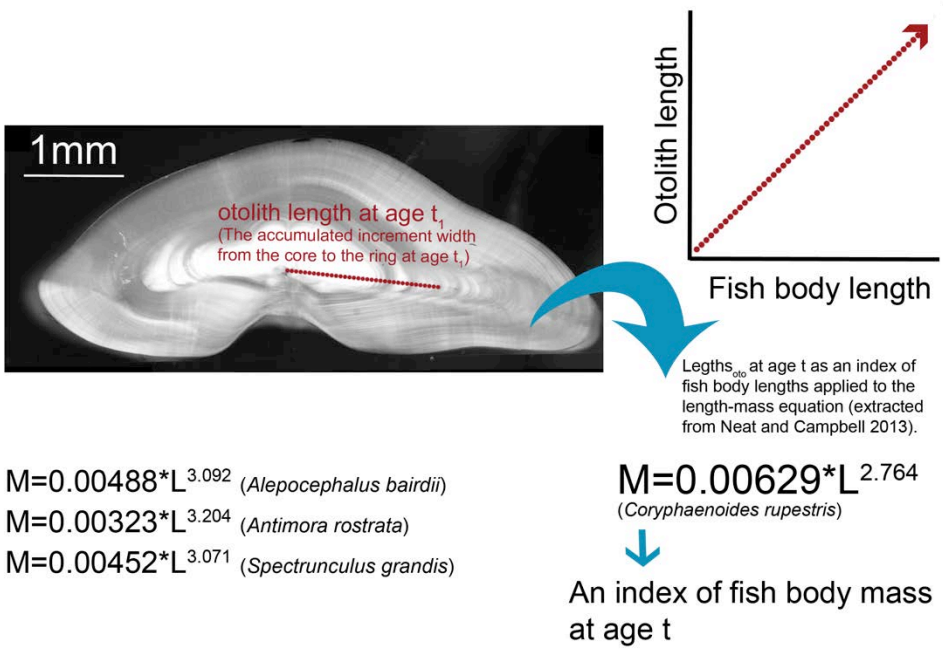

Figure 4.4. Using otolith length as an index of fish body lengths to calculate the body mass index at each age. For example, the accumulated otolith length at age t_1 is X_1 mm (from the otolith core to the ring at age t_1 along the maximum growth axis), and then the value X_1 is applied to the length-weight relationship equation to calculate the body mass index Y_1. Repeating the measurements and calculations, we can acquire body mass index values $Y_{1\ to\ n}$ through the life of each individual. These mass index values do not represent the exact fish body mass but provide the relative mass variance through the ontogeny and let us assess ontogenetic-related mass variance influencing on $\delta^{13}C_{oto}$ values.

Finally, these three metabolism-related factors were combined within a multiple linear regression model to explore ontogenetic influences on the otolith $\delta^{13}C_{oto}$ values. Model residuals were explored to examine the chronological pattern of mass and temperature corrected $\delta^{13}C_{oto}$ values in each species to explain weather other possible factors, especially the foraging activity, influence on ontogenetic variations of $\delta^{13}C_{oto}$ values. All statistical analyses were conducted with the software R (R Development Core Team 2012).

4.3 Results

4.3.1 Growth rate

Limited captures of juvenile deep-sea fish and insufficient samples may bias the growth rate estimated by fish body length. Thus, this study applied the otolith length (the accumulated increment width) on the back-calculation of fish size in order to obtain a relative growth rate. This procedure had several advantages: (1) each sample provided not only one length data point but also considerable data at different ages; and (2) it double-checked the rationality of the age determination and the growth rate. As a result, the growth rates (*k*) estimated from the fish body length and otolith increment width were recorded, as shown in Figure 4.5. In all cases, previously determined estimates of growth rates were consistent within error with the new data (Fig. 4.5). According to the results, *A. rostrata* had a relatively higher growth rate than the other three species.

Juvenile growth in four species was reconstructed following the equation published by Campana (1990):

$$L_t = L_c + (O_t - O_c) \times (L_c - L_i) \times (O_c - O_i)^{-1}$$

where L and O represent the fish body length and otolith radius, respectively. L_t and O_t are values at the age *t*, and O_t was derived from the accumulated widths of growth increments, which have been measured in the microstructure analysis. L_c and O_c are the captured fish body length and the maximum otolith radius on the sectioning plane. L_i and O_i are the biological intercepts, the values at age 0 from the von Bertalanffy growth curves established before (Fig 4.5). This equation is considering individual variance of growth and taking account the Rosa Lee's phenomena (the great growth rate in the older fish) (Campana 1990; Ricker 1969; Thresher *et al*. 2007). These effects can be corrected by the otolith microstructure because increment widths indicate growth rates in fish individuals. The reconstructed juvenile growths were shown in Figure 4.6, revealing the growth rate in the early life is slower for the *S. grandis* compared to other three species.

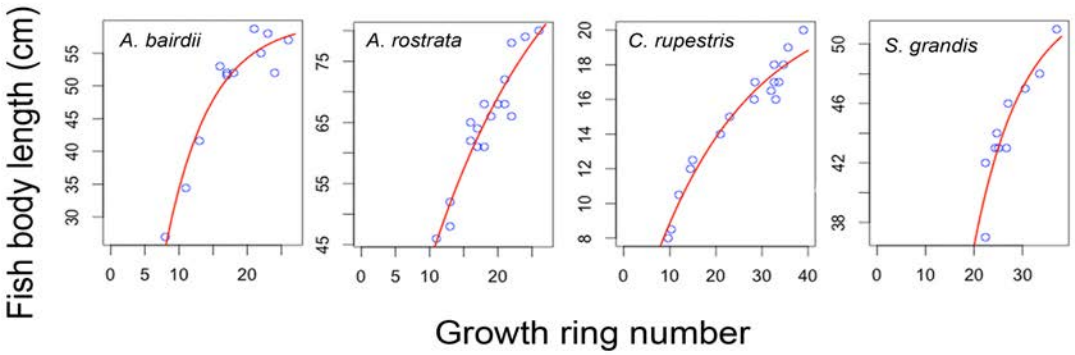

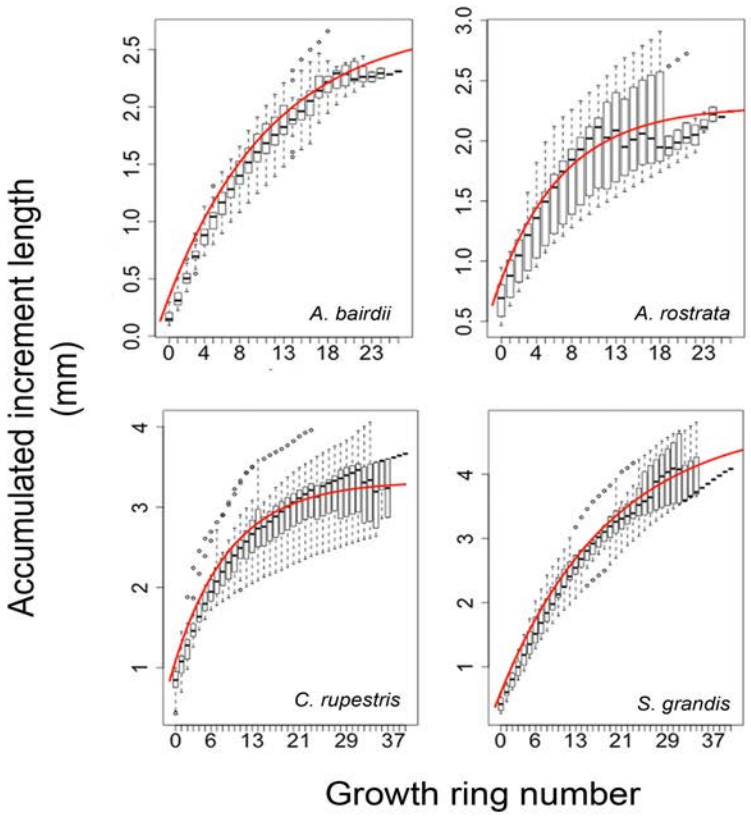

	A. bairdii	*A. rostrata*	*C. rupestris*	*S. grandis*
$k_{fish\ body\ length}$	0.054±0.042	0.15±0.040	0.047±0.020	0.099±0.082
$k_{otolith\ increment\ length}$	0.084±0.0052	0.13±0.019	0.10±0.0071	0.052±0.0039
$k_{references}$	0.077[1]	0.10[2]; 0.089[3]	0.03-0.128[4]	NA

Figure 4.5. Estimated growth rates of four target species. The growth rate value, k, is estimated with fish body length and otolith length in this study and the values in literatures are estimated from fish body length ([1]Allain and Lorance 2000; [2]Fossen and Bergstad 2006; [3]Magnússon 2001; [4]Lorance *et al*. 2008 and citations therein).

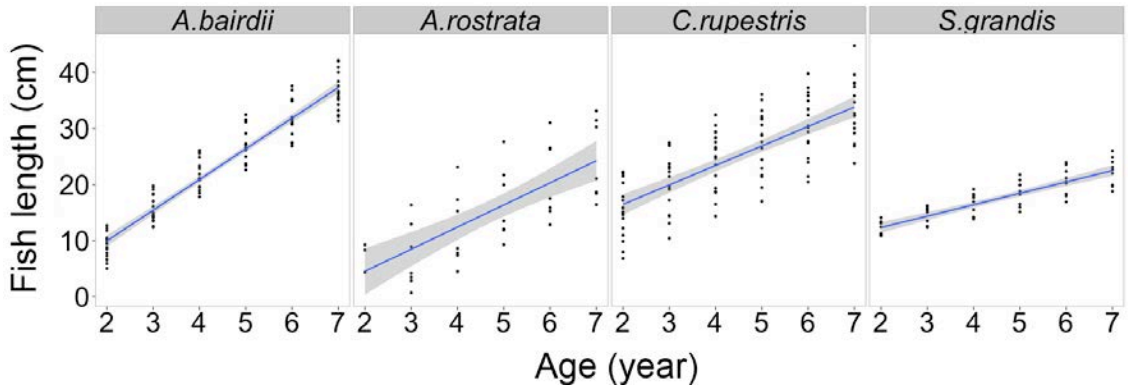

Figure 4.6. Reconstruction of juvenile growth in four representative species. Fish length is transferred to total length in all species. The comparison is based on the age between 2 and 7 years, in which four species show obvious changes in growth rate observed from otolith increment widths.

4.3.2 Predicted otolith oxygen isotope values with respect to depth gradients

The relationship of $\delta^{18}O_{oto}$ values and temperature showed a significant trend in deep-sea fishes (n=25, t value=-8.25, R^2=0.736, p<0.01). The temperature equation was expressed as:

$$\delta^{18}O_{oto} - \delta^{18}O_{water(SMOW)} = 4.12(\pm 0.182) - 0.272(\pm 0.0276)(T℃)$$

Based on the temperature equation and observed temperature and salinity gradients from 2010 to 2013 in the Rockall area, we applied the Monte Carlo simulation to predict $\delta^{18}O_{oto}$ values throughout the depth range studied (Fig. 4.7). Predicted $\delta^{18}O_{oto}$ values showed a sharp gradient in 750-1500m, with relatively consistent values above 750m and below 1500m. Above 750m, seawater temperature and salinity showed annual and seasonal variations but was relatively steady in the mixed layer regarding to depth gradients compared to the values in depth range of 750-1500m. Below the mixed layer, observed temperature and salinity sharply decreased, contributing to a greater sensitivity in $\delta^{18}O_{oto}$ values. The salinity kept constant in deeper waters over 1500m and the temperature dominantly influenced on $\delta^{18}O_{oto}$ values. However, the acquired variable $\delta^{18}O_{water(SMOW)}$ values in relation to salinity was based on surface water in the North Atlantic Ocean (Craig & Gordon 1965) (section 4.2.3.1) and its application to the deeper waters in this study could cause bias of expected $\delta^{18}O_{oto}$ values, particularly if differing water masses mix.

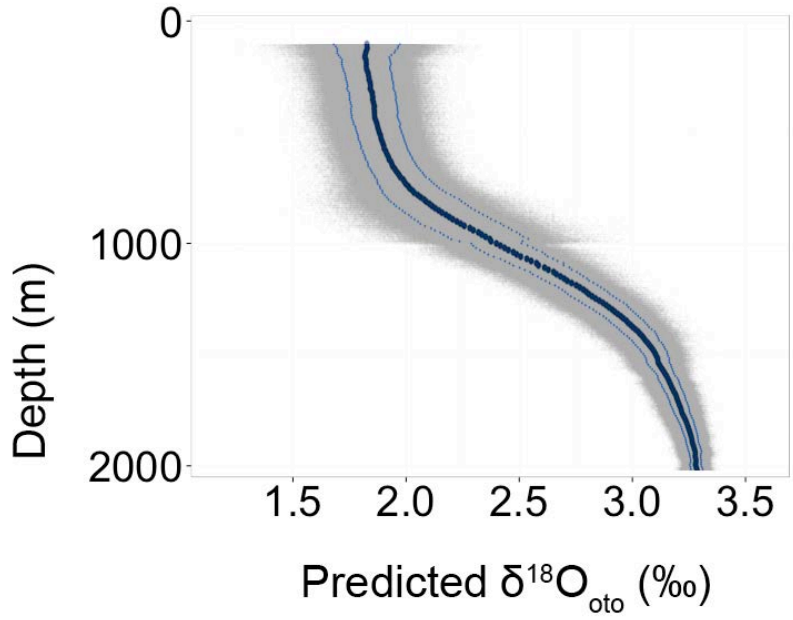

Figure 4.7. Monte Carlo simulation of predicted $\delta^{18}O_{oto}$ values in depth gradients based on the temperature equation established from deep-sea species. The grey dots are predicted values under 10000 simulations at every 10m-interval depth stratum. The dark blue dots are mean values at each depth stratum and light blue dots represent one standard deviation.

4.3.3 Ontogenetic trend of otolith oxygen isotope values in four target species

Ontogenetic increases of $\delta^{18}O_{oto}$ values were found in all investigated species other than the morid *A. rostrata*, which showed almost constant $\delta^{18}O_{oto}$ values of 3.0-3.5‰ (Fig. 4.8). $\delta^{18}O_{oto}$ values in *S. grandis* and *C. rupestris* ranged from 1.8 to 4.1‰ and 1.6 to 3.9‰, respectively, and *A. bairdii* showed a narrower range between 2.6 and 3.9‰. Ontogenetic increases in $\delta^{18}O_{oto}$ values are sharp in the early life stages of *S. grandis* and *C. rupestris* but gentle and continuous for *A. bairdii*. Juvenile size in relation to temperature in terms of locations was shown in Figure 4.9.

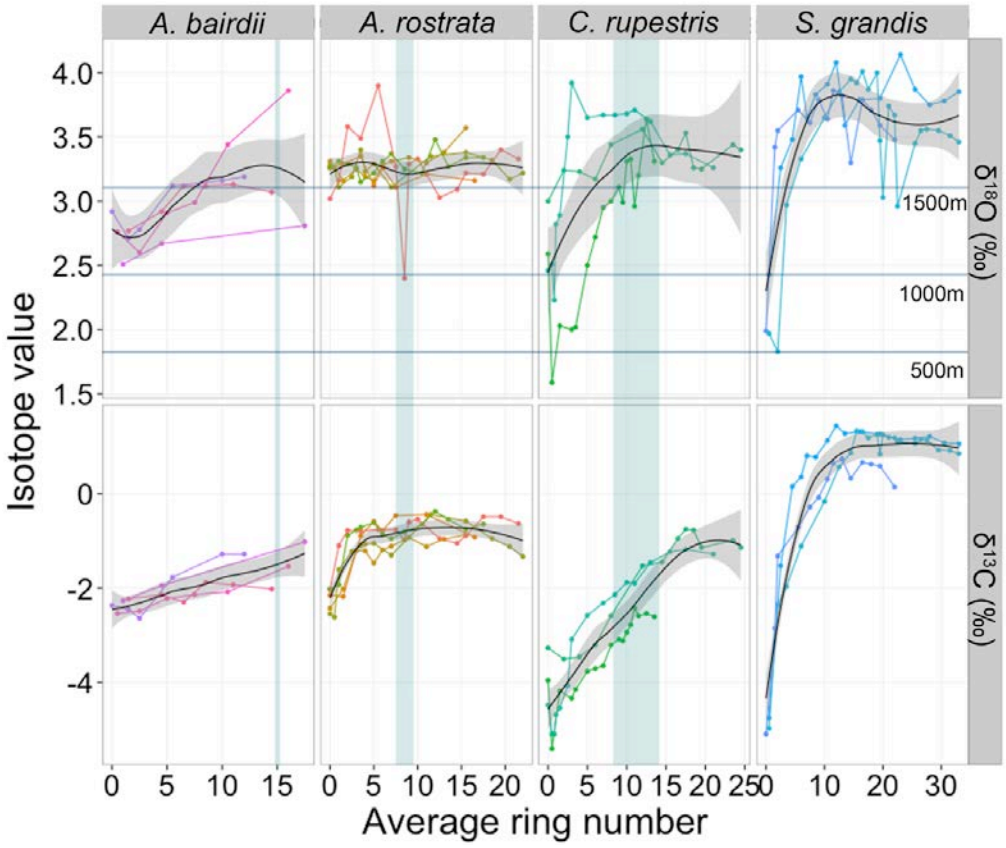

Figure 4.8. Stable isotope values recorded in otoliths. The green bands arethe maturity age: 15 years old for *A. bairdii* (Allain 2001), 8-9 years old for *A. rostrata* (Magnússon 2001) and 8-14 for *C. rupestris* (Lorance *et al*. 2008 and citations therein). The light blue lines are the mean predicted $\delta^{18}O_{oto}$ value from Monte Carlo simulation at three depths.

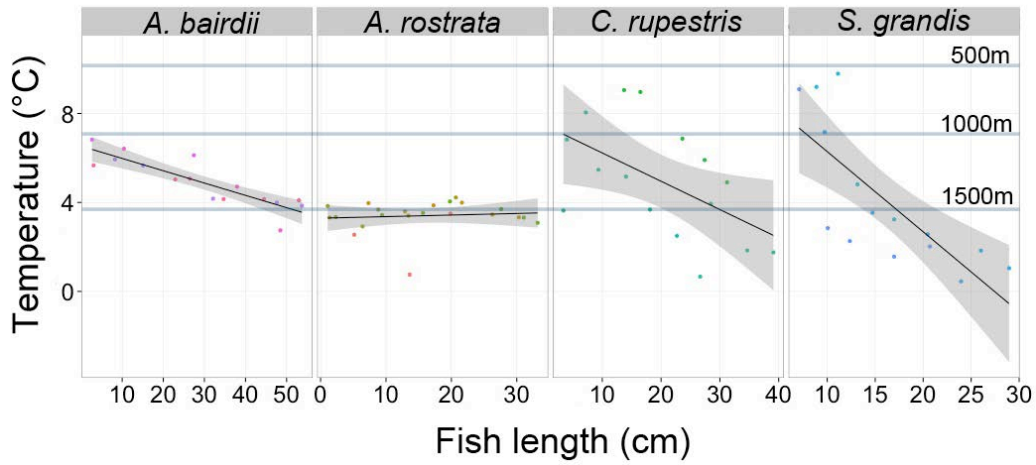

Figure 4.9. Vertical migration in the early life stage. Fish length is the total length.

The difference between the within-species average of the maximum and minimum $\delta^{18}O_{oto}$ values showed that the *A. bairdii, C. rupestris* and *S. grandis* individuals experienced ontogenetic thermal decreases of 2.5, 4.5 and 7.5°C, respectively. The otolith-recorded ontogenetic temperature differences (especially found in *S grandis*) are equivalent to the difference in water temperature between the surface mixed layer and 1500-1800m (about 7.5-8.0°C, Fig. 4.3), implying the potential depth migration for each of the three species.

A. rostrata is found over a wide depth distribution from 300-3000m in different areas, but is restricted to ambient water temperatures no higher than 4.5°C (Magnússon 2001 and citations therein). In the Rockall area, water temperatures below 4°C are found at depths greater than 1500m. Predicted $\delta^{18}O_{oto}$ values show relatively little variation below this depth (Fig. 4.7) and therefore we cannot determine with precision weather *A. rostrata* individuals inhabited depths significantly below 1500m. Nontheless it is clear that unlike the other samples species, *A. rostrata* individuals sampled here were experienced limited ontogenetic change in $\delta^{18}O_{oto}$ values and thus ambient temperature.

4.3.4 Stable carbon isotopes

The chronological patterns of $\delta^{13}C$ values in the sampled four species can be categorised into two types: (1) a sharp increase in the early life stage; (2) a gradual increase throughout the life. *A. rostrata* and *S. grandis* belong to the first type but differ in absolute $\delta^{13}C$ values and the duration of early life stage minima (Fig. 4.8). $\delta^{13}C$ values in *A. rostrata* ranged from -2.62 to -0.37‰, and showed a quick increase in the first 5 years. $\delta^{13}C$ values of *S. grandis* rose from -5.10 to 1.44‰ and reached a plateau at around 10-15 years old. Within the second group, *A. bairdii* otoliths showed a gradual increase in $\delta^{13}C$ values with a relatively narrow range between -2.64 and -1.02‰. *C. rupestris* otoliths showed a continuous increase of $\delta^{13}C_{oto}$ values throughout most of the life-span between -5.41 and -0.75‰, but the increase tended to be gentler after the transition age at around 15-20 years old.

According to the mass balance equation, two factors, $\delta^{13}C_{diet}$ and $\delta^{13}C_{w}$ values, affected the relationship between the $\delta^{13}C_{oto}$ value and the metabolism index, but in different aspects (Fig. 4.10). We showed the different influences between these two effects, respectively. Diet preferences change the slope of this relationship, showing that the inferred metabolic contribution to otolith carbon increases as $\delta^{13}C_{diet}$ increase

(i.e. if fish share a common $\delta^{13}C_{oto}$ value, those with more pelagic diets should yield lower inferred metabolic index values). In contrast, the minor differences in $\delta^{13}C_w$ values slightly influenced the slope and intercept of the relationship and if fish share a common $\delta^{13}C_{oto}$ value, those with higher $\delta^{13}C_w$ values should yield higher inferred metabolic index values. These comparison give possible uncertainties associated with measurement and estimation in the relationship between $\delta^{13}C_{oto}$ values and metabolic rates.

Given the known $\delta^{13}C_{oto}$, $\delta^{13}C_{diet}$ (isotopic compositions of carbon in muscle tissues) and $\delta^{13}C_w$ values (assumed as 1‰), the deduced metabolic index values between species and life stages were shown in the Figure 4.11 and Table 4.2. M values were found in higher for adult *A. bairdii* and *C. rupestris* and the lowest in adult *S. grandis*. Juveniles showed higher metabolism than adult fishes, but the ontogenetic difference is more obvious in *C. rupestris* and *H. atlanticus* than other species.

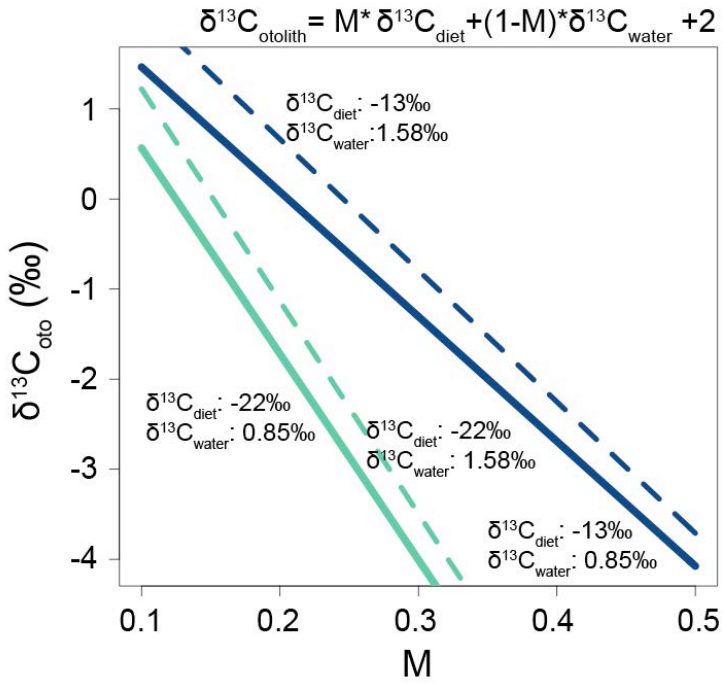

Figure 4.10. Predicted relationship between $\delta^{13}C_{oto}$ values and metabolism. The relationship is based on the mass balance equation and controlled by $\delta^{13}C_{diet}$ and $\delta^{13}C_w$ values. The range of $\delta^{13}C_{diet}$ value is based on Figure 1 and the range of $\delta^{13}C_w$ value is based on the data published in Kroopnick 1985. Blue lines are set as the same $\delta^{13}C_{diet}$ value (-13‰) and cover a possible range of $\delta^{13}C_w$ values between 0.85‰ (full line) and 1.58‰ (dashed line). Similarily, Green lines are resulted from the same $\delta^{13}C_{diet}$

value (-13‰), but in two different $\delta^{13}C_w$ values (0.85‰ in full line and 1.58‰ in dashed line).

Several environmental and physiological factors driving metabolic rate changes must therefore explain the ontogenetic variations in $\delta^{13}C_{oto}$ values. A better approach is to use modelling to remove size and temperature effects and then any diet-related effects should appear in the residuals. The relationship between $\delta^{13}C_{oto}$ value (and thus metabolic rate) and temperature, growth rate and body mass was explored to evaluate likely influences on metabolic rates (Fig. 4.12). Multiple linear regression modelling explained 78.1%, 71.1%, 89.8% and 96.7% of the variation in $\delta^{13}C_{oto}$ values for four target species, *A. bairdii, A. rostrata, C. rupestris* and *S. grandis*, respectively (Appendix D). However, the main explanatory variable differed in each species owing to distinct life history traits between them. Mass-related variables explained the most variance for *A. rostrata* and *S. grandis,* while all variables were important to *C. rupestris.*

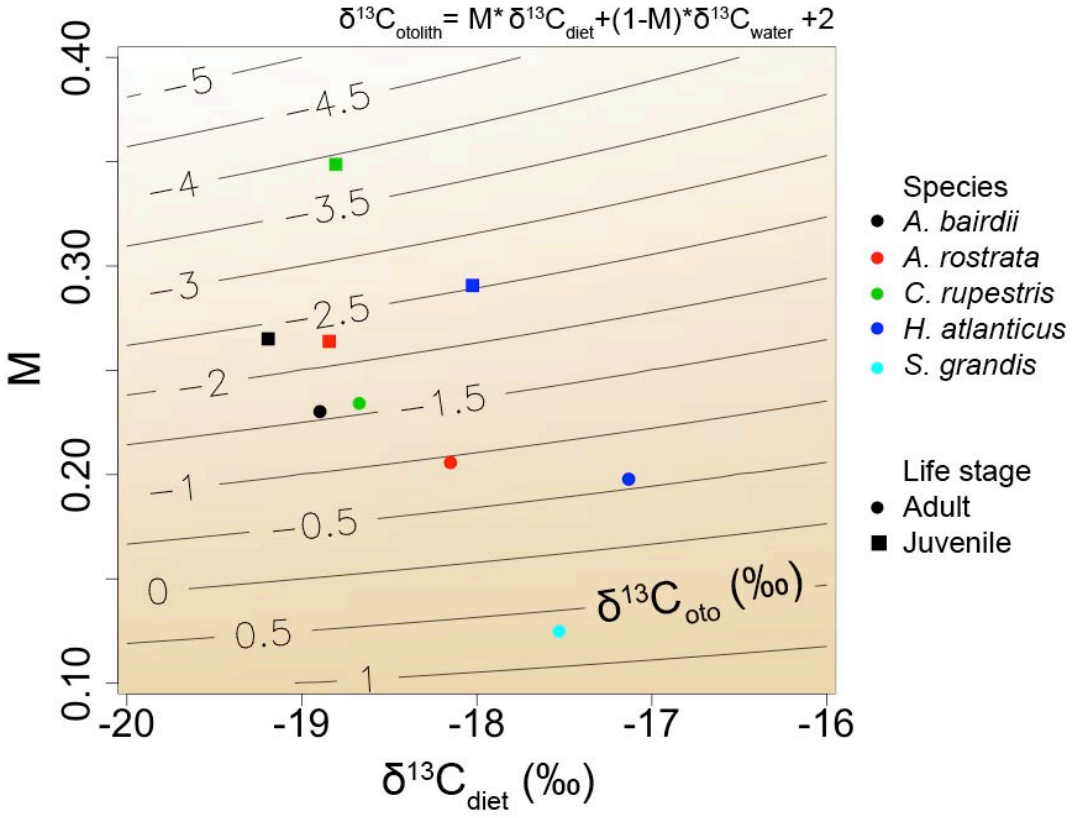

Figure 4.11. Estimated potential contribution of diet derived (metabolic) carbon to otolith arangonite from $\delta^{13}C_{oto}$ values and $\delta^{13}C_{diet}$ values (used as $\delta^{13}C_{muscle}$ values). *Hoplostethus atlanticus* otoliths have been investigated in Trueman

et al. (2013) and are compared to new results. The values used in this calculation are shown in Table 4.2.

Table 4.2. Data for Figure 4.11.

Species	Life stage	$\delta^{13}C_{oto}$	N	$\delta^{13}C_{muscle}$	N (body mass, g)	Predicted M
Alepocephalus bairdii	Juvenile	-2.35±0.138	4	-19.2±0.304	12 (13-30)	0.265
	Adult	-1.58±0.434	7	-18.9±0.306	18(3722-4735)	0.230
Antimora rostrata	Juvenile	-2.24±0.241	5	-18.8±0.236	5 (124-341)	0.264
	Adult	-0.940±0.282	7	-18.2±0.243	4 (1660-2146)	0.206
Coryphaenoides rupestris	Juvenile	-3.91±0.612	3	-18.8±0.350	5 (11-37)	0.349
	Adult	-1.56±0.795	8	-18.7±0.560	10 (1340-2084)	0.234
Hoplostethus atlanticus	Juvenile	-2.53±0.0930	6	-18.0±0.291	12 (20-31)	0.291
	Adult	-0.587±0.283	6	-17.1±0.479	12 (3603-4713)	0.198
Spectrunculus grandis	Adult	0.687±0.476	3	-17.5±0.253	5 (542-834)	0.125

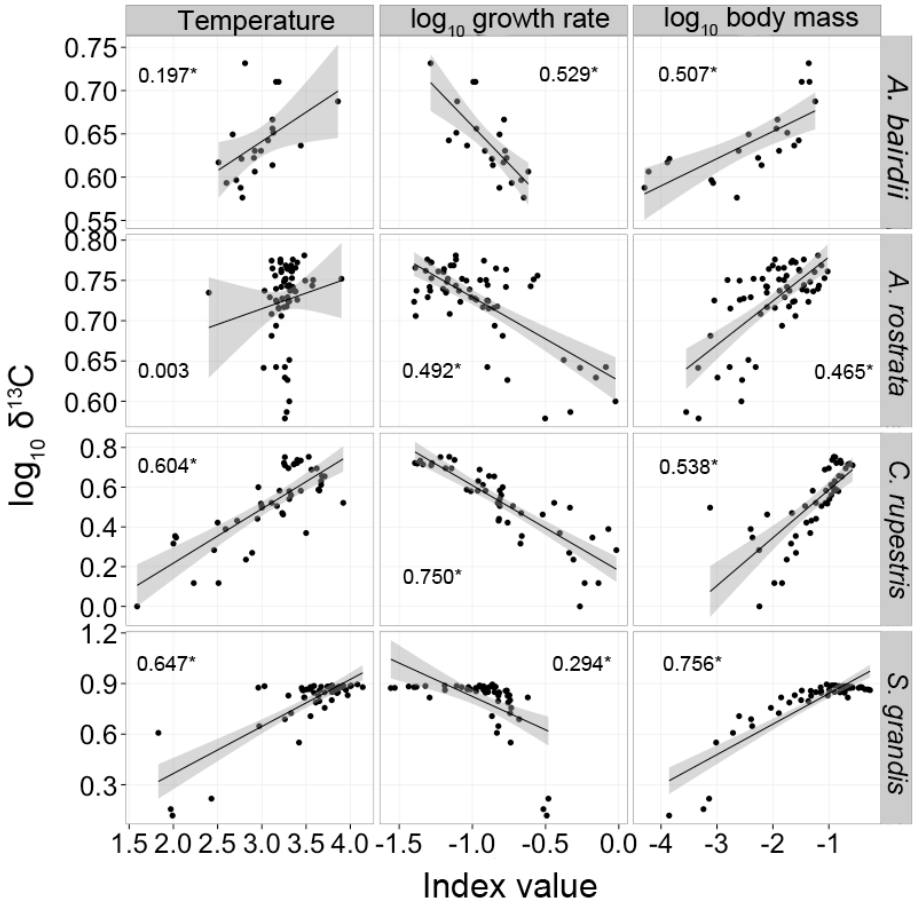

Figure 4.12. Relationships between $\delta^{13}C_{oto}$ values and metabolism-related factors in each species. The numbers represent R square in each regression line (*significant).

Model residuals were not evenly distributed against fish age and the ontogenetic trend of residuals was different between species. The residual analysis displayed less/no change in *A. bairdii* and *A. rostrata,* a slight increase at the early life stage of *S. grandis*, and a fluctuation during the life-span of *C. rupestris* (Fig. 4.13).

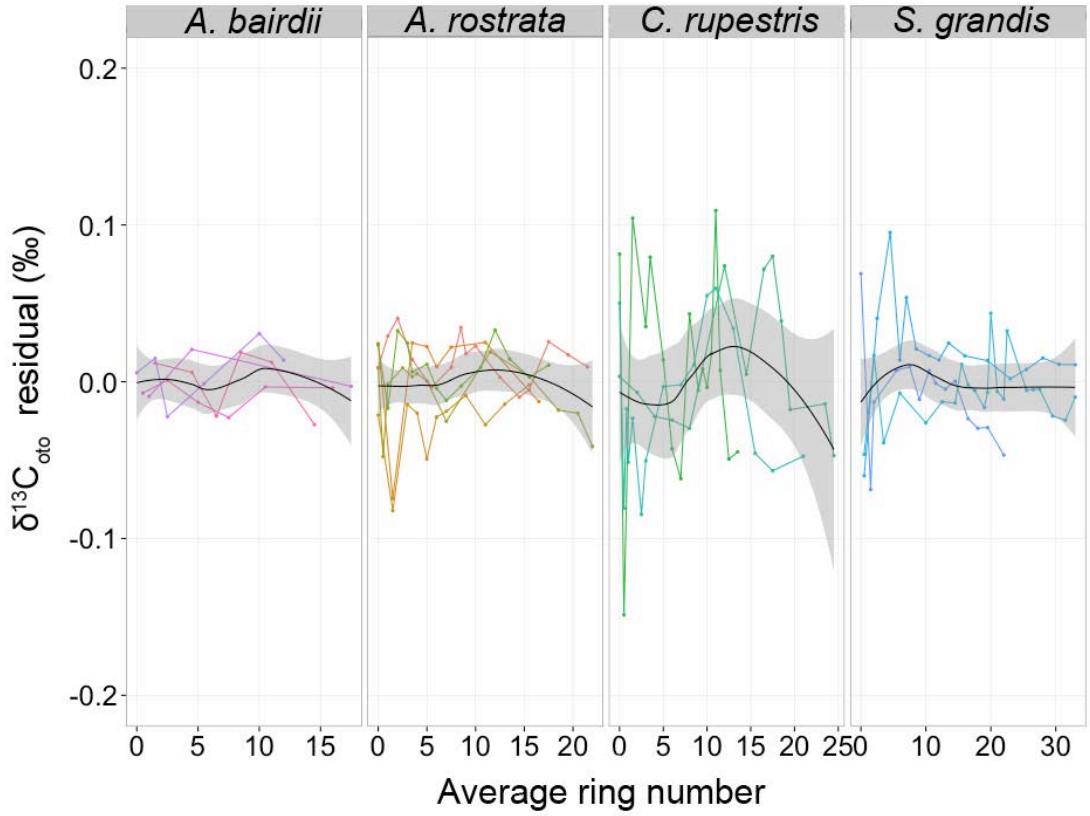

Figure 4.13. Ontogenetic changes of $\delta^{13}C_{oto}$ residuals in four target species.

4.4 Discussion

4.4.1 Thermal life history and migration patterns

In order to have a better understanding of the relationship between depth migration patterns and other life-history traits, two questions associated with ontogenetic depth migrations are discussed: (1) how shallow the larval/juvenile phase is; (2) how long the shallower larval/juvenile phase lasts. To answer the first one, the migration patterns of *A. bairdii* and *C. rupestris* are compared. These two species have different spawning strategies in that macrourids have buoyant eggs (Marshall 1965; Merrett 2004) but alepocephalids have demersal spawning (Crabtree & Sulak 1986). The buoyant eggs let larval macrourids hatch and live in shallower layers with more abundant food

supplies (Marshall 1965; Merrett 2004). However, greater threats from predators in the shallow environment mean that macrorids must spawn abundant eggs and thus have higher fecundity and reproductive costs (Allain 2001) to ensure larval/juvenile survivorship. Conversely, larval/juvenile fish hatched from the demersal eggs confront fewer threats from predators in the deeper early life, allowing lower fecundity and reproductive costs for alepocephalids (Allain 2001). Orange roughy, *Hoplostethus atlanticus* have a shallower juvenile phase (Trueman et al. 2013) and relatively high investment in eggs (Minto & Nolan 2006), but unknown period between spawning events for individuals.

The duration of larval/juvenile shallow water phase as shown by oxygen iisotope analyses varies from short to covering much of the juvenile life history that reflects larval/juvenile settlement and/or dispersal (Fig. 4.14). $\delta^{18}O_{oto}$ values reveal that *H. atlanticus* descend to deep waters in the early juvenile phase for settlement (Shephard et al. 2007, Trueman et al. 2013). A sharp decrease of $\delta^{18}O_{oto}$ values in the very early life of cusk eels (this study; Chung 2010; Shiao et al., 2014) implies behaviours of juvenile settlement. Juvenile settling is accompanied with diet shifts from pelagic- to benthic-dominated contributions (an example of *H. atlanticus* in Trueman et al. 2013). The diet shift is also expected for cusk eels owing to pelagic larvae found in the shallow waters (Okiyama & Kato 1997; Fukui & Kuroda 2007) and adults preying on more benthic dietary items (indicated by $\delta^{13}C_{muscle}$ values, Table 4.2). However, less dramatic transformations of diet preferences are related to a longer duration of larval/juvenile dispersal, such as *A. bairdii* and *C. rupestris*. These two species show progressive downward depth migration from larval/juvenile stages until maturity (Fig. 4.14) and during the process, pelagic organisms are usually the primary dietary items for both species. Thus, it is suggested that benthopelagic foragers have a longer duration of juvenile dispersal with an advantage of a wider spread following current flows. However, diet shifts make benthic fish settling down in the very early life for alternative (benthic) food sources to avoid resource competitions and release predator pressure from the shallower waters.

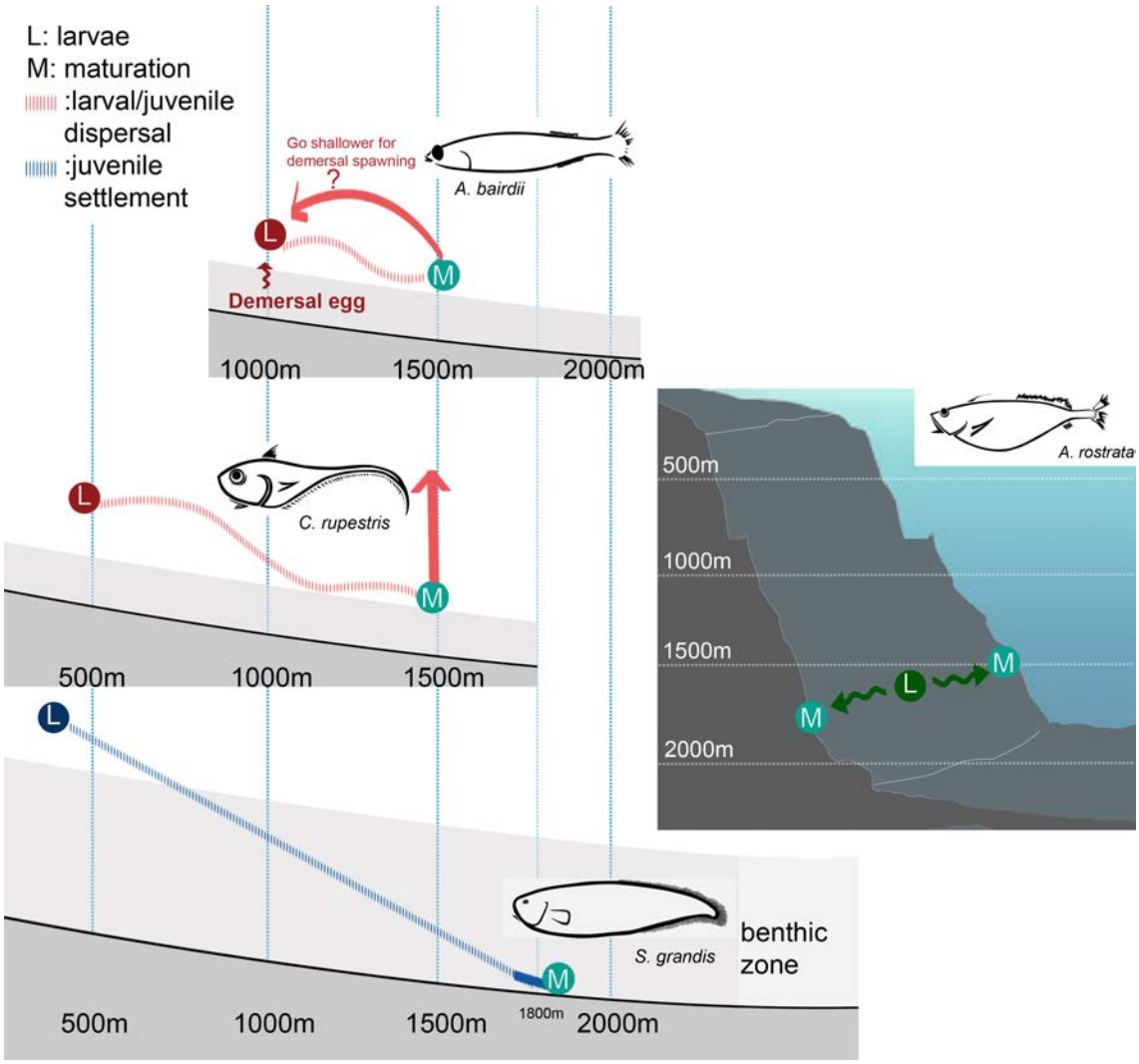

Figure 4.14. Vertical migration patterns of 4 deep-sea fishes species. *A. bairdii* have demersal eggs (Crabtree & Sulak 1986) and after hatching, larvae move off the seafloor and change their dietary items from benthic to pelagic organisms (Mauchline & Gordon 1983). *C. rupestris* show larval/juvenile dispersal and reach the maximum depth until the first maturation, but *S. grandis* show juvenile settlement and they will reach the maximum depth before maturation. *A. rostrata* have a very deep larval/juvenile stage and stay close to the benthic zone in the whole life (revealed by muscle isotope values, Trueman unpublished data) but possibly have horizontal migration along the continent below a certain depth at 1500m.

Larval/juvenile shallow water phase has been found in several deep-sea species (Merrett 1978; Fukui *et al.* 2003; Okiyama & Kato 1997; Smith & Brown 1983, Lin et al. 2012; Hsiao et al. 2014), but depth migration patterns of deep-sea fishes vary in either spatial or temporal scaling. Furthermore, the horizontal migrations (*Aphanopus carbo*, Longmore *et al*. 2014) and no migration (*A. rostrata*, this study) are also found. In brief, deep demersal fishes display a range of ontogenetic depth migration, which may respond to life-history traits as reproductive and feeding strategies, and is also associated with environmental influences as food availability and predator pressure.

4.4.2 Ontogenetic change of metabolism

Ontogenetic metabolic rate dominate the variation of $\delta^{13}C_{oto}$ values (Fig. 4.11). Thus, we apply the metabolic theory of ecology on $\delta^{13}C_{oto}$ values and find that the ontogenetic change of $\delta^{13}C_{oto}$ values is primarily influenced by temperature and body mass. Metabolic theory predicts relationship between metabolic rate and temperature and body mass. However, the field metabolic rate recorded in otolith carbon isotopes do not follow the this trend (Fig. 4.15), implying other biological traits may also contribute the variation of metabolic rates that is in terms of beyond the influence of temperature and body mass, such as the locomotor activity (Sherwood & Rose 2003).

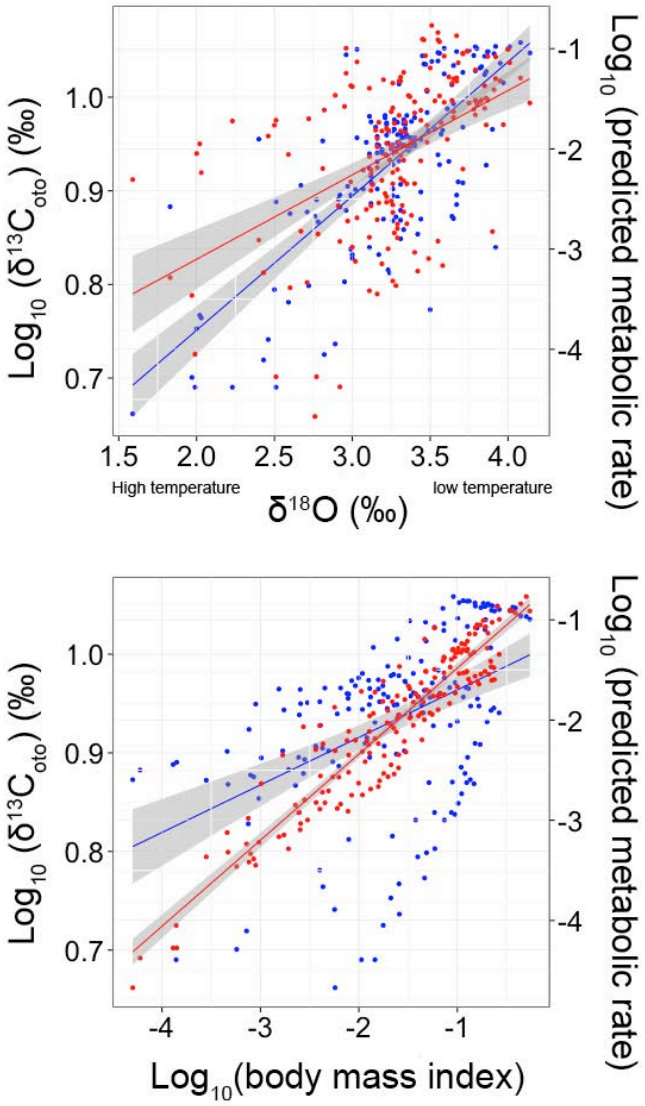

Figure 4.15. Trends differ between theoretical and field metabolic rate ($\delta^{13}C_{oto}$ values). The predicted metabolic rate follows the metabolic theory and is acquired from the temperature, body mass and growth rate (more explanation shown in Section 4.2.3.2). Each dot represents individuals analysed in this study. Blue and red dots are $\delta^{13}C_{oto}$ values and predicted metabolic rate, respectively. Grey areas show the 95% confidence interval. $\delta^{13}C_{oto}$ values reveal that field deep-sea fishes respond more sensitively to temperature changes than the prediction and diplay a less biomass inffllence on the metabolic rate.

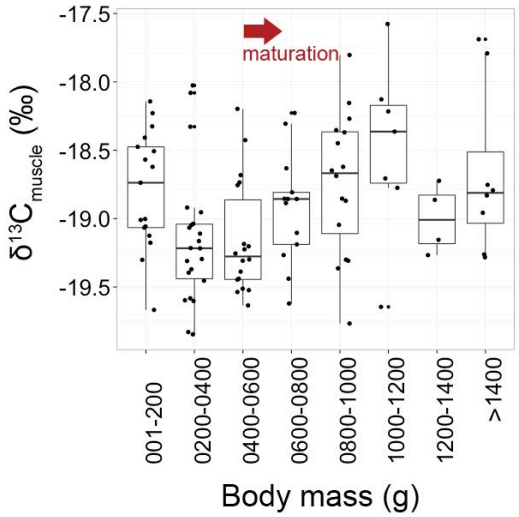

Figure 4.16. $\delta^{13}C_{muscle}$ values of *C. rupestris* in different size ranges (Trueman *et al*. 2014; Trueman unpublished data). The maturation indicates that fish reach the body size at the first maturation not the annual gonad maturation stage. Carbon isotope ratios are reported in delta notation relative to Pee Dee Belemnite.

Fluctuated $\delta^{13}C_{oto}$ residual values of *C. rupestris* (Fig. 4.13) can be explained by the foraging activity in three life stages. *C. rupestris* shows three stages of dietary preferences from the stomach content analysis (Mauchline & Gordon 1984a). During the first several years after hatching, *C. rupestris* is suggested as actively feeding on pelagic prey in shallow waters. While juveniles progressively descend to the seafloor (the second stage), *C. rupestris* behaves relatively passive to find benthic food items, such as polychaetes (but pelagic organisms are still dominated items). As bigger individuals (the third stage), *C. rupestris* then migrate to deeper habitats but perch in the water column several metres above the sea floor (Haedrich 1974). At this stage, *C. rupestris* prey on more pelagic organisms, such as copepods, fish and so on, and leaving from the bottom makes *C. rupestris* relatively active in the water column. The three stages of diet shifts are supported by $\delta^{13}C_{muscle}$ values (Trueman unpublished data) (Fig. 4.16) that isotopic signals increase in the second life stage but decrease afterward. *C. rupestris* is expected having different locomotor activities in response to diet shifts and it reflects on the fluctuation of $\delta^{13}C_{oto}$ residual values as three-stage behavioural changes (Fig. 4.13).

Although $\delta^{13}C_{muscle}$ of *A. bairdii* values continuously increase after maturation till the late adult stage (Trueman unpublished data) (Fig. 4.17), the trend cannot be observed from $\delta^{13}C_{oto}$ values owing to lacks of data points after maturity age (Fig. 4.13).

Nevertheless, *A. bairdii* is supposed to behave consistently according to nearly constant $\delta^{13}C_{oto}$ residual values. *A. bairdii* exploit pelagic-dominated diets in entire life and the increase of $\delta^{13}C_{muscle}$ values is believed as *A. bairdii* preying on larger organisms with higher trophic levels rather than diet shift to benthic food sources.

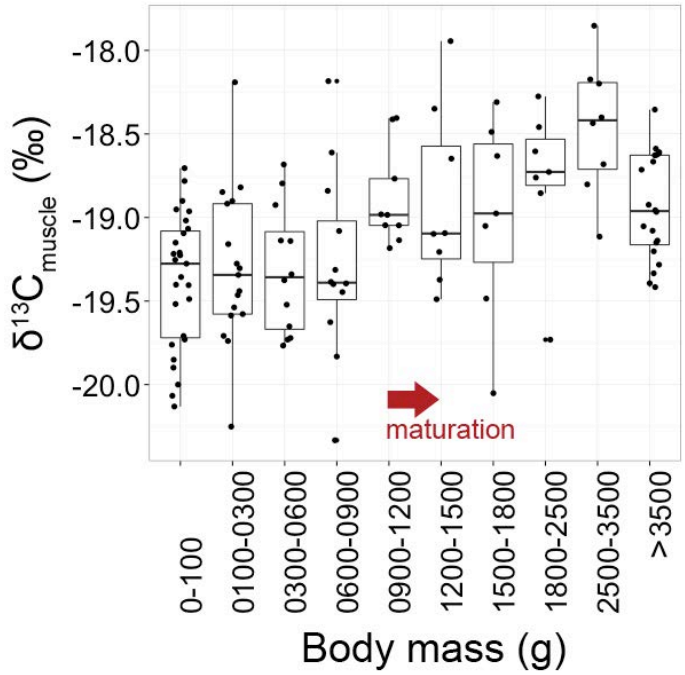

Figure 4.17. $\delta^{13}C_{muscle}$ values of *A. bairdii* in different size ranges (Trueman *et al*. 2014; Trueman unpublished data). The maturation indicates that fish reach the body size at the first maturation not the annual gonad maturation stage. Carbon isotope ratios are reported in delta notation relative to Pee Dee Belemnite.

For species with a short shallow larval/juvenile phase, such as cusk eels and orange roughy, metabolic rates decrease in the early life owing to juvenile settlement with a behavioural change from pelagic to benthic realm/feeding (Fig 4.13 and Fig. 4.18). The diet shift during juvenile settlement is significantly observed from $\delta^{13}C_{muscle}$ values in an example of *H. atlanticus* (Fig. 4.19). However, *H. atlanticus* have a more complex life history than cusk eels that *H. atlanticus* ascend to shallower layers in the middle life and migrate to deeper again in the late adult stage (Trueman et al. 2013). The activity of *H. atlanticus* during the ascending is higher, which is suggested by an increase of metabolic rates (Fig. 4.18), but it is hard to tell if the change is related to feeding or reproductive activities because our $\delta^{13}C_{muscle}$ values lack for the body mass range in the middle life. *H. atlanticus* have a relatively decreasing metabolic rate observed from

the late adult stage that is a different ontogenetic trend compared to other four deep-sea fish species (Fig. 4.13 and Fig. 4.18). The decreasing metabolic rates associated with less energy expense may explain a longer life span of orange roughy (Tacey & Horn 1999; Drazen & Haedrich 2012).

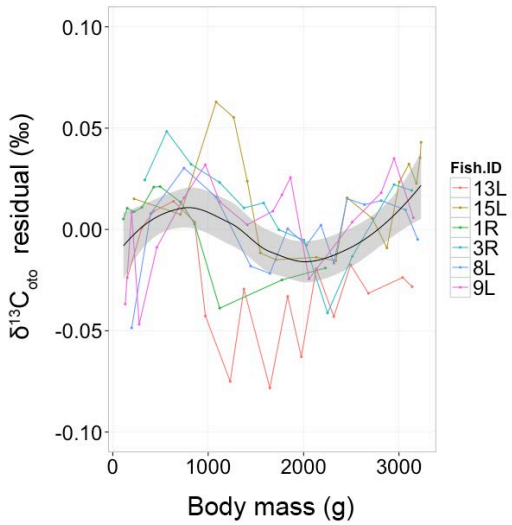

Figure 4.18. $\delta^{13}C_{oto}$ residual analysis of the multiple linear regression model (with three metabolic related factors) in *H. atlanticus*. Values of $\delta^{13}C_{oto}$ and three metabolic related factors are extracted from Trueman *et al*. (2013).

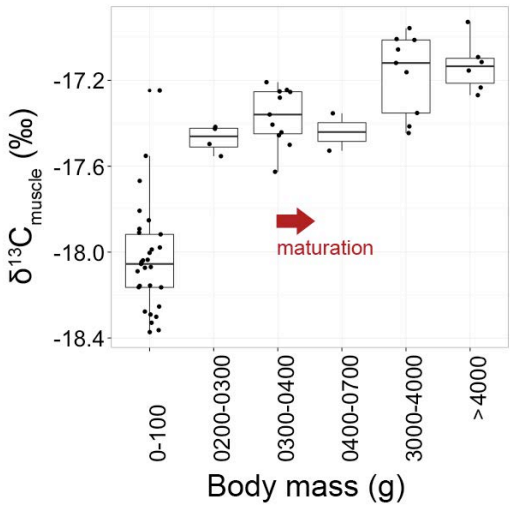

Figure 4.19. $\delta^{13}C_{muscle}$ values of *H. atlanticus* in different size ranges (Trueman *et al*. 2014; Trueman unpublished data). The maturation indicates that fish reach the body size at the first maturation not the annual gonad maturation stage. Carbon isotope ratios are reported in delta notation relative to Pee Dee Belemnite.

Based on the residual analysis, there are common negative $\delta^{13}C_{oto}$ residuals with size (in late adult stage) in relatively benthopelagic foragers (*A. bairdii* and *C. rupestris*) compared to passive feeders (*H. atlanticus* and *S. grandis*), that could be increasing efficiency of movement when benthopelagic fishes get bigger. It also corresponds to more negative $\delta^{13}C_{muscle}$ values in terms of more pelagic intake. Although insufficient information of life history in *A. rostrata*, negative $\delta^{13}C_{oto}$ values in biggest sizes may imply benthopelagic foraging rather than passive feeding (Mauchline & Gordon 1984b; Bailey *et al*. 2003)

This study uses stable isotope records in otolith to investigate the life history traits in deep-sea fishes and tries to connect life-history information with migration patterns and metabolic rates. However, still few fish species have been studied in deep-sea ecology, and therefore the expansion of species will be the future works. Furthermore, in order to better explain metabolism in deep-sea fishes, other biological and ecological conditions and ecosystem progress, such as population density, trophic dynamics and so on, should be deeply considered (Brown 2004).

Chapter 5: Synthesis and conclusion

In the previous chapters, functional and life history traits are analysed separately and the discussions focus more on the deep-sea fish samples collected in this thesis. However, this evidence gives only a partial interpretation of deep-sea fish ecology. In this chapter, more analyses and discussions are presented based on (1) expanding the comparison between results in this thesis and data from literatures and (2) integrating multiple evidences. Following the objectives, two main topics are highlighted:

- Ecological trend of sensory capacity
  The perception, the sense of vision and hearing/balance, is used as an index for identifying functional groups in this thesis, but the sensory capability is found to change with depth gradients. This trend may explain more about the feeding behaviours of deep-sea fishes and predict the differences between pelagic and benthic assemblages.
- Life history traits in relation to functional behaviours
  Functional groups of deep-sea fish are supposed to be well defined by integrating the information of multiple traits. Although the life history of only four species is studied, the possible relationship between life history and functional groups is discussed in the following content.

5.1 Ecological trend of sensory capability

The ecological trend of sensory abilities has been simply described in the Chapter 2 (visual capability) and 3 (vestibular capability), and the acuity of both two senses shows a general decreases with depth. Moreover, the influence of depth on sensory ability is more pronounced for pelagic species compared to demersal species. More knowledge of sensory abilities may aid us explaining the trait evolution of deep-sea fishes and deep-sea fish ecology. In the following sections, there are further discussions expanded from the data in previous chapters, especially explaining the consistent functional behavioural change between visual and vestibular abilities found in deep-sea fishes.

5.1.1 Visual behaviour

The visual resolution of fish has been reported to have a tendency to increase with depth, based on the observation from pelagic species (Warrant 2000). Compared to

the pelagic species, vision is generally regarded as less important for demersal fish, but according to our results, and widespread possession of well developed eyes, deep-sea demersal species still need vision to facilitate and evade predator-prey interactions. The visual fields of deep-sea demersal fishes closely correspond to stomach content and stable isopte records of diet type, indicating that vision is implicated in prey acquisition in all major functional groups across the depth range 500-2000m.

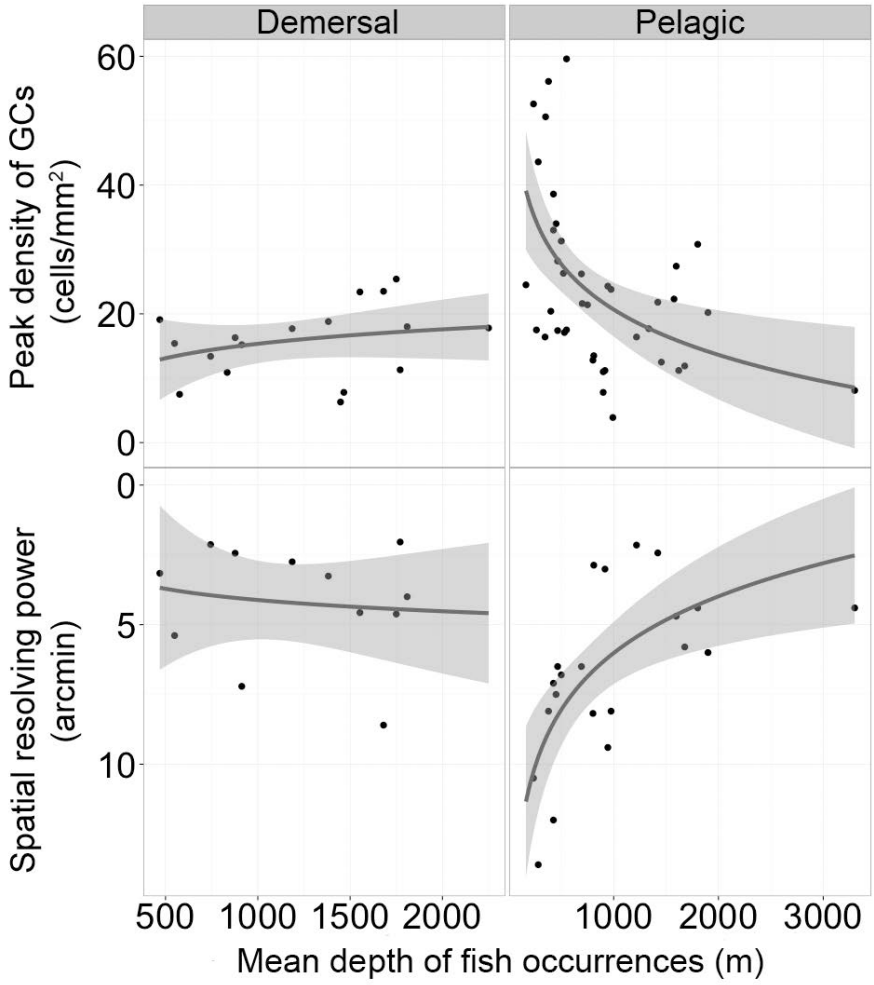

Figure 5.1. Visual capabilities between two functional groups. The data is from chapter 2 and Wagner *et al*. (1998), and species is categorised by habitat as pelagic or demersal. The trends of peak density of GCs for pelagic and benthic foraging species are $y=337*x^{-0.407}$ ($p<0.01$) and $y=3.23*x^{0.225}$ ($p=0.274$), respectively. The trends of resolving power for pelagic and benthic foraging species are $y=165*x^{-0.489}$ ($p<0.01$) and $y=1.51*x^{0.145}$ ($p=0.676$), respectively.

Fish show an exponential decrease of the peak density of ganglion cells and increases in spatial resolving power with depth that is described in Chapter 2 (Fig. 2.9 and Fig. 5.1), which is more pronounced in pelagic fish rather than demersal species. According to discussions in Chapter 2, the higher spatial resolving power of deep-sea pelagic fishes apparently results from the increase of lens size. In addition, the larger lens increases the sensitivity to bioluminescence for pelagic foraging species. In contrast, the spatial resolving power of demersal fishes remains high because demersal fishes have relatively large lens in every depth strata.

5.1.2 Vestibular ability, locomotion-related metabolism and visual interaction hypothesis

Differences in depth-dependent changes in acitivity between benthic and pelagic species have been described previously in terms of the visual interaction hypothesis (Seibel *et al*. 2000; Seibel & Drazen 2007; Seibel *et al*. 1997; Childress *et al*. 1990a). The visual interaction hypothesis proposes that in sunlit waters efficient vision imposes a high selective pressure towards active locomotion in pelagic animals. In benthic animals with the possibility of crypsis, and sessile or infaunal prey, visual based predation may be less intense. Thus depth-dependent reductions in light intensity would be expected to more effectively release pelagic animals from selection pressure for active models of life. The visual interaction hypothesis assumes that light intensity controls the sensory interaction between prey and predator (Drazen & Seibel 2007; Seibel & Drazen 2007; Childress 1995; Childress *et al*. 1990a, 1990b). In bright shallow zones, the longer detectable distance for predator pursuit and evasion favours high mobility and fast swimming. The exponential decrease of light intensity reduces the opportunity for visual interaction that in turn influences the swimming performance of fish. Lower locomotion activity in the deep also reflects on the reduction of fish metabolism (Drazen & Seibel 2007).

The visual interaction hypothesis thus predicts that depth gradients should have a greater influence on vestibular capabilities of pelagic fish compared to benthic foraging species, and further that increases in depth should weaken selection pressure for vestibular sensory perception in pelagic fishes. According to our findings, the otolith SO ratio shows an overall reduction with depth similar to metabolic capacity, with the implication that the SO ratio reflects the sensory demand associated with active locomotion.

5.1.3 Auditory and vestibular adaptation

Otolith received and integrated auditory and vestibular stimulations and the SO ratio values reveal the ability of both sensory perception. For example, higher SO ratio is found in the auditory specialized species, sciaenid fishes (Aguirre 2003), and in the high mobility species (Gauldie 1988). Therefore, the following points are given to interpret the decreasing trend of SO ratio found in deep-sea demersal fishes:

(1) Vision is the important sensory ability in both deep-sea pelagic and demersal fishes (Wagner 2001a; Wagner 2001b). Auditory compensation is believed to benefit deep-sea fish locating their prey in the dim environment. Mesopelagic fishes demonstrate obvious auditory compensation that is observed from a strong negative relationship between optic tectum and trigeminal/octavolateral area size in the brain (Fig. 5.2). However, the correlation is not significant in the demersal assemblages and olfactory system plays a more important role as fishes have weakened visual capabilities (Fig. 5.3). As the observation in brain sensory size, the enhancement of hearing ability is not equal as demersal fishes progressively lost their visual scene in the deep sea because of olfactory compensation. Moreover, the greater otolith size, found in the most of demersal fishes, provide sufficient acoustic sensitivity (Lychakov & Rebane 2000), explaining the enhancement of auditory ability in less functional demand, especially compared to pelagic fishes. On the other hand, in spite of deep demersal fishes with a specialised inner ear structure for hearing, for example, *A. rostrata* show a change of sulcus area shape (anterior enlargement) and complex hair bundle orientation patterns (Deng *et al*. 2011) rather than an increase of SO ratio, which the value is lower than that of other shallower gadiform fishes. These observations giving open questions are how the auditory compensation for demersal deep-sea fishes is and how the auditory enhancement reflects on otolith morphology.

(2) SO ratio also corresponds to the threshold of auditory frequency and fishes with low SO ratio is adapted to low frequency acoustic signals (Gauldie 1988). However, the background noise in deep sea is in a higher level of lower frequencies (Urick 1984). Thus, to deal with ambient noise in terms of low signal to noise ratio in low frequencies, reduced SO ratio across the depth gradients may be an adaptive strategy.

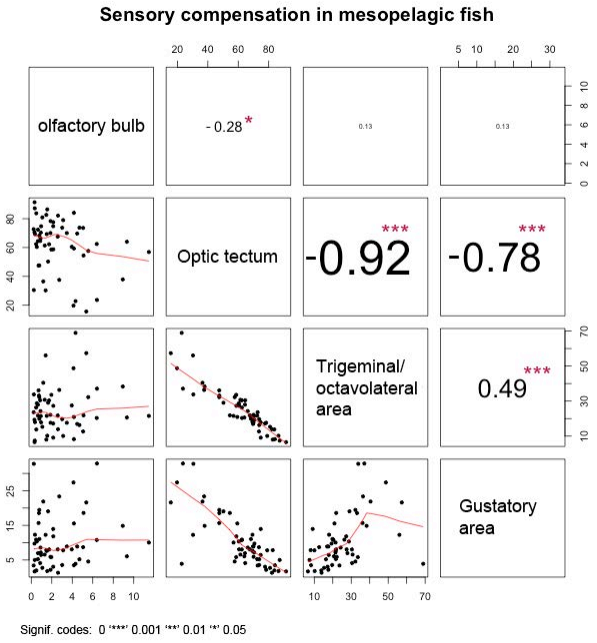

Figure 5.2. Correlations between brain sizes of four sensory areas (a relative percentage in the total area) in mesopelagic fishes. Data is extracted from Wagner (Wagner 2001b).

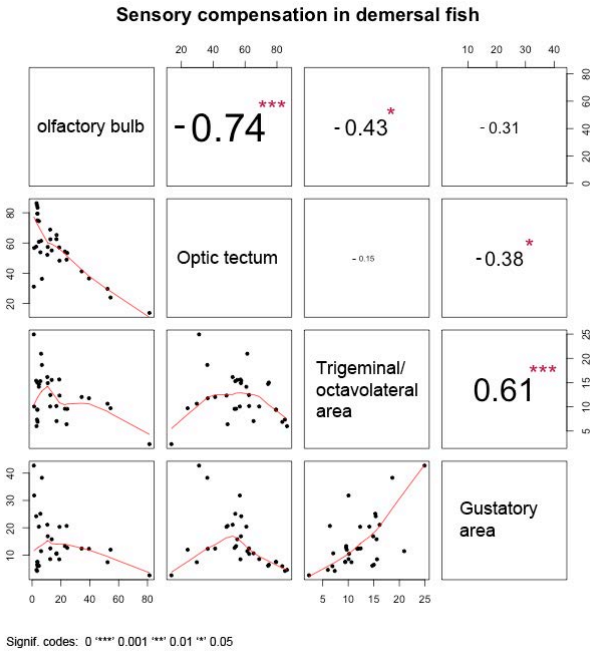

Figure 5.3. Correlations between brain sizes of four sensory areas (a relative percentage in the total area) in deep-sea demersal fishes. Data is extracted from Wagner(Wagner 2001a).

(3) Feeding activity in relation to SO ratio is observed in the literature (Gauldie 1988; Aguirre & Lombarte 1999; Arellano *et al*. 1995) and more discussions in Chapter 3. Depth-related decreasing trend of SO ratio may be in relation to more intakes of benthic foods and also imply the metabolism constraint. A great depth-dependent reduction in metabolic rate is reflecting on a decrease of enzyme activity (Drazen & Seibel 2007), a transform of anguilliform swimming (Neat & Campbell 2013) and reduced red muscle proportions (Drazen *et al*. 2013). A striking finding is SO ratio significantly corresponding to the index of elongated body form (Fig. 5.4) and the red muscle proportion (Fig. 5.5), supporting that the decrease of SO ratio is vestibular adaptation for deep-sea fishes.

We agree that numerous factors may influence fish auditory/vestibular capability and change SO ratio, especially above 500m, which has higher light intensity, higher levels of ambient noise, more complex trophic structures and prey-predator interactions and different environmental conditions from region to region, but this study tries to explore the auditory and vestibular adaptation across a large-scale depth gradient in deep-sea demersal fishes and the results are supported by other sensory abilities.

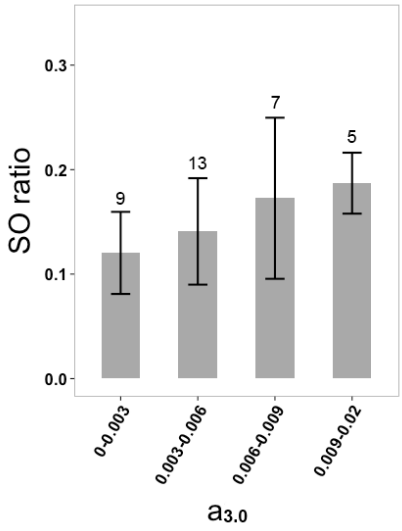

Figure 5.4. An increase of SO ratio with $a_{3.0}$ values (regression model: n=34, t value=2.8, R^2=0.17, p<0.01). $a_{3.0}$ is an index of fish body elongation and the lower $a_{3.0}$ value the higher elongation. These values are extracted from Neat & Campbell (2013).

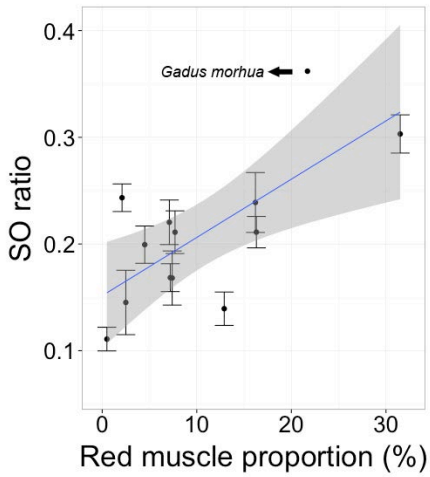

Figure 5.5. An increase of otolith SO ratio with red muscle proportions in deep-sea fishes (regression model: n=13, t value= 3.3, R^2=0.46, p>0.01). Red muscle proportions values are extracted from a review paper of Drazen *et al*. (2013). The SO ratio of Atlantic cod, *Gadus morhua,* (Gauldie 1988) is incorporated.

5.2 Functional groups and life history

5.2.1 Feeding behavioural groups inferred multiple functional traits

Body morphology is a common approach to discuss feeding or functional behaviours (Reecht *et al*. 2013 and citations therein). However, this thesis provides evidence of sensory performance as a potential additional tool for discriminating between groups, and two senses, vision and balance, are discussed. Using multiple functional traits can give more information about fish behaviour in an ecosystem and therefore, in this section, different functional traits are assimilated and analysed.

Five aspects of functional traits were compared among 22 species. (1) The visual fields revealed the feeding strategies (Chapter 2), and five simple categories - peripheral, temporal, nasal, dorsal and ventral direction - were used. (2) Otolith shape was measured by five morphological indices (the ellipticity, rectangularity, form factor, roundness and irregularity) and the index values were extracted from Chapter 3. (3) Neat and Campbell (2013) indicated the $a_{3.0}$ (form factor) value of a fish body form to be an index of anguilliform swimming and these values were assimilated in the dataset. (4) Fish mouth size was an indicator of prey size and type *(*Reecht *et al*. 2013; Scharf

et al. 2000) and the mean mouth diameter was used to represent the mouth size, which value was calculated as the equation:

$$Mean\ mouth\ diameter = 0.5(mouth\ width + mouth\ height)$$

(5) Space use and prey approaching were indicated by the relative mouth opening (Reecht *et al*. 2013; Albouy *et al*. 2011; Villeger *et al*. 2010), which index was calculated as the following equation:

$$Relative\ mouth\ opening = \frac{[2\pi \times 0.5(mouth\ width) \times 0.5(mouth\ height)]}{\left[[2\pi \times 0.5(body\ width) \times 0.5(body\ depth)]\right]}$$

The values of functional traits are shown in Appendix E. The dataset with multiple functional traits were analysed in two ways by the package "FactorMineR (factominer.free.fr/)" in R (R Development Core Team, 2012). One was the multiple factor analysis, which gave the correlation between traits. The second was the hierarchical clustering based on principle components that grouped species in line with the similarity of functional behaviours.

There are several striking findings from the multiple factor analysis shown in Figure 5.6. First, a high correlation is found between the irregular otolith and the peripheral field. Although both irregular otoliths and the peripheral fields are characteristics of pelagic fish, some deep-sea fish species contradict this assumption (Myctophid fish are exclusively pelagic species with a peripheral visual field but round otoliths) (Wagner *et al*. 1998; Campana 2004) and having only two species with a peripheral field in our dataset limits the explanation of this relationship. Secondly, fish with a highly elongated body (in lower $a_{3.0}$ values) have round, square or rectangular otoliths, indicating that the anguilliform swimming mode corresponds to benthic/passive feeding in the deep sea. This also strengthens the suggestion that otolith morphology predicts the mode of fish movement. Thirdly, the relationship between the mouth size and the elliptic otolith shape suggests that fish need a better vestibular capability while they prey on large swimming prey such as fish and cephalopods (the elliptic otolith shape benefits the development of the sulcus area and enhances the vestibular ability mentioned in Chapter 3). The fish eater, European hake (*M. merluccius*), is a good example, which has both distinctive functional traits. Fourthly, a bigger relative mouth opening represents feeding strategies as suction, pursuit and ambush (Reecht *et al*. 2013) and the temporal and nasal visual fields support these kinds of feeding behaviours. According to these findings from Figure 5.6, a correlation circle is simply divided into two areas by the value of dimension 1. Traits associated with pelagic or active foragers

are in the area of positive dimension-one values, and traits indicative of benthic or passive feeders are in the area of negative values.

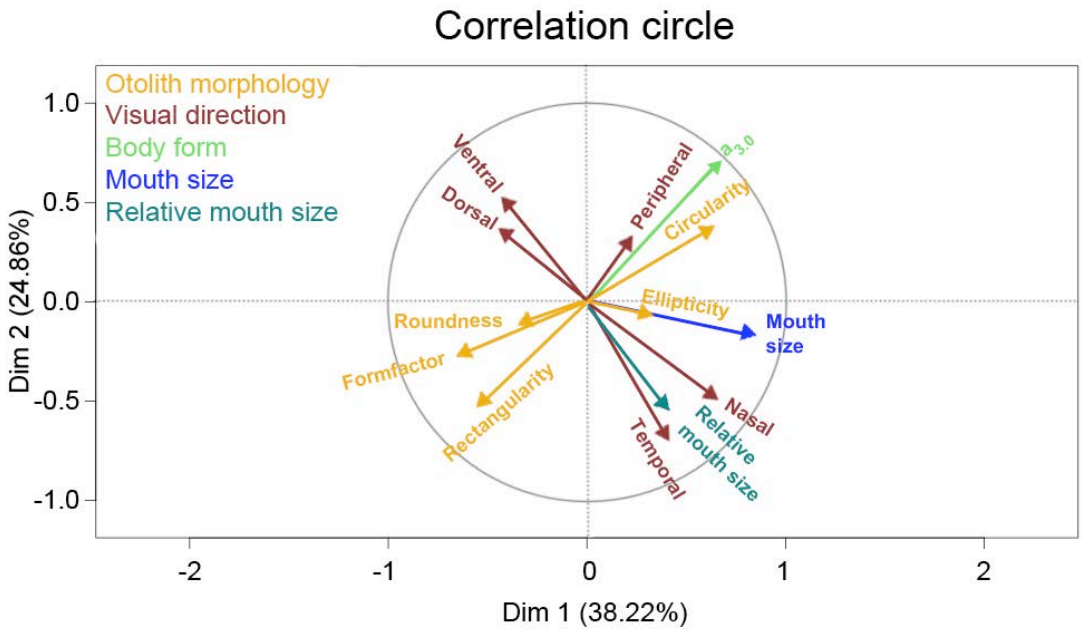

Figure 5.6. Correlations between functional traits.

In the cluster analysis, otolith morphology is displayed as the groups identified in Chapter 3 instead of raw index values, in order to easily discuss functional groups (Fig. 5.7). The functional groups identified by agglomerative clustering with multiple traits are named as Cluster 1-4 as distinct from the otolith morphological Group A-D. Although otolith morphological indices are poorly correlated with visual fields (Fig. 5.6), otolith morphological groups show obvious correlations, such as a connection between Group B and the dorsal/ventral field or between Group A and the temporal/nasal field (Fig. 5.7). The otolith morphological group integrates all the morphological information rather than a single morphological index (Chapter 3) and is more able to explain the fish behaviours at species level.

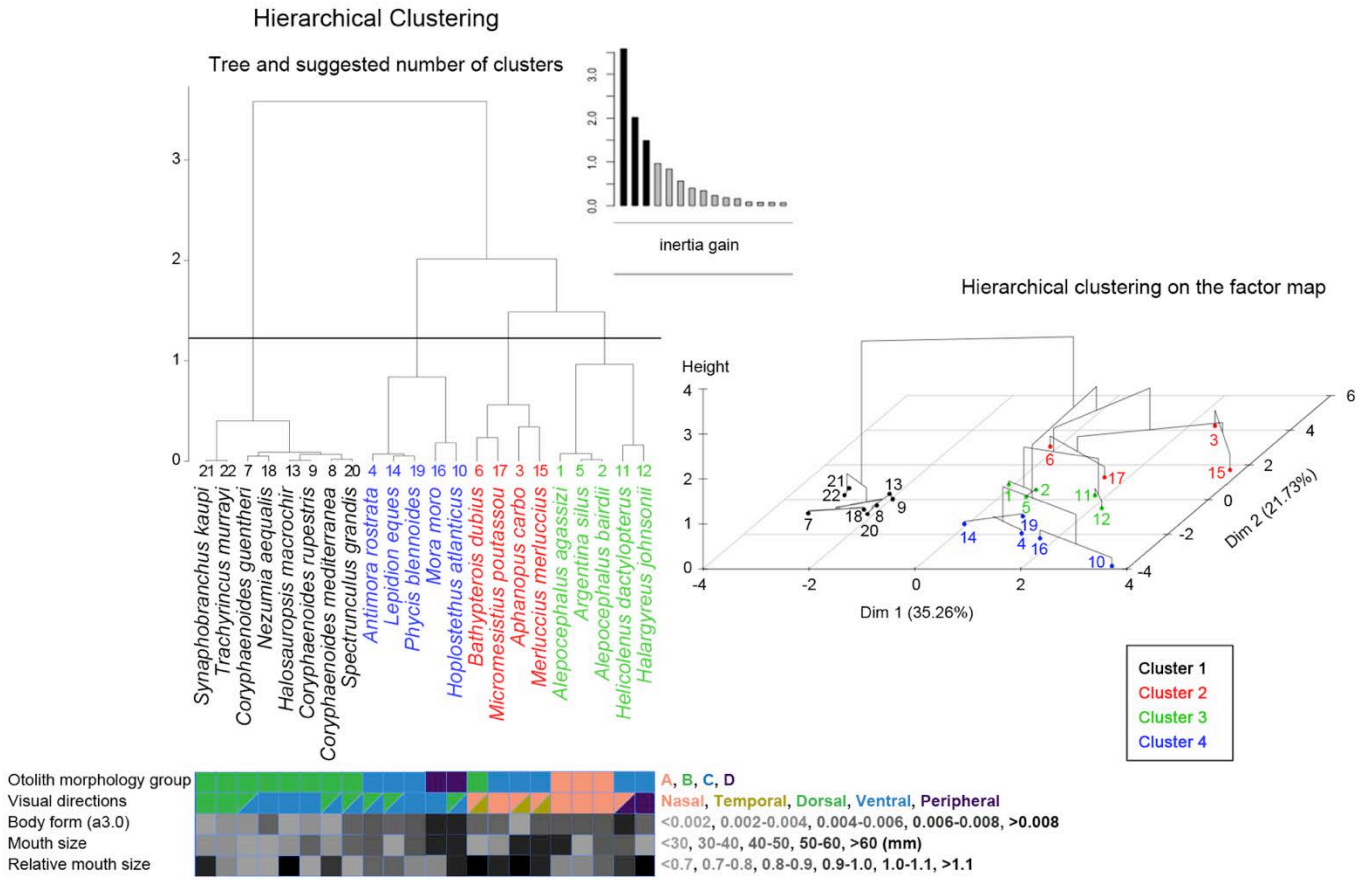

Figure 5.7. Four clusters in 22 deep-sea fish species grouped with multiple functional traits. Colourful grids at the bottom show the range of values in each functional trait and colour lightness corresponds to the value range next to the grids (the darker the higher values). Otolith morphology is the identified groups pointed out in Chapter 3.

The species comprising Cluster 1 are all Group B members (benthic or passive feeders including grenadiers, halosaurs, cusk eels and cutthroat eels) and all have a dorsal/ventral visual field, a smaller mouth size and an elongated body form. Cluster 2 fishes, with a temporal/nasal field and higher relative mouth size, include piscivores (hake and black scabbardfish) and filter feeders (blue whiting and tripodfish). Cluster 3 and 4 fishes have a similar range of $a_{3.0}$, mouth size and relative mouth opening. The most obvious difference is their visual fields. Pelagic feeders in Cluster 3 characterized by a nasal or peripheral visual field are supposed to live in the water column. However, the species in Cluster 4 inhabit regions closer to the bottom as indicated by the dorsal/ventral visual field. This difference suggests an ecological role of Cluster 3 species as dominant in the pelagic or benthopelagic realms, while Cluster 4 species connect the benthopelagic and benthic food web in the deep sea.

Benthic fishes in Cluster 1 have consistent features for five functional traits (fewer variations in each trait between species). In spite of different species/families/orders, benthic foraging fish demonstrate similar functional demands, such as the efficient low-speed swimming and the selection of smaller dietary items near the seafloor. Conversely, pelagic/benthopelagic tendency species (Clusters 2-4) have a wide range of diet preferences and habitat usage either between or within clusters, implying highly diverse feeding strategies. In particular, an explanation is provided by the differing evidences of functional behaviours, such as sensory capabilities, swimming performance and predator-prey interactions.

When the trophic information ($\delta^{15}N$ and $\delta^{13}C$ values in muscle tissue show in Appendix E, Trueman unpublished data) is incorporated in the analyses, the visual field is more highly correlated with $\delta^{15}N_{muscle}$ and $\delta^{13}C_{muscle}$ values in that dorsal and ventral fields correspond to fish having higher trophic niches and benthic dietary choices (Fig. 5.8). Including stable isotope data does not alter the general structure of the cluster analysis but reveals a stronger separation between benthic and pelagic/benthopelagic foragers (Fig. 5.9).

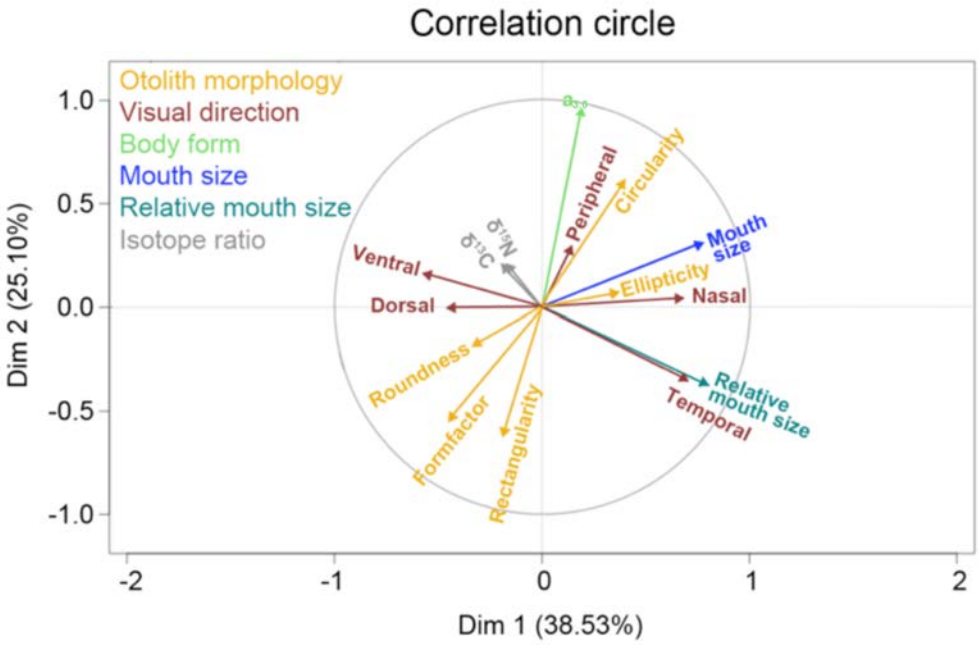

Figure 5.8. Correlation of functional traits and $\delta^{15}N_{muscle}$ and $\delta^{13}C_{muscle}$ values.

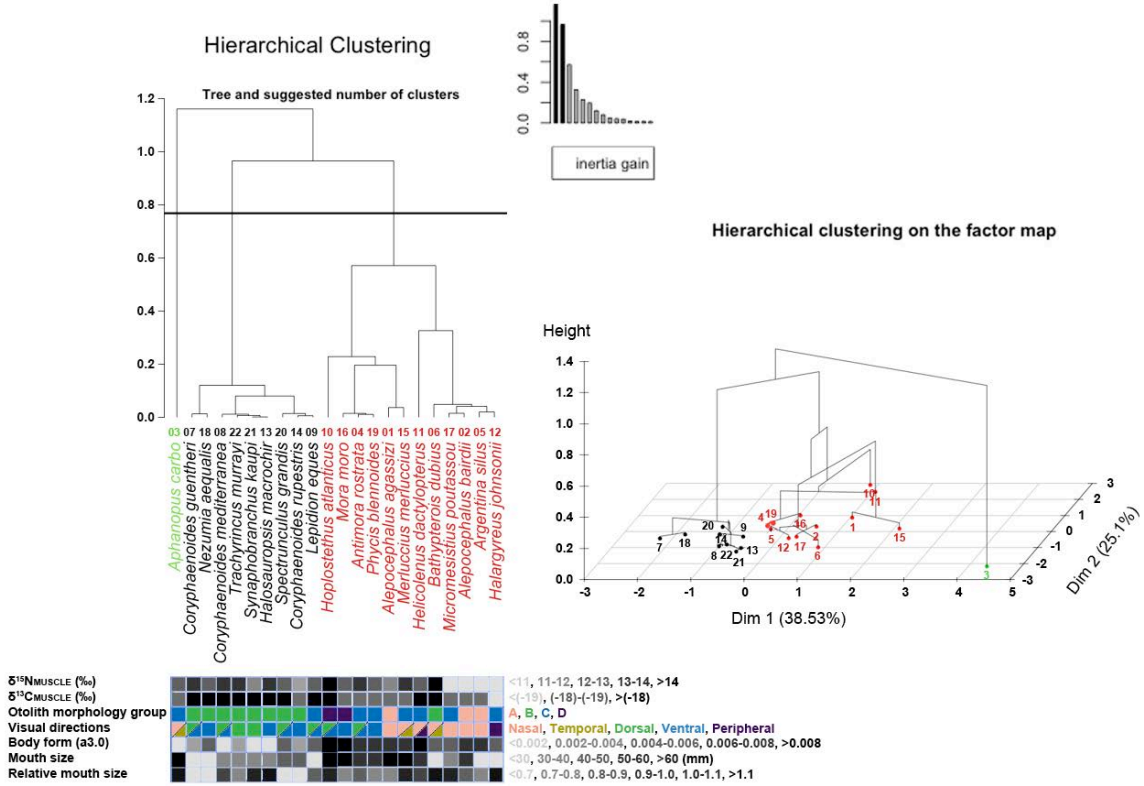

Figure 5.9. Cluster analysis of deep-sea fishes with functional traits and trophic information ($\delta^{15}N_{muscle}$ and $\delta^{13}C_{muscle}$ values). Species in black and red is indicting benthic and pelagic/benthopelagic foragers, respectively, and *A. carbo* is more closed to pelagic/benthopelagic feeders although this species is identified in an isolated group. Colourful grids at the bottom show the range of values in each functional trait and colour lightness corresponds to the value range next to the grids (the darker the higher values). Otolith morphology is the identified groups pointed out in Chapter 3.

5.2.2 Life history (ontogenetic vertical migration) among functional groups

According to the groupings in Figure 5.7, four main deep-sea fish taxa, macrourids, eels, spiny eels and cusk eels, comprise Cluster 1. These fish species are observed as having ontogenetic vertical migration, revealed by the thermal history recorded in the otolith or the capture of shallow larvae/juveniles recorded in the literature. Although the vertical migration has not been proven in each macrourid species, ontogenetic increases in water depth in the early life history of macrourids have been widely discussed based on the otolith oxygen isotope (Lin *et al*. 2012) and the buoyant eggs and pelagic larval phase (Fukui *et al*. 2008; Stein 1980) (more discussions in Chapter 4). Similar findings and evidences are found in *S. grandis* and other cusk eels (Fahay 1992; Fukui & Kuroda 2007; Shiao *et al*. 2014; Chapter 4). *S. kaupi* has a pelagic leptocephalus larval stage, and the habitat depth of leptocephali is recorded as 10m to 350m (Bruun 1937; Svendsen 2009). After maturation, adult *S. kaupi* descend to the bottom and can reach a depth of 6000m which downward migration is further supported by otolith oxygen isotope (Shiao *et al*. 2014). Information on the life history of Notacanthiformes is very limited, but leptocephalus larvae have been described by Smith (Smith 1970), implying that the notacanthiformes fish possibly have descending behaviours similar to Anguilliformes. However, species in Clusters 2-4 show dissimilar migration patterns. For example, *H. atlanticus*, *H. johnsonii* and *M. merluccius* have a shallower larval stage and adult fish migrate to a deeper habitat (Trueman *et al*. 2013; Shephard *et al*. 2007; Fukui *et al*. 2003; Palomera *et al*. 2005; Arneri & Morales-Nin 2000), but the vertical migration is absent in *A. rostrata* (Chapter 4) and the horizontal migration is of more importance than the vertical movement in *A carbo* and *H. dactylopterus* (Longmore *et al*. 2014; Aboim *et al*. 2005).

Thus, benthic foraging fish (Cluster 1) show consistent ontogenetic patterns of vertical migration, whereas benthoeplagic fishes have a diversity of depth-life histories. It is possible that benthic feeder are less diverse in terms of life histories, but life history cannot be explained purely by the functional behaviours, as life history traits also preserve evolutionary information (Inoue *et al*. 2010). At fish family level, macrourids and cusk eels share the similar evolutionary behaviour in terms of the nature of vertical migration between different species. However, equally closely related morid species *A. rostrata* (non-migratory species, Chapter 4) and *H. johnsonii* (migratory species, speculated to originate from a shallow larval phase and deep adult stage recorded in literature) contradict the phylogenetic-related life history traits. Therefore, how the functional or life history traits differently evolve in deep-sea fish phylogeny that is

interesting but unresolved. This is a potential topic in future works and should be studied on a greater number of species.

5.3 Summary of conclusions

- Sensory perception requirement reveals different types of foraging. Functional groups of deep-sea fishes are well defined by two sensory indices, otolith morphology and visual field, which reveal the vestibular and visual ability, respectively. The functional groups are discriminated as the pelagic and benthic foraging assemblages and the classification is further supported by other functional traits such as fish body morphology. Benthic foraging fish have consistent functional demands, such as slow and efficient swimming, the dorsal/ventral visual field and passive feeding on small prey near the seafloor. However, the pelagic foraging species develop diverse functional behaviours and they can have different visual fields, swimming performances, predator-prey interactions and so that depend on diet preferences and habitat usage.
- Sensory abilities of vision and balance are strongly influenced by the depth effect (ecological control). Fish have a higher visual sensitivity and spatial resolving power when adapted for the transformation of light sources from diffuse sunlight to pointed-source bioluminescence and the decrease of light intensity with depths. In addition, a release from selective pressure of light-dependent hunting and escape reduces the stimuli of movement that make fish have a lower level of function demand in terms of vestibular capability. The ecological trend is more significant for pelagic fish than benthic foraging species. Pelagic fish are viewed to be more reliant on light for actively feeding/swimming in the three dimensional environment (water column). However, the demersal realm is less influenced by the environmental effect with respect to depth gradients that makes benthic foraging fish have similar behaviours in the deep.
- The passive or benthic foraging fish have evolved in large-scale ontogenetic vertical migrations. In contrast, relatively active or benthopelagic species develop diverse patterns, in which vertical, horizontal and limited migrations are found. Although the hypothesis of functional behaviours in relation to fish life history still needs further validation, these observations give a new insight into deep-sea fishes ecology. For instance, benthic fishes have similar functional behaviours and life history migration patterns, and species avoid niche competitions and show clear interspecific depth distributions. Moreover, several successful taxonomic groups, especially as macrourids, cusk eels and eel-like fishes, dominate the benthic realms. For the benthopelagic

assemblage, we can find the diversity not only in life histories but also in taxonomy. This may imply a higher genetic diversity in benthopelagic fishes, facilitating biological nutrition flows and connectivity of populations in the deep-sea environment.

Appendix A : Dataset of functional groups, visual capacities and stable isotope values (SIA) in deep-sea fishes.

Order	Species	Mean depth of fish occurren-ces (m)	Peak density of GCs (cells/mm^2)	Spatial resolution (cells/ degree)	Spatial resolution (arcmin)	Lens radius (mm)	Functional groups	$\delta^{15}N_{muscle}$ (‰)	$\delta^{13}C_{muscle}$(‰)	Sample numbers for SIA	Mass ranges of samples in SIA (g)
Anguilliformes	*Serrivomer beanii*	1455	12.50	NA	NA	NA	P	10.42±0.626	-19.05±0.474	6	105-235
Anguilliformes	*Synaphobranchus kaupi*	1448	6.300	NA	NA	NA	DDV	11.63±1.039	-18.75±0.558	9	200-361
Aulopiformes	*Bathypterois dubius*	1466	7.80	NA	NA	NA	DTN	14.71±0.467	-17.84±0.113	7	42.8-79
Aulopiformes	*Bathysaurus ferox*	1750	25.35	13.00	4.617	3.65	DTN	NA	NA	NA	NA
Aulopiformes	*Omosudis lowei*	550	59.60	NA	NA	NA	PDV	NA	NA	NA	NA
Aulopiformes	*Scopelarchus michaelsarsi*	378	56.10	7.400	8.100	3.7	TE	NA	NA	NA	NA
Beryciformes	*Hoplostethus atlanticus*	1218	16.43	27.96	2.146	9.80	PDV	14.63±0.314	-17.13±0.156	12	3603-4714
Gadiformes	*Antimora rostrata*	1421	21.76	24.74	2.425	7.53	PDV	13.12±0.182	-18.32±0.328	6	1457-2146
Gadiformes	*Coryphaenoides guentheri*	1553	23.38	13.12	4.573	3.84	DDV	14.55±1.40	-17.43±0.618	7	210-473
Gadiformes	*Coryphaenoides mediterranea*	1576	22.32	NA	NA	NA	PDV	13.31±0.560	-17.64±0.610	7	1082-1748
Gadiformes	*Coryphaenoides rupestris*	1335	17.74	NA	NA	NA	PDV	11.01±0.574	-18.74±0.560	10	1340-2084
Gadiformes	*Halargyreus johnsonii*	802	12.75	7.333	8.182	2.90	P	10.07±0.373	-19.20±0.256	7	113-119
Gadiformes	*Lepidion eques*	834	10.89	NA	NA	NA	DDV	12.06±0.309	-17.90±0.470	7	166-451
Gadiformes	*Merluccius merluccius*	511	3.636	6.100	4.900	NA	DTN	13.26±0.402	-18.52±0.385	6	2378-3678
Gadiformes	*Micromesistius poutassou*	465	17.36	NA	NA	NA	PTN	10.84±0.515	-18.77±0.470	10	203-364
Gadiformes	*Molva dypterygia*	877	16.32	24.59	2.440	8.64	DTN	13.58±0.146	-18.58±0.383	4	2852-8175
Gadiformes	*Mora moro*	810	13.48	20.89	2.872	8.08	PDV	12.69±0.713	-18.17±0.358	12	1208-2344
Gadiformes	*Nezumia aequalis*	913	15.16	8.326	7.206	3.02	DDV	12.56±0.684	-17.59±0.290	11	50-85
Gadiformes	*Phycis blennoides*	549	15.39	11.14	5.387	4.02	DDV	12.72±0.653	-18.00±0.556	6	885-1816
Gadiformes	*Trachyrincus murrayi*	1382	18.82	18.41	3.259	6.02	DDV	13.20±0.583	-17.74±0.319	10	230-377
Lampriformes	*Stylephorus chordatus*	465	28.20	9.200	6.500	2.45	TE	NA	NA	NA	NA

Appendices

Order	Species	Mean depth of fish occurren -ces (m)	Peak density of GCs (cells/mm^2)	Spatial resolution (cells/ degree)	Spatial resolution (arcmin)	Lens radius (mm)	Functional groups	$\delta^{15}N_{muscle}$ (‰)	$\delta^{13}C_{muscle}$ (‰)	Sample numbers for SIA	Mass ranges of samples in SIA (g)
Myctophiformes	*Diaphus effulgens*	345	16.40	NA	NA	NA	P	NA	NA	NA	NA
Myctophiformes	*Lampanyctus ater*	520	26.30	1.300	NA	0.575	P	NA	NA	NA	NA
Myctophiformes	*Lampanyctus festivus*	400	20.40	2.000	NA	1.15	P	NA	NA	NA	NA
Myctophiformes	*Lampanyctus macdonaldi*	530	17.10	NA	NA	NA	P	NA	NA	NA	NA
Myctophiformes	*Lobianchia gemellarii*	262.5	17.50	NA	NA	NA	P	NA	NA	NA	NA
Myctophiformes	*Myctophum punctatum*	550	17.50	NA	NA	NA	P	NA	NA	NA	NA
Notacanthiformes	*Halosauropsis macrochir*	1681	23.47	6.976	8.601	2.02	DDV	13.58±0.696	-17.36±0.144	12	213-350
Notacanthiformes	*Notacanthus bonapartei*	992	3.900	NA	NA	NA	PDV	NA	NA	NA	NA
Ophidiiformes	*Spectrunculus grandis*	1809	17.96	15.01	3.998	5.02	DDV	12.91±0.453	-17.53±0.253	5	542-834
Osmeriformes	*Alepocephalus agassizi*	1771	11.30	29.39	2.042	12.42	DTN	11.85±0.714	-18.53±0.298	9	2086-2996
Osmeriformes	*Alepocephalus bairdii*	1186	17.73	21.80	2.752	7.35	DTN	10.24±0.465	-18.90±0.306	18	3722-4735
Osmeriformes	*Alepocephalus productus*	2250	17.80	NA	NA	NA	DTN	NA	NA	NA	NA
Osmeriformes	*Argentina silus*	576	7.457	NA	NA	NA	DTN	10.31±0.730	-18.89±0.603	10	550-685
Osmeriformes	*Bathytroctes microlepis*	1802	30.80	13.50	4.400	3.45	PTN	NA	NA	NA	NA
Osmeriformes	*Conocara macroptera*	1678	11.90	10.40	5.800	4.25	PTN	NA	NA	NA	NA
Osmeriformes	*Conocara murrayi*	1621	11.20	NA	NA	NA	PTN	NA	NA	NA	NA
Osmeriformes	*Conocara salmonea*	3300	8.100	13.50	4.400	6.75	PTN	NA	NA	NA	NA
Osmeriformes	*Narcetes stomias*	1900	20.20	10.00	6.000	3.15	PTN	NA	NA	NA	NA
Osmeriformes	*Opisthoproctus grimaldii*	235	52.60	5.700	10.50	1.075	TE	NA	NA	NA	NA
Osmeriformes	*Opisthoproctus soleatus*	280	43.60	4.300	13.60	0.875	TE	NA	NA	NA	NA
Osmeriformes	*Platytroctes apus*	692.5	26.20	9.300	6.500	2.55	PTN	NA	NA	NA	NA
Osmeriformes	*Rouleina attrita*	1597	27.40	12.70	4.700	1.715	PTN	NA	NA	NA	NA
Osmeriformes	*Searsia koefoedi*	975	23.80	7.400	8.100	2.125	PTN	NA	NA	NA	NA
Osmeriformes	*Xenodermichthys copei*	944	24.30	6.400	9.400	0.92	PTN	8.574±0.803	-19.30±0.580	9	40-52
Perciformes	*Aphanopus carbo*	917	11.19	19.94	3.008	8,47	PTN	12.39±0.619	-18.01±0.246	6	1041-1926
Perciformes	*Epigonus telescopus*	744	13.41	28.13	2.133	10.91	DTN	9.45±2.30	-18.37±0.353	2	1160-1296
Perciformes	*Howellasherborni*	162.5	24.50	NA	NA	NA	PTN	NA	NA	NA	NA

Order	Species	Mean depth of fish occurren -ces (m)	Peak density of GCs (cells/mm^2)	Spatial resolution (cells/ degree)	Spatial resolution (arcmin)	Lens radius (mm)	Functional groups	$\delta^{15}N_{muscle}$ (‰)	$\delta^{13}C_{muscle}$ (‰)	Sample numbers for SIA	Mass ranges of samples in SIA (g)
Scorpaeniformes	*Helicolenus dactylopterus*	469	19.11	18.96	3.165	6.16	DTN	12.23±0.499	-17.43±0.197	7	216-511
Stephanoberyciformes	*Poromitra capito*	900	11.00	NA	NA	NA	P	NA	NA	NA	NA
Stephanoberyciformes	*Scopelogadus beanii*	900	7.800	NA	NA	NA	P	NA	NA	NA	NA
Stomiiformes	*Argyropelecus aculeatus*	350	50.60	NA	NA	NA	TE	NA	NA	NA	NA
Stomiiformes	*Argyropelecus affinis*	450	34.00	7.900	7.500	1.9	TE	NA	NA	NA	NA
Stomiiformes	*Argyropelecus gigas*	500	31.30	8.700	6.800	2.2	TE	NA	NA	NA	NA
Stomiiformes	*Argyropelecus hemigymnus*	425	33.00	5.000	12.00	NA	TE	NA	NA	NA	NA
Stomiiformes	*Argyropelecus sladeni*	425	38.60	8.400	7.100	1.9	TE	NA	NA	NA	NA
Stomiiformes	*Chauliodus sloani*	750	21.40	NA	NA	NA	P	NA	NA	NA	NA
Stomiiformes	*Sternoptyx diaphana*	700	21.60	NA	NA	NA	TE	NA	NA	NA	NA

Appendix B : Otolith functional indices values and fish muscle stable isotope values.

Species	Otolith morphological analysis							Muscle isotope analysis				
	Depth (m)	Fish number	Fish body weight (g)	Otolith weight (mg)	OB ratio	SO ratio	Assigned group	Depth (m)	Fish number	Fish body weight (g)	$\delta^{15}N$ (‰)	$\delta^{13}C$ (‰)
Anguilliformes												
Serrivomer beani	1800-2000	3	105-189	1.48	0.00977	0. 066	B	1800-2000	6	105-235	10.4	-19.1
Synaphobranchus kaupi	1800	10	82-256	5.63	0.0381	0.112	B	1500-1800	10	200-361	11.6	-18.8
Aulopiformes												
Bathypterois dubius	1500	6	43-73	31.2	0.126	0.119	B	1500	7	43-79	14.7	-17.8
Bathysaurus ferox	2000	1	485	33.7	0.0695	0.129	C	NA	NA	NA	NA	NA
Beryciformes												
Hoplostethus atlanticus	1500	15	2062-4591	413	0.112	0.199	D	1500	6	3810-4714	14.6	-17.1
Gadiformes												
Brosme brosme	540-760	4	1486-2714	158	0.0821	0.145	B	500	3	2034-4132	14.7	-17.4
Molva dypterygia	680-910	37	656-8400	276	0.0914	0.189	C	1000	4	2852-8175	13.6	-18.6
Merluccius merluccius	500	10	474-3678	473	0.245	0.220	C	500	6	2378-3678	13.3	-18.5
Molva molva	500	3	780-2060	116	0.0946	0.243	C	500	6	2060-5106	13.6	-17.8
Micromesistius poutassou	500	17	108-364	179	0.827	0.239	C	500	10	203-364	10.8	-18.8
Phycis blennoides	500	15	372-2038	318	0.494	0.303	C	500	6	885-1816	12.7	-18.0

Species	Otolith morphological analysis							Muscle isotope analysis				
	Depth (m)	Fish number	Fish body weight (g)	Otolith weight (mg)	OB ratio	SO ratio	Assigned group	Depth (m)	Fish number	Fish body weight (g)	$\delta^{15}N$ (‰)	$\delta^{13}C$ (‰)
Gadiformes												
Coelorhynchus coelorhynchus	540	17	119-296	212	1.25	0.139	B	500	10	107-267	11.8	-17.5
Coryphaenoides guentheri	1500-1850	21	60-400	75.1	0.621	0.129	B	1500-2000	7	210-473	14.5	-17.4
Coelorhynchus labiatus	1800	10	74-111	138	1.53	0.098	B	1500	7	30-53	12.5	-17.8
Coryphaenoides mediterranea	1500-1800	10	789-1748	205	0.173	0.137	B	1500-1800	7	1082-1748	13.3	-17.6
Coryphaenoides rupestris	1500-1650	21	106-2484	228	0.429	0.156	B	500-1500	10	1340-2084	11.0	-18.7
Nezumia aequalis	650	21	38-76	73.15	1.39	0.111	B	750-1000	11	50-85	12.6	-17.6
Trachyrincus murrayi	1500-1850	15	38-259	185	1.66	0.165	B	1000-1500	9	236-377	13.2	-17.7
Antimora rostrata	1800-2000	13	1250-2146	335	0.477	0.141	C	1800-2000	12	1040-2146	13.1	-18.3
Halargyreus johnsonii	760-1000	14	40-119	76.8	1.01	NA	C	1000	7	113-119	10.1	-19.2
Lepidion eques	760-1000	20	115-442	260	1.48	NA	C	500-1000	7	166-451	12.1	-17.9
Mora moro	610-810	18	1012-2754	567	0.388	NA	D	500-1000	12	1208-2344	12.7	-18.2
Notacanthiformes												
Halosauropsis macrochir	1750-1800	10	195-426	15.0	0.0538	0.082	B	1800	12	213-350	13.6	-17.4
Polyacanthonotus rissoanus	1500	7	33-190	1.15	0.0136	0.110	B	1500	9	33-190	14.6	-17.4

Species	Otolith morphological analysis							Muscle isotope analysis				
	Depth (m)	Fish number	Fish body weight (g)	Otolith weight (mg)	OB ratio	SO ratio	Assigned group	Depth (m)	Fish number	Fish body weight (g)	$\delta^{15}N$ (‰)	$\delta^{13}C$ (‰)
Ophidiiformes												
Cataetyx laticeps	1500-1800	25	2812-5662	1000	0.251	0.155	B	1500	9	2883-4660	15.2	-16.3
Spectrunculus grandis	1850	11	262-834	247	0.476	0.168	B	1800	5	542-834	12.9	-17.5
Osmeriformes												
Argentina silus	500	19	302-764	75.3	0.142	0.214	A	500-750	10	550-685	10.3	-18.9
Alepocephalus agassizi	1650	10	1572-4645	26.9	0.00892	0.095	A	1800-2000	9	2086-2996	11.8	-18.5
Alepocephalus bairdii	1000-1500	26	116-3930	19.1	0.0261	0.109	A	1000-1800	18	3722-4735	10.2	-18.9
Rouleina attrita	1750	5	343-822	19.5	0.0350	0.090	A	NA	NA	NA	NA	NA
Xenodermichthys copei	1000	10	21-43	2.18	0.0676	0.094	A	1000	9	40-52	8.6	-19.3
Perciformes												
Aphanopus carbo	850	23	598-1894	23.1	0.0214	0.094	C	750-1000	6	1041-1926	12.4	-18.0
Centrolophus niger	500	2	984-1260	135	0.101	0.145	C	NA	NA	NA	NA	NA
Epigonus telescopus	900-1000	4	998-2118	246	0.205	0.211	A	1000	2	1100-1296	9.4	-18.4
Lycodes atlanticus	2000	3	51-106	26.9	0.342	0.095	A	NA	NA	NA	NA	NA
Nesiarchus nasutus	800	2	1078-1168	13.3	0.0120	0.149	C	NA	NA	NA	NA	NA

Species	Otolith morphological analysis							Muscle isotope analysis				
	Depth (m)	Fish number	Fish body weight (g)	Otolith weight (mg)	OB ratio	SO ratio	Assigned group	Depth (m)	Fish number	Fish body weight (g)	$\delta^{15}N$ (‰)	$\delta^{13}C$ (‰)
Scorpaeniformes												
Helicolenus dactylopterus	680	49	192-716	95.4	0.315	0.211	C	500	7	216-511	12.2	-17.4
Sebastes mentella	600	14	968-1842	613	0.391	0.168	C	NA	NA	NA	NA	NA
Stomiiformes												
Borostomias antarcticus	1800	2	107-201	0.15	0.0147	0.092	A	NA	NA	NA	NA	NA

Appendix C: SO ratio measured from otolith images in Campana (2004). Values in brackets are the median depth of fish occurrences (Neat & Campbell, 2013). [P]Pleagic; [D]demersal.

Species	Length (cm)	SO ratio	Depth of occurrences (m)	Species	Length (cm)	SO ratio	Depth of occurrences (m)
Anguilliformes				*Alosa sapidissima*[P]	44	0.29	0-259
Derichthys serpentinus[P]	26	0.24	200-700	*Brevoortia tyrannus*[P]	16	0.26	0-50
Ilyophis brunneus[P]	57	0.18	450-3120	*Clupea harengus harengus*[D]	26	0.25	0-200
Simenchelys parasiticus (parasitica)[D]	45	0.18	500-1800				
Venefica procera[D]	101	0.16	326-2304	**Gadiformes**			
Anguilla rostrata[D]	37	0.23	0-464	*Boreogadus saida*[D]	17	0.20	0-400
Nemichthys scolopaceus[P]	121	0.14	450-1800(975)	*Enchelyopus cimbrius*[D]	11	0.15	20-265
Nessorhamphus ingolfianus[P]	25	0.22	550-1500(995)	*Gadus morhua*[D]	31	0.26	150-200
				Gadus ogac[D]	29	0.27	0-200
Aulopiformes				*Gaidropsarus argentatus*[D]	29	0.13	400-2260
Alepisaurus brevirostris[P]	125	0.18	140-1590	*Gaidropsarus ensis*[D]	19	0.14	0-2000
Bathypterois quadrifilis[D]	17	0.16	402-1408	*Halargyreus johnsoni*[P]	44	0.18	650-1700
Chlorophthalmus agassizi[D]	12	0.23	500-1000	*Macrourus berglax*[D]	23	0.18	300-500
Notolepis rissoi (Arctozenus risso)[P]	22	0.18	0-2200	*Melanogrammus aeglefinus*[D]	11	0.23	10-200
Paralepis atlantica (Magnisudis atlantica)[P]	12	0.20	0-4750	*Melanonus zugmayeri*[P]	10	0.14	750-1800(978)
Parasudis truculenta[D]	14	0.22	133-181	*Merluccius albidus*[D]	34	0.20	160-640
				Merluccius bilinearis[D]	15	0.25	55-914
Belonifonnes				*Microgadus tomcod*[D]	8	0.26	0-69
Scomberesox saurus[P]	25	0.21	0-30	*Nezumia bairdi*[D]	16	0.19	90-700
				Nezumia sclerorhynchus[P]	28	0.17	450-730
Beryciformes				*Pollachius virens*[D]	32	0.26	37-364
Hoplostethus mediterraneus[D]	13	0.28	600-900(662)	*Urophycis chesteri (Phycis chesteri)*[D]	32	0.24	360-800
				Urophycis chuss[D]	24	0.29	110-130
Clupeiformes				*Urophycis regia*[D]	14	0.30	110-185
Alosa aestivalis[P]	24	0.33	0-55	*Urophycis tenuis*[D]	20	0.28	180-1000
Alosa pseudoharengus[P]	29	0.25	5-145				

Species	Length (cm)	SO ratio	Depth of occurrences (m)	Species	Length (cm)	SO ratio	Depth of occurrences (m)
Lophiifomies				*Narcetes stomias*[P]	59	0.16	1800-2100
Cryptopsaras couesi[P]	21	0.12	500-1250	*Osmerus mordax*[P]	17	0.22	0-425
Dibranchus atlanticus[D]	5	0.09	300-823				
Lophius americanus[D]	38	0.10	0-668	**Perciformes**			
				Acanthoeybium solandri[P]	129	0.30	0-12
Myctophiformes				*Ammodytes americanus / dubius*[D]	12	0.20	0-73
Benthosema glaciale[P]	6	0.16	300-400	*Anarhichas denticulatus*[D]	76	0.16	100-900
Diaphus dumerilii[P]	5	0.24	450-500	*Anarhichas lupus*[D]	64	0.16	18-110
Diaphus metopoclampus[P]	8	0.26	90-1080	*Anarhichas minor*[D]	31	0.15	100-400
Diaphus rafinesquii[P]	8	0.21	40-1200	*Benthodesmus elongatus*[D]	32	0.19	178-950
Lampadena speculigera[P]	16	0.21	0-1000	*Brama brama*[P]	64	0.32	400-1800(652)
Lampanyctus macdonaldi[P]	12	0.15	60-762	*Callionymus agassizi* [D]	18	0.14	250-700
Lobianchia gemellarii[P]	6	0.23	25-800	*(Foetorepus agassizii)*			
Myctophum punctatum[P]	5	0.21	0-1000	*Caranx crysos*[P]	16	0.26	0-100
Notoscopelus resplendens[P]	9	0.21	0-2121	*Caranx hippos*[P]	19	0.22	1-200
				Caristius groenlandicus[P]	17	0.12	100-420
Notacanthiformes				*Chiasmodon niger*[P]	11	0.15	750-2745
Notacanthus chemnitzi[D]	87	0.15	622-2000(1319)	*Coryphaena hippurus*[P]	75	0.26	5-10
Lipogenys gilli[D]	63	0.16	400-2000	*Echeneis naucrates*[P]	19	0.26	1-50
				Eumesogrammus praecisus[D]	16	0.13	5-400
Ophidiiformes				*Howella sherborni*[P]	11	0.21	26-950
Dicrolene intronigra[D]	19	0.14	1000-1600				
Lepophidium cervinum[D]	14	0.17	60-399				
Osmeriformes							
Bajacalifornia megalops[P]	36	0.17	800-1400				
Bathylagus euryops[P]	14	0.16	750-2030(1554)				
Holtbyrnia macrops[D]	14	0.13	910-2012(1516)				
Mallotus villosus[P]	17	0.17	0-725				

Species	Length (cm)	SO ratio	Depth of occurrences (m)	Species	Length (cm)	SO ratio	Depth of occurrences (m)
Perciformes				*Taractichthys longipinnis*[P]	71	0.32	42-200
Katsuwonus pelamis[P]	61	0.34	0-260	*Tautoga onitis*[P]	12	0.17	1-75
Lepidocybium flavobrunneum[D]	79	0.25	200-1100	*Tautogolabrus adspersus*[P]	27	0.18	10-128
Lopholatilus chamaeleonticeps[D]	42	0.15	80-540	*Tetrapturus albidus*[P]	144	0.22	0-100
Lumpenus lumpretaeformis[D]	53	0.12	40-100	*Thunnus alalunga*[P]	96	0.40	0-100
Lumpenus maculatus[D]	13	0.08	2-607	*Thunnus albacares*[P]	134	0.40	1-100
Lycenchelys verrilli[D]	14	0.16	46-1100	*Thunnus obesus*[P]	74	0.40	0-50
Lycenchelys paxillus[D]	7	0.15	46-1525	*Thunnus thynnus*[P]	76	0.38	0-100
Lycodes esmarki[D]	34	0.15	251-350				
Lycodes lavalaei[D]	28	0.14	57-535	**Pleuronectiforrnes**			
Lycodes reticulatus[D]	48	0.16	100-930	*Citharichthys arctifrons*[D]	16	0.13	46-366
Lycodes vahlii[D]	18	0.12	65-1200	*Glyptocephalus cynoglossus*[D]	49	0.13	300-1500(643)
Macrozoarces americanus[D]	61	0.12	0-388	*Hippoglossoides platessoides*[D]	22	0.11	90-250
Melanostigma atlanticum[P]	6	0.11	500-1800(914)	*Hippoglossus hippoglossus*[D]	43	0.21	50-2000
Mullus auratus[D]	14	0.15	10-60	*Limanda ferruginea*[D]	31	0.18	36-91
Peprilus tricanthus[D]	22	0.27	15-420	*Paralichthys dentatus*[D]	22	0.18	10-37
Pholis gunnellus[D]	13	0.19	0-30	*Pseudopleuronectes americanus*[D]	67	0.14	5-143
Polyprion americanus[D]	102	0.20	100-200	*Reinhardtius hippoglossoides*[D]	24	0.11	1500-1529(1503)
Pomatomus saltatrix[P]	28	0.28	0-200	*Scophthalmus aquosus*[D]	21	0.15	55-73
Ruvettus pretiosus[D]	23	0.25	200-400	*Symphurus pterospilotus* [D]	11	0.11	201-380
Sarda sarda[P]	56	0.36	80-200	*(Symphurus billykrietei)*			
Scomber japonicus[P]	22	0.37	50-200				
Scomber scombrus[P]	21	0.38	0-200	**Polymixiiformes**			
Scomberomorus maculatus[P]	45	0.39	10-35	*Polymixia lowei*[D]	16	0.22	150-600
Scomberornorus cavalla[P]	71	0.37	5-15				
Selene setapinnis[D]	5	0.16	0-55	**Saccopharyngiformes**			
Seriola dumerili[P]	24	0.24	18-72	*Eurypharyrvc pelecanoides*[P]	31	0.16	1200-1400
Synagrops bellus[D]	7	0.19	107-179				
Synagrops spinosa[D]	5	0.25	300-500				

Species	Length (cm)	SO ratio	Depth of occurrences (m)	Species	Length (cm)	SO ratio	Depth of occurrences (m)
Salmoniformes				*Peristedion miniatum*[D]	11	0.18	64-910
Coregonus clupeaformis[D]	16	0.24	12-128	*Prionotus carolinus*[D]	26	0.22	15-170
Oncorhynchus mykiss[D]	24	0.22	0-200	*Sebastes fasciatus*[D]	26	0.20	128-366
Salmo salar[D]	26	0.26	10-23	*Sebastes marinus*[P]	16	0.15	100-500
Salmo trutta[P]	41	0.27	0-10	*Triglops murrayi*[D]	12	0.15	7-530
Salvelinus alpinus[D]	41	0.29	30-70	*Triglops nybelini*[D]	13	0.11	200-600
Salvelinus fontinalis[D]	21	0.25	15-27	*Triglops pingeli*[D]	11	0.14	18-91
Scorpaeniformes				**Stephanoberyciformes**			
Agonus decagonus[D]	17	0.12	75-230	*Poromitra megalops*[P]	14	0.14	150-1000
(Leptagonus decagonus)				*Rondeletia loricata*[P]	9	0.14	100-3500
Artediellus atlanticus[D]	7	0.15	35-900	*Scopelogadus beanii*[P]	12	0.14	0-2500
Aspidophoroides monopterygius[D]	11	0.13	60-150				
Aspidophoroides olriki[D]	8	0.090	7-520	**Stomiiformes**			
Careproctus reinhardti[D]	13	0.10	75-1750	*Argyropelecus aculeatus*[P]	9	0.14	100-600
Cottunculus microps[D]	15	0.10	165-215	*Argyropelecus gigas*[P]	7	0.14	400-600
Cottunculus thomsonii[D]	26	0.10	540-1800(1122)	*Chauliodus sloani*[P]	17	0.16	494-1000
Cyclopterus lumpus[D]	22	0.17	50-150	*Cyclothone microdon*[P]	5	0.11	500-2700
Ectreposebastes imus[P]	9	0.17	500-850	*Malacosteus niger*[P]	20	0.13	500-3886
Eumicrotremus spinosus[D]	6	0.17	60-200	*Maurolicus muelleri*[P]	5	0.19	300-400
Gymnocanthus tricuspis[D]	19	0.13	0-451	*Polyipnus asteroides*[P]	3	0.13	366-732
Icelus bicornis[D]	7	0.11	0-930	*Sternoptyx diaphana*[P]	6	0.14	500-800
Icelus spatula[D]	9	0.11	125-150	*Stomias boa*[P]	19	0.19	200-1500
Liparis atlanticus[D]	19	0.16	0-145	*Vinciguerria nimbaria*[P]	6	0.15	20-400
Liparis fabricii[D]	13	0.13	12-1800				
Liparis gibbus[D]	24	0.16	100-200	**Zeiformes**			
Myoxocephalus scorpioides[D]	17	0.16	0-275	*Cyttopsis roseus (rosea)*[P]	9	0.085	330-690
Myoxocephalus scorpius[D]	19	0.16	0-145	*Daramattus americanus*[P]	9	0.12	500-700
Paraliparis calidus[D]	8	0.11	150-1207	*(Grammicolepis brachiusculus)*			
Paraliparis copei[D]	10	0.12	200-1976	*Zenopsis conchifera (conchifer)*[D]	33	0.13	150-330

Appendix D : Multiple linear regression model of ontogenetic $\delta^{13}C_{oto}$ changes in four target deep-sea fishes

Regression model: *Alepocephalus bairdii*

$Log_{10}(\delta^{13}C_{oto}) \sim \delta^{18}O_{oto} * Log_{10}$[iGR(index of growth rate)] * log_{10}[iBM(index of body mass)]

	Estimate	Std. Error	t value	Pr(>|t|)
(Intercept)	-0.107	1.52	-0.007	0.995
$\delta^{18}O_{oto}$	0.185	0.518	0.358	0.726
Log_{10}(iGR)	0.175	1.55	0.113	0.911
Log_{10}(iBM)	0.964	0.721	1.34	0.204
$\delta^{18}O_{oto}$: Log_{10}(iGR)	-0.141	0.526	-0.267	0.793
$\delta^{18}O_{oto}$: Log_{10}(iBM)	-0.346	0.246	-1.40	0.184
Log_{10}(iGR) : Log_{10}(iBM)	1.57	0.835	1.88	0.0825
$\delta^{18}O_{oto}$: Log_{10}(iGR) : Log_{10}(iBM)	-0.573	0.287	-2.00	0.0669

Signif. codes: 0 '***' 0.001 '**' 0.01 '*' 0.05

Residual standard error: 0.0198 on 13 degrees of freedom
Multiple R-squared: 0.8574, Adjusted R-squared: 0.7806
F-statistic: 11.17 on 7 and 13 DF, p-value: 0.0001333

Regression model: *Antimora rostrata*

$Log_{10}(\delta^{13}C_{oto}) \sim \delta^{18}O_{oto} + Log_{10}$[iGR(index of growth rate)] + log_{10}[iBM(index of body mass)]+ $\delta^{18}O_{oto}$:Log_{10}[iGR(index of growth rate)]+ Log_{10}[iGR(index of growth rate)]:log_{10}[iBM(index of body mass)]

	Estimate	Std. Error	t value	Pr(>|t|)
(Intercept)	1.69	0.37	4.51	<0.001 ***
$\delta^{18}O_{oto}$	-0.235	0.112	-2.10	0.0402 *
Log_{10}(iGR)	0.916	0.341	2.69	0.00945**
Log_{10}(iBM)	0.113	0.0180	6.33	<0.001***
$\delta^{18}O_{oto}$: Log_{10}(iGR)	-0.238	0.101	-2.35	0.0225*
Log_{10}(iGR): Log_{10}(iBM)	0.0914	0.0184	4.982	<0.001***

Signif. codes: 0 '***' 0.001 '**' 0.01 '*' 0.05

Residual standard error: 0.02629 on 55 degrees of freedom
Multiple R-squared: 0.7347, Adjusted R-squared: 0.7106
F-statistic: 30.46 on 5 and 55 DF, p-value: 1.059e-14

Regression model: *Coryphaenoides rupestris*

$Log_{10}(\delta^{13}C_{oto}) \sim \delta^{18}O_{oto} * Log_{10}$[iGR(index of growth rate)] * log_{10}[iBM(index of body mass)]

	Estimate	Std. Error	t value	Pr(>|t|)
(Intercept)	-2.345	0.727	-3.224	0.00260 **
$\delta^{18}O_{oto}$	0.742	0.224	3.311	0.00204 **
Log_{10}(iGR)	-3.194	0.913	-3.499	0.00121 **
Log_{10}(iBM)	-0.972	0.342	-2.844	0.00714 **
$\delta^{18}O_{oto}$: Log_{10}(iGR)	0.808	0.278	2.91	0.00602 **
$\delta^{18}O_{oto}$: Log_{10}(iBM)	0.260	0.109	2.38	0.02243 *
Log_{10}(iGR) : Log_{10}(iBM)	-1.33	0.515	-2.58	0.0138*
$\delta^{18}O_{oto}$: Log_{10}(iGR) : Log_{10}(iBM)	0.364	0.165	2.20	0.0341*

Signif. codes: 0 '***' 0.001 '**' 0.01 '*' 0.05

Residual standard error: 0.0591 on 38 degrees of freedom

Multiple R-squared: 0.9135, Adjusted R-squared: 0.8976

F-statistic: 57.33 on 7 and 38 DF, p-value: < 2.2e-16

Regression model: *Spectrunculus grandis*

$Log_{10}(\delta^{13}C_{oto}) \sim \delta^{18}O_{oto} * log_{10}$[iBM(index of body mass)] * Log_{10}[iGR(index of growth rate)]

	Estimate	Std. Error	t value	Pr(>|t|)
(Intercept)	0.815	0.488	1.67	0.102
$\delta^{18}O_{oto}$	0.0701	0.129	0.544	0.589
Log_{10}(iGR)	0.170	0.517	0.329	0.743
Log_{10}(iBM)	0.610	0.155	3.93	<0.001***
$\delta^{18}O_{oto}$: Log_{10}(iGR)	-0.00476	0.138	-0.034	0.973
$\delta^{18}O_{oto}$: Log_{10}(iBM)	-0.102	0.0502	-2.03	0.0488*
Log_{10}(iGR) : Log_{10}(iBM)	0.645	0.198	3.27	0.00211**
$\delta^{18}O_{oto}$: Log_{10}(iGR) : Log_{10}(iBM)	-0.127	0.0663	-1.92	0.0612

Signif. codes: 0 '***' 0.001 '**' 0.01 '*' 0.05

Residual standard error: 0.03171 on 44 degrees of freedom
Multiple R-squared: 0.9716, Adjusted R-squared: 0.967
F-statistic: 214.8 on 7 and 44 DF, p-value: < 2.2e-16

Appendix E : Dataset for multiple factor analysis

	Otolith morphological indices					Visual fields				
Species	FormFactor	Roundness	Rectangularity	Circularity	Ellipticity	Nasal	Temporal	Dorsal	Ventral	Peripheral
Alepocephalus agassizi	0.604	0.792	0.666	20.97	0.149	1	0	0	0	0
Alepocephalus bairdii	0.544	0.644	0.643	24.04	0.207	1	0	0	0	0
Aphanopus carbo	0.578	0.443	0.719	21.89	0.378	1	1	0	0	0
Antimora rostrata	0.473	0.358	0.624	26.74	0.425	0	0	1	1	0
Argentina silus	0.534	0.589	0.602	23.82	0.224	1	0	0	0	0
Bathypterois dubius	0.715	0.579	0.731	17.61	0.285	1	1	0	0	0
Coryphaenoides guentheri	0.778	0.663	0.743	16.17	0.199	0	0	1	1	0
Coryphaenoides mediterranea	0.708	0.577	0.746	17.80	0.249	0	0	1	1	0
Coryphaenoides rupestris	0.744	0.637	0.734	16.94	0.218	0	0	0	1	0
Hoplostethus atlanticus	0.302	0.438	0.536	42.18	0.258	0	0	1	1	0
Helicolenus dactylopterus	0.587	0.544	0.667	21.63	0.297	1	0	0	0	1
Halargyreus johnsonii	0.446	0.383	0.594	28.57	0.367	0	0	0	0	1
Halosauropsis macrochir	0.733	0.661	0.731	17.19	0.180	0	0	0	1	0
Lepidion eques	0.513	0.400	0.714	24.63	0.387	0	0	1	1	0
Merluccius merluccius	0.401	0.342	0.684	31.94	0.467	1	1	0	0	0
Mora moro	0.413	0.554	0.535	30.62	0.254	0	0	0	1	0
Micromesistius poutassou	0.515	0.320	0.764	24.62	0.510	1	0	0	0	0
Nezumia aequalis	0.725	0.645	0.705	17.40	0.205	0	0	0	1	0
Phycis blennoides	0.533	0.373	0.695	23.82	0.431	0	0	0	1	0
Spectrunculus grandis	0.749	0.593	0.738	16.79	0.268	0	0	1	1	0
Synaphobranchus kaupi	0.778	0.792	0.723	16.16	0.101	0	0	1	0	0
Trachyrincus murrayi	0.783	0.811	0.692	16.12	0.112	0	0	1	0	0

Species	$a_{3.0}$	Mean mouth diameter (mm)	Relative mouth opening	$\delta^{15}N_{muscle}$ (‰)	$\delta^{13}C_{muscle}$ (‰)
Alepocephalus agassizi	0.00745	77.0	0.718	11.84	-18.53
Alepocephalus bairdii	0.00651	54.4	0.818	10.24	-18.90
Aphanopus carbo	0.00063	90.5	2.930	12.39	-18.01
Antimora rostrata	0.00611	57.7	0.807	13.12	-18.32
Argentina silus	0.00722	27.5	0.725	10.31	-18.89
Bathypterois dubius	0.00527	27.6	1.290	14.71	-17.83
Coryphaenoides guentheri	0.00297	18.0	0.261	14.55	-17.43
Coryphaenoides mediterranea	0.00187	34.0	0.977	13.31	-17.64
Coryphaenoides rupestris	0.00301	46.5	0.679	11.01	-18.74
Hoplostethus atlanticus	0.01853	77.1	1.100	14.63	-17.13
Helicolenus dactylopterus	0.01632	51.2	0.969	12.23	-17.43
Halargyreus johnsonii	0.00519	26.9	1.430	10.07	-19.20
Halosauropsis macrochir	0.00174	34.6	1.110	13.58	-17.36
Lepidion eques	0.00538	29.8	0.821	12.06	-17.90
Merluccius merluccius	0.00676	80.8	1.060	13.26	-18.52
Mora moro	0.00848	65.4	0.717	12.69	-18.17
Micromesistius poutassou	0.00551	36.1	1.090	10.84	-18.77
Nezumia aequalis	0.00484	15.2	0.393	12.56	-17.59
Phycis blennoides	0.00717	51.3	0.747	12.72	-18.00
Spectrunculus grandis	0.00564	42.4	0.467	12.90	-17.53
Synaphobranchus kaupi	0.00069	37.1	1.010	11.63	-18.75
Trachyrincus murrayi	0.00245	33.4	0.797	13.20	-17.74

List of References

Aboim, M.A., Menezes, G.M., Schlitt, T. & Roger, A.D., 2005. Genetic structure and history of populations of the deep-sea fish *Helicolenus dactylopterus* (Delaroche, 1809) inferred from mtDNA sequence analysis. *Molecular Ecology*, 14(5), pp.1343–1354. Available at: http://doi.wiley.com/10.1111/j.1365-294X.2005.02518.x.

Abecasis, D., Costa, A.R., Pereira, J.G. & Pinho, M.R., 2006. Age and growth of bluemouth, *Helicolenus dactylopterus* (Delaroche, 1809) from the Azores. *Fisheries Research*, 79(1-2), pp.148–154. Available at: http://linkinghub.elsevier.com/retrieve/pii/S0165783606000725.

Aguirre, H. & Lombarte, A., 1999. Ecomorphological comparisons of sagittae in *Mullus barbatus* and *M. surmuletus*. *Journal of Fish Biology*, 555, pp.105–114.

Aguirre, W.E., 2003. Allometric growth of the sulcus in *Cynoscion* spp. (Sciaenidae). *Journal of Fish Biology*, 63, pp.1341–1346.

Albikovskaya, L.K. & Gerasimova, O.V., 1993. Food and feeding patterns of cod (*Gadus morhua* L.) and beaked redfish (*Sebastes mentella* Travin) on Flemish Cap. *NAFO Scientific Council Studies,* 19, pp.31–39.

Albouy, C., Guilhaumon, F., Villéger, S., Mouchet, M., Mercier, L., Culioli, J.M., Tomasini, J.A., Le Loc'h, F. & Mouillot, D., 2011. Predicting trophic guild and diet overlap from functional traits: statistics, opportunities and limitations for marine ecology. *Marine Ecology Progress Series*, 436, pp.17–28.

Allain, V., 2001. Reproductive strategies of three deep-water benthopelagic fishes from the northeast Atlantic Ocean. *Fisheries Research*, 51, pp.165–176.

Allain, V. & Lorance, P., 2000. Age estimation and growth of some deep-sea fish from the northeast Atlantic ocean. *Cybium*, 24(3), pp.7–16.

Allain, V., Biseau, A. & Kergoat, B., 2003. Preliminary estimates of French deepwater fishery discards in the Northeast Atlantic Ocean. *Fisheries Research*, 60(1), pp.185–192.

Allmendinger, R. 2011. http://www.geo.cornell.edu/geology/faculty/RWA/programs/stereonet.html

Andrews, A.H., Tracey, D.M. & Dunn, M.R., 2009. Lead-radium dating of orange roughy (*Hoplostethus atlanticus*): validation of a centenarian life span. *Canadian Journal of Fisheries and Aquatic Sciences*, 66(7), pp.1130–1140.

Andriashev, A.P., 1953. *Ancient deep-water and secondary deepwater fishes and their importance in a zoogeographical analysis*, Akad. Nauk SSSR.

Angel, M.V., 1997. What is the deep sea. In D. J. Randall & A. P. Farrell, eds. *Deep-sea fishes*. Academic Press, pp. 1–41.

Arellano, R.V., Hamerlynck, O., Vincx, M., Mees, J., Hostens, K. & Gijselinck, W., 1995. Changes in the ratio of the sulcus acusticus area to the sagitta area of *Pomatoschistus minutus* and *P. lozanoi* (Pisces, Gobiidae). *Marine Biology*, 122, pp. 355–360.

References

Arneri, E. & Morales-Nin, B., 2000. Aspects of the early life history of European hake from the central Adriatic. *Journal of Fish Biology*, 56(6), pp.1368–1380.

Bailey, D.M., Bagley, P.M., Jamieson, A.J., Collins, M.A. & Priede, I.G., 2003. In situ investigation of burst swimming and muscle performance in the deep-sea fish *Antimora rostrata*. *Journal of Experimental Marine Biology and Ecology*, 285, pp.295–311.

Bailey, D.M., Bagley, P.M., Jamieson, A.J., Collins, M.A. & Priede, I.G., 2002. Measurement of in situ oxygen consumption of deep-sea fish using an autonomous lander vehicle. *Deep-Sea Research Part I*, 49(8), pp.1519–1529.

Bailey, D.M., King, N.J. & Priede, I.G., 2007. Cameras and carcasses: historical and current methods for using artificial food falls to study deep-water animals. *Marine Ecology Progress Series*, 350, pp.179–191. Available at: http://www.int-res.com/abstracts/meps/v350/p179-191/.

Baker, K.D., Haedrich, R.L., Snelgrove, P.V.R., Wareham, V.E., Edinger, E.N. & Gilkinson, K.D., 2012. Small-scale patterns of deep-sea fish distributions and assemblages of the Grand Banks, Newfoundland continental slope. *Deep-Sea Research Part I*, 65, pp.171–188.

Bemis, B.E., Kendall, C., Wankel, S.D., Lange,T. & Krabbenhoft, D.P., 2003. Isotopic evidence for spatial and temporal changes in Everglades food web structure. Poster presented at Greater Everglades Ecosystem Restoration Conference . Palm Harbor, Florida.

Bergstad, O.A., 1990. Distribution, population structure, growth and reproduction of the roundnose grenadier *Coryphaenoides rupestris* (Pisces: Macrouridae) in the deep waters of the Skagerrak. *Marine Biology*, 107(1), pp.25–39.

Bergstad, O.A., 1991. Distribution and trophic ecology of some gadoid fish of the Norwegian Deep 2. Food-web linkages and comparisons of diets and distributions. *Sarsia*, 75(4), pp.315–325.

Bergstad, O.A., Gjelsvik, G., Schander, C. & Høines, Å.S., 2010. Feeding ecology of *Coryphaenoides rupestris* from the mid-atlantic ridge. *PLoS ONE*, 5(5), pp.e10453–e10453.

Bergstad, O.A., Wik, Å.D. & Hildre, Ø., 2003. Predator-prey relationships and food sources of the Skagerrak deep-water fish assemblage. *Journal of Northwest Atlantic Fishery Science*, 31, pp.165–180.

Bergstad, O.A., Clark, L., Hansen, H. Ø. & Cousins, N., 2012. Distribution, population biology, and trophic ecology of the deepwater demersal fish *Halosauropsis macrochir* (pisces: halosauridae) on the mid-atlantic ridge. *PLoS ONE*, 7(2), pp.e31493–e31493.

Bett, B.J., Malzone, M.G., Narayanaswamy, B.E. & Wigham, B.D., 2001. Temporal variability in phytodetritus and megabenthic activity at the seabed in the deep Northeast Atlantic. *Progress In Oceanography*, 50(1), pp.349–368.

Blondel, J., 2003. Guilds or functional groups: does it matter? *Oikos*, 100(2), pp.223–231.

Boyle, M.D., Ebert, D.A. & Cailliet, G.M., 2012. Stable-isotope analysis of a deep-sea

benthic-fish assemblage: evidence of an enriched benthic food web. *Journal of Fish Biology*, 80(5), pp.1485–1507.

Bozzano, A., 2004. Retinal specialisations in the dogfish Centroscymnus coelolepis from the Mediterranean deep-sea. *Scientia Marina*, 68, pp.185–195.

Bozzano, A. & Catalán, I.A., 2002. Ontogenetic changes in the retinal topography of the European hake, Merluccius merluccius : implications for feeding and depth distribution. *Marine Biology*, 141(3), pp.549–559. Available at: http://www.springerlink.com/openurl.asp?genre=article&id=doi:10.1007/s00227-002-0840-7.

Bozzano, A., Recasens, L. & Sartor, P., 1997. Diet of the European hake *Merluccius merluccius* (Pisces: Merluciidae) in the Western Mediterranean (Gulf of Lions). *Scientia Marina*, 61, pp.1–8.

Brown, A. & Thatje, S., 2014. Explaining bathymetric diversity patterns in marine benthic invertebrates and demersal fishes: physiological contributions to adaptation of life at depth. *Biological Reviews*, 89(2), pp.406–426.

Bruun, A.F., 1937. *Contributions to the life histories of the deep sea eels: synaphobranchidae*. Dana-report, no. 9, Oxford University Press, London, UK.

Bulman, C.M. & Koslow, J.A., 1992. Diet and food consumption of a deep-sea fish, orange roughy *Hoplostethus Atlanticus* (Pisces, Trachichthyidae), off southeastern Australia. *Marine Ecology Progress Series*, 82(2), pp.115–129.

Cailliet, G.M.G., Andrews, A.H., Burtona, E.J., Watters, D.L., Kline, D.E. & Ferry-Grahamd, L.A., 2001. Age determination and validation studies of marine fishes: do deep-dwellers live longer? *Experimental Gerontology*, 36(4-6), pp.739–764. Available at: http://www.sciencedirect.com/science/article/pii/S0531556500002394.

Campbell, N., Neat, F., Burns, F. & Kunzlik, P., 2011. Species richness, taxonomic diversity, and taxonomic distinctness of the deep-water demersal fish community on the Northeast Atlantic continental slope (ICES Subdivision VIa). *ICES Journal of Marine Science*, 68(2), pp.365–376.

Campana, S.E., 1999. Chemistry and composition of fish otoliths: pathways, mechanisms and applications. *Marine Ecology Progress Series*, 188, pp.263–297.

Campana, S.E., 1990. How reliable are growth back-calculations based on otoliths?. *Canadian Journal of Fisheries and Aquatic Sciences*, 47(11), pp.2219–2227.

Campana, S.E., 2004. *Photographic atlas of fish otoliths of the Northwest Atlantic Ocean*, NRC Research Press.

Campana, S.E. & Neilson, J.D., 1985. Microstructure of fish otoliths. *Canadian Journal of Fisheries and Aquatic Sciences*, 42(5), pp.1014–1032.

Cardinale, M., Doering-Arjes, P., Kastowsky, M. & Mosegaard, H., 2004. Effects of sex, stock, and environment on the shape of known-age Atlantic cod (*Gadus morhua*) otoliths. *Canadian Journal of Fisheries and Aquatic Sciences*, 61(2), pp.158–167. Available at: http://www.nrcresearchpress.com/doi/abs/10.1139/f03-151.

Carrassón, M. & Cartes, J.E., 2002. Trophic relationships in a Mediterranean deep-sea fish community: partition of food resources, dietary overlap and connections within

the benthic boundary layer. *Marine Ecology Progress Series*, 241, pp.41–55.

Carrassón, M., Matallanas, J. & Casadevall, M., 1997. Feeding strategies of deep-water morids on the western Mediterranean slope. *Deep-Sea Research I*, 44(9-10), pp.1685–1699. Available at: http://www.sciencedirect.com/science/article/pii/S0967063797000447.

Carlsson, J., Shephard, S., Coughlan, J., Trueman, C.N., Rogan, E. & Cross, T.F., 2011. Fine-scale population structure in a deep-sea teleost (orange roughy, *Hoplostethus atlanticus*). *Deep Sea Research Part I: Oceanographic Research Papers*, 58(6), pp.627–636.

Cartes, J.E., Hidalgo, M., Papiol, V., Massutí, E & Moranta, G., 2009. Changes in the diet and feeding of the hake *Merluccius merluccius* at the shelf-break of the Balearic Islands: Influence of the mesopelagic-boundary community. *Deep-Sea Research Part I*, 56(3), pp.344–365. Available at: http://linkinghub.elsevier.com/retrieve/pii/S0967063708002033.

Casas, J.M. & Pineiro, C., 2000. Growth and age estimation of greater fork-beard (*Phycis blennoides brunnich*, 1768) in the north and northwest of the iberian peninsula (ICES division VIIIc and IXa). *Fisheries Research*, 47(1), pp.19–25.

Childress, J.J., 1995. Are there physiological and biochemical adaptations of metabolism in deep-sea animals? *Trends in Ecology & Evolution*, 10(1), pp.30–36.

Childress, J.J. & Seibel, B.A., 1998. Life at stable low oxygen levels: Adaptations of animals to oceanic oxygen minimum layers. *Journal of Experimental Biology*, 201(8), pp.1223–1232.

Childress, J.J., Cowles, D.L., Favuzzi, J.A. & Mickel, T.J., 1990a. Metabolic rates of benthic deep-sea decapod crustaceans decline with increasing depth primarily due to the decline in temperature. *Deep Sea Research Part A. Oceanographic Research Papers*, 37(6), pp.929–949.

Childress, J.J., Price, M.H., Favuzzi, J. & Cowles, D., 1990b. Chemical composition of midwater fishes as a function of depth of occurrence off the Hawaiian islands: food availability as a selective factor? *Marine Biology*, 105(2), pp.235–246.

Chung, M.-T., 2010. *The life history of the deep-water cusk eel Cataetyx laticeps: evidence from the microstructure and stable isotope of otoliths.* Master degree thesis, University of Southampton.

Clark, M.R., Althaus, F., Williams, A., Niklitschek, E., Menezes, G.M., Hareide, N.-R., Sutton, P. & O'Donnell., C., 2010. Are deep-sea demersal fish assemblages globally homogenous? Insights from seamounts. *Marine Ecology*, 31, pp.39–51.

Clarke, G.L. & Denton, E.J., 1962. Light and animal life. In M.N. Hill, eds. *The Sea Volume I: Physical oceanography*. John Wiley & Sons Lid, New York pp. 456-468.

Collin, S.P. & Pettigrew, J.D., 1989. Quantitative comparison of the limits on visual spatial resolution set by the ganglion cell layer in twelve species of reef teleosts. *Brain, Behavior and Evolution*, 34(3), pp.184–192.

Collin, S.P. & Partridge, J.C., 1996. Retinal specializations in the eyes of deep-sea teleosts. *Journal of Fish Biology*, 49(1), pp.157–174.

Collin, S.P. & Shand, J., 2003. Retinal Sampling and the Visual Field in Fishes. In *Sensory processing in aquatic environments*. New York, NY: Springer New York, pp. 139–169.

Collins, M.A., Priede, I.G. & Bagley, P.M., 1999. In situ comparison of activity in two deep-sea scavenging fishes occupying different depth zones. *Proceedings of the Royal Society B: Biological Sciences*, 266(1432), pp.2011–2016. Available at: http://rspb.royalsocietypublishing.org/cgi/doi/10.1098/rspb.1999.0879.

Crabtree, R.E. & Sulak, K.J., 1986. A contribution to the life history and distribution of Atlantic species of the deep-sea fish genus Conocara (Alepocephalidae). *Deep Sea Research Part A. Oceanographic Research Papers*, 33, pp.1183–1201.

Craig, H. & Gordon, L.I., 1965. Deuterium and oxygen 18 variations in the ocean and marine atmosphere. In E. Tongiorgi, ed. *Proceedings of the conference on stable isotopes in oceano-graphic studies and paleotemperatures.* Laboratory of Geology and Nuclear Science, Pisa, pp. 9–130.

Craig, J., Jamieson, A.J., Heger, A. & Priede, I.G., 2009. Distribution of bioluminescent organisms in the Mediterranean Sea and predicted effects on a deep-sea neutrino telescope. *Nuclear Instruments and Methods in Physics Research A*, 602(1), pp.224–226.

Craig, J., Jamieson, A.J., Bagley, P.M. & Priede, I.G., 2011. Naturally occurring bioluminescence on the deep-sea floor. *Journal of Marine Systems*, 88, pp.563–567.

de Busserolles, F., Fitzpatrick, J.L., Marshall, J. & Collin, S.P., 2014. The influence of photoreceptor size and distribution on optical sensitivity in the eyes of lanternfishes (myctophidae). *PLoS ONE*, 9(6), pp.e99957–e99957.

Danovaro, R., Company, J.B., Corinaldesi, C., D'Onghia, G., Galil, B., Gambi, C., Gooday, A.J., Lampadariou, N., Luna, G.M., Morigi, C., Olu, K., Polymenakou, P., Ramirez-Llodra, E., Sabbatini, A., Sardà, F., Sibuet, M. & Tselepides, A., 2010. Deep-Sea Biodiversity in the Mediterranean Sea: The Known, the Unknown, and the Unknowable. *PloS one*, 5(8), pp.e11832.

Davis, M.P. & Chakrabarty, P., 2011. Tripodfish (Aulopiformes: *Bathypterois*) locomotion and landing behaviour from video observation at bathypelagic depths in the Campos Basin of Brazil. *Marine Biology Research*, 7(3), pp.297–303.

Degens, E.T., Deuser, W.G. & Haedrich, R.L., 1969. Molecular structure and composition of fish otoliths. *Marine Biology*, 2(2), pp.105–113.

Deng, X., Wagner, H.-J. & Popper, A.N., 2011. The inner ear and its coupling to the swim bladder in the deep-sea fish *Antimora rostrata* (Teleostei: Moridae). *Deep-Sea Research Part I*, 58, pp.27–37.

DeNiro, M. & Epstein, S. 1978. Influence of diet on the distribution of carbon isotopes in animals. *Geochimica et Cosmochimica Acta*, 42, pp.495–506.

Douglas, R.H., Partridge, J.C. & Marshall, N.J., 1998. The eyes of deep-sea fish I: Lens pigmentation, tapeta and visual pigments. *Progress in Retinal and Eye Research*, 17(4), pp.597–636.

Drazen, J.C., Buckley, T.W. & Hoff, G.R., 2001. The feeding habits of slope dwelling

macrourid fishes in the eastern North Pacific. *Deep Sea Research Part I: Oceanographic Research Papers*, 48(3), pp.909–935.

Drazen, J.C., Dugan, B. & Friedman, J.R., 2013. Red muscle proportions and enzyme activities in deep-sea demersal fishes. *Journal of Fish Biology*, 83, pp.1592–1612.

Drazen, J.C., Popp, B.N., Choy, C.A., Clemente, T., De Forest, L & Smith, Jr., K.L., 2008. Bypassing the abyssal benthic food web: Macrourid diet in the eastern North Pacific inferred from stomach content and stable isotopes analyses. *Limnology and oceanography*, 53(6), pp.2644–2654.

Drazen, J.C. & Haedrich, R.L., 2012. A continuum of life histories in deep-sea demersal fishes. *Deep-Sea Research Part I*, 61, pp.34-42.

Drazen, J.C. & Robison, B.H., 2004. Direct observations of the association between a deep-sea fish and a giant scyphomedusa. *Marine and Freshwater Behaviour and Physiology,* 37(3), pp.209-214.

Drazen, J.C. & Seibel, B.A., 2007. Depth-related trends in metabolism of benthic and benthopelagic deep-sea fishes. *Limnology and Oceanography*, 53, pp.2306–2316.

Drazen, J.C. & Yeh, J., 2012. Respiration of four species of deep-sea demersal fishes measured in situ in the eastern North Pacific. *Deep-Sea Research Part I*, 60, pp.1–6.

DuBuit, M.H., 1996. Diet of hake (*Merluccius merluccius*) in the Celtic Sea. *Fisheries Research,* 28, pp.381–394.

Fahay, M.P., 1992. Development and distribution of cusk eel eggs and larvae in the middle atlantic bight with a description of *Ophidion robinsi* n. sp. (Teleostei: Ophidiidae). *Copeia*, (3), pp.799–819.

Fanelli, E. & Cartes, J., 2010. Temporal variations in the feeding habits and trophic levels of three deep-sea demersal fishes from the western Mediterranean Sea, based on stomach contents and stable isotope analyses. *Marine Ecology Progress Series*, 402, pp.213–232. Available at: http://www.int-res.com/abstracts/meps/v402/p213-232/.

Filiz, H., Bilge, G., Irmak, E., Togulga, M., Uckun, D. & Akalin, S., 2006. Age and growth of the hollowsnout grenadier, *Caelorinchus caelorhincus* (Risso, 1810), in the Aegean Sea. *Journal of Applied Ichthyology*, 22(4), pp.285–287.

Fossen, I. & Bergstad, O.A., 2006. Distribution and biology of blue hake, *Antimora rostrata* (Pisces: Moridae), along the mid-Atlantic Ridge and off Greenland. *Fisheries Research*, 82(1-3), pp.19–29.

Fowler, S.W. & Knauer, G.A., 1986. Role of large particles in the transport of elements and organic compounds through the oceanic water column. *Progress In Oceanography*, 16(3), pp.147–194.

Freckleton, R.P., Harvey, P.H. & Pagel, M., 2002. Phylogenetic analysis and comparative data: a test and review of evidence. *The American Naturalist,* 160, pp.712–726.

Friedman, I. & O'Neil, J.R., 1977. Compilation of stable isotope fractionation factors of geochemical interest. In F. M, ed. *Data of Geochemistry*. US Government Printing

Office, Washington, DC, p. 12.

Frigstad, H., Henson, S.A., Hartman, S.E., Omar, A.M., Jeansson, E., Cole, H., Pebody, C. & Lampitt, R.S., 2015. Links between surface productivity and deep ocean particle flux at the Porcupine Abyssal Plain (PAP) sustained observatory. *Biogeosciences Discussions*, 12, pp. 5169-5199.

Fritsches, K.A., Marshall, N.J. & Warrant, E.J., 2003. Retinal specializations in the blue marlin: eyes designed for sensitivity to low light levels. *Marine and Freshwater Research*, 54(4), pp.333–341.

Froese, R. & Pauly, D. eds., *Fishbase*, World Wide Web electronic publication. Available at: http://www.fishbase.org/ [Accessed January 1, 2013].

Fukui, A. & Kuroda, H., 2007. Larvae of *Lamprogrammus shcherbachevi* (Ophidiiformes: Ophidiidae) from the western North Pacific Ocean. *Ichthyological Research*, 54(1), pp.74–80.

Fukui, A., Tsuchiya, T., Sezaki, K. & Watabe, S., 2008. Pelagic eggs and larvae of *Coryphaenoides marginatus* (Gadiformes: Macrouridae) collected from Suruga Bay, Japan. *Ichthyological Research*, 55(3), pp.284–293.

Fukui, A., Tsuchiya, T. & Uotani, I., 2003. Pelagic juvenile of *Halargyreus johnsonii* (Gadiformes: Moridae) from Suruga Bay, Japan. *Ichthyological Research*, 50(2), pp.186–189. Available at: http://www.springerlink.com/Index/10.1007/s10228-002-0150-6.

Gage, J.D., 2003. Food inputs, utilization, carbon flow and energetics. In P. A. Tyler, ed. *Ecosystems of the deep oceans*. Elsevier, pp. 313–380.

Gage, J.D. & Tyler, P.A., 1991. *Deep-sea biology: A natural history of organisms at the deep-sea floor*, Cambridge University Press.

Gagliano, M & McCormick, M.I., 2004. Feeding history influences otolith shape in tropical fish. *Marine Ecology Progress Series*. 278, pp. 291–296.

Garland, T., Dickerman, A.W., Janis, C.M. & Jones, J.A., 1993. Phylogenetic Analysis of Covariance by Computer Simulation. *Systematic Biology,* 42, pp.265–292.

Gaskett, A.C., Bulman, C., He, X. & Goldsworthy, S.D., 2001. Diet composition and guild structure of mesopelagic and bathypelagic fishes near Macquarie Island, Australia. *New Zealand Journal of Marine and Freshwater Research*. 35, pp. 469–476.

Gartner, J.V., Jr., Crabtree, R.E. & Sulak, K.J., 1997. Feeding at Depth. In D. J. Randall & A. P. Farrell, eds. *Deep-Sea Fishes*. 16, pp. 115–193.

Gauldie, R.W., 1988. Function, form and time-keeping properties of fish otoliths. *Comparative Biochemistry and Physiology Part A: Physiology*, 91, pp.395–402.

Gauldie, R.W., 1996. Biological factors controlling the carbon isotope record in fish otoliths: principles and evidence. *Comparative Biochemistry and Physiology Part B: Biochemistry and Molecular Biology*, 115(2), pp.201–208.

Gauldie, Gauldie, R. & et, R.W., 2002. An eco-morphological explanation of individual variability in the shape of the fish otolith: comparison of the otolith of *Hoplostethus*

atlanticus with other species by depth. *Journal of Fish Biology*, 60(5), pp.1204–1221. Available at: http://gateway.webofknowledge.com/gateway/Gateway.cgi?GWVersion=2&SrcAuth=mekentosj&SrcApp=Papers&DestLinkType=FullRecord&DestApp=WOS&KeyUT=000177275400011.

Geer, L.Y., Marchler-Bauer, A., Geer, R.C., Han, L., He, J., He, S., Liu, C., Shi, W. & Bryant, S.H., 2010. The NCBI BioSystems database. *Nucleic Acids Research,* 38, pp.D492–D496.

Giering, S.L.C., Sanders, R., Lampitt, R.S., Anderson, T.R., Tamburini, C., Boutrif, M., Zubkov, M.V., Marsay, C.M., Henson, S.A., Saw, K., Cook, K. & Mayor, D.J., 2014. Reconciliation of the carbon budget in the ocean's twilight zone. *Nature*, 507, pp. 480-483.

Gillibrand, E.J.V., Bagley, P., Jamieson, A., Herring, P.J., Partridge, J.C., Collins, M.A., Milne, R. & Priede, I.G., 2007a. Deep sea benthic bioluminescence at artificial food falls, 1,000–4,800 m depth, in the Porcupine Seabight and Abyssal Plain, North East Atlantic Ocean. *Marine Biology*, 150(6), pp.1053–1060.

Gillibrand, E.J.V., Jamieson, A.J., Bagley, P.M., Zuur, A.F. & Priede, I.G., 2007b. Seasonal development of a deep pelagic bioluminescent layer in the temperate NE Atlantic Ocean. *Marine Ecology Progress Series*, 341, pp.37–44.

González, C., Bruno, I. & Paz, X., 2000. Food and Feeding of Deep-sea Redfish (*Sebastes mentella* Travin) in the North Atlantic. *NAFO Scientific Council Studies*, 33, pp.89–101.

Gordon, J.D.M. & Bergstad, O.A., 1987. Species composition of demersal fish in the Rockall Trough, north-eastern atlantic, as determined by different trawls. *Journal of the Marine Biological Association of the United Kingdom*, 72, pp.213–230.

Gordon, J.D.M. & Duncan, J.A.R., 1987. Deep-sea bottom-living fishes at two repeat stations at 2 200 and 2 900 m in the Rockall Trough, northeastern Atlantic Ocean. *Marine Biology*, 96(3), pp.309–325.

Gordon, J.D.M. & Mauchline, J., 1996. The distribution and diet of the dominant, slope-dwelling eel, *Synaphobranchus kaupi*, of the Rockall Trough. *Journal of the Marine Biological Association of the United Kingdom*, 76, pp.493–503.

Graham, A.S., HaedrichR.L. & Fletcher, G.L., 1985. Hematology of three deep-sea fishes: a reflection of low metabolic rates. *Comparative Biochemistry and Physiology Part A: Physiology*, 80(1), pp.79–84.

Haddock, S. & Case, J.F., 1999. Bioluminescence spectra of shallow and deep-sea gelatinous zooplankton: ctenophores, medusae and siphonophores. *Marine Biology*, 133(3), pp.571–582.

Haddock, S.H.D., Moline, M.A. & Case, J.F., 2010. Bioluminescence in the Sea. *Annual Review of Marine Science*, 2, pp.443–493.

Haedrich, R.L., 1974. Pelagic capture of the epibenthic rattail *Coryphaenoides rupestris*. *Deep-Sea Research*, 21(11), pp.977–979.

Haedrich, R.L., 1997. Distribution and population ecology. In D. J. Randall & A. P. Farrell, eds. *Deep-sea fishes*. Academic Press, pp. 79–114.

Haedrich, R.L. & Merrett, N.R., 1988. Summary atlas of deep-living demersal fishes in the North Atlantic Basin. *Journal of Natural History*, 22 (5), pp. 1325–1362.

Haedrich, R.L. & Merrett, N.R., 1992. Production/biomass ratios, size frequencies and biomass spectra in deep-sea demersal fishes. In G. T. Rowe & V. Pariente, eds. *Deep-Sea Food Chains and the Global Carbon Cycle*. Dordrecht: Springer Netherlands, pp. 157–182.

Hareide, N.R., 1995. Comparison between longlining and trawling for deep-water species-selectivity, quality and catchability- a review. In A.G. Hopper, eds. *Deep-Water Fisheries of the North Atlantic Oceanic Slope*. Kluwer Academic Publishers, Dordrecht, pp. 227–234.

Harmon, L.J., Weir, J.T., Brock, C.D., Glor, R.E. & Challenger, W., 2008. GEIGER: investigating evolutionary radiations. *Bioinformatics,* 24, pp.129–131.

Heger, A., Ieno, E.N., King, N.J., Morris, K.J., Bagley, P.M. & Priede, I.G., 2008. Deep-sea pelagic bioluminescence over the Mid-Atlantic Ridge. *Deep Sea Research Part II: Topical Studies in Oceanography*, 55(1-2), pp.126–136.

Henriques, C., Priede, I.G. & Bagley, P.M., 2002. Baited camera observations of deep-sea demersal fishes of the northeast Atlantic Ocean at 15-28 degrees N off West Africa. *Marine Biology*, 141(2), pp.307–314.

Henson, S.A., Sanders, R., Madsen, E., Morris, P.J., Le Moigne, F. & Quartly, G.D., 2011. A reduced estimate of the strength of the ocean's biological carbon pump. *Geophysical Research Letters*, 38, pp. L04606

Hoie, H., Otterlei, E. & Folkvord, A., 2004. Temperature-dependent fractionation of stable oxygen isotopes in otoliths of juvenile cod (*Gadus morhua* L.). *ICES Journal of Marine Science: Journal du Conseil*, 61(2), pp.243–251.

Hortson, M., 2010. *Eye*. Open.Michigan, Regents of the University of Michigan, http://open.umich.edu/education/med/resources/second-look-series/materials; (Accessed 6, September 2014).

Hunt, J.J., 1992. Morphological characteristics of otoliths for selected fish in the Northwest Atlantic. *Journal of Northwest Atlantic Fishery Science*, 13, pp. 63-75.

Husebø, Å., Nøttestad, L., Fosså, J.H., Furevik, D.M. & Jørgensen, S.B., 2002. Distribution and abundance of fish in deep-sea coral habitats. *Hydrobiologia*, 471, pp. 91-99.

Hussey, N.E., MacNeil, M.A., McMeans, B.C., Olin, J.A., Dudley, S.F.J., Cliff, G., Wintner, S.P., Fennessy, S.T. & Fisk, A.T., 2014. Rescaling the trophic structure of marine food webs. *Ecology Letters*, 17, pp.239-250.

Hüssy, K., 2008. Otolith accretion rates: Does size really matter? *Journal of Experimental Marine Biology and Ecology*, 362(2), pp.131–136.

Hüssy, K. & Mosegaard, H., 2004. tlantic cod (*Gadus morhua*) growth and otolith accretion characteristics modelled in a bioenergetics context. *Canadian Journal of Fisheries and Aquatic Sciences*, 61, pp.1021–1031.

Iken, K., Brey, T., Wand, U., Voigt, J. & Junghans, P., 2001. Food web structure of the benthic community at the Porcupine Abyssal Plain (NE Atlantic): a stable isotope

analysis. *Progress In Oceanography*, 50, pp.383–405.

Inoue, J.G., Miya, M., Miller, M.J., Sado, T., Hanel, R., Hatooka, K., Aoyama, J., Minegishi, Y., Nishida, M. & Tsukamoto, K., 2010. Deep-ocean origin of the freshwater eels. *Biology Letters*, 6(3), pp.363–366.

Jamieson, A.J.A., Fujii, T., Matsumoto, A.K., Bagley, P.M. & Priede, I.G., 2009. Liparid and macrourid fishes of the hadal zone: in situ observations of activity and feeding behaviour. *Proceedings of the Royal Society B-Biological Sciences*, 276(1659), pp.1037–1045.

Jamieson, R.E., Schwarcz, H.P. & Brattey, J., 2004. Carbon isotopic records from the otoliths of Atlantic cod (*Gadus morhua*) from eastern Newfoundland, Canada. *Fisheries Research*, 68, pp.83–97.

Jenkins, G.P., Shaw, M. & Stewart, B.D., 1993. Spatial variation in food-limited growth of juvenile greenback flounder, *Rhombosolea tapirina*: evidence from otolith daily increments and otolith scaling. *Canadian Journal of Fisheries and Aquatic Sciences*, 50, pp.2558–2567.

Johnsen, S., Frank, T.M., Haddock, S.H.D., Widder, E.A. & Messing, C.G., 2012. Light and vision in the deep-sea benthos: I. Bioluminescence at 500-1000. m depth in the Bahamian Islands. *Journal of Experimental Biology*, 215(19), pp.3335–3343.

Jones, M.R.L. & Breen, B.B., 2013. Food and feeding relationships of three sympatric slickhead species (Pisces: Alepocephalidae) from northeastern Chatham Rise, New Zealand. *Deep-Sea Research Part I*, 79, pp.1–9.

Jónsdóttir, I.G., Campana, S.E. & Marteinsdottir, G., 2006. Otolith shape and temporal stability of spawning groups of Icelandic cod (*Gadus morhua* L.). *ICES Journal of Marine Science*, 63, pp.1501–1512.

Jørgensen, O.A., 1995. A comparison of deep-water trawl and longline fishing in the Davis Strait. In A.G. Hopper, eds. *Deep-Water Fisheries of the North Atlantic Oceanic Slope*. Kluwer Academic Publishers, Dordrecht, pp. 227–234.

Kalish, J.M., 1991a. C-13 and O-18 isotopic disequilibria in fish otoliths: metabolic and kinetic effects. *Marine Ecology Progress Series*, 75, pp.191–203.

Kalish, J.M., 1991b. Oxygen and carbon stable isotopes in the otoliths of wild and laboratory-reared Australian salmon (*Arripis trutta*). *Marine Biology*, 110(1), pp.37–47.

Kawasaki, T., 1980. Fundamental relations among the selections of life history in the marine teleosts. *Bulletin of the Japanese Society of Scientific Fisheries*, 463(3), pp.289–293.

Kelly, C.J., Connolly, P.L. & Bracken, J.J., 1997. Age estimation, growth, maturity and distribution of the roundnose grenadier from the Rockall trough. *Journal of Fish Biology*, 50(1), pp.1–17.

Kelly, C.J., Connolly, P.L. & Bracken, J.J., 1999. Age estimation, growth, maturity, and distribution of the bluemouth rockfish *Helicolenus d. dactylopterus* (Delaroche 1809) from the Rockall Trough. *ICES Journal of Marine Science*, 56(1), pp.61–74.

Kerr, L.A., Andrews, A.H., Frantz, B.R., Coale, K.H., Brown, T.A. & Cailliet, G.M., 2004.

Radiocarbon in otoliths of yelloweye rockfish (*Sebastes ruberrimus*): a reference time series for the coastal waters of southeast Alaska. *Canadian Journal of Fisheries and Aquatic Sciences*, 61(3), pp.443–451.

Koslow, J.A., 1996. Energetic and life-history patterns of deep-sea benthic, benthopelagic and seamount-associated fish. *Journal of Fish Biology*, 49, pp.54–74.

Kroopnick, P.M., 1985. The distribution of 13C of ΣCO2 in the world oceans. *Deep Sea Research Part A. Oceanographic Research Papers*, 32(1), pp.57–84.

Lampitt, R.S., 1985. Evidence for the seasonal deposition of detritus to the deep-sea floor and its subsequent resuspension. *Deep Sea Research Part A. Oceanographic Research Papers*, 32(8), pp.885–897.

Lampitt, R.S., Wishner, K.F., Turley, C.M. & Angel, M.V., 1993. Marine snow studies in the Northeast Atlantic Ocean: distribution, composition and role as a food source for migrating plankton. *Marine Biology*, 116(4), pp.689–702.

Laws, E.A., Falkowski, P.G., Smith Jr., W.O., Ducklow, H. & McCarthy, J.J., 2000. Temperature effects on export production in the open ocean. *Global Biogeochemical Cycles*, 14, pp. 1231-1246.

Levin, L.A., Etter, R.J., Rex, M.A., Gooday, A.J., Smith, C.R., Pineda, J., Stuart, C.T., Hessler, R.R. Pawson, D., & 2001. Environmental influences on regional deep-sea species diversity. *Annual Review of Ecology and Systematics*, 32, pp.51–93.

Lin, H.-Y., Shiao, J.-C., Chen, Y.-G. & Iizuka, Y., 2012. Ontogenetic vertical migration of grenadiers revealed by otolith microstructures and stable isotopic composition. *Deep-Sea Research Part I*, 61(C), pp.123–130.

Locket, N.A., 1977. Adaptations to the Deep-Sea Environment. In *The visual system in vertebrates*. Handbook of Sensory Physiology. Berlin, Heidelberg: Springer Berlin Heidelberg, pp. 67–192.

Lombarte, A., 1992. Changes in otolith area: sensory area ratio with body size and depth. *Environmental Biology of Fishes*, 33, pp.405–410.

Lombarte, A. & Cruz, A., 2007. Otolith size trends in marine fish communities from different depth strata. *Journal of Fish Biology*, 71, pp.53–76.

Lombarte, A. & Lleonart, J., 1993. Otolith size changes related with body growth, habitat depth and temperature. *Environmental Biology of Fishes,* 37, pp.297–306.

Lombarte, A. & Castellón, A., 1991. Interspecific and intraspecific otolith variability in the genus *Merluccius* as determined by image analysis. *Canadian Journal of Zoology,* 69, pp.2442–2449.

Lombarte, A., Palmer, M., Matallanas, J., Gómez-Zurita, J. & Morales-Nin, B., 2010. Ecomorphological trends and phylogenetic inertia of otolith sagittae in Nototheniidae. *Environmental Biology of Fishes,* 89, pp.607–618.

Longmore, C., Fogarty, K., Neat, F., Brophy, D., Trueman, C., Milton, A. & Mariani, S., 2010. A comparison of otolith microchemistry and otolith shape analysis for the study of spatial variation in a deep-sea teleost, *Coryphaenoides rupestris*. *Environmental Biology of Fishes*, 89(3), pp.591–605.

References

Longmore, C., Trueman, C.N., Neat, F., Jorde, P.E., Knutsen, H., Stefanni, S., Catarino, D., Milton, J.A. & Mariani, S., 2014. Ocean-scale connectivity and life cycle reconstruction in a deep-sea fish. *Canadian Journal of Fisheries and Aquatic Sciences*, 71, pp.1–12.

Longmore, C., Trueman, C.N., Neat, F., O'Gorman, E.J., Milton, J.A. & Mariani, S., 2011. Otolith geochemistry indicates life-long spatial population structuring in a deep-sea fish, *Coryphaenoides rupestris*. *Marine Ecology Progress Series*, 435, pp.209–224.

Lorance, P., Large, P.A. & Bergstad, O.A., 2008. Grenadiers of the Northeast Atlantic—Distribution, biology, fisheries, and their impacts, and developments in stock assessment and management. *American Fisheries Society Symposim*, 63, pp.365–397.

Lorance, P. & Trenkel, V.M., 2006. Variability in natural behaviour, and observed reactions to an ROV, by mid-slope fish species. *Journal of Experimental Marine Biology and Ecology*, 332(1), pp.106–119.

Lychakov D.V. & Rebane Y.T., 2000. Otolith regularities. *Hearing Research*, 143, pp.83–102.

MacArthur R.H. & Wilson E.O., 1967. *The Theory of Island Biogeography*. Princeton University Press.

Magnússon, J.V., 2001. Distribution and some other biological parameters of two morid species *Lepidion eques* (Günther, 1887) and *Antimora rostrata* (Günther, 1878) in Icelandic waters. *Fisheries Research*, 51(2-3), pp.267–281.

Marshall, N.B., 1965. Systematic and biological studies of the Macrourid fishes (Anacanthini-Teleostii). *Deep Sea Research and Oceanographic Abstracts*, 12(3), pp.299–322.

Massutí, E., Morales-Nin, B. & Moranta, J., 2000. Age and growth of blue-mouth, *Helicolenus dactylopterus* (Osteichthyes: Scorpaenidae), in the western Mediterranean. *Fisheries Research*, 46(1-3), pp.165–176.

Mauchline, J. & Gordon, J.D.M., 1980. The food and feeding of the deep-sea morid fish *Lepidion eques* (gunther, 1887) in the Rockall Trough. *Journal of the Marine Biological Association of the United Kingdom*, 60(4), pp.1053–1059.

Mauchline, J. & Gordon, J.D.M., 1983. Diets of clupeoid, stomiatoid and salmonoid fish of the Rockall Trough, northeastern Atlantic Ocean. *Marine Biology*, 77(1), pp.67–78.

Mauchline, J. & Gordon, J.D.M., 1984a. Diets and bathymetric distributions of the macrourid fish of the Rockall Trough, northeastern Atlantic Ocean. *Marine Biology*, 81(2), pp.107–121.

Mauchline, J. & Gordon, J.D.M., 1984b. Feeding and bathymetric distribution of the gadoid and morid fish of the Rockall Trough. *Journal of the Marine Biological Association of the United Kingdom*, 64(3), pp.657–665.

Mauchline, J. & Gordon, J.D.M., 1984c. Occurrence and feeding of berycomorphid and percomorphid teleost fish in the Rockall Trough. *Journal du Conseil International pour l'Exploration de la Mer*, 41(3), pp.239–247.

Mauchline, J. & Gordon, J.D.M., 1985. Trophic Diversity in Deep-Sea Fish. *Journal of Fish Biology*, 26(5), pp.527–535.

Mauchline, J. & Gordon, J.D.M., 1986. Foraging strategies of deep-sea fish. *Marine Ecology Progress Series*, 27(3), pp.227–238.

Mauchline, J. & Gordon, J.D.M., 1991. Oceanic pelagic prey of benthopelagic fish in the benthic boundary layer of a marginal oceanic region. *Marine Ecology Progress Series*, 74, pp.109–115.

McLellan, T., 1977. Feeding strategies of the macrourids. *Deep-Sea Research*, 24(11), pp.1019–1036.

Mérigot, B., Letourneur, Y. & Lecomte-Finiger, R., 2007. Characterization of local populations of the common sole *Solea solea* (Pisces, Soleidae) in the NW Mediterranean through otolith morphometrics and shape analysis. *Marine Biology*, 151, pp.997–1008.

Merrett, N.R., 1978. On the identity and pelagic occurrence of larval and juvenile stages of rattail fishes (family Macrouridae) from 60° N, 20°W and 53° N, 20°W. *Deep-Sea Research*, 25(2), pp.147–160.

Merrett, N.R., 2004. Bathygadidae and macrouridae: grenadiers. In W. J. Richards, ed. *Early stages of atlantic fishes: an identification guide for the western central north atlantic*. CRC Press, pp. 595–615.

Merrett, N.R. & Haedrich, R.L., 1997. *Deep-sea demersal fish and fisheries.* Chapman & Hall, London, UK.

Merrett, N.R. & Marshall, N.B., 1980. Observations on the ecology of deep-sea bottom-living fishes collected off northwest Africa (08°–27°N). *Progress in Oceanography*, 9, pp. 185–244.

Minagawa, M. & Wada, E., 1984. Stepwise enrichment of ^{15}N along food chains: Further evidence and the relation between $\delta^{15}N$ and animal age. *Geochimica et Cosmochimica Acta* , 48, pp.1135–1140.

Montgomery, J. & Pankhurst, N., 1997. Sensory Physiology. In D. J. Randall & A. P. Farrell, eds. *Deep-Sea Fishes*. Academic Press, pp. 325–349.

Mora, C., Tittensor, D.P. & Myers, R.A., 2008. The completeness of taxonomic inventories for describing the global diversity and distribution of marine fishes. *Proceedings of the Royal Society B-Biological Sciences*, 275(1631), pp.149–155.

Morales-Nin, B., 2000. Review of the growth regulation processes of otolith daily increment formation. *Fisheries Research*, 46(1), pp.53–67.

Morales-Nin, B. & Sena-Carvalho, D., 1996. Age and growth of the black scabbard fish (*Aphanopus carbo*) off Madeira. *Fisheries Research*, 25, pp.239–251.

Morte, M.S., Redón, M.J. & Sanz-Brau, A., 2002. Diet of *Phycis blennoides* (Gadidae) in relation to fish size and season in the western Mediterranean (Spain). *Marine Ecology*, 23(2), pp.141–155.

Murayama, E., Takagi, Y., Ohira, T., Davis, J.G., Greene, M.I. & Nagasawa, H., 2002. Fish otolith contains a unique structural protein, otolin-1. *European Journal of*

Biochemistry, 269(2), pp.688–696.

Murayama, E., Herbomel, P., Kawakami, A., Takeda, H. & Nagasawa, H., 2005. Otolith matrix proteins OMP-1 and Otolin-1 are necessary for normal otolith growth and their correct anchoring onto the sensory maculae. *Mechanisms of Development*, 122(6), pp.791–803. Available at: http://gateway.webofknowledge.com/gateway/Gateway.cgi?GWVersion=2&SrcAuth=mekentosj&SrcApp=Papers&DestLinkType=FullRecord&DestApp=WOS&KeyUT=000230037100004.

Near, T.J., Eytan, R.I., Dornburg, A., Kuhn, K.L., Moore, J.A., Davis, M.P., Wainwright, P.C., Friedman, M. & Smith, W.L., 2012. Resolution of ray-finned fish phylogeny and timing of diversification. *Proceedings of the National Academy of Sciences of the United States of America*, 109(34), pp.13698–13703.

Neat, F., Burns, F. & Drewery, J., 2008. *The deepwater ecosystem of the continental shelf slope and seamounts of the rockall trough: a report on the ecology and biodiversity based on FRS scientific survey*, Fisheries Research Services, Aberdeen.

Neat, F.C. & Campbell, N., 2013. Proliferation of elongate fishes in the deep sea. *Journal of Fish Biology*, 83(6), pp.1576–1591.

Nolf, D., 1993. A survey of perciform otoliths and their interest for phylogenetic analysis, with an iconographic synopsis of the Percoidei. *Bulletin of Marine Science,* 52, pp. 220–239.

Okiyama, M. & Kato, H., 1997. A pelagic juvenile of *Barathronus pacificus* (Ophidiiformes: Aphyonidae) from the southwest Pacific, with notes on its metamorphosis. *Ichthyological Research*, 44(2), pp.222–226.

Orme, D., 2012. The caper package: comparative analysis of phylogenetics and evolution in R. http:// caper.r-forge.r-project.org.

Pagel, M., 1999. Inferring the historical patterns of biological evolution. *Nature,* 401, pp.877–884.

Pagel, M.D., 1992. A method for the analysis of comparative data. *Journal of Theoretical Biology,* 156, pp.431–442.

Pannella, G.G., 1971. Fish otoliths: daily growth layers and periodical patterns. *Science*, 173(2), pp.1124–1127.

Partridge, J.C., Douglas, R.H., Marshall,N.J., Chung, W.-S., Jordan, T.M. & Wagner, H.-J., 2014. Reflecting optics in the diverticular eye of a deep-sea barreleye fish (*Rhynchohyalus natalensis*). *Proceedings of the Royal Society B-Biological Sciences*, 281(1782), pp.20133223.

Payan, P., De Pontual, H., Bœuf, G. & Mayer-Gostan, N., 2004. Endolymph chemistry and otolith growth in fish. *Comptes Rendus Palevol*, 3(6-7), pp.535–547. Available at: http://www.sciencedirect.com/science/article/pii/S1631068304001381.

Payne, M.R., Egan, A., Fässler, S.M.M., Hátún, H., Holst, J.C., Jacobsen, J.A., Slotte, A. & Loeng, H., 2012. The rise and fall of the NE Atlantic blue whiting (*Micromesistius poutassou*). *Marine Biology Research*, 8(5-6), pp.475–487.

Peterson, B.J. & Fry, B., 1987. Stable Isotopes in Ecosystem Studies. *Annual Review of Ecology and Systematics*, 18, pp.293–320.

Petko, J.A., Millimaki, B.B., Canfield, V.A., Riley, B.B. & Levenson, R., 2008. Otoc1: A novel otoconin-90 ortholog required for otolith mineralization in zebrafish. *Developmental Neurobiology*, 68(2), pp.209–222. Available at: http://doi.wiley.com/10.1002/dneu.20587.

Pinet, P.R., 2009. *Invitation to oceanography* 5 ed., Jones and Bartlett Publisher, LLC.

Polunin, N., Morales-Nin, B., Pawsey, W.E., Cartes, J.E., Pinnegar, J.K. & Moranta, J., 2001. Feeding relationships in Mediterranean bathyal assemblages elucidated by stable nitrogen and carbon isotope data. *Marine Ecology Progress Series*, 220, pp.13–23.

Popper, A.N., 1997. A scanning electron microscopic study of the sacculus and legena in the ears of fifteen species of teleost fishes. *Journal of Morphology*, 153, pp.397–417.

Popper, A.N. & Fay, R.R., 1993. Sound detection and rocessing by Fish: critical review and major research questions. *Brain, Behavior and Evolution*, 41, pp.14–38.

Popper A.N. & Lu Z, 2000. Structure-function relationships in fish otolith organs. *Fisheries Research*, 46, pp.15–25.

Post, D.M., 2002. Using stable isotopes to estimate trophic position: models, methods, and assumptions. *Ecology*, 83(3), pp.703–718.

Preikshot, D., Froese, R. & Pauly, D. (2000). The ORDERS table. In R. Froese & D. Pauly, eds. *FishBase 2000: Concepts, Design and Data Sources*, pp. 55–59. Los Banos: ICLARM.

Priede, I.G., Bagley, P.M., Smith, A., Creasey, S. & Merrett, N.R., 1994. Scavenging deep demersal fishes of the Porcupine Seabight, north-east Atlantic: observations by baited camera, trap and trawl. *Journal of the Marine Biological Association of the United Kingdom,* 74, pp.481-198.

Priede, I.G., Godbold, J.A., King, N.J., Collins, M.A., Bailey, D.M. & Gordon, J.D.M., 2010. Deep-sea demersal fish species richness in the Porcupine Seabight, NE Atlantic Ocean: global and regional patterns. *Marine Ecology*, 31, pp.247–260.

Priede, I.G. & Froese, R., 2013. Colonization of the deep sea by fishes. *Journal of Fish Biology*, 83, pp.1528-1550.

Priede, I.G., Bagley, P.M. & Smith, A., 1994. Scavenging deep demersal fishes of the Porcupine Seabight, north-east Atlantic: observations by baited camera, trap and trawl. *Journal of the Marine Biological Association of the United Kingdom*, 74, pp.481–498.

Rex, M.A. & Etter, R.J., 2010. *Deep-sea biodiversity: pattern and scale*, Harvard University Press.

R Development Core Team, 2012. R: A language and environment for statistical computing. http://www.r-project.org/

Reecht, Y., Rochet, M.-J., Trenkel, V.M., Jennings, S. & Pinnegar, J.K., 2013. Use of

morphological characteristics to define functional groups of predatory fishes in the Celtic Sea. *Journal of Fish Biology*, 83(2), pp.355–377.

Reichert, M.J.M., Dean, J.M., Feller, R.J. & Grego, J.M., 2000. Somatic growth and otolith growth in juveniles of a small subtropical flatfish, the fringed flounder, *Etropus crossotus*. *Journal of Experimental Marine Biology and Ecology*, 254(2), pp.169–188.

Renaud, P.E., Tessmann, M., Evenset, A. & Christensen, G.N., 2011. Benthic food-web structure of an Arctic fjord (Kongsfjorden, Svalbard). *Marine Biology Research*, 7(1), pp.13–26.

Revell, L.J., 2012. phytools: an R package for phylogenetic comparative biology (and other things). *Methods in Ecology and Evolution,* 3, pp.217–223.

Rice, A.L., Billett D.S.M., Fry, J., John, A.W.G., Lampitt, R.S., Mantoura, R.F.C. & Morris, R.J., 1986. Seasonal deposition of phytodetritus to the deep-sea floor. *Proceedings of the Royal Society of Edinburgh. Section B. Biological Sciences*, 88(1), pp.265–279.

Ricker, W.E., 1969. Effects of size-selective mortality and sampling bias on estimates of growth, mortality, production, and yield. *Journal of the Fisheries Research Board of Canada,* 26(3), pp. 479-541.

Roff, D.A., 1988. The evolution of migration and some life-history parameters in marine fishes. *Environmental Biology of Fishes*, 22(2), pp.133–146.

Rose, S.W. & Quattrini, A.M.,1988. T Deep-sea reef fish assemblage patterns on the Blake Plateau (Western North Atlantic Ocean). *Marine Ecology*, 30(1), pp.74–92.

Ryther, J.H., 1956. Photosynthesis in the ocean as a function of light intensity. *Limnology and oceanography*, 1(1), pp.61–70.

Santos, A.R., Trueman, C., Connolly, P. & Rogan, R., 2013. Trophic ecology of black scabbardfish, *Aphanopus carbo* in the NE Atlantic—Assessment through stomach content and stable isotope analyses. *Deep-Sea Research Part I*, 77, pp.1–10.

Scharf, F.S., Juanes, F. & Rountree, R.A., 2000. Predator size - prey size relationships of marine fish predators: interspecific variation and effects of ontogeny and body size on trophic-niche breadth. *Marine Ecology Progress Series*, 208, pp.229–248.

Schwarcz, H.P., Gao, Y., Campana, S., Browne, D., Knyf, M. & Brand, U., 1998. Stable carbon isotope variations in otoliths of Atlantic cod (*Gadus morhua*). *Canadian Journal of Fisheries and Aquatic Sciences*, 55(8), pp.1798–1806.

Seibel, B.A., 2011. Critical oxygen levels and metabolic suppression in oceanic oxygen minimum zones. *Journal of Experimental Biology*, 214(2), pp.326–336.

Seibel, B.A. & Drazen, J.C., 2007. The rate of metabolism in marine animals: environmental constraints, ecological demands and energetic opportunities. *Philosophical Transactions of the Royal Society B: Biological Sciences*, 362(1487), pp.2061–2078.

Seibel, B.A., Thuesen, E.V., Childress, J.J. & Gorodezky, L.A., 1997. Decline in pelagic cephalopod metabolism with habitat depth reflects differences in locomotory efficiency. *Biological Bulletin*, 192(2), pp.262–278.

Seibel, B.A., Thuesen, E.V. & Childress, J.J., 2000. Light-limitation on predator-prey interactions: consequences for metabolism and locomotion of deep-sea cephalopods. *Biological Bulletin*, 198(2), pp.284–298.

Sedberry, G.R. & Musick, J.A., 1978. Feeding strategies of some demersal fishes of the continental slope and rise off the mid-Atlantic coast of the USA. *Marine Biology,* 44, pp.357–375.

Sequeira, V., Neves, A., Vieira, A.R., Figueiredo, I. & Gordo, L.S., 2009. Age and growth of bluemouth, *Helicolenus dactylopterus*, from the Portuguese continental slope. *ICES Journal of Marine Science*, 66(3), pp.524–531.

Shephard, S., Trueman, C., Rickaby, R. & Rogan, E., 2007. Juvenile life history of NE Atlantic orange roughy from otolith stable isotopes. *Deep Sea Research Part I: Oceanographic Research Papers*, 54(8), pp.1221–1230.

Sherwood, G.D. & Rose, G.A., 2003. Influence of swimming form on otolith delta C-13 in marine fish. *Marine Ecology Progress Series*, 258, pp.283–289.

Sherwood, G.D. & Rose, G.A., 2005. Stable isotope analysis of some representative fish and invertebrates of the Newfoundland and Labrador continental shelf food web. *Estuarine, Coastal and Shelf Science*, 63(4), pp.537–549.

Shiao, J.-C., Itoh, S., Yurimoto, H., Iizuka, Y. & Liao, Y.-C., 2014. Oxygen isotopic distribution along the otolith growth axis by secondary ion mass spectrometry: Applications for studying ontogenetic change in the depth inhabited by deep-sea fishes. *Deep Sea Research Part I: Oceanographic Research Papers*, 84, pp.50–58.

Smith, D.G., 1970. Notacanthiform leptocephali in the western North Atlantic. *Copeia*, pp.1–9.

Smith, K.L. & Brown, N.O., 1983. Oxygen consumption of pelagic juveniles and demersal adults of the deep-sea fish *Sebastolobus altivelis*, measured at depth. *Marine Biology*, 76(3), pp.325–332.

Somero, G.N., 1992. Adaptations to high hydrostatic pressure. *Annual Review of Physiology*, 54, pp.557–577.

Stein, D.L., 1980. Description and occurrence of macrourid larvae and juveniles in the northeast Pacific Ocean off Oregon, U.S.A. *Deep Sea Research Part A. Oceanographic Research Papers*, 27(11), pp.889–900.

Stein, D.L., Felley, J.D. & Vecchione, M., 2005. ROV observations of benthic fishes in the Northwind and Canada Basins, Arctic Ocean. *Polar Biology*, 28(3), pp.232–237.

Steneck, R.S., 2001. Functional groups. In S. Levin, ed. *Encyclopedia of Biodiversity*. Academic Press, pp. 121–139.

Stockton, W.L. & DeLaca, T.E., 1982. Food falls in the deep sea: occurrence, quality, and significance. *Deep Sea Research Part A. Oceanographic Research Papers*, 29(2), pp.157–169.

Stowasser, G., McAllen, R., Pierce, G.J., Collins, M.A., Moffat, C.F., Priede, I.G. & Pond, W.B., 2009. Trophic position of deep-sea fish-Assessment through fatty acid

and stable isotope analyses. *Deep Sea Research Part I: Oceanographic Research Papers*, 56(5), pp.812–826. Available at: http://www.sciencedirect.com/science/article/pii/S0967063709000041.

Sulak, K.J., 1977. The systematics and biology of *Bathypterois* (Pisces, Chlorophthalmidae). *Galathea Report 14*, ed Wolff T (Copenhagen: Danish Science Press, Ltd), pp.49–108.

Sulak, K.J., Wenner, C.A., Sedberry, G.R. & Van Guelpen, L., 1985. The life history and systematics of deep-sea lizard fishes, genus *Bathysaurus* (Synodontidae). *Canadian Journal of Zoology*, 63(3), pp.623–642.

Svendsen, F.M., 2009. *Morphological and genetic variation in North Atlantic synaphobranchid eels in relation to species diagnostics*. University of Bergen, Bergen, Norway.

Swan, S.C. & Gordon, J.D.M., 2001. A review of age estimation in macrourid fishes with new data on age validation of juveniles. In Fisheries Research. pp. 177–195.

Swan, S.C., Gordon, J.D.M., Morales-Nin, B., Shimmield, T., Sawyer, T. & Geffen, A.J., 2003. Otolith microchemistry of *Nezumia aequalis* (Pisces: Macrouridae) from widely different habitats in the Atlantic and Mediterranean. *Journal of the Marine Biological Association of the UK*, 83(4), pp.883–886.

Swan, S.C., Geffen, A.J., Morales-Nin, B., Gordon, J.D.M., Shimmield, T., Sawyer, T. & Massutí, E., 2006. Otolith chemistry: an aid to stock separation of *Helicolenus dactylopterus* (bluemouth) and *Merluccius merluccius* (European hake) in the Northeast Atlantic and Mediterranean. *ICES Journal of Marine Science*, 63(3), pp.504–513. Available at: http://icesjms.oxfordjournals.org/cgi/doi/10.1016/j.icesjms.2005.08.012.

Swan, S.C., Gordon, J.D.M. & Shimmield, T., 2003. Preliminary investigations on the uses of otolith microchemistry for stock discrimination of the deep-water black scabbardfish (*Aphanopus carbo*) in the North East Atlantic. *Journal of Northwest Atlantic Fishery Science*, 31, pp.1–11.

Tamura, K., Peterson, D., Peterson, N, Stecher, G., Nei, M. & Kumar, S., 2011. MEGA5: molecular evolutionary genetics analysis using maximum likelihood, evolutionary distance, and maximum parsimony methods. *Molecular Biology and Evolution,* 28, pp.2731–2739.

Torres, G.J., Lombarte, A. & Morales-Nin, B., 2000. Variability of the sulcus acusticus in the sagittal otolith of the genus *Merluccius* (Merlucciidae). *Fisheries Research*, 46, pp.5–13.

Thresher, R.E., Koslow, J.A., Morison, A.K. & Smith, D.C., 2007. Depth-mediated reversal of the effects of climate change on long-term growth rates of exploited marine fish. *Proceedings of the National Academy of Sciences*, 104(18), pp.7461–7465.

Thorrold, S.R., Campana, S., Jones, C. & Swart, K., 1997. Factors determining delta C-13 and delta O-18 fractionation in aragonitic otoliths of marine fish. *Geochimica et Cosmochimica Acta*, 61(14), pp.2909–2919.

Trenkel, V.M. & Lorance, P., 2011. Estimating *Synaphobranchus kaupii* densities:

Contribution of fish behaviour to differences between bait experiments and visual strip transects. *Deep-Sea Research Part I*, 58(1), pp.63–71. Available at: http://dx.doi.org/10.1016/j.dsr.2010.11.006.

Trenkel, V.M., Francis, R.I.C.C., Lorance, P., Mahévas, S., Rochet, M.-J. & Tracey, D.M., 2004a. Availability of deep-water fish to trawling and visual observation from a remotely operated vehicle (ROV). *Marine Ecology Progress Series*, 284, pp.293–303.

Trenkel, V.M., Lorance, P. & Mahévas, S., 2004b. Do visual transects provide true population density estimates for deepwater fish? *ICES Journal of Marine Science: Journal du Conseil*, 61(7), pp.1050–1056.

Trueman, C.N., Johnston, G., O'Hea, B. & MacKenzie, K.M., 2014. Trophic interactions of fish communities at midwater depths enhance long-term carbon storage and benthic production on continental slopes. *Proceedings of the Royal Society B-Biological Sciences*, 281: 20140669.

Trueman, C.N., Rickaby, R. & Shephard, S., 2013. Thermal, trophic and metabolic life histories of inaccessible fishes revealed from stable-isotope analyses: a case study using orange roughy *Hoplostethus atlanticus*. *Journal of Fish Biology*, 83, pp.1613–1636.

Tuset, V.M., Lombarte, A., González, J.A., Pertusa, J.F. & Lorente, M.J., 2003. Comparative morphology of the sagittal otolith in *Serranus* spp. *Journal of Fish Biology*, 63, pp.1491–1504.

Tuset, V.M., Piretti, S., Lombarte, A. & González, J.A., 2010. Using sagittal otoliths and eye diameter for ecological characterization of deep-sea fish: *Aphanopus carbo* and *A. intermedius* from NE Atlantic waters. *Scientia Marina*, 74(4), pp.807–814.

Tuset, V.M., Rosin, P.L. & Lombarte, A., 2006. Sagittal otolith shape used in the identification of fishes of the genus *Serranus*. *Fisheries Research*, 81, pp.316–325.

Uiblein, F., Lorance, P. & Latrouite, D., 2003. Behaviour and habitat utilization of seven demersal fish species on the Bay of Biscay continental slope, NE Atlantic. *Marine Ecology Progress Series*, 257, pp.223–232.

Ullmann, J.F.P.J., Moore, B.A., Temple, S.E., Fernández-Juricic, E. & Collin, S.P., 2012. The retinal wholemount technique: a window to understanding the brain and behaviour. *Brain, Behavior and Evolution*, 79(1), pp.26–44.

Urick, R.J., 1984. *Ambient Noise in the Sea.* Undersea Warfare Technology Office, Naval Sea Systems Command, Department of the Navy, *Washington, D.C.*

van Aken, H.M., 2000. The hydrography of the mid-latitude Northeast Atlantic Ocean II: The intermediate water masses. *Deep-Sea Research Part I*, 47(5), pp.789–824.

van der Merwe, N.J., 1982. Carbon Isotopes, photosynthesis, and archaeology: Different pathways of photosynthesis cause characteristic changes in carbon isotope ratios that make possible the study of prehistoric human diets. *American Scientist*, 70(6), pp.596–660.

Vieira, A.R., Farias, I., Figueiredo, I., Neves, A., Morales-Nin, B., Sequeira, V., Martins, M.R. & Serrano Gordo, L., 2009. Age and growth of black scabbardfish (*Aphanopus carbo* Lowe, 1839) in the southern NE Atlantic. *Scientia Marina*,

73(S2), pp.33–46.

Vieira, A.R., Figueiredo, I., Figueiredo, C. & Menezes, G.M., 2013. Age and growth of two deep-water fish species in the Azores Archipelago: *Mora moro*(Risso, 1810) and *Epigonus telescopus*(Risso, 1810). *Deep Sea Research Part II: Topical Studies in Oceanography*, 98, pp.148–159.

Vignon, M. & Morat, F., 2010. Environmental and genetic determinant of otolith shape revealed by a non-indigenous tropical fish. *Marine Ecology Progress Series*, 411, pp.231–241.

Villeger, S., Ramos Miranda, J., Flores Hernandez, D. & Mouillot, D., 2010. Contrasting changes in taxonomic vs. functional diversity of tropical fish communities after habitat degradation. *Ecological Applications*, 20(6), pp.1512–1522.

Volpedo, A. & Echeverría, D.D., 2003. Ecomorphological patterns of the sagitta in fish on the continental shelf off Argentine. *Fisheries Research*, 60, pp.551–560.

Volpedo, A.V., Tombari, A.D. & Echeverría, D.D., 2008. Eco-morphological patterns of the sagitta of Antarctic fish. *Polar Biology*, 31, pp.635–640.

Vorus, W.S. & Taravella, B.M., 2011. Anguilliform fish propulsion of highest hydrodynamic efficiency. *Journal of Marine Science and Application*, 10(2), pp.163–174.

Wagner, H.J., 2001a. Brain areas in abyssal demersal fishes. *Brain, Behavior and Evolution*, 57(6), pp.301–316.

Wagner, H.J., 2001b. Sensory brain areas in mesopelagic fishes. *Brain, Behavior and Evolution*, 57(3), pp.117–133.

Wagner, H.J., Fröhlich, E., Negishi, K. & Collin, S.P., 1998. The eyes of deep-sea fish II. Functional morphology of the retina. *Progress in Retinal and Eye Research*, 17(4), pp.637–685.

Warrant, E., 2000. The eyes of deep-sea fishes and the changing nature of visual scenes with depth. *Philosophical Transactions of the Royal Society B: Biological Sciences*, 355(1401), pp.1155–1159. Available at: http://rstb.royalsocietypublishing.org/cgi/doi/10.1098/rstb.2000.0658.

Warrant, E.J. & Johnsen, S., 2013. Vision and the light environment. *Current Biology*, 23(22), pp.R990–R994.

Warrant, E.J. & Locket, N.A., 2004. Vision in the deep sea. *Biological Reviews*, 79(3), pp.671–712. Available at: http://doi.wiley.com/10.1017/S1464793103006420.

Was, A., Gosling, E., McCrann, K. & Mork, J., 2008. Evidence for population structuring of blue whiting (*Micromesistius poutassou*) in the Northeast Atlantic. *ICES Journal of Marine Science*, 65(2), pp.216–225.

Whitehead, P.J.P., Bauchot, M.L., Hureau, C., Nielsen, J. & Tortonese, E., eds., 1984. *Fishes of the north-eastern Atlantic and the Mediterranean Vol. 1*, UNESCO.

Whitehead, P.J.P., Bauchot, M.L., Hureau, C., Nielsen, J. & Tortonese, E., eds., 1986. *Fishes of the north-eastern Atlantic and the Mediterranean Vol.2 and Vol. 3*, UNESCO.

Widder, E.A., 2002. Bioluminescence and the pelagic visual environment. *Marine and Freshwater Behaviour and Physiology*, 35(1-2), pp.1–26.

Wickham, H., 2009. *ggplot2: Elegant Graphics for Data Analysis* (Springer Publishing Company, Incorporated).

Williams, H.A. & Lowe, M.K., 1997. Growth rates of four Hawaiian deep slope fishes: A comparison of methods for estimating age and growth from otolith microincrement widths. *Canadian Journal of Fisheries and Aquatic Sciences*, 54(1), pp.126–136.

Winemiller, K.O. & Rose, K.A., 1992. Patterns of life-history diversification in North American fishes: implications for population regulation. *Canadian Journal of Fisheries and Aquatic Sciences*, 49(10), pp.2196–2218.

Wiser, W., 1994. Cost of growth in cells and organisms: general rules and comparative aspects. *Biological Reviews*, 68, pp.1–33.

Witbaard, R., Duineveld, G.C.A., Van der Weele, J.A., Berghuis, E.M. & Reyss, J.P., 2000. The benthic response to the seasonal deposition of phytopigments at the Porcupine Abyssal Plain in the North East Atlantic. *Journal of Sea Research*, 43(1), pp.15–31.

Wright, P.J., Panfili, J., Morales-Nin, B. & Geffen, A.J., 2002. Types of calcified structures: otoliths. In J. Panfili,H. De Pontual, H. Troadec & P.J. Wright eds. *Manual of fish sclerochronology*. Brest, France: Ifremer-IRD coedition, pp. 31–57.

Wysocki, L.E. & Ladich F., 2001. The ontogenetic development of auditory sensitivity, vocalization and acoustic communication in the labyrinth fish *Trichopsis vittata*. *Journal of Comparative Physiology A*, 187, pp.177–187.

Yancey, P.H., Gerringer, M.E., Drazen, J.C., Rowden, A.A. & Jamieson, A., 2014. Marine fish may be biochemically constrained from inhabiting the deepest ocean depths. *Proceedings of the National Academy of Sciences of the United States of America*, 111(12), pp.4461–4465.

Yeh, J. & Drazen, J.C., 2011. Baited-camera observations of deep-sea megafaunal scavenger ecology on the California slope. *Marine Ecology Progress Series*, 424, pp.145–156.